Eigenvalue Optimization with respect to Shape-Variations in Electromagnetic Systems

Eigenvalue Optimization with respect to Shape-Variations in Electromagnetic Systems

Accepted doctoral thesis by Christine Eva Herter, M.Sc.

Darmstadt, Technische Universität Darmstadt

Date of thesis defense: September 16, 2024
Year of publication on TUprints: 2024

Acknowledgments

In the past five years, I met various people who supported me with my thesis and influenced my life in many ways. First and foremost, I would like to thank my supervisor Winnifried Wollner. After supervising my master thesis, he gave me the chance to continue working as a PhD knowing that I was more a computational engineer than a mathematician. He supported me a lot and was always really patient. I am thankful for the time he spend discussing about mathematical problems and the implementation. Also, he gave me the possibility to travel to several conferences for presenting my research and networking to people, which I really enjoyed.

Furthermore, I want to thank my co-supervisor Sebastian Schöps for his ideas and discussions regarding the application part. Besides, I would like to thank Stefan Ulbrich, who already supported me during my studies in Computational Engineering as professorial mentor, and Christian Stinner. Both accepted to be part of the examination committee for my thesis.

I thank all the colleagues from the AG Optimization at TU Darmstadt, where I worked the first three years of my PhD. I have many great memories of this time - all the group lunches (Blitz friday), nice discussions during coffee-cookie-meetings and all the great activities beyond work, such as going to Boulder and Running, Boardgame and Doppelkopf nights as well as Kleinwalsertal. In this context, I would like to thank Oli, who was my biggest emotional support, knowing all the struggles which I had. Moreover, I thank Fred, who was a great office mate, and Oliver, for many nice coffee breaks and always an open ear, especially in the end of the dissertation. Also, both proofread parts of my thesis. I thank the colleagues from GSC with whom I enjoyed the exchange during the salad days and cake meetings. I thank the colleagues from TEMF who had a workplace for me while visiting Darmstadt in the last months of my PhD, especially to Anna for the discussions about cavities and proofreading parts of my thesis, and Timon, who was also proofreading parts of my thesis.

Zusammenfassung

Diese Arbeit beschäftigt sich mit der Freiformoptimierung eines Eigenwertproblems abhängig von kleinen Formvariationen, um die optimale Geometrie in elektromagnetischen Systemen zu finden. Die Arbeit ist motiviert durch die Kavitäten eines Teilchenbeschleunigers, welche sensibel gegenüber kleiner Verformungsänderungen sind. Wir formulieren ein optimales Steuerungsproblem, das wir durch die gemischte Variationsformulierung des normierten zeitharmonischen Maxwell-Eigenwertproblems von Kikuchi beschränken. Dabei kontrollieren wir die Verformung des Gebietes durch Gebietstransformationen.

Darüber hinaus sind wir an der Lösung des Optimierungsproblems interessiert. Dafür berechnen wir zunächst mithilfe des adjungierten Kalküls die Ableitung des reduzierten Kostenfunktionals für ein verallgemeinertes Eigenwertoptimierungsproblem. Anschließend wenden wir diesen Ansatz auf das konkrete Optimierungsproblem an, welches wir durch das Maxwell-Eigenwertproblem beschränken, und diskutieren zwei Optimierungsverfahren zur Lösung des Problems. Wir betrachten zum einen ein Gradientenverfahren und zum anderen ein gedämpftes inverses Broyden-Fletcher-Goldfarb-Shanno (BFGS)-Verfahren, wobei wir bei letzterem die positive Definitheit für die Operatoren beweisen, die den Hesse-Operator des reduzierten Kostenfunktionals approximieren. Wir validieren diese Methoden anhand numerischer Beispiele, um die Funktionalität ihrer Implementierung zu zeigen. Dabei diskutieren wir zunächst den Einfluss der Regularitätsparameter, die wir für das Optimierungsproblem verwenden. Außerdem untersuchen wir den Einfluss des gewählten Ziel-Eigenwertes auf die Verformung der betrachteten Gebiete.

Abschließend diskutieren wir die Erweiterung dieses Ansatzes auf praktische Probleme, wie zum Beispiel einer Kavität eines Teilchenbeschleunigers, die die Motivation dieser Arbeit war. Wir zeigen Ergebnisse zu zweidimensionalen Kavitäten und erweitern diesen Ansatz auf dreidimensionale Probleme.

Abstract

In this thesis, we consider a freeform optimization problem of eigenvalues by means of shape-variations with respect to small deformations in order to find the optimal geometry in electromagnetic systems. This is motivated by the application of a particle accelerator cavity. We formulate an optimal control problem constrained by the mixed variational formulation by Kikuchi of the normalized time-harmonic Maxwell eigenvalue problem. By applying the method of mappings, we control the deformation of the domain.

Moreover, we are interested in solving the optimization problem. Therefore, we first calculate the derivative of the reduced cost functional for a generalized eigenvalue optimization problem using the adjoint calculus. Then, we apply this approach to the considered freeform optimization problem constrained by the Maxwell eigenvalue problem. In order to solve this problem, we discuss two optimization methods. Here, we consider a gradient method and a damped inverse Broyden-Fletcher-Goldfarb-Shanno (BFGS) method, where we prove the positive definiteness of the operators which approximate the Hessian of the reduced cost functional for the latter. Further, we validate these methods on numerical examples to demonstrate the functionality of their implementation. We discuss the influence of the regularity parameters and a chosen target value on the optimization methods and on the final deformation of the considered domains.

Finally, we discuss the extension of this approach to more realistic problems, such as a particle accelerator cavity, which was the motivation of this thesis. We present results on two-dimensional cavity domains and the extend this approach to three-dimensional problems.

Contents

Introduction

Shape optimization has its application in numerous crucial fields in engineering and industry. In the last decades, it inspired deep mathematical theories and had an intense development. One goal of shape optimization is to optimize the produced components from the early stages of design, so that they fulfill and optimize their intended purpose. The rise of computational power and the development of advanced mathematical programming methods made shape as well as topology optimization a very popular discipline in many scientific fields, e.g., structural mechanics, including civil engineering or architecture or in fluid mechanics, see [5].

In this thesis, we consider an eigenvalue optimization with shape-variations in electromagnetic systems, such as particle accelerator cavities. The general goal of an accelerator is to propel charged particles at high speed, close to the speed of light, to smash them either onto a target or against other particles circulating in the opposite direction. Physicists study these collisions to probe the world of the infinitely small. One famous example of a particle collider is the Large Hadron Collider from the CERN [1] which is, with 27 km rings of superconducting magnets, the longest and most powerful accelerator.

One crucial component of these accelerators is the cavity, which is responsible for the acceleration of particles. So-called superconducting Radio Frequency (RF) particle accelerator cavities are used to transfer energy to a charged particle beam by applying an electric field. Cavities excite electromagnetic fields of various frequencies. For each frequency, there exists a corresponding electric field, a so-called eigenmode, which varies in its shape, see [9].

The goal of superconducting RF cavities is to achieve an acceleration mode, which accelerates the particles inside the cavity forward. The most relevant acceleration eigenmode is the fundamental Transverse Magnetic (TM) mode. The shape of the TM_{010}-mode, also called π-mode, is shown in Figure 1.1. The
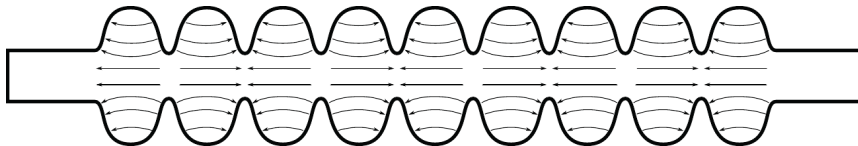
Figure 1.1. Electric field of the TM_{010}, also called π-mode

electromagnetic field distribution and resonating frequency of various modes in superconducting cavities are sensitive to small geometric deformations and their effectiveness is mainly determined by their geometry. Therefore, it is common to tune the achieved eigenfrequencies to derive a more precise electric field for the acceleration. A freeform optimization allows us to find the optimal geometry. For a detailed description of cavities as well as their associated components, we refer to the paper about superconducting TESLA cavities [12] and also to [36,46].

1.1. Eigenvalue Optimization for Electromagnetic Cavities

Since RF cavities highly depend on their exact shape, the optimization of the shape is of deep interest and has already been studied a lot in the past. In this context, a wide research area is the optimization with respect to several parameters of the geometry of the concerning cavity. This area is mainly a field of applied engineering and contains essentially numerical studies. For the optimization, a common way is to compute the directional derivatives of the cost function with respect to the considered parameters. Depending on the number of parameters and the size of the design space, the computation of the gradient can get very costly. One way to deal with this problem is to use gradient-free methods, see, e.g., [43, 69, 70], where evolutionary algorithms are used to solve multi-objective shape optimization problems, and [90], where a stochastic setting is used. Another way is the optimization with gradient-based methods. One example is the computation of the derivatives of stiffness and mass matrices with respect to geometric changes which are closely related to the computation of shape derivatives, see, e.g., in [113].

In all the mentioned references, the deformation of a cavity always depends on certain parameters defining the geometry of the domain. The motivation of this thesis is to allow a shape-deformation in every direction to achieve the optimal shape. Therefore, we consider a freeform optimization problem. Compared to parameter optimization, the freeform optimization is more costly in computation of the derivatives because the number of unknowns increases. To handle this problem, we consider the approach of adjoint calculus which is well-explained for optimization problems subject to partial differential equations (PDEs), see, e.g., [59].

In [78], it is explained that the origin of the approach of adjoint calculus lies in the Pontryagin's principle and the practical use with perspective of the Lagrange multipliers is introduced in [33]. The adjoint method has already been applied to many applications of control problems as well as shape and topology optimization problems, e.g., in the domain of structural optimization of solid bodies, see [4, 6–8], or in fluid mechanics, see, e.g., [54, 62]. Further, optimization problems where the functionals depend on the eigenvalues are studied in, e.g., [67] and discussed in [101]. Moreover, this work is inspired by [58, 92], where the adjoint calculus is done for elliptic eigenvalue problems.

In the context of the optimization of Maxwell's eigenvalue problem, the adjoint method has already been applied for optimization with respect to certain parameters, see, e.g., [3]. In the authors work [57], we introduce adjoint calculus in order to solve a freeform optimization problem constrained by Maxwell's eigenvalue problem. In this thesis, we explain this approach in more detail. We use adjoint calculus to obtain the reduced gradient for a generalized eigenvalue optimization problem. Furthermore, we apply this approach to the freeform optimization problem constrained by Maxwell's eigenvalue problem with respect to shape-variations in order to find the optimal shape of a considered domain, e.g., a cavity domain.

Based on this approach, we are able to compute the first derivatives of the considered problem. One strategy to solve this kind of optimization problem is a line search method, where in each iteration a search direction and a step length is computed, see, e.g., [40, 84, 103]. In this thesis, we consider two well-known line search methods, a gradient method and a quasi-Newton's method, namely an inverse damped BFGS method. We expect a better convergence on the second method, see [89]. The origin of the damping step is shown in [89], which we extend from the finite-dimensional to the infinite-dimensional setting. Further,

in the origin, the damping is applied to the classical BFGS method. In this thesis, we show that a damping is also applicable to the inverse BFGS method.

The eigenvalue optimization with respect to shape-variations is closely related to the context of shape optimization. For the computation of shape derivatives in PDE-constrained optimization, we refer to [41, 52, 99]. For the adjoint approach, we require the differentiability of the control-to-state operator associated with Maxwell's eigenvalue problem in a sufficiently strong topology. Therefore, we need to take into account that the results depend on a shape-variation. This variation can be expressed by the method of mappings, see, e.g., [79, 80], and is based on kinematic statements from continuum mechanics. The method of mappings is already applied to several shape optimization problems to derive Fréchet derivatives with respect to shape-variations. For example, we refer to [42], where properties of Fréchet differentiability are derived in the context of Navier-Stokes problems. For the analysis of a linear elasticity eigenvalue problem without domain mapping, we refer to [44]. In this thesis, we assume continuity and differentiability in order to apply adjoint calculus for the considered freeform optimization problem constrained by Maxwell's eigenvalue problem depending on a domain mapping.

The mathematical model for high frequency electromagnetic fields is the following eigenvalue problem solving Maxwell's equations

$$
\begin{aligned}
\nabla \times (\nabla \times E) &= k^2 E &&\text{in } \Omega, \\
\nabla \cdot E &= 0 &&\text{in } \Omega, \\
E \times n &= 0 &&\text{on } \partial\Omega,
\end{aligned}
\tag{1.1}
$$

in a bounded domain Ω. Here, E describes the electric field, k is the wave number and n is the outward normal to the domain, see [60]. Historically, the attempts to solve such Maxwell's eigenvalue problems suffered from so-called spurious modes that disturbed the searched eigenmodes. In particular, by using the finite element discretization with Lagrange elements, problems arise chiefly for three-dimensional problems. Moreover, spurious modes appear by ignoring the divergence-free constraint, i.e.,

$$
\nabla \cdot E = 0.
$$

A method invented between 1975 and 1980 by Weiland [107, 108], the so called finite integration technique (FIT), could completely avoid the problem of spuri-

ous modes. The drawback of this method is the price of going back to a finite difference scheme. Real cavities have, next to their smooth inner surfaces, special points with fine structural details, e.g., at a coupling loop for feeding in the RF power. This strong variations of scale favour the use of finite element methods against finite difference schemes. It is also possible to avoid spurious modes by the use of the finite element method. In the paper [9], two methods are well discussed. The first method is a penalty method introduced in [72], which uses a variational formulation neglecting the divergence-free constraint. The discretization of the electric field is represented by ordinary node based elements. A penalization shifts the spurious eigenfrequencies to the right of the desired part of the spectrum. The other introduced method to avoid spurious modes is a mixed variational formulation which includes the divergence-free constraint. The components of the electric field are discretized by edge elements, e.g., Nédélec elements, whereas the variational term of the divergence-free constraint is discretized by node based elements. By using edge elements, the computed approximated eigenmodes are naturally split into curl-free and (in a discrete sense) divergence-free modes. Hence, these elements ensure proper subspaces of the space of the electric field. For more details of edge elements, we refer to [77, 105]. Here, the advantages and disadvantages of these elements are intensely discussed. Furthermore, for edge elements in context of cavity shapes, we refer to [29, 34, 105].

In this thesis, we consider a mixed variational formulation, namely the formulation introduced by Kikuchi [65] which distinguishes in its discretization between the electric field and the divergence-free space, see [83]. It is clear that the matrix of the discretized problem is simpler to solve in case of node based elements or neglecting the divergence-free constraint in comparison with the mixed formulation. Nevertheless, we choose the mixed formulation because in an optimization loop, a particular eigenvalue needs to be selected automatically. With this setting, we ensure the selection of a physical eigenvalue which is no spurious solution.

1.2. Contribution

This work focuses on the eigenvalue optimization with respect to shape-variations in electromagnetic systems. The contributions of this thesis are the following.

In Chapter 3, we discuss a suitable variational formulation for the eigenvalue optimization problem and state the concrete formulation with domain mapping.

Furthermore, we show the Fréchet differentiability of the functions concerning the domain mapping in order to compute the derivatives of the domain dependent Maxwell eigenvalue problem.

Based on a normalization of the eigenfunctions, local uniqueness of the solution allows us to derive adjoint formulas for the derivatives of the eigenvalues with respect to domain variations. We compute the derivatives for a generalized eigenvalue problem and apply this approach to the concrete Maxwell eigenvalue optimization problem. The results and formulation have been announced by the author in [57]. In this thesis, we explain this approach in detail, see Section 4.1.

To solve freeform optimization problems, we consider two optimization methods, namely a gradient and a damped inverse BFGS method. For the latter, we prove the preservation of the positive definiteness property of the operator, which updates in every iteration to approximate the Hessian of the reduced cost functional. With this property, we ensure that the curvature condition is fulfilled. The proof can be found in Section 4.2.

A further contribution is the implementation and simulation of the considered freeform optimization problem constrained by Maxwell's eigenvalue problem with respect to shape-variations. All computations base on the finite element library `deal.II` [10, 11]. Here, the author fixed bugs concerning the provided mixed finite element system. Moreover, the optimization is implemented within the optimization library `DOpElib` [49]. Here, the author extended the framework for PDE optimization problems for eigenvalue optimization problems. Moreover, the author fixed bugs in the BFGS method and extended the method to an inverse damped BFGS method, which we use for the numerical examples in this thesis.

In Section 4.4, we demonstrate the functionality of the extension of the library, the implementation of the damped inverse BFGS method as well as the computation of the derivatives using adjoint calculus, we show numerical examples on simple geometries. In this context, we study the regularization parameters of the cost functional and the influence of different target values in the objective functional on the domain deformation.

We extend the optimization to more realistic geometries, such as two-dimensional cavity domains and three-dimensional geometries. The numerical results are stated in Chapter 5.

1.3. Outline

This thesis is structured as follows. After the introduction, we continue with the preliminaries of this thesis in Chapter 2. In detail, we introduce shortly the theory of functional analysis in Section 2.1. For the computation of the deformation gradient and its derivative, we introduce the needed matrix algebra in Section 2.2. We shortly treat the theory of eigenvalues in Section 2.3. Furthermore, we consider definitions of differentiability of operators in Banach spaces in Section 2.4. Afterwards, in Section 2.5, we explain reduced problems and the theory of adjoint calculus in context of PDE constrained optimization problem. In Section 2.6 we treat optimality conditions. We conclude this chapter with explaining a general descent method for unconstrained optimization problems in Section 2.7.

In Chapter 3, we discuss the theory of Maxwell's eigenvalue problem. For that, we consider the time-harmonic Maxwell eigenvalue problem and discuss shortly two different variants of variational formulations of this problems regarding the occurrence of so-called spurious modes in Section 3.1. Further, in Section 3.2, we formulate the introduced variational formulation of the previous section depending on a domain mapping. Hence, we define the deformation gradient and distinguish between the function spaces of $H_0(\mathrm{curl})$ and H_0^1. In Section 3.3, we discuss the existence and properties of eigenvalues and associated eigenfunctions of Maxwell's eigenvalue problem.

Chapter 4 deals with the eigenvalue optimization. In order to compute the reduced gradient, we discuss the adjoint calculus in Section 4.1. First, we consider the derivatives for a general eigenvalue problem depending on a domain mapping. Afterwards, we compute the derivatives for the concrete Maxwell eigenvalue optimization problem. In order to solve the considered problem, we introduce two optimization methods in Section 4.2. On the one hand, we discuss a gradient method. On the other hand, we treat a quasi-Newton method, to be precise a damped inverse BFGS method, to increase the convergence rate. Here, we show the concrete methods applied on the considered eigenvalue optimization problem. Afterwards, we consider the discretization of Maxwell's eigenvalue problem in Section 4.3, where we use a mixed finite element method (FEM) to discretize the function spaces. Here, we discretize the $H_0^1(\Omega)$-space with Lagrange elements and the $H_0(\mathrm{curl}; \Omega)$ with Nédélec elements. We conclude this section with the matrix formulation of the discretized Maxwell eigenvalue problem and by mentioning some implementation details, i.e., about the library `deal.II` and

its hurdles with mixed finite elements as well as saddle point problems and the eigenvalue solver library `SLEPc` which we use for solving this kind of problems. In Section 4.4, we conclude this chapter with numerical results. We show solutions of the optimization problem on two simple geometries, i.e., a rectangle with free boundaries, in Section 4.4.1, and a quarter circle with fixed edges, in Section 4.4.2. Here, we compare the optimization methods which we introduced in the previous section and observe the influence of regularization parameters of the considered cost functional and various target values on the domain deformation. Finally, in Section 4.4.3, we conclude this section by a discussion of the obtained numerical results.

In Chapter 5, we present discuss the extension of approach to more realistic problems. We present results of eigenvalue optimization on two-dimensional planar cavity domains, in Section 5.1. First, we show results of the optimization of a 1-cell cavity in Section 5.1.1. Afterwards, we consider a 5-cell cavity model in Section 5.1.2. Here, we optimize the first eigenvalue to a target value by using the damped inverse BFGS method. In Section 5.2, we extend the approach to three-dimensional geometries. Here, we show numerical results of the optimization on a cuboid in Section 5.2.1 and an optimization example of cylindrical geometry in Section 5.2.2.

In Chapter 6, we conclude this thesis and discuss open questions for the analysis and for the application. In Appendix A.1, we show a documentation of the extension for eigenvalue optimization problems of the PDE optimization software `DOpElib`. Furthermore, we treat a concrete example of the implementation of Maxwell's eigenvalue optimization problem with domain mapping. Moreover, in Appendix A.2, we show further numerical solutions tables of the optimization examples for completion.

CHAPTER 2

Preliminaries

In this thesis, we consider optimization problems constrained by an eigenvalue problem. To be able to analyze and discuss this kind of problems, we introduce in Section 2.1 the functional analysis background. Further, in Section 2.2, we consider some basic matrix algebra which we need for the computation of the domain mapping and its derivatives. In Section 2.3, we treat the eigenvalue theory, which we use in Section 3.3 to show the existence of eigenvalues and associated eigenvectors in cavity problems. Further, in Section 2.4, we introduce the different concepts of differentiability of operators in Banach spaces. Moreover, we consider the optimality theory for optimization problems with PDE-constraints in infinite dimensional spaces. Therefore, we treat in Section 2.5 the theory of reduced problems and adjoint calculus in context of PDE optimization problems. Further, we consider optimality conditions in Section 2.6 and conclude this chapter with an introduction to unconstrained optimization in Section 2.7.

2.1. Functional Analysis

In this section, we introduce the functional analytical background which we need for this thesis. First, we consider Banach and Hilbert spaces in Section 2.1.1. In the context of PDE optimization, we do not necessarily have classical solutions. Therefore, we introduce in Section 2.1.2 the Sobolev spaces. By using these spaces and functional analysis, there exist a satisfactory solution theory which provides a suitable framework to derive optimality conditions. For the theory of Banach and Hilbert spaces as well as Sobolev spaces, we refer to [59, 81, 93]. To later on formulate and discuss Maxwell's eigenvalue problem, we introduce

vector functions with curl and divergence. For this theory and more details, we refer to [24, 76]

2.1.1. Banach and Hilbert Spaces

Definition 2.1 (Norm, Banach space)**.** *Let X be a real vector space.*

1. A mapping $\|\cdot\|\colon X \mapsto [0, \infty)$ is a norm on X, if

$$
\begin{aligned}
a) \quad & \|u\| = 0 \ \Leftrightarrow \ u = 0 & & \forall u \in X, \\
b) \quad & \|\lambda u\| = |\lambda|\,\|u\| & & \forall u \in X, \lambda \in \mathbb{R}, \\
c) \quad & \|u + v\| \leq \|u\| + \|v\| & & \forall u, v \in X.
\end{aligned}
$$

2. A normed real vector space X is called (real) Banach space if it is complete, i.e., if every Cauchy sequence (u_n) has a limit $u \in X$, more precisely, if $\lim_{m,n\to\infty} \|u_m - u_n\| = 0$ then there is $u \in X$ with $\lim_{n\to\infty} \|u_n - u\| = 0$.

Example 2.2. Let $\Omega \subset \mathbb{R}$ be open. For a multi-index $\alpha = (\alpha_1, \ldots, \alpha_n) \in \mathbb{N}_0^n$ we define its order by $|\alpha| := \sum_{i=1}^n \alpha_i$ and associate the $|\alpha|$-th order partial derivative at x by

$$
D^\alpha u(x) := \frac{\partial^{|\alpha|} u}{\partial x_1^{\alpha_1} \ldots \partial x_n^{\alpha_n}}(x).
$$

We define

$$
C^k(\Omega) = \{u \in C(\Omega)\colon D^\alpha u \in C(\Omega) \text{ for } |\alpha| \leq k\}.
$$

For $\Omega \subset \mathbb{R}^n$ open and bounded, let

$$
C^k(\bar{\Omega}) = \{u \in C^k(\Omega)\colon D^\alpha u \text{ has a continuous extension to } \bar{\Omega} \text{ for } |\alpha| \leq k\}.
$$

Then the spaces $C^k(\bar{\Omega})$ are Banach spaces with the norm

$$
\|u\|_{C^k(\bar{\Omega})} := \sum_{|\alpha| \leq k} \|D^\alpha u\|_{C(\bar{\Omega})}.
$$

Definition 2.3. *Two normed vector spaces X, Y are called isometric, if there is a linear bijection $L\colon X \to Y$ such that $\|L(x)\| = \|x\|$ for every $x \in X$.*

Definition 2.4 (Inner product, Hilbert space)**.** *Let H be a real vector space.*

1. A mapping $(\cdot, \cdot) \colon H \times H \mapsto \mathbb{R}$ is an inner product on H, if

    a) $(u, v) = (v, u) \quad \forall u, v \in H$,

    b) for every $v \in H$, the mapping $u \in H \mapsto (u, v)$ is linear,

    c) $(u, u) \geq 0 \quad \forall u \in H$ and $(u, u) = 0 \Leftrightarrow u = 0$.

2. A vector space H with inner product $(\cdot, \cdot)$ and associated norm

$$\|u\| := \sqrt{(u, u)}$$

    is called Pre-Hilbert space.

3. A Pre-Hilbert space $(H, (\cdot, \cdot))$ is called Hilbert space if it is complete under its norm $\|u\| := \sqrt{(u, u)}$.

Example 2.5. Let $\emptyset \neq \Omega \subset \mathbb{R}^n$ be open and bounded. Then $(C(\bar{\Omega}), (\cdot, \cdot)_{L^2})$ is a Pre-Hilbert space with the L^2-inner product

$$(u, v)_{L^2} = \int_\Omega u(x) v(x) \mathrm{d}x.$$

Theorem 2.6 (Cauchy-Schwarz Inequality)**.** *Let H be a Pre-Hilbert space. Then the Cauchy-Schwarz inequality holds*

$$|(u, v)| \leq \|u\| \|v\| \quad \forall u, v \in H.$$

Definition 2.7. *A Hilbert (or, more generally, a Banach) space X is called separable if it contains a countable dense subset. That is, there exists $Y = \{x_i \in X \colon i \in \mathbb{N}\} \subset X$ such that*

$$\forall x \in X, \quad \forall \varepsilon > 0 \colon \exists y \in Y \quad \|x - y\|_X < \varepsilon.$$

Example 2.8. For bounded Ω the space $C(\bar{\Omega})$ is separable.

Definition 2.9. *Let H be a Hilbert space. We say that two elements x and y of H are orthogonal if $(x, y) = 0$. For any subspace M of H, we define the orthogonal complement by*

$$M^\perp = \{x \in H \,|\, (x, y) = 0 \,\forall y \in M\}.$$

For the following Projection Theorem, we refer to [93, Theorem 6.26].

Theorem 2.10 (Projection Theorem). *Let H be a Hilbert space and let M be a closed subspace of H. Then every $u \in H$ has a unique decomposition $u = v + w$, where $v \in M$ and $w \in M^\perp$.*

Linear partial differential operators define linear mappings between function spaces. We recall the definition of linear operators.

Definition 2.11 (Linear operator). *Let X, Y be normed real vector spaces with norms $\|\cdot\|_X, \|\cdot\|_Y$.*

1. *A mapping $A\colon X \to Y$ is called linear operator if it satisfies*

$$A(\lambda u + \mu v) = \lambda Au + \mu Av \quad \forall u, v \in X, \ \lambda, \mu \in \mathbb{R}.$$

   The range of A is defined by

$$R(A) \coloneqq \{y \in Y \colon \exists x \in X \colon y = Ax\}$$

   and the null space of A by

$$N(A) \coloneqq \{x \in X \colon Ax = 0\}.$$

2. *A linear mapping $L\colon X \to Y$ is called bounded if there is a constant C such that $\|Lx\| \leq C\|x\|$ for all $x \in X$.*

3. *An operator $L\colon X \to Y$ is sequentially continuous at a point $x \in X$ if, whenever $x_n \in X$ is a sequence such that $x_n \to x$, we have $L(x_n) \to L(x)$.*

Theorem 2.12. *Let X, Y be normed real vector spaces with norms $\|\cdot\|_X, \|\cdot\|_Y$. Let $L\colon X \to Y$ be a linear mapping.*

1. *If L is sequentially continuous at the origin, it is continuous at every $x \in X$.*

2. *L is sequentially continuous if and only if it is bounded.*

The set of all bounded linear mappings forms a vector space. Taking the smallest possible constant in Definition 2.11, then this quantity gives us a measure of the size of a linear mapping. By that, the following theorem is motivated.

Theorem 2.13. *Let X, Y be normed real vector spaces with norms $\|\cdot\|_X, \|\cdot\|_Y$. By $\mathcal{L}(X, Y)$ we denote the space of all linear operators $A\colon X \to Y$ that are*

bounded in the sense that

$$\|A\|_{X,Y} := \sup_{\|u\|_X = 1} \|Au\|_Y < \infty.$$

$\mathcal{L}(X,Y)$ *is a normed space with the operator norm* $\|\cdot\|_{X,Y}$.

Theorem 2.14. *If* Y *is a Banach space then* $\mathcal{L}(X,Y)$ *is a Banach space.*

If Y is a Banach space, any operator $A \in \mathcal{L}(X,Y)$ is determined uniquely by its action on a dense subspace.

Theorem 2.15. *Let* X *be a normed space,* Y *be a Banach space and let* $U \subset X$ *be a dense subspace. Then for all* $A \in \mathcal{L}(U,Y)$, *there exists a unique extension* $\tilde{A} \in \mathcal{L}(X,Y)$ *with* $\tilde{A}|_U = A$. *For this extension, there holds* $\|\tilde{A}\|_{X,Y} = \|A\|_{U,Y}$.

Definition 2.16 (Linear functionals, dual space).

1. *Let* X *be a Banach space. A bounded linear operator* $u^* \colon X \to \mathbb{R}$, *i.e.,* $u^* \in \mathcal{L}(X, \mathbb{R})$ *is called a bounded linear functional on* X.

2. *The space* $X^* := \mathcal{L}(X, \mathbb{R})$ *of linear functionals in* X *is called dual space of* X *and is (by Theorem 2.14) a Banach space with the operator norm*

$$\|u^*\| := \sup_{\|u\|_X = 1} |u^*(u)|.$$

3. *We use the notation*
$$\langle u^*, u \rangle_{X^*, X} := u^*(u).$$

   $\langle \cdot, \cdot \rangle_{X^*, X}$ *is called dual pairing of* X^* *and* X.

The dual space of a Hilbert space is isometric to the space itself. This result is known as the Riesz Representation Theorem.

Theorem 2.17 (Riesz Representation Theorem). *The dual space* H^* *of a Hilbert space* H *is isometric to* H *itself. More precisely, for every* $v \in H$ *the linear functional* u^* *defined by*

$$\langle u^*, u \rangle_{H^*, H} := (v, u)_H \quad \forall u \in H$$

is in H^* with norm $\|u^*\|_{H^*} = \|v\|_H$. *Vice versa, for any $u^* \in H^*$ there exists a unique $v \in H$ such that*

$$\langle u^*, u \rangle_{H^*, H} = (v, u)_H \quad \forall u \in H$$

and $\|u^*\|_{H^*} = \|v\|_H$. In particular, a Hilbert space is reflexive.

Definition 2.18. *Let X, Y be Banach spaces. Then for an operator $A \in \mathcal{L}(X, Y)$ the dual operator $A^* \in \mathcal{L}(Y^*, X^*)$ is defined by*

$$\langle A^* v, u \rangle_{X^*, X} = \langle v, Au \rangle_{Y^*, Y} \qquad \forall v \in Y^*, u \in X.$$

It holds that $\|A^*\|_{Y^*, X^*} = \|A\|_{X, Y}$.

2.1.2. Sobolev Spaces

For the theory for PDEs, we replace the classical function space $C^k(\bar{\Omega})$ by the Sobolev space $W^{k,p}(\Omega)$, which consists of all functions $u \in L^p(\Omega)$ that possess (weak) partial derivatives $D^\alpha u \in L^p(\Omega)$ for $|\alpha| \leq k$. The so-called p-Lebesgue space $L^p(\Omega)$ is complete under the L^p-norm, where

$$\|u\|_{L^p(\Omega)} = \left(\int_\Omega |u(x)|^p \mathrm{d}x \right)^{1/p}, \qquad p \in [1, \infty),$$

$$\|u\|_{L^\infty(\Omega)} = \operatorname*{ess\,sup}_{x \in \Omega} |u(x)| \quad (= \sup_{x \in \Omega} |u(x)| \text{ for } u \in C(\bar{\Omega})).$$

The L^p-norm can be extended to Lebesgue measurable functions. Therefore, we introduce the σ-algebra on $\mathbb{R}^n$.

Definition 2.19 (σ-Algebra)**.** *A collection $\mathcal{S} \subset \mathcal{P}(\mathbb{R}^n)$ of subsets of $\mathbb{R}^n$ is called σ-algebra on $\mathbb{R}$ if*

1. *$\emptyset, \mathbb{R}^n \in \mathcal{S}$,*

2. *$A \in \mathcal{S}$ implies $\mathbb{R}^n \setminus A \in \mathcal{S}$,*

3. *If $(A_k)_{k \in \mathbb{N}} \subset \mathcal{S}$ then $\bigcup_{k=1}^\infty A_k \in \mathcal{S}$.*

A measure $\mu \colon \mathcal{S} \to [0, \infty]$ is a mapping with the following properties:

1. *$\mu(\emptyset) = 0$.*

2. If $(A_k)_{k \in \mathbb{N}} \subset \mathcal{S}$ is a sequence of pairwise disjoint sets then

$$\mu \left(\bigcup_{k=1}^{\infty} A_k \right) = \sum_{k=1}^{\infty} \mu(A_k) \qquad \sigma\text{-additivity.}$$

It holds the following theorem for the σ-algebra of Lebesgue measurable sets with corresponding Lebesgue measure.

Theorem 2.20. *There exists the σ-algebra $\mathcal{B}_n$ of Lebesgue measurable sets on $\mathbb{R}^n$ and the Lebesgue measure $\mu \colon \mathcal{B}_n \to [0, \infty]$ with the properties:*

1. $\mathcal{B}_n$ contains all open sets (and thus all closed sets).

2. μ is a measure on $\mathcal{B}_n$.

3. If B is any ball in $\mathbb{R}^n$ then $\mu(B) = |B|$, where $|B|$ is the volume of B.

4. If $A \subset B$ with $B \in \mathcal{B}_n$ and $\mu(B) = 0$ then $A \in \mathcal{B}_n$ and $\mu(A) = 0$. This means that $(\mathbb{R}^n, \mathcal{B}_n, \mu)$ is a complete measure space.

The sets $A \in \mathcal{B}_n$ are called Lebesgue measurable.

If some property holds for all $x \in \mathbb{R} \setminus N$ with $N \subset \mathcal{B}_n, \mu(N) = 0$, then we say that it holds almost everywhere (a.e.). A function is Lebesgue measurable by the following definition.

Definition 2.21. *We say that $f \colon \mathbb{R}^n \to [-\infty, \infty]$ is Lebesgue measurable if*

$$\{x \in \mathbb{R}^n \colon f(x) > \alpha\} \in \mathcal{B}_n \quad \forall \alpha \in \mathbb{R}.$$

Now, we extend the L^p-norm to Lebesgue measurable functions. For this and for further details, as well as the definitions of Lebesgue integrals to the literature, we refer to, e.g., [59, Section 1.2.2].

Definition 2.22. *Let $\Omega \in \mathcal{B}_n$. We define for $p \in [1, \infty)$ the seminorm*

$$\|u\|_{L^p(\Omega)} := \left(\int_\Omega |u(x)|^p dx \right)^{1/p}$$

and

$$\|u\|_{L^\infty(\Omega)} := \operatorname*{ess\,sup}_{x \in \Omega} |u(x)| := \inf\{\alpha \geq 0 : \mu(\{|u| > \alpha\}) = 0\}.$$

Now, for $1 \leq p \leq \infty$ we define the spaces

$$\mathcal{L}^p(\Omega) := \{u \colon \Omega \to \mathbb{R} \text{ Lebesgue measurable} \colon \|u\|_{L^p(\Omega)} < \infty\}.$$

These spaces are not normed because there exist measurable functions $u \colon \Omega \to \mathbb{R}$, $u \neq 0$, with $\|u\|_{L^p} = 0$. By the following Lemma, we define $L^p(\Omega) = \mathcal{L}^p(\Omega)/\sim$ as the space of equivalence classes of a.e. identical functions, equipped with the norm $\|\cdot\|_{L^p}$. With that, we define

$$\mathcal{L}^p_{\mathrm{loc}}(\Omega) := \{u \colon \Omega \to \mathbb{R} \text{ Lebesgue measurable} \colon u \in \mathcal{L}^p(K) \text{ for all } K \subset \Omega \text{ compact}\}$$

and set $L^p_{\mathrm{loc}}(\Omega) := \mathcal{L}^p_{\mathrm{loc}}(\Omega)/\sim$, with the equivalence relation

$$f \sim g \colon \iff \quad \|f - g\|_{L^p(\Omega)} = 0 \quad \iff f = g \quad \text{a.e.}.$$

For Lebesgue spaces, it holds the following lemma.

Lemma 2.23. *For all $u, v \in \mathcal{L}^p(\Omega)$, $p \in [1, \infty]$, we have*

$$\|u - v\|_{L^p} = 0 \quad \Leftrightarrow \quad u = v \quad \text{a.e.}$$

Theorem 2.24 (Fischer-Riesz). *The spaces $L^p(\Omega), p \in [1, \infty]$, are Banach spaces. The space $L^2(\Omega)$ is a Hilbert space with inner product*

$$(u, v)_{L^2} := \int_\Omega uv \mathrm{d}x.$$

Lemma 2.25 (Hölder inequality). *Let $\Omega \in \mathcal{B}_n$. Then for all $p \in [1, \infty]$ we have with the dual exponent $q \in [1, \infty]$ satisfying $\frac{1}{p} + \frac{1}{q} = 1$ for all $u \in L^p(\Omega)$ and $v \in L^q(\Omega)$ the Hölder inequality*

$$uv \in L^1(\Omega) \quad \text{and} \quad \|uv\|_{L^1} \leq \|u\|_{L^p}\|v\|_{L^q}.$$

Now we can characterize the dual space of L^p-spaces.

Theorem 2.26. *Let $\Omega \in \mathcal{B}_n$, $p \in [1, \infty)$ and $q \in (1, \infty]$ the dual exponent satisfying $\frac{1}{p} + \frac{1}{q} = 1$. Then the dual space $(L^p(\Omega))^*$ can be identified with $L^q(\Omega)$ by*

means of the isometric isomorphism

$$u \in L^q(\Omega) \mapsto u^* \in (L^p(\Omega))^*, \textit{where } \langle u^*, v \rangle_{(L^p)^*, L^p} := \int_\Omega u(x)v(x)\mathrm{d}x.$$

Lemma 2.27. *Let $\Omega \subset \mathbb{R}^n$ be open and $f \in L^1_{\mathrm{loc}}(\Omega)$ with*

$$\int_\Omega f(x)\varphi(x)\mathrm{d}x = 0 \quad \forall \varphi \in C^\infty_c(\Omega).$$

Then $f = 0$ a.e.

Now, we introduce the definition of weak derivatives.

Definition 2.28. *Let $\Omega \subset \mathbb{R}^n$ be open and let $u \in L^1_{\mathrm{loc}}(\Omega)$. If there exists a function $w \in L^1_{\mathrm{loc}}(\Omega)$ such that*

$$\int_\Omega w\varphi\mathrm{d}x = (-1)^{|\alpha|} \int_\Omega u D^\alpha \varphi\mathrm{d}x, \qquad \forall \varphi \in C^\infty_c(\Omega), \tag{2.1}$$

then $D^\alpha u := w$ is called the α-th weak partial derivative of u.

Remark 2.29.
   1. By Lemma 2.27, Definition 2.28 determines the weak derivative $D^\alpha u \in L^1_{\mathrm{loc}}(\Omega)$ uniquely.
   2. The weak derivative is consistent with the classical derivative.

Definition 2.30 ($C^{k,\beta}$-boundary and Lipschitz-boundary)**.** *Let $\Omega \subset \mathbb{R}^n$ be open and bounded. We say that Ω has a $C^{k,\beta}$- boundary, $k \in \mathbb{N}_0 \cup \{\infty\}, 0 \leq \beta \leq 1$, if for any $x \in \partial\Omega$ there exists $r > 0, l \in \{1, \ldots, n\}, \sigma \in \{-1, +1\}$, and a function $\gamma \in C^{k,\beta}(\mathbb{R}^{n-1})$ such that*

$$\Omega \cap B(x; r) = \{y \in B(x; r) \colon \sigma y_l < \gamma(y_1, \ldots, y_{l-1}, y_{l+1}, \ldots, y_n)\},$$

where $B(x; r)$ denotes the open ball around x with radius r. We call the $C^{0,1}-$boundary also Lipschitz-boundary.

The Gauß-Green Theorem is then the following.

Theorem 2.31 (Gauß-Green Theorem)**.** *Let $\Omega \subset \mathbb{R}^n$ be open and bounded with Lipschitz-boundary and the normal vector n exists for $x \in \partial\Omega$ a.e.. Then for*

all $u, v \in C^1(\bar{\Omega})$

$$\int_\Omega u_{x_i}(x)v(x)\mathrm{d}x = -\int_\Omega u(x)v_{x_i}(x)\mathrm{d}x + \int_{\partial\Omega} u(x)v(x)n_i(x)\mathrm{d}S(x),$$

where n_i is the i-th component of the outward normal vector.

Now, we introduce Sobolev spaces, which are subspaces $W^{k,p}(\Omega)$ of functions $u \in L^p(\Omega)$, for which the weak derivatives $D^\alpha u$, $|\alpha| \leq k$, are in $L^p(\Omega)$.

Definition 2.32 (Sobolev spaces). *Let $\Omega \subset \mathbb{R}^n$ be open. For $k \in \mathbb{N}_0, p \in [1,\infty]$, we define the Sobolev space $W^{k,p}(\Omega)$ by*

$$W^{k,p}(\Omega) = \{u \in L^p(\Omega) \colon u \text{ has weak derivatives } D^\alpha u \in L^p(\Omega) \text{ for all } |\alpha| \leq k\}$$

equipped with the norm

$$\|u\|_{W^{k,p}(\Omega)} := \left(\sum_{|\alpha|\leq k} \|D^\alpha u\|_{L^p}^p\right)^{1/p}, \quad p \in [1,\infty),$$

$$\|u\|_{W^{k,\infty}(\Omega)} := \sum_{|\alpha|\leq k} \|D^\alpha u\|_{L^\infty(\Omega)}.$$

Remark 2.33.

1. For $p = 2$ we define $H^k(\Omega) := W^{2,k}(\Omega)$. We note that $W^{0,p}(\Omega) = L^p(\Omega)$ for $p \in [1,\infty]$.

2. Weak partial derivatives will also be denoted by $u_{x_i}, u_{x_i x_j}, \ldots$.

3. For $u \in H^1(\Omega)$ we set

$$\nabla u(x) = \begin{pmatrix} u_{x_1}(x) \\ \vdots \\ u_{x_n}(x) \end{pmatrix}.$$

Further, the following density results hold.

Theorem 2.34. *Let $\Omega \subset \mathbb{R}^n$ be open. Then the following holds.*

1. *The set $C^\infty(\Omega) \cap W^{k,p}(\Omega), k \in \mathbb{N}_0, 1 \leq p < \infty$, is dense in $W^{k,p}(\Omega)$. Hence, $W^{k,p}(\Omega)$ is the completion of $\{u \in C^\infty(\Omega) \colon \|u\|_{W^{k,p}} < \infty\}$ with respect to the norm $\|\cdot\|_{W^{k,p}}$.*

2. If Ω is a bounded domain with Lipschitz-boundary then $C^\infty(\bar{\Omega})$ is dense in $W^{k,p}(\Omega), k \in \mathbb{N}_0, 1 \le p < \infty$.

Weak differentiability does not necessarily ensure continuity. We have for examples with $\Omega := B(0;1)$ and $u(x) := \|x\|^{-\beta}$ that

$$u \in W^{1,p}(\Omega) \quad \Leftrightarrow \quad \beta < \frac{n-p}{p}.$$

Theorem 2.35. *Let $\Omega \subset \mathbb{R}^n$ be open, $k \in \mathbb{N}_0$, and $p \in [1, \infty]$. Then $W^{k,p}(\Omega)$ is a Banach space. Moreover, the space $H^k(\Omega) = W^{k,2}(\Omega)$ is a Hilbert space with inner product*

$$(u,v)_{H^k(\Omega)} = \sum_{|\alpha| \le k} (D^\alpha u, D^\alpha v)_{L^2(\Omega)}.$$

Definition 2.36. *Let $\Omega \subset \mathbb{R}^n$ be open. For $k \in \mathbb{N}_0$, $p \in [1, \infty]$, we denote by*

$$W_0^{k,p}(\Omega)$$

the closure of $C_c^\infty(\Omega)$ in $W^{k,p}(\Omega)$. The space is equipped with the same norm as $W^{k,p}(\Omega)$ and is a Banach space. The space $H_0^k(\Omega) = W_0^{k,2}(\Omega)$ is a Hilbert space.

Remark 2.37. $W_0^{k,p}(\Omega)$ *contains exactly all $u \in W^{1,p}(\Omega)$ such that $D^\alpha u = 0$ for $|\alpha| \le k-1$ on $\partial\Omega$ with an appropriate interpretation of the traces $D^\alpha u|_{\partial\Omega}$.*

Theorem 2.38. *We assume that $\Omega \subset \mathbb{R}^n$ is open and bounded with Lipschitz-boundary. Then for all $p \in [1, \infty]$ there exists a unique bounded linear operator*

$$T \colon W^{1,p}(\Omega) \to L^p(\partial\Omega)$$

such that

$$Tu = u|_{\partial\Omega} \quad \forall u \in W^{1,p}(\Omega) \cap C(\overline{\Omega}).$$

Here, $\|T\|_{W^{1,p}(\Omega),L^p(\partial\Omega)}$ depends only on Ω and p. Tu is called the trace of u on $\partial\Omega$.

The semi-norm

$$|u|_{H^k(\Omega)} := \left(\sum_{|\alpha|=k} \|D^\alpha u\|_{L^2}^2 \right)^{1/2}$$

defines an equivalent norm on the Hilbert space $H_0^k(\Omega)$ and it holds Poincaré's inequality.

Theorem 2.39 (Poincaré's inequality). *Let $\Omega \subset \mathbb{R}^n$ be open and bounded. Then there exists a constant $C > 0$ with*

$$|u|_{H^k(\Omega)} \leq \|u\|_{H^k(\Omega)} \leq C|u|_{H^k(\Omega)} \qquad \forall u \in H_0^k(\Omega). \tag{2.2}$$

For the embedding of Sobolev spaces, we refer to [59, Section 1.2.2.9].

We define

$$H_0^1(\Omega) := \{v | v \in H^1(\Omega), \ v|_{\partial\Omega} = 0\}. \tag{2.3}$$

The dual space of the Hilbert space H_0^1 is denoted by $H^{-1}(\Omega)$ and characterized by the following theorem.

Theorem 2.40. *For the space $H^{-1}(\Omega)$, $\Omega \subset \mathbb{R}^n$ open, the following holds*

$$H^{-1}(\Omega) = \left\{ v \in H_0^1(\Omega) \mapsto (f^0, v)_{L^2} + \sum_{j=1}^{n}(f^j, v_x)_{L_2} : f^j \in L^2(\Omega) \right\}.$$

Furthermore, for $f \in H^{-1}(\Omega)$, it holds that

$$\|f\|_{H^{-1}} = \min \left\{ \left(\sum_{j=0}^{n} \|f^j\|_{L^2}^2 \right)^{\frac{1}{2}} : \ \langle f, v \rangle_{H^{-1}, H_0^1} \right.$$

$$\left. = (f^0, v)_{L^2} + \sum_{j=1}^{n}(f^j, v_{x_j})_{L^2}, \ f^j \in L^2(\Omega) \right\}.$$

2.1.3. Vector Functions with Curl or Divergence

We extend the $L^2(\Omega)$ inner product to vector functions of the dimension d, where $d = \{2, 3\}$. We suppose that

$$u = (u_1, u_2)^T \in (L^2(\Omega))^2 \qquad \text{or} \qquad u = (u_1, u_2, u_3)^T \in (L^2(\Omega))^3,$$

and

$$v = (v_1, v_2)^T \in (L^2(\Omega))^2 \qquad \text{or} \qquad v = (v_1, v_2, v_3)^T \in (L^2(\Omega))^3,$$

where u and v are assumed to have the same dimension. Then, the $(L^2(\Omega))^d$-inner product is then defined by

$$(u, v) = \int_\Omega \sum_{j=1}^d u_j \bar{v}_j \, \mathrm{d}x.$$

We denote the gradient, which is an operator from $C_0^\infty(\Omega)'$ to $(C_0^\infty(\Omega)')^d$ by

$$\nabla u = \begin{pmatrix} \frac{\partial u}{x_1} \\ \vdots \\ \frac{\partial u}{x_d} \end{pmatrix}.$$

In the following, we define the curl and divergence. In a domain $\Omega \subset \mathbb{R}^3$, the curl operator for three-dimensional vector functions $u \in (C_0^\infty(\Omega)')^3$ is defined by

$$\nabla \times u \stackrel{d=3}{=} \left(\frac{\partial u_3}{\partial x_2} - \frac{\partial u_2}{\partial x_3}, \frac{\partial u_1}{\partial x_3} - \frac{\partial u_3}{\partial x_1}, \frac{\partial u_2}{\partial x_1} - \frac{\partial u_1}{\partial x_2} \right)^T.$$

By applying Definition 2.28 to each component of the curl, it holds that

$$(\nabla \times u, \varphi) = (u, \nabla \times \varphi) \qquad \forall \, \varphi \in (C_0^\infty(\Omega))^3. \tag{2.4}$$

Further, in a domain $\Omega \subset \mathbb{R}^2$, the curl operator for two-dimensional vector functions $u \in (C_0^\infty(\Omega)')^2$ is a scalar and defined by

$$\nabla \times u \stackrel{d=2}{=} \frac{\partial u_2}{\partial x_1} - \frac{\partial u_1}{\partial u_2}.$$

The curl operator for a given differentiable scalar function $\varphi \in C_0^\infty(\Omega)'$ is defined by

$$\nabla \times \varphi \stackrel{d=2}{=} \left(\frac{\partial \varphi}{\partial x_2}, \frac{\partial \varphi}{\partial x_1} \right)^T.$$

To define the divergence operator in a domain $\Omega \subset \mathbb{R}^d$, let $u \in (C_0^\infty(\Omega)')^d$. The operator is defined by

$$\nabla \cdot u = \sum_{i=1}^d \frac{\partial u_i}{\partial x_i}.$$

By applying Definition 2.28 to each component of the divergence, we see that

$$(\nabla \cdot u, \varphi) = -(u, \nabla \cdot \varphi) \qquad \forall \, \varphi \in (C_0^\infty(\Omega))^d. \tag{2.5}$$

With the weak definition of the derivative, we obtain

$$\nabla \times (\nabla p) = 0 \qquad \forall \, p \in C_0^\infty(\Omega)',$$
$$\nabla \cdot (\nabla \times u) = 0 \qquad \forall \, u \in (C_0^\infty(\Omega)')^3.$$

Now, we introduce the function space $H(\text{curl}; \Omega)$ which is of central impor-
tance in the context of Maxwell's equations. First, we define the space of three-
dimensional vector functions with curl in L^2 by

$$H(\text{curl}; \Omega) := \{u | \, u \in (L^2(\Omega))^3, \nabla \times u \in (L^2(\Omega))^3\}, \tag{2.6}$$

equipped with the norm

$$\|u\|_{H(\text{curl}; \, \Omega)} = \left(\|u\|^2_{(L^2(\Omega))^3} + \|\nabla \times u\|^2_{(L^2(\Omega))^3} \right)^{\frac{1}{2}}. \tag{2.7}$$

In the two-dimensional case, we define vector functions with curl in L^2 by

$$H(\text{curl}; \Omega) := \{u | \, u \in (L^2(\Omega))^2, \, \nabla \times u \in L^2(\Omega)\}, \tag{2.8}$$

equipped with the norm

$$\|u\|_{H(\text{curl}; \, \Omega)} = \left(\|u\|^2_{(L^2(\Omega))^2} + \|\nabla \times u\|^2_{L^2(\Omega)} \right)^{\frac{1}{2}}. \tag{2.9}$$

We denote the space of functions in $H(\text{curl}; \Omega)$ with vanishing tangential trace
by

$$H_0(\text{curl}; \Omega) = \{u \in H(\text{curl}; \Omega); \, u \times n = 0 \text{ on } \partial\Omega\}. \tag{2.10}$$

For more details of this function spaces and density results, we refer to [24, 76].
In order to show the surjectivity of the div operator, we introduce the de Rham
complex,

$$\mathbb{R} \xrightarrow{\text{id}} H^1(\Omega) \xrightarrow{\nabla} H(\text{curl}; \Omega) \xrightarrow{\nabla \times} H(\text{div}; \Omega) \xrightarrow{\nabla \cdot} L_2(\Omega) \xrightarrow{0} \{0\},$$

where we refer for details as well as the definition of the $H(\text{div}; \Omega)$ space to [76].
The main property of this complex is the coincidence of ranges and kernels of

consecutive operators. We assume a bounded, simply connected domain Ω. Then the following identities hold.

$$\ker(\nabla) = \mathbb{R},$$
$$\ker(\nabla \times, H(\mathrm{curl};\,\Omega)) = \nabla H^1(\Omega),$$
$$\ker(\nabla \cdot, H(\mathrm{div};\,\Omega)) = \nabla \times H(\mathrm{curl};\,\Omega),$$
$$L_2(\Omega) = \nabla \cdot H(\mathrm{div};\,\Omega).$$

From that it follows that the div operator is surjective. It holds that

$$
\begin{aligned}
\nabla \times (\nabla w) &= 0 \qquad \forall\, w \in H^1(\Omega), \\
\nabla \cdot (\nabla \times u) &= 0 \qquad \forall\, u \in H(\mathrm{curl};\,\Omega).
\end{aligned}
\tag{2.11}
$$

2.2. Matrix Algebra

For the computation of the inverse of the deformation tensor and its derivatives, which we consider in this thesis, we introduce some basics of matrix algebra, which is stated in [45, Chapter 3]. We define the transposed of a matrix $A \in \mathbb{R}^{m \times n}$, with elements a_{ij}, by

$$A^T = (a_{ji}),$$

for $i = 1, \ldots, m$ and $j = 1, \ldots, n$. We denote that

$$A_{ij} = (a_{ij}).$$

We note that $(A^T)^T = A$. Furthermore, we call a square matrix $A \in \mathbb{R}^{n \times n}$ symmetric, if for all elements i, j

$$a_{ij} = a_{ji}.$$

Furthermore, we need the computation of the determinant of the deformation tensor for two-dimensional and three-dimensional square matrices. For a 2×2 matrix

$$
A = \begin{bmatrix} a_{11} & a_{12} \\ a_{21} & a_{22} \end{bmatrix},
$$

the corresponding determinant is defined by

$$\det(A) = a_{11}a_{22} - a_{12}a_{21}.$$

Now, let A be a 3×3 matrix

$$A = \begin{bmatrix} a_{11} & a_{12} & a_{13} \\ a_{21} & a_{22} & a_{23} \\ a_{31} & a_{32} & a_{33} \end{bmatrix}.$$

For the computation of the 3×3 matrix, we define determinants of the 2×2 submatrices, which are called minors or complementary minors of the associated element, and can be extended to $(n-1) \times (n-1)$ submatrices of an $n \times n$ matrix, for $n \geq 2$. The minor associated with the a_{ij} element is defined by

$$\det(A_{-(i)(j)}),$$

where $A_{-(i)(j)}$ denotes the submatrix that is formed from A by removing the i-th row and the j-th column. The sign corresponding to a_{ij} is $(-1)^{i+j}$.

We express the determinant in terms of determinants of submatrices as

$$\det(A) = a_{11}(-1)^{1+1} \det \left(\begin{bmatrix} a_{22} & a_{23} \\ a_{32} & a_{33} \end{bmatrix} \right)$$
$$+ a_{12}(-1)^{1+2} \det \left(\begin{bmatrix} a_{21} & a_{23} \\ a_{31} & a_{33} \end{bmatrix} \right)$$
$$+ a_{13}(-1)^{1+3} \det \left(\begin{bmatrix} a_{21} & a_{22} \\ a_{31} & a_{32} \end{bmatrix} \right).$$

By that, we define the cofactor of a_{ij} as

$$a_{(ij)} = (-1)^{i+j} \det(A_{-(i)(j)}).$$

By that, the adjugate of a matrix $A \in \mathbb{R}^{n \times n}$ is defined by

$$\mathrm{adj}(A) = (a_{(ji)}) = (a_{(ij)})^T.$$

For example, the adjugate for a 2×2 matrix is

$$\text{adj}(A) = \begin{bmatrix} a_{22} & -a_{12} \\ -a_{21} & a_{11} \end{bmatrix}.$$

For a matrix $A \in \mathbb{R}^{n \times n}$, with $n \geq 2$ and a nonzero determinant, the inverse matrix is defined by

$$A^{-1} = \frac{1}{\det(A)} \text{adj}(A).$$

Finally, let $A \in \mathbb{R}^{n \times n}$ be a nonsingular square matrix. The determinant of the inverse matrix is

$$\det(A^{-1}) = (\det(A))^{-1},$$

and so $\det(A) = 0$ if and only if A is singular.

2.3. Eigenvalue Theory

In the following, we define eigenvalues and eigenfunctions. For details, we refer to [76, Chapter 2.2.5].

Definition 2.41. *A function $u \in H$, where H is a Hilbert-space and a scalar $\lambda \in \mathbb{C}$ are respectively an eigenfunction and corresponding eigenvalue of an operator $A \colon H \to H$ if*

$$Au = \lambda u \qquad \text{and } u \neq 0.$$

For a general compact operator A, we cannot conclude that there exist eigenvalues and eigenvectors without further conditions on A. An important case in electromagnetism occurs when A is self-adjoint.

Definition 2.42. *An operator $A \colon H \to H$ is self-adjoint if*

$$(Au, v)_H = (u, Av)_H \qquad \forall \, u, v \in H.$$

We further introduce the Fredholm alternative.

Lemma 2.43 (Fredholm alternative). *Let $B \colon x \to H$ be a bounded linear operator where H is a Hilbert space. Suppose $B = I + A$, where A is a compact operator and I is the identity operator. Then either*

1. The homogeneous equation $Bu = 0$ has only the trivial solution $u = 0$ in H. In this case, for every $f \in H$, the inhomogeneous equation $Bu = f$ has a unique solution depending on f, or

2. The homogeneous equation $Bu = 0$ has exactly p linearly independent solutions for some finite integer $p > 0$.

2.4. Differentiability

In this section we introduce the different concepts of differentiability of operators in Banach spaces. For the theory of differentiability of this section, we refer to [59, 96]. First, we introduce the semi-differentiability. The limit does not need to fulfill any linearity or continuity assumptions, and the variation is only performed along a fixed positive direction.

Definition 2.44 (Semi-differentiability)**.** *Let X, Y be Banach spaces and let $D \subseteq X$ be an open subset. Then the map $F : D \to Y$ is called semi-differentiable at the point $x \in D$ if for all $h \in X$, there exists $y(x, h) \in Y$ such that*

$$\lim_{\substack{t \to 0 \\ t > 0}} \frac{F(x + th) - F(x)}{t} = dF(x, h).$$

In this case we write $F'(x)h = dF(x, h)$ to denote the semi-derivative of F at the point x with respect to the direction h. If F is semi-differentiable at every $x \in V$, where $V \subset D$ is open, then F is called semi-differentiable in V.

Remark 2.45. This concept is also known as directional differentiability. In this case we should name $F'(x)h = dF(x, h)$ the directional derivative of F in the direction h. An example of a directionally differentiable function is shown in Figure 2.1.

An extended notion of differentiability of operators between Banach spaces is given in the following. For details, we refer again to [59].

Definition 2.46 (Gâteau and Fréchet differentiability)**.** *Let $F : u \subset X \to Y$ be an operator with Banach spaces X, Y and $U \neq \emptyset$ open.*

1. *F is called Gâteau differentiable at $x \in U$ if F is directionally differentiable at x and the directional derivative $F'(x) : X \ni h \mapsto dF(x, h) \in Y$ is bounded and linear, i.e., $F'(x) \in \mathcal{L}(X, Y)$.*
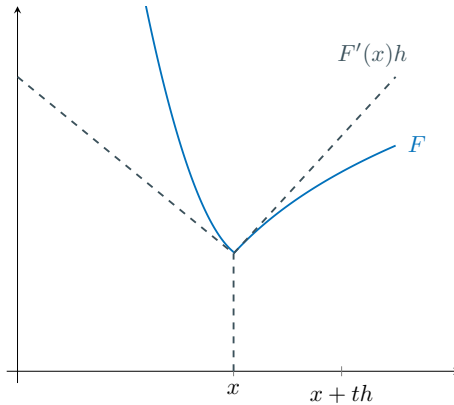
Figure 2.1. A directionally differentiable function

2. *F is called Fréchet differentiable at $x \in U$ if F is Gâteau differentiable and the following approximation condition holds:*

$$\|F(x+h) - F(x) - F'(x)h\|_Y = o(\|h\|_X) \qquad \text{for } \|h\|_X \to 0.$$

3. *If F is Gâteau/Fréchet differentiable at every $x \in V$, $V \subset U$ open, then F is called Gâteau-/Fréchet-differentiable in V.*

Further, the following rules hold.

1. For Fréchet differentiable operators the chain rule $H(x) = G(F(x))$ holds. F, G are Fréchet differentiable at x and $F(x)$, respectively. H is Fréchet differentiable at x with

$$H'(x) = G'(F(x))F'(x).$$

2. The sum rule holds for Fréchet- and Gâteaux differentials.

3. If F is Gâteaux differentiable on a neighborhood of x and F' is continuous at x then F is Fréchet differentiable at x.

4. If $F \colon X \times Y \to Z$ is Fréchet differentiable at (x, y) then $F(\cdot, y)$ and $F(x, \cdot)$ are Fréchet differentiable at x and y, respectively. These derivatives are called partial derivatives and denoted by $F_x(x, y)$ and $F_y(x, y)$, respectively. Since F is Fréchet differentiable it holds that

$$F'(x, y)(h_x, h_y) = F_x(x, y)h_x + F_y(x, y)h_y.$$

5. If F is Gâteaux differentiable in a neighborhood V of x, then for all $h \in X$ with $\{x + th : t \in [0,1]\} \subset V$, the following holds

$$\|F(x+h) - F(x)\|_Y \leq \sup_{0<t<1} \|F'(x+th)h\|_Y.$$

If $t \in [0,1] \mapsto F'(x+th)h \in Y$ is continuous, then

$$F(x+h) - F(x) = \int_0^1 F'(x+th)h \, \mathrm{d}x,$$

where the Y-valued integral is defined as a Riemann integral.

The following important theorem, see [59, Theorem 1.4.1], shows that $e(q,u) = 0$ defines a locally continuously Fréchet differentiable control-to-state map $q \mapsto u(q)$ when $e(q,u) = 0$ where $e \colon Q \times U \to Z$ is continuous Fréchet differentiable and $e_u(q,u) \in \mathcal{L}(Y,Z)$ has a bounded inverse.

Theorem 2.47 (Implicit Function Theorem). *Let X, Y, Z be Banach spaces and let $F \colon G \to Z$ be a continuously Fréchet differentiable map from an open set $G \subset X \times Y$ to Z. Let $(\overline{x}, \overline{y}) \in G$ be such that $F(\overline{x}, \overline{y}) = 0$ and that $F_y(\overline{x}, \overline{y}) \in \mathcal{L}(Y, Z)$ has a bounded inverse.*

Then there exists an open neighborhood $U_X(\overline{x}) \times U_Y(\overline{y}) \subset G$ of $(\overline{x}, \overline{y})$ and a unique continuous function $w \colon U_X(\overline{x}) \to Y$ such that

1. $w(\overline{x}) = \overline{y}$,

2. for all $x \in U_X(\overline{x})$ there exists exactly one $y \in U_Y(\overline{y})$ with $F(x, y) = 0$, namely $y = w(x)$.

Moreover, the mapping $w \colon U_X(\overline{x}) \to Y$ is continuously Fréchet differentiable with derivative

$$w'(x) = F_y(x, w(x))^{-1} F_x(x, w(x)).$$

If $F_G \to Z$ is m-times continuously Fréchet differentiable then also $w \colon U_X(\overline{x}) \to Y$ is m-times continuously Fréchet differentiable.

Definition 2.48 (Gradient). *If Q is a Banach space, we denote Q^* its dual space. The Fréchet derivative of an operator $G \colon X \to Y$ between Banach spaces is denoted by $G' \colon X \to \mathcal{L}(X, Y)$, where $\mathcal{L}(X, Y)$ are the bounded linear operators $A \colon X \to Y$. In particular, the derivative of a real-valued function $f \colon Q \to \mathbb{R}$ is denoted by $f' \colon Q \to Q^*$.*

In case of a Hilbert space Q, the gradient $\nabla_Q f \colon Q \to Q$ is the Riesz representation of f', i.e.,

$$(\nabla_Q f(w), v)_Q = \langle f'(w), v \rangle_{Q^*, Q} \qquad \forall v \in Q.$$

2.5. Reduced Problem and Adjoint Calculus

In optimization with PDE constraints, there are two common ways to formulate optimality conditions and solve the eigenvalue optimal control problem, the sensitivity approach and the approach of adjoint calculus, see [59]. In the sensitivity approach all directional derivatives have to be computed. In the context of shape optimization, problems have a large number of variables which makes this approach very costly. Thus, computing the derivatives of the reduced cost function with the adjoint approach is more efficient in computations.

In the adjoint approach for PDE optimization problems, we consider the optimization problem

$$\min_{(q,u)} J(q,u), \quad \text{s.t.} \ \ e(q,u) = 0, \quad (q,u) \in X^{\mathrm{ad}}, \tag{2.12}$$

where we define u as the state variable and q as the control variable, respectively. Further, let $X = Q \times U$. The objective function is defined as $J \colon Q \times U \to \mathbb{R}$ and the PDE constraint $e \colon Q \times U \to Z$ is an operator between Banach spaces. We call this operator the state equation. We define X^{ad} as a nonempty closed set which collects additional constraints on the control q and state u. Additionally, to compute the derivatives, we assume J and e to be continuously Fréchet-differentiable. For each $q \in Q$, we assume that the state equation $e(q,u) = 0$ admits a (locally) unique solution $u = u(q)$ with a solution operator $q \mapsto u(q)$. With the assumption that $e'_u(q, u(q)) \in \mathcal{L}(Q, U)$ is continuously invertible, the Implicit Function Theorem (2.47) ensures that $u(q)$ is continuously differentiable.

Using these assumptions, we compute the derivative $u(q)$ by differentiating the equation $e(q, u(q)) = 0$ with respect to q. From the chain rule, it follows that

$$e'_u(q, u(q)) u'(q) + e'_q(q, u(q)) = 0.$$

Inserting $u(q)$ in (2.12), we obtain the reduced problem

$$\min_q j(q) \coloneqq J(q, u(q)) \quad \text{s.t.} \ \ q \in Q^{\mathrm{ad}} \coloneqq \{ q \in Q \mid (q, u(q)) \in X^{\mathrm{ad}} \}. \tag{2.13}$$

To formulate the derivatives via adjoint calculus, we formally define the Lagrangian $\mathcal{L}: Q \times U \times Z^* \to \mathbb{R}$ of the reduced problem (2.13) by

$$\mathcal{L}(q, u, z) = J(q, u) - \langle e(q, u), z \rangle_{Z, Z^*}.$$

By the definition of $u(q)$, it holds that

$$j(q) = \mathcal{L}(q, u(q), z).$$

Further, taking $z = z(q)$, we compute the derivative $j'(q)$ as

$$j'(q) = \mathcal{L}'_q(q, u(q), z(q)) + \mathcal{L}'_u(q, u(q), z(q)) \circ u'(q) + \mathcal{L}'_z(q, u(q), z(q)) \circ z'(q).$$

Because we choose $u = u(q)$ it holds that

$$\mathcal{L}'_z(q, u(q), z(q)) = e(q, u) = 0.$$

Equivalently, we define the adjoint equation by using $z = z(q)$ to solve

$$e'_u(q, u(q), z(q)) = 0.$$

In more detail, $z = z(q)$ is the solution of the equation

$$\mathcal{L}'_u(q, u(q), z(q)) = J'_u(q, u(q)) - e'_u(q, u(q), z(q))^* z = 0.$$

With the choice of $z(q)$ it holds that

$$j'(q) = \mathcal{L}'_q(q, u(q), z(q)) = J'_q(q, u(q)) - e'_q(q, u(q))^* z(q).$$

The sign of the multiplier z is arbitrary, i.e., we could also have used the Lagrangian

$$J(q, u) + \langle e(q, u), z \rangle$$

to obtain z with the opposite sign.

The whole approach to obtain $j'(q)$ is summarized by the following three steps:

1. **The State Problem:** We solve the state problem

$$e(q, u) = 0$$

to get $u = u(q) \in U$.

2. **The Adjoint Problem:** We solve the adjoint problem

$$e_u'(q, u)^* z = J_u'(q, u)$$

to get $z = z(q) \in Z^*$.

3. **The Gradient**: After computing the state solution u and the adjoint solution z, we obtain the derivative of the reduced cost functional by computing

$$j'(q) = J_q'(q, u) - e_q'(q, u)^* z.$$

Now, utilizing standard Lagrange techniques, see, e.g., [18, 102], we compute the Q-gradient $\nabla_Q j(q)$ by inverting the Riesz isomorphism, i.e., solving

$$(\nabla_Q j(q), \delta q)_Q = j'(q)\delta q \qquad \forall \delta q \in Q.$$

In contrast to the sensitivity approach, the biggest advantage of the adjoint approach is that we do not need the operator $u'(q) \in \mathcal{L}(Q, U)$. We only require the vector $u'(q)^* J_q'(q, u(q)) \in Q^*$.

2.6. Optimality Conditions

All efficient optimization methods to solve the infinite-dimensional problem stated in (2.12) are based on first order optimality conditions (or Karush-Kuhn-Tucker (KKT) conditions), see [59]. We consider the general problem

$$\min_{q \in Q} J(q) \qquad \text{s.t.} \quad q \in Q_{\text{ad}}, \tag{2.14}$$

where Q is a Banach space, $J : Q \to \mathbb{R}$ is Gâteaux-differentiable and $Q_{\text{ad}} \subset Q$ is nonempty, closed and convex. With that, the following theorem holds.

Theorem 2.49. *Let Q be a Banach space and $Q_{\text{ad}} \subset Q$ be nonempty and convex. Furthermore, let $J : V \to \mathbb{R}$ be defined on an open neighborhood of Q_{ad}. Let $\bar{q}$ be a local solution of (2.14) at which J is Gâteaux-differentiable. Then the following optimality conditions holds:*

$$\bar{q} \in Q_{\text{ad}}, \quad \langle J'(\bar{q}), q - \bar{q} \rangle_{Q^*, Q} \geq 0 \quad \forall q \in Q_{\text{ad}}. \tag{2.15}$$

1. If J is convex on Q_{ad}, (2.15) is necessary and sufficient for global optimality.

2. If, in addition, J is strictly convex on Q_{ad}, then there exists at most one solution of (2.14), or, equivalently, of (2.15).

3. If Q if reflexive, Q_{ad} is closed and convex, and J is convex and continuous with

$$\lim_{q \in Q_{\mathrm{ad}}, \|q\|_Q \to \infty} J(q) = \infty,$$

then there exists a (global = local) solution of (2.14).

Now, we consider a general nonlinear problem of the form

$$\min_{(q,u) \in Q \times U} J(q,u) \qquad s.t. \quad e(q,u) = 0, \quad q \in Q_{\mathrm{ad}}. \tag{2.16}$$

By the Implicit Function Theorem 2.47, we ensure that the mapping $u \in V \mapsto u(q) \in U$ is continuous Fréchet differentiable with the following assumptions.

Assumption 2.50.
1. $Q_{\mathrm{ad}} \subset Q$ is nonempty, convex and closed.
2. $J \colon Q \times U \to \mathbb{R}$ and $e \colon Q \times U \to Z$ are continuously Fréchet differentiable and Q, U, Z are Banach spaces.
3. For all $q \in V$ in a neighborhood $V \subset Q$ of Q_{ad}, the state equation $e(q,u) = 0$ has a unique solution $u = u(q) \in U$.
4. $e_u'(q, u(q)) \in \mathcal{L}(U, Z)$ has a bounded inverse for all $q \in V \supset Q_{\mathrm{ad}}$.

Let Assumption 2.50 hold for (2.16). With it, we consider the reduced problem

$$\min_{q \in Q} j(q) := J(q, u(q)) \qquad s.t. \quad q \in Q_{\mathrm{ad}}, \tag{2.17}$$

where $V \ni u \mapsto u(q) \in U$ is the solution operator of the state equation. If Assumption 2.50 holds for (2.16), we can formulate the following theorem which can be proved with Theorem 2.49, see [59].

Theorem 2.51. *Let Assumption 2.50 hold. If $\bar{q}$ is a local solution of the reduced problem stated in (2.17) then $\bar{q}$ satisfies the variational inequality*

$$\bar{q} \in Q_{ad} \qquad and \qquad \langle j'(\bar{q}), q - \bar{q} \rangle_{Q^*, Q} \geq 0 \qquad \forall\, q \in Q_{\mathrm{ad}}.$$

The adjoint representative of the derivative is given by

$$j'(q) = J'_q(q, u(q)) - e'_q(q, u(q))^* z(q), \qquad (2.18)$$

where the adjoint state $z(q) \in Z^*$ solves the adjoint equation

$$e'_u(q, u(q))^* z = J'_u(q, u(q)). \qquad (2.19)$$

The Lagrangian associated with (2.16) is

$$\mathcal{L} \colon Q \times U \times Z^* \to \mathbb{R}, \qquad \mathcal{L}(q, u, z) = J(q, u) + \langle z, e(q, u) \rangle_{Z^*, Z}.$$

The representation (2.18) of $j'(q)$ yields the following corollary of Theorem 2.51.

Corollary 2.52. *Let $(\overline{q}, \overline{u})$ be an solution of (2.16) and let Assumption 2.50 hold. Then there exists an adjoint state (or Lagrange multiplier) $\overline{z} \in Z^*$ such that the following optimality conditions hold*

$$e(\overline{q}, \overline{u}) = 0, \qquad (2.20)$$
$$e_u(\overline{q}, \overline{u})^* \overline{z} = -J'_u(\overline{q}, \overline{z}), \qquad (2.21)$$
$$\overline{q} \in Q_{\mathrm{ad}}, \quad \langle J'_q(\overline{q}, \overline{u}) + e'_q(\overline{q}, \overline{u})^* \overline{z}, q - \overline{q} \rangle_{Q^*, Q} \geq 0 \quad \forall q \in Q_{\mathrm{ad}}. \qquad (2.22)$$

The optimality conditions are represented with the Lagrangian in the compact form

$$\mathcal{L}'_z(\overline{q}, \overline{u}, \overline{z}) = 0, \qquad (2.23)$$
$$\mathcal{L}'_u(\overline{q}, \overline{u}, \overline{z}) = 0, \qquad (2.24)$$
$$\overline{q} \in Q_{\mathrm{ad}}, \quad \langle \mathcal{L}'_q(\overline{q}, \overline{u}, \overline{z}), q - \overline{q} \rangle_{Q^*, Q} \geq 0, \quad \forall q \in Q_{\mathrm{ad}}. \qquad (2.25)$$

2.7. Unconstrained Optimization

For the theory of global convergence, we first introduce unconstrained optimization problem of the form

$$\min_{q \in Q} j(q),$$

where Q is a real Banach space and $j \colon Q \to \mathbb{R}$ is continuously Fréchet-differentiable. By that, the first optimality condition for a local minimum $\overline{q} \in Q$

is that $\bar{q}$ satisfies

$$j'(\bar{q}) = 0,$$

see [59, Chapter 2.2.1]. A global convergent class of methods are descent methods. The general idea is shown in Algorithm 2.1.

Algorithm 2.1 General descent method

Input: Choose initial point $q_0 \in Q$.
  For $k = 1, \ldots, k_{\max}$ **do**
    If $j'(q^k) = 0$ **then**
      STOP
    Choose a descent direction $d^k \in Q : \langle j'(q^k), d^k \rangle_{Q^*,Q} < 0$.
    Choose a step size $t_k > 0$ such that $j(q^k + t_k d^k) < j(q^k)$.
    Set $q^{k+1} := q^k + t_k d^k$.
    $k \leftarrow k + 1$.

To prove global convergence, additional requirements on the quality of the descent direction and the step sizes need to be fulfilled.

1. **Admissibility of the search directions:**

$$\frac{\langle j'(q^k), d^k \rangle_{Q^*,Q}}{\|d^k\|_Q} \overset{k \to \infty}{\longrightarrow} 0 \quad \implies \quad \|j'(q^k)\|_{Q^*} \overset{k \to \infty}{\longrightarrow} 0.$$

This means that if the slopes along the directions d^k become smaller and smaller then the steepest possible slopes have to become smaller and smaller.

2. **Admissibility of the step sizes:**

$$j(q^k + t_k d^k) < j(q^k) \qquad \forall k$$

$$\text{and} \quad j(q^k + t_k d^k) - j(q^k) \overset{k \to \infty}{\longrightarrow} 0 \quad \implies \quad \frac{\langle j'(q^k), d^k \rangle_{Q^*,Q}}{\|d^k\|_Q} \overset{k \to \infty}{\longrightarrow} 0.$$

$$(2.26)$$

This means that if the j-decreases become smaller and smaller then the slopes along the d^k have to become smaller and smaller.

With these two conditions, we can prove global convergence, see [59, Theorem 2.2].

Theorem 2.53. *Let $j \colon Q \to \mathbb{R}$ be continuously Fréchet-differentiable and $(q^k), (d^k), (t_k)$ be generated by Algorithm 2.1. We assume that (d^k) and (t_k)*

are admissible and that $(j(q^k))$ is bounded below. Then Algorithm 2.1 converges, i.e.,

$$\lim_{k \to \infty} j'(q^k) = 0.$$

To this end, there are two open questions:

- How can we check in practice if a search direction is admissible or not?
- How can we compute admissible step sizes?

For the first question is provided by the following Lemma:

Lemma 2.54. *If the search directions (d^k) satisfy the angle condition*

$$\langle j'(q^k), d^k \rangle_{Q^*,Q} \leq -\eta \|j'(q^k)\|_{Q^*} \|d^k\|_Q$$

then they are admissible.

Theory of Maxwell's Eigenvalue Problem

The aim of this chapter is to study the obtained Maxwell eigenvalue problem and it is structured as follows. In Section 3.1, we introduce Maxwell's equations [73–75]. The theory is also well discussed in the literature, see, e.g., [60, 76]. We establish the time-harmonic formulation of Maxwell's equations which describe the electromagnetic field in RF cavities. For further literature on the time-harmonic case, we refer to [65]. Additionally, for the concrete context of the theory of electromagnetic fields in RF cavities, we refer to [23, 36, 46, 76].

In order to control the change of the domain, we introduce a domain mapping in Section 3.2. The mapping bases on the method of mappings, which was mainly introduced in [79, 80], and on kinematic statements from continuum mechanics. In the theory of continuum mechanics, a material body can be identified with different parts of space at different moments in time, and is simultaneously the carrier of the physical process, see [53]. For the domain mapping, we refer to [68]. The method of mappings is also well known in the context of shape optimization and shape derivatives. It is suitable for deriving rigorous Fréchet derivatives with respect to shape-variations. For example, in [42] the method of mappings is used to derive properties of Fréchet differentiability of the state as well as for an object function w.r.t. domain variations in context of Navier-Stokes problems. Besides the domain mapping, we introduce the mapping of the function spaces of H^1 in Section 3.2.1, and of $H(\text{curl})$ in Section 3.2.2. By that, we ensure that the transformed functions have an appropriate and well-defined gradient, curl and divergence. For the details and specific properties of the function spaces, we refer

to [35,76]. We apply the introduced mapping on the Maxwell eigenvalue problem and show the domain dependent formulation in Section 3.2.3. Furthermore, we calculate the Fréchet derivatives of the functions concerning the domain mapping and show the derivatives of the domain depending Maxwell eigenvalue problem with respect to the displacement.

In Section 3.3, we discuss, based on [76, Chapter 4] and [23], a proper formulation of the time-harmonic Maxwell eigenvalue problem depending on a domain mapping, under which it has a unique solution. We also present the required uniqueness results, which we need for the further analysis in the two remaining sections.

3.1. Maxwell's Eigenvalue Problem

Maxwell's equations were formulated by various scientists and collected by James Clerk Maxwell to describe the phenomena of electromagnetism. The equations were published first in 1861 in [73]. Further, the final mathematical formulation of Maxwell's equations is stated in [74] and the whole summary of Maxwell's work is published in [75]. The theory of Maxwell is also well discussed in [60,76], from where we state the main aspects of this section.

The formulation in form of a system of partial differential equations (PDEs) is the following

$$\nabla \times E = -\frac{\partial B}{\partial t}, \qquad \text{(Faraday's Law)}$$

$$\nabla \times H = \frac{\partial D}{\partial t} + J, \qquad \text{(Ampere's Law)}$$

$$\nabla \cdot D = \rho, \qquad \text{(Coulomb's Law)}$$

$$\nabla \cdot B = 0, \qquad \text{(Absence of free magnetic poles)}$$

where E describes the electric field, D the electric displacement, H the magnetic field and B the magnetic induction. These fields arise in the presence of static electric charges, whose distribution is given by the density function ρ, and flow of electric charges, i.e., currents, described by the vector density function J. The quantities with their corresponding units are given in Table 3.1. Faraday's law gives the relation between the time variation of the magnetic induction field and the circulation of the electric field. Ampere's law defines the effect of transport and displacement currents on the circulation of the magnetic field. Coulomb's

Physical quantity	symbol	unit
Electric field	E	V/m
Magnetic field	H	A/m
Electric displacement	D	As/m^2
Magnetic induction	B	Vs/m^2
Current density	J	A/m^2
Charge density	ρ	C/m^3

Table 3.1. Table of physical quantities of Maxwell's equations

law gives the effect of the charge density on the electric displacement. The last law describes the absence of free magnetic poles. For the completeness of the system material laws relate the fields E and H with the flux quantities to D and B and the current density J, see [76].

In this thesis, we consider the domain of a particle accelerator cavity $\Omega \subset \mathbb{R}^d$, where $d = \{2, 3\}$, to be open, bounded, simply connected and Lipschitz continuous. Further, we apply linear, isotropic, non-dispersive, non-permanent-magnetic constitutive laws, which are a good approximation in many cases for high-frequency problems, i.e.,

$$B = \mu H, \quad J = \sigma E, \quad D = \varepsilon E, \tag{3.1}$$

where ε is the electric permittivity, μ the magnetic permeability and σ the conductivity. Since we consider isotropic media, these quantities are positive, bounded scalar functions of the position. Inside the cavity, we assume vacuum. The cavity walls are made of superconducting material (lossless, closed structures), where the electromagnetic fields resonate with specific eigenmodes. Additionally, we assume the cavity to be source-free, i.e., no currents are applied and no charges are present. Hence, we assume the electromagnetic field to be time-harmonic, i.e., for an angular frequency $\omega \geq 0$, we express the fields as

$$\begin{aligned}
E(r,t) &= \mathscr{R}\{E(r)\exp^{-i\omega t}\}, \\
H(r,t) &= \mathscr{R}\{H(r)\exp^{-i\omega t}\},
\end{aligned} \tag{3.2}$$

where $\mathscr{R}(\cdot)$ denotes the real part of the complex expression it is applied to. With that and (3.1), we obtain the classical formulation of Maxwell's eigenvalue problem by eliminating H: Find the wave number $k := \omega\sqrt{\mu_0\varepsilon_0} \in \mathbb{R}$ with

constants μ_0, ε_0 and $E \neq 0$ such that

$$
\begin{aligned}
\nabla \times (\nabla \times E) &= k^2 E && \text{in } \Omega, \\
\nabla \cdot E &= 0 && \text{in } \Omega, \\
E \times n &= 0 && \text{on } \partial\Omega.
\end{aligned}
\tag{3.3}
$$

The boundary condition $E \times n = 0$ is called Perfectly Electric Conducting (PEC) boundary condition where n is the outward normal to the domain of interest. It prescribes zero tangential electric field on the conducting walls.

In context of particle colliders, we are interested in the propagation or excitation of electromagnetic waves. For a given k, only certain frequencies ω will be allowed. The fields divide themselves in two distinct categories, i.e., transverse magnetic (TM) and transverse electric (TE). To achieve an acceleration of the particles, TE is unsuitable because there does not exist a electrical component in longitudinal direction, i.e., it holds $E_z = 0$ everywhere. For that reason, the field needs to be TM. In that case, it holds $B_z = 0$ everywhere and the boundary condition is $E_z|_S = 0$. In electron or proton linear accelerators, the most cavities are derived from a cylindrical or pillbox cavity. In a cylindrical geometry, it is possible to compute the TM and TE modes analytically. Here, the nomenclature of the TM$_{mnp}$ modes is defined as follows. The subscript $m \in \mathbb{N}$ is the number of full period variations in ω of the field components, $n \in \mathbb{N}$ is the number of the axial field component in the radial direction in the range $0 < r \leq R_c$, excluding $r = 0$ and where R_c is the radius of the cylinder. Further, $p \in \mathbb{N}$ is the number of half period variations in z of the fields. For details, we refer to [60, 104].

Clearly, (3.3) is an eigenvalue problem for the real eigenvalue $\lambda = k^2$. In order to numerically solve this problem, we need to formulate a variational formulation. One possible variational formulation of the problem formulation stated in (3.3) is the formulation by Kikuchi, to find an eigenvalue λ and an associated eigenvector $u \in H_0(\mathrm{curl}; \Omega)$, which is a non-trivial electric field ($u = E$) with $u \neq 0$, and $\psi \in H_0^1(\Omega)$, such that

$$
\begin{aligned}
(\nabla \times u, \nabla \times v)_\Omega + (\nabla\psi, v)_\Omega &= \lambda(u, v)_\Omega && \forall\, v \in H_0(\mathrm{curl};\, \Omega), \\
(u, \nabla\varphi)_\Omega &= 0 && \forall\, \varphi \in H_0^1(\Omega).
\end{aligned}
\tag{3.4}
$$

This formulation was introduced in 1987, see [65] and can also be found in [23]. Here, $(\cdot, \cdot)_\Omega = \int_\Omega \mathrm{d}x$ denotes the scalar product over the domain Ω.

In practice, a more common and simplified formulation of Maxwell's eigenvalue problem is to consider the symmetric variational problem of finding non-trivial pairs $u \in H_0(\mathrm{curl}; \Omega)$ and $\lambda \in \mathbb{R}$, such that

$$(\nabla \times u, \nabla \times v)_\Omega = \lambda(u, v)_\Omega \qquad \forall \, v \in H_0(\mathrm{curl}; \Omega). \tag{3.5}$$

We justify the choice of the formulation by Kikuchi (3.4) instead of the common formulation (3.5) by the aspect, that in the (3.5), the curl operator has a large null space regarding to the divergence condition

$$\nabla \cdot E = 0.$$

In (3.5), we cannot ensure that this space is removed from the $H_0(\mathrm{curl}; \Omega)$-space. In contrast, (3.4) removes the concerning null space and guarantees with the divergence constraint to get rid of these so-called spurious modes by guaranteeing that $\lambda = 0$ is no longer a permissible solution. Then, the only solution corresponding to the $\lambda = 0$ is the trivial one $E = 0$.

An alternative way is to consider (3.5) in a constructed divergence-free space by using the Helmholtz decomposition, which we will discuss in Section 3.3. Both formulations, (3.4) and the one using the Helmholtz decomposition, are similar. In the first, we enforce the divergence-free space by an additional constraint whereas we construct directly a divergence-free space in the latter.

3.2. Domain Mapping

In this section, we study kinematics which describe the motion and deformation of domains, in order to describe Maxwell's eigenvalue problem dependent on a domain mapping. For the theory of kinematics, we refer to [28, 53] and for the mapping in the function spaces H^1 and $H(\mathrm{curl})$, we refer to [76].

We introduce two different coordinate systems, namely the Lagrangian coordinates $\widehat{x}$ in a reference domain $\widehat{\Omega}$ (also known as material coordinates), and the Eulerian coordinates x in a physical (or current) domain Ω_q. Here, $q \colon \widehat{\Omega} \to \mathbb{R}^d$ describes the domain change from the reference domain to the physical domain by a deformation $\Omega_q = (\mathrm{I} + q)\,\widehat{\Omega}$, where $\widehat{\Omega}, \Omega_q \subset \mathbb{R}^d$ with $d = \{2, 3\}$. Further, I denotes the $d \times d$ identity matrix.

Definition 3.1 (Domains). *We denote*

1. $\widehat{\Omega}$: *the reference/non-deformed configuration,*
2. Ω_q: *the physical/deformed configuration.*

Furthermore, if $q = 0$, then $\widehat{\Omega} = \Omega_q$ is the reference configuration.

Remark 3.2. It is common, that problems described of solids/elasticity are usually described in the Lagrangian system. Therefore, we stay in the Lagrangian configuration.

In the following, we introduce a domain mapping, which transforms the reference domain $\widehat{\Omega}$ to the physical domain Ω_q. We assume the reference domain $\widehat{\Omega}$ to be a bounded Lipschitz domain. To map between these two domains, we introduce the displacement q by the following definition.

Definition 3.3 ((Lagrangian) Description of the displacement field). *We define the displacement q by*

$$q \colon \widehat{x} \to q(\widehat{x}) = x(\widehat{x}) - \widehat{x}. \tag{3.6}$$

It relates a particle's position in the reference configuration $\hat{x}$ to its corresponding position in the physical configuration x.

In order to define Q^{ad}, we introduce the two key quantities, which we require to study the changes of size and shape of a body. These quantities are the deformation gradient DF_q and the deformation determinant J_q. Therefore, we define the deformation.

Definition 3.4 (Deformation). *We define the transformation of a point $\widehat{x} \subset \widehat{\Omega}$ to a point $x \subset \Omega_q$ by*

$$x = \mathrm{F}_q(\widehat{x}) = q(\widehat{x}) + \widehat{x}. \tag{3.7}$$

The function $\mathrm{F}_q \colon \mathbb{R}^d \to \mathbb{R}^d$ is known as deformation. We represent the deformed configuration with $\Omega_q = \mathrm{F}_q(\widehat{\Omega})$.

We show the deformation applied on a reference domain $\widehat{\Omega}$ to a physical domain Ω_q in Figure 3.1. With that, the definition of the deformation gradient is the following.

Definition 3.5 (Deformation gradient). *Let $\hat{x}$ be a point in the reference configuration $\widehat{\Omega}$ and, let x be a point in the current configuration. Further, we assume F_q*
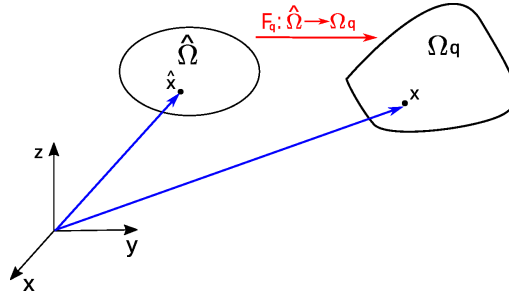
Figure 3.1. Definition of the deformation F_q.

to be differentiable. Then, we define the deformation gradient DF_q in terms of q by

$$\mathrm{DF}_q(\widehat{x}) = \widehat{\nabla}\mathrm{F}_q(\widehat{x}) = \mathrm{I} + \widehat{\nabla}q(\widehat{x}), \tag{3.8}$$

where I denotes the $d \times d$ identity matrix, i.e., $(\mathrm{DF}_q)_{ij} = \frac{\partial (\mathrm{F}_q)_i}{\partial \widehat{x}_j}$.

Moreover, we define the determinant of the deformation $\mathrm{J}_q \in \mathbb{R}$, also known as Jacobi determinant, by the following definition.

Definition 3.6 (Jacobi determinant)**.** *Let* DF_q *be a deformation gradient as defined in* (3.8)*. Then*

$$\mathrm{J}_q(\widehat{x}) = \det(\mathrm{DF}_q(\widehat{x})) \tag{3.9}$$

is the Jacobi determinant. Assuming that $\mathrm{J}_q(\widehat{x}) \neq 0$ *for all* $\widehat{x} \subset \widehat{\Omega}$*, the Jacobi determinant relates volume changes between infinitesimal reference and current domains*

$$\int_{\Omega_q} \mathrm{d}x = \int_{\widehat{\Omega}} \mathrm{J}_q \mathrm{d}\widehat{x}. \tag{3.10}$$

Remark 3.7 (Properties of DF_q and J_q)**.** The following properties for DF_q and J_q hold.

1. The determinant J_q characterizes the volume ratio.

2. We preserve the orientation of F_q with assuming $\mathrm{J}_q > \varepsilon > 0$. This assumption is a restriction to q.

3. We physically do not allow negative volumes $\mathrm{J}_q < 0$ and also not $\mathrm{J}_q = 0$. For the latter DF_q would not be invertible.

4. For $\mathrm{DF}_q = \mathrm{I}$, it follows that $\mathrm{J}_q = 1$. In this case, the domain is not deforming.

5. For $\mathrm{J}_q = 1$ with possibly $\mathrm{DF}_q \neq \mathrm{I}$, the volume does not change and a motion is called isochoric.

6. For $\mathrm{J}_q > 1$, it follows that the domain is growing and for $\mathrm{J}_q < 1$ (and $\mathrm{J}_q > 0$), it follows that the domain is shrinking.

In the following, we assume that the shapes of the domain can be described with a set of admissible transformations F_{ad} by

$$\mathcal{O}_{\mathrm{ad}} = \left\{ \mathrm{F}_q(\widehat{\Omega}) \colon \mathrm{F}_q \in F_{\mathrm{ad}} \right\}.$$

The admissible domains $\Omega_q \in \mathcal{O}_{\mathrm{ad}}$ can be interpreted as images of $\widehat{\Omega}$ under suitable transformations $\mathrm{F}_q \colon \mathbb{R}^d \to \mathbb{R}^d$. By this we tacitly assume F_{ad} to be chosen such that $\mathrm{F}_q \colon \widehat{\Omega} \to \mathrm{F}_q(\widehat{\Omega})$ is invertible and $\mathrm{F}_q(\widehat{\Omega})$ is a bounded Lipschitz domain. We require that

$$\mathrm{F}_q \in W^{1,\infty}(\widehat{\Omega})^d, \qquad\qquad \mathrm{F}_q^{-1} \in W^{1,\infty}(\mathrm{F}_q(\widehat{\Omega}))^d.$$

Since we will be working with the control q our above requirements on F_{ad} can be asserted considering a suitable admissible domain for the controls, we define

$$\begin{aligned} Q^{\mathrm{ad}} = \{ q \in W^{1,\infty}(\widehat{\Omega})^d \colon & F_q^{-1} \in W^{1,\infty}(F_q(\widehat{\Omega}))^d, \\ & \Omega_q \text{ is a bounded Lipschitz domain,} \qquad (3.11) \\ & \operatorname*{essinf}_{x \in \widehat{\Omega}} \mathrm{J}_q > \varepsilon > 0 \}. \end{aligned}$$

3.2.1. Domain Mapping of the Function Space H^1

To transform a scalar function $\widehat{p} \in H^1(\widehat{\Omega})$ to a scalar function $p \in H^1(\Omega_q)$, we consider the non-degenerate mapping

$$F_q \colon \widehat{\Omega} \to F_q(\widehat{\Omega}) = \Omega_q,$$

introduced in (3.7), with the associated Jacobian $\mathrm{DF}_q(\widehat{x})$, $\widehat{x} \in \widehat{\Omega} \subset \mathbb{R}^d$. For the scalar function $\widehat{p}$, the mapping $\mathcal{F}$ is defined by

$$p = \mathcal{F}_q(\widehat{p}) = \widehat{p} \circ F_q^{-1} \qquad (3.12)$$

which is an isomorphism from $H^1(\widehat{\Omega})$ to $H^1(\Omega_q)$ because of the bijectivity of the transformation. By applying the chain rule it holds that for a mapping of a

gradient of the function $\widehat{p}$ to p it holds that

$$\nabla p = \mathrm{DF}_q^{-T} \widehat{\nabla} \widehat{p}.$$

The same mapping approach is used in the construction of parametric H^1-conforming finite element (FE).

3.2.2. Domain Mapping of the Function Space $H(\mathbf{curl})$

For the mapping from the function space $H(\mathrm{curl}; \widehat{\Omega})$ to $H(\mathrm{curl}; \Omega_q)$, it follows from Stokes' Theorem, that tangential continuity is required. A proper mapping can be preserved by applying the so-called covariant Piola mapping. For details we refer to [31, 76] and [94].

Definition 3.8 (Covariant Piola mapping)**.** *Let $\widehat{\Omega} \subset \mathbb{R}^n$ and F_q be the non-degenerate mapping (3.7) from $\widehat{\Omega}$ onto $\Omega_q = F_q(\widehat{\Omega})$, and let $\widehat{u} \in H_0(\mathrm{curl}; \widehat{\Omega})$. The covariant Piola mapping is defined by*

$$u = \mathcal{F}_q^{\mathrm{curl}}(\widehat{u}) = \mathrm{DF}_q(\widehat{x})^{-T} \widehat{u} \circ F_q^{-1} \quad \in H(\mathrm{curl}; \Omega_q). \tag{3.13}$$

Because of the bijectivity of the transformation, the covariant Piola mapping is an isomorphism of $H(\mathrm{curl}; \widehat{\Omega})$ onto $H(\mathrm{curl}; \Omega_q)$. It preserves tangential traces and thus the tangential continuity of the $H(\mathrm{curl})$-spaces. For the curl of those functions it holds in the three-dimensional case

$$\nabla \times u \circ F_q = \mathrm{J}_q^{-1} \mathrm{DF}_q \widehat{\nabla} \times \widehat{u},$$

and in the two-dimensional case it holds

$$\nabla \times u \circ F_q = \mathrm{J}_q^{-1} \widehat{\nabla} \times \widehat{u}.$$

The same mapping approach is used in the construction of parametric $H(\mathrm{curl})$-conforming FE.

3.2.3. Maxwell's Eigenvalue Problem with Domain Mapping

Now, we apply the introduced transformation rules from the previous subsections to consider the variational formulations (3.4) and (3.5) depending on the domain mapping. By applying (3.10) for the domain integration, and (3.12)

and (3.13) for the function spaces $H_0^1(\Omega)$ and $H_0(\mathrm{curl})$, we obtain the following integration formulas. Let $\widehat{u}, \widehat{v} \in H_0(\mathrm{curl}; \widehat{\Omega})$ and $u, v \in H_0(\mathrm{curl}; \Omega_q)$, as well as $\widehat{\psi}, \widehat{\varphi} \in H_0^1(\widehat{\Omega})$ and $\psi, \varphi \in H_0^1(\Omega_q)$ be corresponding functions defined by the mappings $\mathcal{F}_q$ and $\mathcal{F}_q^{\mathrm{curl}}$, respectively. Together with the properties for the deformation gradient and the Jacobi determinant, we are able to define the following scalar products on $L^2(\widehat{\Omega})$ depending on $q \in Q^{\mathrm{ad}}$. We are able to rewrite the terms in the weak form on the reference domain. Therefore, we define for the notation for the physical domain

$$a(q; u, v) := (\nabla \times u, \nabla \times v)_{\Omega_q}, \tag{3.14}$$

$$b(q; \psi, v) := (\nabla \psi, v)_{\Omega_q}, \tag{3.15}$$

$$m(q; u, v) := (u, v)_{\Omega_q}, \tag{3.16}$$

and for the reference domain

$$\widehat{a}(q; \widehat{u}, \widehat{v}) \overset{d=2}{:=} \left(\mathrm{J}_q^{-1} \cdot \widehat{\nabla} \times \widehat{u}, \widehat{\nabla} \times \widehat{v} \right)_{\widehat{\Omega}}, \tag{3.17}$$

$$\widehat{a}(q; \widehat{u}, \widehat{v}) \overset{d=3}{:=} \left(\mathrm{J}_q^{-1} \cdot \mathrm{DF}_q \widehat{\nabla} \times \widehat{u}, \mathrm{DF}_q \widehat{\nabla} \times \widehat{v} \right)_{\widehat{\Omega}}, \tag{3.18}$$

$$\widehat{b}(q; \widehat{\psi}, \widehat{v}) := \left(\mathrm{J}_q \cdot \mathrm{DF}_q^{-T} \widehat{\nabla} \widehat{\psi}, \mathrm{DF}_q^{-T} \widehat{v} \right)_{\widehat{\Omega}}, \tag{3.19}$$

$$\widehat{m}(q; \widehat{u}, \widehat{v}) := \left(\mathrm{J}_q \cdot \mathrm{DF}_q^{-T} \widehat{u}, \mathrm{DF}_q^{-T} \widehat{v} \right)_{\widehat{\Omega}}, \tag{3.20}$$

where we differentiate for the curl-equation between the two-dimensional case (3.17), and the three-dimensional case (3.18). We see directly the equivalence between (3.14) and (3.17) by considering the weak form of the two-dimensional curl-curl equation, i.e.,

$$(\nabla \times u, \nabla \times v)_{\Omega_q} \overset{d=2}{=} \int_{\Omega_q} (\nabla \times u, \nabla \times v) \, \mathrm{d}x$$

$$= \int_{\widehat{\Omega}} \mathrm{J}_q \left(\mathrm{J}_q^{-1} \widehat{\nabla} \times \widehat{u}, \mathrm{J}_q^{-1} \widehat{\nabla} \times \widehat{v} \right) \mathrm{d}\widehat{x}$$

$$= \int_{\widehat{\Omega}} \mathrm{J}_q^{-1} \left(\widehat{\nabla} \times \widehat{u}, \widehat{\nabla} \times \widehat{v} \right) \mathrm{d}\widehat{x}$$

$$= \left(\mathrm{J}_q^{-1} \cdot \widehat{\nabla} \times \widehat{u}, \widehat{\nabla} \times \widehat{v} \right)_{\widehat{\Omega}}.$$

For three-dimensional problems, it holds equivalence between (3.14) and (3.18). The weak form is

$$
\begin{aligned}
(\nabla \times u, \nabla \times v)_{\Omega_q} \overset{d=3}{=}& \int_{\Omega_q} (\nabla \times u, \nabla \times v)\,\mathrm{d}x \\
=& \int_{\widehat{\Omega}} \mathrm{J}_q \left(\mathrm{J}_q^{-1}\,\mathrm{DF}_q\,\widehat{\nabla} \times \widehat{u}, \mathrm{J}_q^{-1}\,\mathrm{DF}_q\,\widehat{\nabla} \times \widehat{v} \right)\mathrm{d}\widehat{x} \\
=& \int_{\widehat{\Omega}} \mathrm{J}_q^{-1} \left(\mathrm{DF}_q\,\widehat{\nabla} \times \widehat{u}, \mathrm{DF}_q\,\widehat{\nabla} \times \widehat{v} \right)\mathrm{d}\widehat{x} \\
=& \left(\mathrm{J}_q^{-1} \cdot \mathrm{DF}_q\,\widehat{\nabla} \times \widehat{u}, \mathrm{DF}_q\,\widehat{\nabla} \times \widehat{v} \right)_{\widehat{\Omega}}.
\end{aligned}
$$

For the integration over the variational form of the divergence-free constraint, we consider equivalence between (3.15) and (3.19), i.e.,

$$
\begin{aligned}
(\nabla \psi, v)_{\Omega_q} =& \int_{\Omega_q} (\nabla \psi, v)\,\mathrm{d}x \\
=& \int_{\widehat{\Omega}} \mathrm{J}_q \left(\mathrm{DF}_q^{-T}\widehat{\nabla}\widehat{\psi}, \mathrm{DF}_q^{-T}\,\widehat{v} \right)\mathrm{d}\widehat{x} \\
=& \left(\mathrm{J}_q \cdot \mathrm{DF}_q^{-T}\widehat{\nabla}\widehat{\psi}, \mathrm{DF}_q^{-T}\,\widehat{v} \right)_{\widehat{\Omega}}.
\end{aligned}
$$

Finally, for the right-hand side of the variational formulation, we receive the equivalence of (3.16) and (3.20), i.e.,

$$
\begin{aligned}
(u, v)_{\Omega_q} =& \int_{\Omega_q} (u, v)\,\mathrm{d}x \\
=& \int_{\widehat{\Omega}} \mathrm{J}_q \left(\mathrm{DF}_q^{-T}\,\widehat{u}, \mathrm{DF}_q^{-T}\,\widehat{v} \right)\mathrm{d}\widehat{x} \\
=& \left(\mathrm{J}_q \cdot \mathrm{DF}_q^{-T}\,\widehat{u}, \mathrm{DF}_q^{-T}\,\widehat{v} \right)_{\widehat{\Omega}}.
\end{aligned}
$$

The induced norm on $L^2(\Omega_q)$ is

$$
\|u\|_{L^2(\Omega_q)} = \sqrt{(u, u)_{\Omega_q}}. \tag{3.21}
$$

We recall that the variational formulations of Maxwell's eigenvalue problem, i.e., (3.4) and (3.5), are

$$
\begin{aligned}
(\nabla \times u, \nabla \times v)_{\Omega_q} + (\nabla \psi, v)_{\Omega_q} &= \lambda(u, v)_{\Omega_q} \quad \forall\, v \in H_0(\mathrm{curl};\, \Omega_q), \\
(u, \nabla \varphi)_{\Omega_q} &= 0 \qquad\qquad \forall\, \varphi \in H_0^1(\Omega_q),
\end{aligned} \tag{3.22}
$$

and,

$$(\nabla \times u, \nabla \times v)_{\Omega_q} = \lambda(u,v)_{\Omega_q} \qquad \forall\, v \in H_0(\text{curl}; \Omega_q), \tag{3.23}$$

on the physical domain Ω_q. Or, in short form, with

$$k(q; u, \psi, v, \varphi) := a(q; u, v) + b(q; \psi, v) + b(q; \varphi, u),$$

we obtain for (3.22)

$$k(q; u, \psi, v, \varphi) = \lambda m(q; u, v) \quad \forall\, v \in H_0(\text{curl}; \Omega_q), \tag{3.24}$$

and for (3.23)

$$a(q; u, v) = \lambda m(q; u, v) \qquad \forall\, v \in H_0(\text{curl}; \Omega_q). \tag{3.25}$$

By the previously discussed transformations, (3.24) is, together with

$$\widehat{k}(q; \widehat{u}, \widehat{\psi}, \widehat{v}, \widehat{\varphi}) := \widehat{a}(q; \widehat{u}, \widehat{v}) + \widehat{b}(q; \widehat{\psi}, \widehat{v}) + \widehat{b}(q; \widehat{\varphi}, \widehat{u}),$$

equivalent to

$$\widehat{k}(q; \widehat{u}, \widehat{\psi}, \widehat{v}, \widehat{\varphi}) = \lambda \widehat{m}(q; \widehat{u}, \widehat{v}) \tag{3.26}$$

and (3.25) is equivalent to

$$\widehat{a}(q; \widehat{u}, \widehat{v}) = \lambda \widehat{m}(q; \widehat{u}, \widehat{v}), \tag{3.27}$$

for all $\widehat{v} \in H_0(\text{curl}; \widehat{\Omega})$ and for all $\widehat{\varphi} \in H_0^1(\widehat{\Omega})$, with $\widehat{u} = (\mathcal{F}_q^{\text{curl}})^{-1}(u)$, where $\widehat{u} \in H_0(\text{curl}; \widehat{\Omega})$, and $\widehat{\psi} = \mathcal{F}_q^{-1}(\psi)$, with $\widehat{\psi} \in H_0^1(\widehat{\Omega})$. Conversely, also finding $\widehat{u}, \widehat{\psi}$ of (3.26) and (3.27) is equivalent to finding $u = \mathcal{F}_q^{\text{curl}}(\widehat{u})$, where $\widehat{u} \in H_0(\text{curl}; \widehat{\Omega})$, and $\psi = \mathcal{F}_q(\widehat{\psi})$, where $\widehat{\psi} \in H_0^1(\widehat{\Omega})$, solving (3.24) and (3.25).

3.2.4. Fréchet Differentiability of the Domain Mapping

In this section, we formulate the Fréchet derivatives of the domain mapping concerning Maxwell's eigenvalue problem. Therefore, we consider the regularity assumptions on the domain transformations which we introduced in beginning of Section 3.2. Let $\widehat{\Omega} \subset \mathbb{R}^d$ be a bounded Lipschitz domain. The admissible domain of controls is defined as in (3.11). For the case that $J_q > \varepsilon$ is small enough, we can ensure that $F_q(\widehat{\Omega})$ is a bounded Lipschitz domain and with that,

there exists a linear bounded extension operator $W^{1,\infty}(\widehat{\Omega}) \to W^{1,\infty}(\mathbb{R}^d)$ for a bounded Lipschitz domain $\widehat{\Omega}$. Taking these assumptions, we prove the Fréchet differentiability from $W^{1,\infty}(\widehat{\Omega})$ to $L^{\infty}(\widehat{\Omega})$ of all important functions concerning the domain mapping in the following lemma.

Lemma 3.9. *Let $\widehat{\Omega} \subset \mathbb{R}^d$ be a bounded Lipschitz domain and $q \in Q_{\mathrm{ad}}$. Then the functions*
$$f_1, f_4, f_5, f_6 \colon (F_{\mathrm{ad}}, \| \cdot \|_{W^{1,\infty}(\widehat{\Omega})}) \to L^{\infty}(\widehat{\Omega})^{d \times d},$$
$$f_2, f_3 \colon (F_{\mathrm{ad}}, \| \cdot \|_{W^{1,\infty}(\widehat{\Omega})}) \to L^{\infty}(\widehat{\Omega}),$$

where
$$\begin{aligned}
f_1(q) &= \mathrm{DF}_q = \widehat{\nabla} q + \mathrm{I}, \\
f_2(q) &= \mathrm{J}_q = \det(\mathrm{DF}_q), \\
f_3(q) &= (\det(\mathrm{DF}_q))^{-1}, \\
f_4(q) &= \mathrm{DF}_q^{-T}, \\
f_5(q) &= \det(\mathrm{DF}_q) \cdot \mathrm{DF}_q^{-T}, \\
f_6(q) &= (\det(\mathrm{DF}_q))^{-1} \cdot \mathrm{DF}_q,
\end{aligned}$$

are continuously Fréchet differentiable in the direction $\delta q \in Q = W^{1,\infty}(\widehat{\Omega})^d$ with the following derivatives:
$$f_1(q)' \delta q = \widehat{\nabla} \delta q,$$

For $f_2(q)$, we differentiate between the two-dimensional and the three-dimensional case. By that, we obtain for $d = 2$

$$\begin{aligned}
f_2(q)' \delta q \overset{d=2}{=} &(\mathrm{DF}_q)_{11} \cdot (\widehat{\nabla} \delta q)_{22} + (\mathrm{DF}_q)_{22} \cdot (\widehat{\nabla} \delta q)_{11} \\
&- (\mathrm{DF}_q)_{21} \cdot (\widehat{\nabla} \delta q)_{12} - (\mathrm{DF}_q)_{12} \cdot (\widehat{\nabla} \delta q)_{21},
\end{aligned}$$

and for $d = 3$

$$\begin{aligned}
f_2(q)' \delta q \overset{d=3}{=} &(\widehat{\nabla} \delta q)_{11} \cdot \det((\mathrm{DF}_q)_{-(1)(1)}) + (\mathrm{DF}_q)_{11} \cdot (\det(\mathrm{DF}_q)_{-(1)(1)})'_q \delta q \\
&+ (\widehat{\nabla} \delta q)_{12} \cdot \det((\mathrm{DF}_q)_{-(1)(2)}) + (\mathrm{DF}_q)_{12} \cdot (\det(\mathrm{DF}_q)_{-(1)(2)})'_q \delta q \\
&+ (\widehat{\nabla} \delta q)_{13} \cdot \det((\mathrm{DF}_q)_{-(1)(3)}) + (\mathrm{DF}_q)_{13} \cdot (\det(\mathrm{DF}_q)_{-(1)(3)})'_q \delta q,
\end{aligned}$$

where $(\mathrm{DF}_q)_{-(i)(j)}$ *are the minors of the deformation gradient* DF_q. *Further, we obtain the derivatives*

$$f_3(q)'\delta q = \frac{-1}{\mathrm{J}_q^2}\mathrm{J}_q'\delta q,$$

$$f_4(q)'\delta q = (\det(\mathrm{DF}_q))^{-1}\cdot \mathrm{adj}(q)'\delta q + \frac{-1}{\mathrm{J}_q^2}\mathrm{J}_q'\delta q\cdot \mathrm{adj}(q),$$

$$f_5(q)'\delta q = f_2(q)'\delta q\cdot f_4(q) + f_2(q)\cdot f_4(q)'\delta q,$$

$$f_6(q)'\delta q = \frac{-1}{\mathrm{J}_q^2}\mathrm{J}_q'\delta q\cdot \mathrm{DF}_q + (\det(\mathrm{DF}_q))^{-1}\cdot \widehat{\nabla}\delta q,$$

where for $d = 2$, *it holds for the derivative of the adjugate that*

$$\mathrm{adj}(q)'\delta q \stackrel{d=2}{=} \begin{pmatrix} (\widehat{\nabla}\delta q)_{22} & -(\widehat{\nabla}\delta q)_{12} \\ -(\widehat{\nabla}\delta q)_{21} & (\widehat{\nabla}\delta q)_{11} \end{pmatrix},$$

and for $d = 3$, *we obtain*

$$\mathrm{adj}(q)'\delta q \stackrel{d=3}{=} \begin{pmatrix} +\det((\mathrm{DF}_q)_{-(1)(1)})'\delta q & -\det((\mathrm{DF}_q)_{-(1)(2)})'\delta q & +\det((\mathrm{DF}_q)_{-(1)(3)})'\delta q \\ -\det((\mathrm{DF}_q)_{-(2)(1)})'\delta q & +\det((\mathrm{DF}_q)_{-(2)(2)})'\delta q & -\det((\mathrm{DF}_q)_{-(2)(3)})'\delta q \\ +\det((\mathrm{DF}_q)_{-(3)(1)})'\delta q & -\det((\mathrm{DF}_q)_{-(3)(2)})'\delta q & +\det((\mathrm{DF}_q)_{-(3)(3)})'\delta q \end{pmatrix}^T.$$

Proof. Since for all $q \in Q_{\mathrm{ad}}$, we have $f_2(q) > 0$ a.e.. With that, we know that $\mathrm{F}_q' = \mathrm{DF}_q$ is invertible a.e. on $\widehat{\Omega}$. The differentiability of the formula for the derivatives now follows from elementary point wise arguments. $\square$

Finally, we compute the derivatives of the domain dependent Maxwell eigenvalue problem (3.22). The derivative of $a_q'(q;(u,\psi),(z,\phi))\delta q$ is for $d = 2$

$$a_q'(q;u,z)\delta q \stackrel{d=2}{=} \int_{\widehat{\Omega}} \frac{-1}{\mathrm{J}_q^2}\mathrm{J}_q'\delta q\left(\widehat{\nabla}\times u, \widehat{\nabla}\times z\right)\mathrm{d}\widehat{x}, \qquad (3.28)$$

whereas for $d = 3$, we obtain

$$a_q'(q;u,z)\delta q \stackrel{d=3}{=} \int_{\widehat{\Omega}} \frac{-1}{\mathrm{J}_q^2}\mathrm{J}_q'\delta q\left(\mathrm{DF}_q\,\widehat{\nabla}\times u, \mathrm{DF}_q\,\widehat{\nabla}\times z\right)\mathrm{d}\widehat{x}$$

$$+ \int_{\widehat{\Omega}} \frac{1}{\mathrm{J}_q}\left(\mathrm{DF}_q'\delta q\,\widehat{\nabla}\times u, \mathrm{DF}_q\,\widehat{\nabla}\times z\right)\mathrm{d}\widehat{x} \qquad (3.29)$$

$$+ \int_{\widehat{\Omega}} \frac{1}{\mathrm{J}_q}\left(\mathrm{DF}_q\,\widehat{\nabla}\times u, \mathrm{DF}_q'\delta q\,\widehat{\nabla}\times z\right)\mathrm{d}\widehat{x}.$$

The remaining derivatives are independent of the dimension. We obtain

$$
\begin{aligned}
b_q'(q; z, \psi)\delta q = {}& \int_{\widehat{\Omega}} \mathrm{J}_q' \delta q \left(\mathrm{DF}_q^{-T} z, \mathrm{DF}_q^{-T} \widehat{\nabla}\psi \right) \mathrm{d}\widehat{x} \\
& + \int_{\widehat{\Omega}} \mathrm{J}_q \left((\mathrm{DF}_q^{-T})' \delta q \, z, \mathrm{DF}_q^{-T} \widehat{\nabla}\psi \right) \mathrm{d}\widehat{x} \\
& + \int_{\widehat{\Omega}} \mathrm{J}_q \left(\mathrm{DF}_q^{-T} z, (\mathrm{DF}_q^{-T})_q' \delta q \, \widehat{\nabla}\psi \right) \mathrm{d}\widehat{x},
\end{aligned}
\tag{3.30}
$$

and

$$
\begin{aligned}
m_q'(q; u, z)\delta q = {}& \int_{\widehat{\Omega}} \mathrm{J}_q' \delta q \cdot (\mathrm{DF}_q^{-T} u, \mathrm{DF}_q^{-T} z)\mathrm{d}\widehat{x} \\
& + \int_{\widehat{\Omega}} \mathrm{J}_q \cdot ((\mathrm{DF}_q^{-T})_q' \delta q \, u, \mathrm{DF}_q^{-T} z)\mathrm{d}\widehat{x} \\
& + \int_{\widehat{\Omega}} \mathrm{J}_q \cdot (\mathrm{DF}_q^{-T} u, (\mathrm{DF}_q^{-T})_q' \delta q \, z)\mathrm{d}\widehat{x}.
\end{aligned}
\tag{3.31}
$$

3.3. Existence of Eigenvalues and associated Eigenfunctions

In this section, we discuss the existence and properties of eigenvalues and eigenfunctions of the Maxwell eigenvalue problem in a cavity domain Ω_q. This is already well discussed in [76, Chapter 4.7], and we summarize the main results to get a better understanding of the problem.

First, we introduce a suitable function space to guarantee divergence-free solutions of (3.3). Therefore, we consider the same assumptions made in Section 3.1, i.e., we assume a bounded, simply connected Lipschitz domain and a current density of $J = 0$ in the cavity resonator. Additionally, we assume that the electric field u is a real-valued function and the parameters $\mu = \mu_0$, $\varepsilon = \varepsilon_0$ are real-valued constants. We assume that $H_0(\mathrm{curl}; \Omega_q)$ be a real Hilbert space. Hence, all further functions we deal with are real-valued and all constants will be real. Moreover, we apply the domain mapping, which we introduced in Section 3.2. With that, we try to solve the problem of finding $u \in H_0(\mathrm{curl}; \Omega_q)$ such that

$$
(\nabla \times u, \nabla \times v)_{\Omega_q} - \lambda(u, v)_{\Omega_q} = (F, v)_{\Omega_q} \qquad \forall\, v \in H_0(\mathrm{curl}; \Omega_q). \tag{3.32}
$$

We call values for λ, which do not have a unique solution, cavity eigenvalues (or resonances) of Ω_q. By computing these eigenvalues, we consider, equivalent

to (3.23), the following problem formulation

$$(\nabla \times u, \nabla \times v)_{\Omega_q} = \lambda(u, v)_{\Omega_q} \qquad \forall\, v \in H_0(\text{curl}; \Omega_q), \qquad (3.33)$$

to find non-trivial pairs $u \in H_0(\text{curl}; \Omega_q)$ and $\lambda \in \mathbb{R}$. For the analysis of this problem, we introduce the Helmholtz decomposition.

Lemma 3.10 (Helmholtz decomposition). *The space $\nabla H_0^1(\Omega_q)$ is a closed subspace of $H_0(curl; \Omega_q)$, and we may write*

$$H_0(curl; \Omega_q) = X_0^q \oplus \nabla H_0^1(\Omega_q),$$

where

$$X_0^q = \{u \in H_0(curl; \Omega_q) | (u, \nabla\psi)_{\Omega_q} = 0 \quad \forall\, \psi \in H_0^1(\Omega_q)\}. \qquad (3.34)$$

By using the Helmholtz decomposition, it is possible to write any solution of the problem stated in (3.33) as

$$u = u_0 + \nabla\psi, \qquad \text{where } u_0 \in X_0^q, \ \psi \in H_0^1(\Omega_q).$$

By choosing $v = \nabla\varphi$ in (3.33), and noting that $\nabla \times (\nabla\varphi) = 0$, see (2.11), it holds for all $\varphi \in H_0^1(\Omega_q)$ that

$$\lambda(\nabla\psi, \nabla\varphi)_{\Omega_q} = 0 \qquad \forall\, \varphi \in H_0^1(\Omega_q).$$

This equation is true if either $\lambda = 0$ or $(\nabla\psi, \nabla\varphi)_{\Omega_q} = 0$. In case that $\lambda \neq 0$ and with choosing $\varphi = \psi$, we see that $\nabla\psi = 0$. By vanishing Dirichlet boundary conditions, we have that $\psi = 0$. In case that $\lambda = 0$, we get from (3.33) that $u_0 \in X_0^q$ satisfies

$$(\nabla \times u_0, \nabla \times v)_{\Omega_q} = 0 \qquad \forall\, v \in X_0^q.$$

Remark 3.11. Drawback of this formulation is that the divergence-free condition contained in the definition of X_0^q is in general difficult to implement. This is well discussed, e.g., in [65]. For that reason, we use the mixed formulation (3.22) for the implementation.

We mention here, regarding an outlook to future analysis of this problem, that the space X_0^q, defined in (3.34), has useful properties. It has a compact embedding into $(L^2(\Omega_q))^3$, see [106], and, because of this compactness property, there exists the following Friedrichs inequality, see [76, Corollary 4.8].

Corollary 3.12 (Friedrichs inequality). *Suppose that Ω_q is a bounded, simply connected, Lipschitz domain with boundary $\partial\Omega_q$. Then there is a constant C such that for every $u \in X_0^q$*

$$\|u\|_{(L^2(\Omega_q))^d} \leq C \left(\|\nabla \times u\|_{(L^2(\Omega_q))^N} \right) \tag{3.35}$$

for $N = 1$ if $d = 2$ and $N = 3$ for $d = 3$.

This inequality shows, that the curl-curl bilinear form is coercive on X_0^q. Further, it is proved that this space removes the null-space of the curl from $H_0(\text{curl}; \Omega_q)$. We know that the solution $\lambda = 0$ of (3.33) has an infinite multiplicity. The corresponding eigenfunctions are $u_0 = \nabla\psi$ for $\psi \in H_0^1(\Omega_q)$ and are called spurious modes. These eigenfunctions are physically not relevant. Thus any scheme for using (3.33) to compute resonances must be able to identify the eigenfunctions corresponding to $\lambda = 0$ and either only compute those for $\lambda \neq 0$ or else compute all eigenpairs for (3.33) and reject those for $\lambda = 0$. To obtain only physical solutions of problem stated in (3.33), we can assume that $\lambda \neq 0$ and we see that (3.33) may be written as either the mixed formulation by Kikuchi (3.22), i.e.,

$$(\nabla \times u, \nabla \times v)_{\Omega_q} + (\nabla\psi, v)_{\Omega_q} = \lambda(u,v)_{\Omega_q} \quad \forall\, v \in H_0(\text{curl}; \Omega_q),$$
$$(u, \nabla\varphi)_{\Omega_q} = 0 \qquad \forall\, \varphi \in H_0^1(\Omega_q),$$

or as the problem of finding $u_0 \in X_0^q$, $u_0 \neq 0$, and $\lambda \in \mathbb{R}$, such that

$$(\nabla \times u_0, \nabla \times v)_{\Omega_q} = \lambda\,(u_0, v)_{\Omega_q} \qquad \forall\, v \in X_0^q. \tag{3.36}$$

By choosing $v = u_0$ and applying the Friedrichs inequality (3.35), it holds

$$\lambda = \frac{(\nabla \times u_0, \nabla \times u_0)_{\Omega_q}}{(u_0, u_0)_{\Omega_q}} > 0.$$

With that, the following existence results of eigenvalues and eigenfunctions of the problem stated in (3.33) and their properties hold. For details, we refer to [76, Theorem 4.18]. By that, we define the eigenvalues and eigenfunctions of the problem stated in (3.36), where Q^{ad} is the space we defined in Section 3.2.

Definition 3.13 (Definition of eigenvalues and eigenfunctions for Maxwell's eigenvalue problem stated in (3.36))**.** *Let* $q \in Q^{\mathrm{ad}}$ *be arbitrary. Then* λ *is called an eigenvalue of the state equation* (3.36) *if there exists a nontrivial weak solution* u *to the system stated in* (3.36)*, i.e.,* $0 \neq u \in X_0^q$ *and it holds that*

$$(\nabla \times u, \nabla \times v)_{\Omega_q} = \lambda(u, v)_{\Omega_q} \quad \forall\, v \in X_0^q \tag{3.37}$$

In this case, the function u *is called an eigenfunction to the eigenvalue* λ*.*

For the solutions of (3.37), we obtain the following properties.

Theorem 3.14 (Existence and properties of eigenvalues and eigenfunctions for Maxwell's eigenvalue problem)**.** *Let* $q \in Q^{\mathrm{ad}}$ *be arbitrary. The solutions of the eigenvalue problem stated in* (3.37) *have the following properties:*

1. *Corresponding to the eigenvalue* $\lambda = 0$ *there is an infinite family of eigenfunctions* $u = \nabla p$ *for any* $p \in H_0^1(\Omega_q)$*.*
2. *There is an infinite discrete set of eigenvalues* λ_j*,* $j = 0, 1, 2, \ldots$ *and corresponding* $u_j \in X_0^q, u_j \neq 0$*, such that*
   a) *Equation* (3.33) *is satisfied*
   b) $0 < \lambda_0 \leq \lambda_1, \leq \ldots$,
   c) $\lim_{j \to \infty} \lambda_j = \infty$,
   d) u_j *is orthogonal to* u_l *in the inner product* $(\cdot; \cdot)_{L^2(\Omega_q)}$ *if* $j \neq l$*.*

Proof. See [76, Theorem 4.18].

$\square$

Optimization of Eigenvalue Problems

In this chapter, we consider an eigenvalue optimization problem in context of time-harmonic Maxwell's equations. In Section 4.1, we use adjoint calculus, which we introduced in Section 2.5 for PDE optimization problems, to obtain derivatives of the reduced eigenvalue optimization problem. The approach of adjoint calculus was already applied for specific eigenvalue optimization problems, such as in application of micro structures, see [101], and for elliptic eigenvalue problems, see [58, 92]. The author introduced this approach for Maxwell's eigenvalue problems in [57] and shows the details in the following section, which is divided in two parts. In Section 4.1.1, we formulate the adjoint calculus for a general eigenvalue optimization problem. Then, in Section 4.1.2, we apply this approach to the specific optimization problem constrained by the time-harmonic Maxwell eigenvalue problem.

In Section 4.2, we introduce optimality conditions and two optimization methods in order to solve reduced optimization problems. In Section 4.2.1, we discuss the reduced gradient method, where we refer for details to [40, 84]. In order to obtain better convergence, we introduce a damped inverse Broyden–Fletcher–Goldfarb–Shanno (BFGS) method in Section 4.2.2. For the classical BFGS, we refer to [40, 84, 103] and for the damping, we refer to [89]. We conclude this section by applying these methods to eigenvalue optimization problems in Section 4.2.3.

In Section 4.3, we discuss the discretization of Maxwell's eigenvalue problem. We explain the choice for Mixed FEM using Nédélec elements for the discretization of the electric field, based on a discussion seen in [9]. By that, we justify why we take the divergence-free constraint into account. Afterwards, we shortly introduce the FEM with the Lagrange, see Section 4.3.1, as well as the Nédélec elements, see Section 4.3.2 and show the matrix formulation of the problem, see Section 4.3.3. For the FE in context of Maxwell's equations, we refer to [24, 76]. We conclude this section by explaining some implementation details in Section 4.3.4. Here we introduce the usage of the library `deal.II` and its hurdles with Mixed Finite Elements as well as saddle point problems and the eigenvalue solver library `SLEPc` which we use for solving this kind of problems.

In Section 4.4, we conclude this chapter by showing the functionality of the introduced optimization methods on numerical examples. We compare the introduced optimization methods on two computational domains. First, we obtain a freeform optimization on a rectangle with free boundaries, see Section 4.4.1. Second, we optimize a domain of a quarter circle with fixed edges, see Section 4.4.2. In both settings, we optimize the first eigenvalue of Maxwell's eigenvalue problem to a certain target value. We show mesh independent convergence of the optimization methods. Further, we compare the solutions regarding iteration steps and accuracy. Moreover, we discuss the influence on the choice of regularization parameters concerning the optimal shape. We conclude this section by a conclusion of the numerical results in Section 4.4.3.

4.1. Adjoint Calculus

In this section, we apply the theory of adjoint calculus for PDE constraint optimization, which we introduced in Section 2.5, to eigenvalue optimization problems in order to obtain derivatives of the reduced problem and formulate optimality conditions. Therefore, we consider the general eigenvalue optimization problem in Section 4.1.1 and the concrete time-harmonic Maxwell eigenvalue problem in Section 4.1.2.

4.1.1. Adjoint Calculus for General Eigenvalue Problems

Let $X^{\mathrm{ad}} \subset X \coloneqq Q^{\mathrm{ad}} \times \mathbb{R} \times \mathbf{U}$ be a non-empty closed set, which collects additional constraints on the control q. Here Q^{ad} is the set of admissible con-

trols and $\mathbf{U}$ is the space of eigenfunctions. In the example considered in Section 4.1.2, it is $\mathbf{U} = H_0(\mathrm{curl}; \Omega_q) \times H_0^1(\Omega_q)$ and functions can be decomposed as $\mathbf{u} = (u, \psi)$ and $\delta\mathbf{u} = (\delta u, \delta\psi)$. We select an appropriate eigenvalue and consider the generalized eigenvalue optimization problem

$$
\begin{aligned}
\min \quad & J(q; \lambda) \\
\text{s.t.} \quad & k(q; \mathbf{u}, \delta\mathbf{u}) = \lambda\, m(q; \mathbf{u}, \delta\mathbf{u}) && \forall\, \delta\mathbf{u} \in \mathbf{U}, \\
& (m(q; \mathbf{u}, \mathbf{u}) - 1)\, \delta\lambda = 0 && \forall\, \delta\lambda \in \mathbb{R}, \\
& (q, \lambda, \mathbf{u}) \in X^{\mathrm{ad}}.
\end{aligned}
\tag{4.1}
$$

We assume the cost functional $J \colon Q \times \mathbb{R} \to \mathbb{R}$ to be continuously Fréchet-differentiable on $Q^{\mathrm{ad}} \times \mathbb{R}$ and the forms $k, m \colon Q \times \mathbf{U} \times \mathbf{U} \to \mathbb{R}$ are linear in the second and third argument. Moreover, m is assumed to be symmetric with respect to the last two arguments. Further, they are both differentiable on $Q^{\mathrm{ad}} \times \mathbf{U} \times \mathbf{U}$. Here, differentiability on Q^{ad} is to be understood in terms of sufficiently regular perturbations $\delta q \in \widetilde{Q}$ such that smallness of δq implies that the forms k, m remain well-defined.

For each $q \in Q^{\mathrm{ad}}$, we assume that the eigenvalue problem $k(q, u) = \lambda\, m(q, u)$ admits a sequence $\lambda_0 \leq \lambda_1 \leq \ldots$ of real eigenvalues. To apply adjoint calculus, we assume that, after normalization, the selected eigenvalue is simple. By that, it follows that the eigenvalue and eigenfunction pair $(\lambda, \mathbf{u})$ is locally unique. The selection rule, e.g., $\lambda = \lambda_0$ is understood implicitly defining a solution operator

$$
S \colon Q^{\mathrm{ad}} \to \mathbb{R} \times \mathbf{U}
$$

by defining

$$
q \mapsto S(q) = (\lambda(q), \mathbf{u}(q)) = (\lambda, \mathbf{u})
$$

to be the particularly chosen eigenvalue-eigenfunction pair. With the help of the solution operator, we define the reduced problem

$$
\begin{aligned}
\min_{q \in Q}\, & j(q) := J(q, \lambda(q), \mathbf{u}(q)) \\
\text{s.t.} \quad & q \in Q^{\mathrm{ad}} := \left\{ q \in Q \,|\, (q, \lambda(q), \mathbf{u}(q)) \in X^{\mathrm{ad}} \right\}.
\end{aligned}
\tag{4.2}
$$

We can now utilize standard Lagrange techniques, see, e.g., [18, 102], to obtain a representation of the derivative $j'(q) \in Q^*$ and the Q-gradient $\nabla_Q j(q) \in Q$. To

this end, we introduce the Lagrangian

$$\mathcal{L} : Q^{\mathrm{ad}} \times (\mathbb{R} \times \mathbf{U}) \times (\mathbb{R} \times \mathbf{U})$$

of problem stated in (4.2) as

$$\mathcal{L}(q, (\lambda, \mathbf{u}), (\mu, \mathbf{z})) = J(q, \lambda) - k(q; \mathbf{u}, \mathbf{z}) + \lambda \, m(q; \mathbf{u}, \mathbf{z}) + \mu \left(m(q; \mathbf{u}, \mathbf{u}) - 1 \right) \quad (4.3)$$

where the adjoint is, same as the state, a pair including

$$(\mu, \mathbf{z}) = (\mu(q), \mathbf{z}(q)) \in \mathbb{R} \times \mathbf{U},$$

with the adjoint state $\mathbf{z} \in \mathbf{U}$ and the multiplier for the normalization of the eigenfunction condition μ . To compute the derivative of the reduced cost functional, we follow the three steps described in Section 2.5:

1. **The state problem**: We recover the state equation (eigenvalue/eigenfunction) by computing the derivatives of the Lagrangian with respect to the Lagrange multipliers component-wise for all $(\delta\mu, \delta\mathbf{z}) \in \mathbb{R} \times \mathbf{U}$

$$
\begin{aligned}
0 &= \mathcal{L}'_{(\mu, \mathbf{z})}(q, (\lambda, \mathbf{u}), (\mu, \mathbf{z}))(\delta\mu, \delta\mathbf{z}) \\
&= \mathcal{L}'_{\mathbf{z}}(q, (\lambda, \mathbf{u}), (\mu, \mathbf{z}))\delta z + \mathcal{L}'_{\mu}(q, (\lambda, \mathbf{u}), (\mu, \mathbf{z}))\delta\mu,
\end{aligned}
\quad (4.4)
$$

where

$$
\begin{aligned}
\mathcal{L}'_z(q, (\lambda, \mathbf{u}), (\mu, \mathbf{z}))\delta\mathbf{z} &= -k(q; \mathbf{u}, \delta\mathbf{z}) + \lambda \, m(q; \mathbf{u}, \delta\mathbf{z}) \\
\mathcal{L}'_\mu(q, (\lambda, \mathbf{u}), (\mu, \mathbf{z}))\delta\mu &= \delta\mu \left(m(q; \mathbf{u}, \mathbf{u}) - 1 \right),
\end{aligned}
\quad (4.5)
$$

using linearity of k, m in the last argument. Thus, solving (4.4) is equivalent to solving the equations

$$k(q; \mathbf{u}, \delta\mathbf{z}) = \lambda \, m(q; \mathbf{u}, \delta\mathbf{z}), \quad (4.6)$$

$$\left(m(q; \mathbf{u}, \mathbf{u}) - 1 \right) \delta\mu = 0. \quad (4.7)$$

These equations are exactly the state eigenvalue problem (4.6) and the normalization of the concerning solution of the eigenvector (4.7). By solving these equations, we obtain the state solution of (4.2), i.e.,

$$(\lambda, \mathbf{u}) = (\lambda(q), \mathbf{u}(q)) \in \mathbb{R} \times \mathbf{U}.$$

2. **The adjoint problem**: Similar to the state problem, we obtain the adjoint state by computing the derivatives component-wise for all $(\delta\lambda, \delta\mathbf{u}) \in \mathbb{R} \times \mathbf{U}$

$$
\begin{aligned}
0 &= \mathcal{L}'_{(\lambda,\mathbf{u})}(q, (\lambda, \mathbf{u}), (\mu, \mathbf{z}))(\delta\lambda, \delta\mathbf{u}) \\
&= \mathcal{L}'_{\mathbf{u}}(q, (\lambda, \mathbf{u}), (\mu, \mathbf{z}))\,\delta\mathbf{u} + \mathcal{L}'_{\lambda}(q, (\lambda, \mathbf{u}), (\mu, \mathbf{z}))\,\delta\lambda,
\end{aligned}
\tag{4.8}
$$

with

$$
\begin{aligned}
\mathcal{L}'_{\mathbf{u}}(q, (\lambda, \mathbf{u}), (\mu, \mathbf{z}))\,\delta\mathbf{u} &= -k(q; \delta\mathbf{u}, \mathbf{z}) + \lambda m(q; \delta\mathbf{u}, \mathbf{z}) \\
&\quad - 2\mu\, m(q; \mathbf{u}, \delta\mathbf{u}), \\
\mathcal{L}'_{\lambda}(q, (\lambda, u), (\mu, z))\delta\lambda &= J'_{\lambda}(q, \lambda)\,\delta\lambda + \delta\lambda m(q; \mathbf{u}, \mathbf{z}),
\end{aligned}
$$

where we use the linearity of k, m in the last two arguments and symmetry of m. Similar to the state problem, we solve the adjoint problem stated in (4.8) by solving each equation separately, namely

$$
k(q; \delta\mathbf{u}, \mathbf{z}) + 2\mu\, m(q; \mathbf{u}, \delta\mathbf{u}) = \lambda m(q; \delta\mathbf{u}, \mathbf{z}), \tag{4.9}
$$

$$
J'_{\lambda}(q, \lambda)\,\delta\lambda = -\delta\lambda m(q; \mathbf{u}, \mathbf{z}). \tag{4.10}
$$

Setting $\mu = 0$ and considering variations in $\delta\mathbf{u}$, we see that $\mathbf{z}$ solves the adjoint eigenvalue problem

$$
k(q; \delta\mathbf{u}, \mathbf{z}) = \lambda\, m(q; \delta\mathbf{u}, \mathbf{z}) \qquad \forall\, \delta\mathbf{u} \in \mathbf{U}.
$$

Variations in $\delta\lambda$ yield a normalization of the adjoint eigenfunction

$$
m(q; \mathbf{u}, \mathbf{z}) = -J'_{\lambda}(q, \lambda).
$$

3. **The gradient**: After computing the state solution $(\lambda, \mathbf{u})$ and the adjoint solution $(\mu, \mathbf{z})$ of (4.2), we obtain the derivative for all $\delta q \in \tilde{Q}$ of the reduced cost functional by computing

$$
\begin{aligned}
j'(q)\delta q &= \mathcal{L}'_q(q; (\lambda, \mathbf{u}), (\mu, \mathbf{z}))\,\delta q \\
&= J'_q(q, \lambda)\delta q - k'_q(q; \mathbf{u}, \mathbf{z})\,\delta q + \lambda m'_q(q; \mathbf{u}, \mathbf{z})\,\delta q,
\end{aligned}
$$

taking into account that $\mu = 0$. Assuming $\tilde{Q} \subset Q$ to be dense and $j'(q)$ to be extendable to a functional on Q, and not just on $\tilde{Q}$, we can compute

the Q-gradient $\nabla_Q j(q)$ by inverting the Riesz isomorphism, i.e., solving

$$(\nabla_Q j(q), \delta q)_Q = j'(q)\delta q \qquad \forall \delta q \in Q.$$

4.1.2. Adjoint Calculus for Maxwell's Eigenvalue Problem

Similar to the adjoint calculus of the generalized eigenvalue optimization problem, which we introduced in the previous subsection, we assume the particular eigenvalue λ to be simple. By using the notations (3.14),(3.15),(3.16), we consider the optimization problem constrained by Maxwell's eigenvalue problem stated in (3.22), i.e., we want to find

$$(q, \lambda, (u, \psi)) \in Q^{\mathrm{ad}} \times \mathbb{R} \times (H_0(\mathrm{curl}; \Omega_q) \times H_0^1(\Omega_q))$$

as solution of the problem

$$
\begin{aligned}
\min \quad & J(q, \lambda) \\
\text{s.t.} \quad a(q; u, \delta u) + b(q; \delta u, \psi) &= \lambda m(q; u, \delta u) && \forall\, \delta u \in H_0(\mathrm{curl}; \Omega_q), \\
b(q; u, \delta \psi) &= 0 && \forall\, \delta \psi \in H_0^1(\Omega_q), \\
\delta \lambda \left(m(q; u, u) - 1 \right) &= 0 && \forall\, \delta \lambda \in \mathbb{R},
\end{aligned}
\tag{4.11}
$$

where the state variables $u = u(q)$ and $\psi = \psi(q)$ depend on the control q. We define the corresponding adjoint variables by

$$(\mu, (z, \phi)) \in \mathbb{R} \times (H_0(\mathrm{curl}; \Omega_q) \times H_0^1(\Omega_q)).$$

By defining the notation

$$k(q; (u, \psi), (\delta u, \delta \psi)) = a(q; u, \delta u) + b(q; \delta u, \psi) + b(q; u, \delta \psi),$$

the Lagrangian of the eigenvalue optimization problem for the admissible set Q^{ad}

$$\mathcal{L} \colon Q^{\mathrm{ad}} \times (\mathbb{R} \times (H_0(\mathrm{curl}; \Omega_q) \times H_0^1(\Omega_q))) \times (\mathbb{R} \times (H_0(\mathrm{curl}; \Omega_q) \times H_0^1(\Omega_q)))$$

of problem stated in (4.11) is

$$
\begin{aligned}
\mathcal{L}(q, (\lambda, (u, \psi)), (\mu, (z, \phi))) = {} & J(q, \lambda) - k(q; (u, \psi), (z, \phi)) + \lambda\, m(q; u, z) \\
& + \mu\left(m(q; u, u) - 1 \right).
\end{aligned}
$$

With the directions

$$
(\delta\mu, (\delta z, \delta\phi)) \in (\mathbb{R} \times (H_0(\mathrm{curl}; \Omega_q) \times H_0^1(\Omega_q))),
$$
$$
(\delta\lambda, (\delta u, \delta\psi)) \in (\mathbb{R} \times (H_0(\mathrm{curl}; \Omega_q) \times H_0^1(\Omega_q))),
$$
$$
\delta q \in Q^{\mathrm{ad}},
$$

we compute the derivative of the reduced cost functional of Maxwell's eigenvalue problem with the three steps, mentioned in Section 4.1.1.

1. **The state problem**: We solve the state problem of Maxwell's eigenvalue problem

$$
k(q; (u, \psi), (\delta z, \delta\phi)) = \lambda\, m(q; u, \delta z),
$$
$$
(m(q; u, u) - 1)\, \delta\mu = 0. \tag{4.12}
$$

   which is similar to solving Maxwell's eigenvalue problem and a normalization of the eigenvector solution u. By that, we achieve the state solution $(\lambda, (u, \psi))$.

2. **The adjoint problem**: We solve the adjoint problem of for Maxwell's eigenvalue problem by solving the following equations

$$
k(q; (\delta u, \delta\psi), (z, \phi)) + 2\mu\, m\,(q; u, \delta u) = \lambda m\,(q; \delta u, z)\,,
$$
$$
J_\lambda'(q, \lambda)\, \delta\lambda + \delta\lambda\, m\,(q; u, z) = 0.
$$

   The system has a solution for $\mu = 0$. In this case, the problem is similar to the transposed eigenvalue problem

$$
k(q; (\delta u, \delta\psi), (z, \phi)) = \lambda m\,(q; \delta u, z)\,, \tag{4.13}
$$

   with a normalization of adjoint eigenvector z dependent on the state solution (λ, u) by

$$
J_\lambda'(q, \lambda) = -m\,(q; u, z)\,. \tag{4.14}
$$

   By that, we obtain the adjoint solution $\mu, (z, \phi)$ with $\mu = 0$.

3. **The gradient**: After computing the state solution $(\lambda, (u, \psi))$ and the adjoint solution $(\mu, (z, \phi))$ of (4.11), we obtain the derivative for all $\delta q \in \tilde{Q}$ of the reduced cost functional, similar to the generalized eigenvalue opti-

mization problem, see Section 4.1.1, by computing

$$
\begin{aligned}
j'(q)\delta q &= \mathcal{L}'_q(q,(\lambda,(u,\psi)),(\mu,(z,\phi)))\,\delta q \\
&= J'_q(q,\lambda)\delta q - k'_q(q;(u,\psi),(z,\phi))\,\delta q \\
&\quad + \lambda m'_q(q;u,z)\,\delta q - \mu(m(q;u,u)-1)'_q\,\delta q,
\end{aligned}
$$

using the derivatives (3.28),(3.29), (3.30),(3.31), the notation

$$
k'_q(q;(u,\psi),(z,\phi))\,\delta q = a'_q(q;u,z)\,\delta q + b'_q(q;z,\psi)\,\delta q + b'_q(q;u,\phi)\,\delta q.
$$

Further, we take into account that $\mu = 0$ and by that, we obtain

$$
j'(q)\delta q = J'_q(q,\lambda)\delta q - k'_q(q;(u,\psi),(z,\phi))\,\delta q + \lambda m'_q(q;u,z)\,\delta q. \qquad (4.15)
$$

Assuming $\widetilde{Q} \subset Q$ to be dense and $j'(q)$ to be extendable to a functional on Q, and not just on $\widetilde{Q}$, we can compute the Q-gradient $\nabla_Q j(q)$ by inverting the Riesz isomorphism, i.e., solving

$$
(\nabla_Q j(q),\delta q)_Q = j'(q)\delta q \qquad \forall \delta q \in Q. \qquad (4.16)
$$

4.2. Optimization Methods

In this section, we introduce two optimization methods utilizing a line search strategy to solve problems of the form

$$
\min_{q \in Q} j(q), \qquad (4.17)
$$

where Q is a Hilbert space and $j \colon Q \to \mathbb{R}$ is continuously Fréchet differentiable. We define the gradient of the reduced cost functional j at q^k by using the Riesz representation, which we introduced in Theorem 2.17. With that, we want to find $\nabla_Q j(q^k) \in Q$ satisfying

$$
(\nabla_Q j(q^k),d)_Q = j'(q^k)d \quad \forall\, d \in Q. \qquad (4.18)
$$

For an optimization method with line search strategy, we compute a direction d^k and search along this direction a lower function value starting from

the current iterate q^k. This new iterate is given by

$$q^{k+1} = q^k + t_k d^k, \qquad (4.19)$$

where t_k is the step size. The convergence of a line search method depends on a good choice of the direction d^k and the step size t_k, see Section 2.7.

We establish a gradient method in Section 4.2.1, and an inverse damped BFGS method in Section 4.2.2. Both methods require the direction chosen as a descent direction

$$(\nabla_Q j(q^k), d^k)_Q \le 0.$$

The exact step size $t_k \in \mathbb{R}$ of the chosen direction can be computed by solving the minimization problem

$$t_k = \arg\min_{t>0} j(q^k + td^k). \qquad (4.20)$$

Solving the exact solution of (4.20) is often expensive and in general not necessary. With a line search, the method generates a limited number of trial step sizes until on find an approximate minimum of (4.20).

It is well-known that gradient methods are stable but really slow in runtime. To increase the performance, we introduce an inverse damped BFGS method. This is a quasi-Newton method which can have an improved convergence rate. In literature, it is shown that a damping update for the classical BFGS ensures the positive definiteness of the operator of the approximated hessian of the reduced cost functional, see, e.g., [89]. In this thesis, we show that it is also possible to apply a damping update to the inverse BFGS method to ensure convergence of the inverse method. We show that the curvature condition is fulfilled which guarantees the positive definiteness of the inverse operator, in Lemma 4.5. For the theory, we refer to [40, 84, 103], where gradient as well as Newton and quasi-Newton methods are well explained.

4.2.1. Gradient Method

In the Hilbert space setting, we can choose $Q^* = Q$ and $\langle \cdot, \cdot \rangle_{Q^*,Q} = (\cdot, \cdot)_Q$ by the Riesz Representation Theorem 2.17, according to [59, Section 2.2]. With that, it holds that $d^k = -\nabla_Q j(q^k)$ is the direction of steepest descent with

$$j'(q^k)d^k = (\nabla_Q j(q^k), d^k)_Q = -\|\nabla_Q j(q^k)\|_Q^2 \le 0.$$

Further, if $j'(q^k)d^k = 0$, it holds that $\nabla_Q j(q^k) = 0$. Thus, the necessary conditions for a minimizer are fulfilled. The steepest descent is an admissible search direction. To guarantee an admissible step size in the sence of (2.26), we consider the Armijo condition. For details, we refer to [59, Section 2.2.1.1].

Definition 4.1 (Armijo Condition). *Let d^k be a descent direction of j at q^k. Then, we choose the maximum $t_k \in \{1, \frac{1}{2}, \frac{1}{4}, \dots\}$ for which*

$$j(q^k + t_k d^k) - j(q^k) \le \gamma t_k (\nabla_Q j(q^k), d^k)_Q. \tag{4.21}$$

This condition means that the reduction in j should be proportional to both, the step length t_k and the directional derivative $\langle \nabla_Q j(q^k), d^k \rangle$. Now, we show the existence of the Armijo step sizes and admissibility of step sizes, where we refer for the proofs to [59, Lemma 2.2. and Lemma 2.3].

Lemma 4.2. *Let j' be uniformly continuous on*

$$N_0^\rho = \{q + d \colon j(q) \le j(q^0), \|d\|_Q \le \rho\}$$

for some $\rho > 0$. Then, for every $\varepsilon > 0$, there exists $\delta > 0$ such that for all $q^k \in Q$ with $j(q^k) \le j(q^0)$ and all $d^k \in Q$ that satisfy

$$\frac{(\nabla_Q j(q^k), d^k)_Q}{\|d^k\|_Q} \le -\varepsilon,$$

there holds

$$j(q^k + td^k) - j(q^k) \le \gamma t (\nabla_Q j(q^k), d^k)_Q \qquad t \in [0, \delta/\|d^k\|_Q].$$

Lemma 4.3. *Let j' be uniformly continuous on*

$$N_0^\rho = \left\{q + d \colon j(q) \le j(q^0), \|d\|_Q \le \rho\right\}$$

for some $\rho > 0$. We consider the general descent method from Algorithm 2.1, where (t_k) is generated by the Armijo rule and the descent directions d^k are chosen such that they are not too short in the following sense:

$$\|d^k\|_Q \ge \phi\left(-\frac{(\nabla_Q j(q^k), d^k)_Q}{\|d^k\|_Q}\right), \tag{4.22}$$

where $\phi\colon [0,\infty) \to [0,\infty)$ is monotonically increasing and satisfies $\phi(t) > 0$ for all $t > 0$. Then the step sizes (t_k) are admissible.

Hence, the Armijo Condition (4.21) guarantees together with (4.22) that the step sizes (t_k) are admissible. With that, it is possibly to apply the global convergence result of Theorem 2.53. In Algorithm 4.1, we consider the gradient method, where we choose the direction of steepest descent as search direction. For the choice of step sizes, we apply the Armijo condition.

Algorithm 4.1 Gradient method

Input: Let $q^0 \in Q$ be an initial guess for the control. We choose the parameter
$k_{\max} \in \mathbb{N}$, and $\gamma \in (0, 0.5)$ for the Armijo Condition (4.21).
   For $k = 1, \ldots, k_{\max}$ **do**
     If $\nabla_Q j(q^k) = 0$ **then**
       STOP
     $d^k = -\nabla_Q\, j(q^k)$.
     Choose $t_k > 0$ with Armijo condition (4.21).
     $q^{k+1} = q^k + t_k d^k$.
     $k \leftarrow k + 1$.

4.2.2. Damped Inverse BFGS Method

Another method to solve the reduced optimization problem stated in (4.2) is a damped inverse BFGS method, which is named for its discoverers Broyden, Fletcher, Goldfarb, and Shanno and is one of the most famous quasi-Newton methods. These methods, similar to the steepest descent method, require only the gradient of the objective function which gets updated in every iteration. Quasi-Newton methods are sometimes more efficient than the classical Newton's method, because the second derivatives are not required. The computation of the second derivative is in many cases very costly or not even possibly. In contrast, quasi-Newton methods only require the gradient of the objective function which is sufficient to produce superlinear convergence. For the theory and more details to quasi-Newton methods, and specifically the BFGS method, can be found in, e.g., [84, 89, 109].

The classical Newton approximation computes the search direction by solving the problem

$$\nabla_Q^2\, j(q^k)d^k = -\nabla_Q\, j(q^k), \tag{4.23}$$

where $\nabla_Q j(q^k) \in Q$ and $\nabla_Q^2 j(q^k) \in \mathcal{L}(Q; Q)$ are the gradient and Hessian of the reduced cost functional at iteration k. Similar to finite dimensional problems, the computation of the Hessian, or the inverse Hessian to avoid its inversion in the computation step of the search direction, has a big computational effort. The idea of the inverse BFGS method is to replace the inverse Hessian by an operator $B_k \colon Q \to Q$ which approximates the inverse Hessian. However, to guarantee that the resulting directions d^k are descent directions, positivity of the operators B_k needs to be maintained. The computation step for the search direction is then given by

$$d^k = -B_k \nabla_Q j(q^k).$$

The inverse BFGS method is derived from the classical BFGS method by applying the so called Sherman-Morrison-Woodbury formula. For details, we refer to [84].

Further, equivalently to finite dimensional problems, we ensure that by updating the operator $B_{k+1} \colon Q \to Q$ fulfills the Secant Equation

$$B_{k+1}\widetilde{d}^k = y^k, \tag{4.24}$$

where $y^k = \nabla_Q j(q_{k+1}) - \nabla_Q j(q_k)$ and $\widetilde{d}^k = t_k d^k = q^{k+1} - q^k$, illustrated in Figure 4.1. The operator B_{k+1} is not uniquely determined by the secant equation.
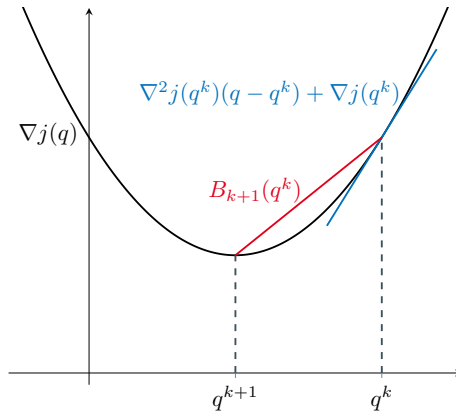
Figure 4.1. Secant equation

If $Q = \mathbb{R}^n$, one possible update formula is the inverse BFGS update for any $v \in \mathbb{R}$

$$B_{k+1}v = B_k v + \frac{(\widetilde{d}^k - B_k y^k)(\widetilde{d}^k, v) + \widetilde{d}^k(\widetilde{d}^k - B_k y^k, v)}{(\widetilde{d}^k, y^k)} - \widetilde{d}^k \frac{(\widetilde{d}^k - B_k y^k, y^k)}{(\widetilde{d}^k, y^k)^2}(\widetilde{d}^k, v),$$

(4.25)

where the operator B_k is a symmetric positive definite (spd) matrix and which will be revised or updated in every iteration. The generalized update formula for $B_{k+1} \in \mathcal{L}(Q, Q)$ to Hilbert spaces yields that for any $p \in Q$ it holds

$$(p, B_{k+1}p)_Q = (p, B_k p)_Q + \frac{(p, \widetilde{d}^k - B_k y^k)_Q (\widetilde{d}^k, p)_Q + (p, \widetilde{d}^k)_Q (\widetilde{d}^k - B_k y^k, p)_Q}{(\widetilde{d}^k, y^k)_Q} - (p, \widetilde{d}^k)_Q \frac{(\widetilde{d}^k - B_k y^k, y^k)_Q}{(\widetilde{d}^k, y^k)_Q^2}(\widetilde{d}^k, p)_Q,$$

(4.26)

where the operator B_k is spd. Similar to the finite dimensional case, this operator will be revised or updated in every iteration.

In the following, we consider the curvature condition which is necessary to guarantee that it follows from B_k is positive definite, it remains that B_{k+1} is positive definite, see [84]. This can be asserted by the curvature condition

$$\langle y^k, \widetilde{d}^k \rangle > 0.$$

(4.27)

In general, it is satisfied by using a line search procedure which fulfills the so-called Wolfe, also known as Powell-Wolfe, conditions

$$j(q^k + t_k d^k) \leq j(q^k) + \gamma t_k (\nabla_Q j(q^k), d^k)_Q$$

(4.28)

$$(\nabla_Q j(q^k + t_k d^k), d^k)_Q \geq \eta (\nabla_Q j(q^k), d^k)_Q$$

(4.29)

with parameters $0 < \gamma < \eta < 1$, see [84]. The first condition (4.28) is the Armijo Condition (4.21) which ensures a sufficient decrease of the function $j(q)$. For quasi-Newton methods, this condition is not enough to ensure a reasonable progress. It is satisfied for sufficient small values of t_k, but it does not avoid unacceptable short values of t_k. The second condition (4.29) ensures that the algorithm makes a reasonable progress. In general, the Wolfe Conditions

(4.28),(4.29) ensure the curvature condition (4.27) and the therein resulting positive definiteness of B_{k+1}.

In Remark 3.7, we introduced properties of the deformation tensor DF_q and its determinant J_q, which need to be fulfilled. In particular, to ensure that the deformation tensor stays invertible in the optimization progress, we need to ensure the positiveness of J_q. Therefore, we will later apply a barrier term in the regularization functional, i.e.,

$$-\beta \int_{\widehat{\Omega}} \ln(\mathrm{J}_q - \varepsilon),$$

with $\beta, \varepsilon > 0$, to the cost functional, see (4.35). In some cases, it happens that applying this barrier term has the consequence, that the mentioned Wolfe Conditions (4.28) and (4.29) end up with a non-feasible line search. One possibility to fix this problem and to guarantee the fulfilling of the curvature condition, is to modify the line search to ensure feasibility. An alternative is to implement a damping step which substitutes the second condition of the Wolfe Conditions (4.29) and fulfills the Curvature Condition (4.27).

That such a damping update fulfills the Curvature Condition, is already proven for the classical (non-inverse) BFGS method in finite-dimensional optimization, see, e.g., [84]. In the following, we show that a damping update fulfills the Curvature Condition also for the inverse method in infinite dimensional optimization. The damping was already introduced for an update for the Hessian approximation by [89]. Here, we show that an analogous approach can be utilized for the approximation of the inverse Hessian. Hence, we define the damping update as follows.

Definition 4.4 (Damping for inverse BFGS method). *Let B_k be given and spd. Further, let*

$$q^{k+1} = q^k + t_k d^k,$$
$$\widetilde{d}^k = t_k d^k = q^{k+1} - q^k,$$
$$and \quad y^k = \nabla_Q j(q^{k+1}) - \nabla_Q j(q^k).$$

Then the inverse BFGS damping is given by

$$\widetilde{d}^k = \theta_k \widetilde{d}^k + (1 - \theta_k) B_k y^k,$$

where $\theta_k \in \mathbb{R}$ is defined as

$$
\theta_k = \begin{cases} 1 & \text{if } (y^k, \widetilde{d}^k)_Q \geq 0.2(y^k, B_k y^k)_Q, \\[2ex] 0.8 \dfrac{(y^k, B_k y^k)_Q}{(y^k, B_k y^k)_Q - (\widetilde{d}^k, y^k)_Q} & \text{else.} \end{cases}
$$

In the following lemma, we show that the damping step ensures that positive definiteness of B_k is sufficient to assert positive definiteness of B_{k+1}.

Lemma 4.5. *Let $\widetilde{d}^k, y^k$ be given and assume that $B_0 \in \mathcal{L}(Q, Q)$ is a symmetric, positive definite operator. Then the damping of Definition 4.4 ensures that it holds that $\langle y^k, \widetilde{d}^k \rangle > 0$ for the BFGS Update (4.26). By induction B_k, and thus B_{k+1}, remains positive definite.*

Proof. First, we verify the claim, that $\langle y^k, \widetilde{d}^k \rangle > 0$ is sufficient to assert positive definiteness of B_{k+1}. The proof of this is almost analog to the finite dimensional case, see, e.g., [103]. To this end, let $p \in Q \setminus \{0\}$, then the update formula asserts

$$
(p, B_{k+1} p)_Q = (p, B_k p)_Q + \frac{(p, \widetilde{d}^k - B_k y^k)_Q (\widetilde{d}^k, p)_Q + (p, \widetilde{d}^k)_Q (\widetilde{d}^k - B_k y^k, p)_Q}{(\widetilde{d}^k, y^k)_Q}
$$
$$
- (p, \widetilde{d}^k)_Q \frac{(\widetilde{d}^k - B_k y^k, y^k)_Q}{(\widetilde{d}^k, y^k)_Q^2} (\widetilde{d}^k, p)_Q
$$

By expanding the second and third summand, it equals to

$$
= (p, B_k p)_Q + 2 \frac{(p, \widetilde{d}^k)_Q^2 - (p, B_k y^k)_Q (p, \widetilde{d}^k)_Q}{(\widetilde{d}^k, y^k)_Q}
$$
$$
- (p, \widetilde{d}^k)_Q^2 \frac{(\widetilde{d}^k, y^k)_Q - (B_k y^k, y^k)_Q}{(\widetilde{d}^k, y^k)_Q^2}
$$

Again, expanding and re-sort terms provides

$$
= (p, B_k p)_Q + \frac{(p, \widetilde{d}^k)_Q^2}{(\widetilde{d}^k, y^k)_Q}
$$
$$
- 2 \frac{(p, B_k y^k)_Q (p, \widetilde{d}^k)_Q}{(\widetilde{d}^k, y^k)_Q} + (p, \widetilde{d}^k)_Q^2 \frac{(B_k y^k, y^k)_Q}{(\widetilde{d}^k, y^k)_Q^2}
$$

By adding $\pm \frac{(B_k y^k, p)^2_Q}{(y^k, B_k y^k)_Q}$, we obtain

$$
\begin{aligned}
= (p, B_k p)_Q &+ \frac{(p, \widetilde{d}^k)^2_Q}{(\widetilde{d}^k, y^k)_Q} - \frac{(B_k y^k, p)^2_Q}{(y^k, B_k y^k)_Q} \\
&+ \frac{(B_k y^k, p)^2_Q}{(y^k, B_k y^k)_Q} - 2\frac{(p, B_k y^k)_Q (p, \widetilde{d}^k)_Q}{(\widetilde{d}^k, y^k)_Q} + (p, \widetilde{d}^k)^2_Q \frac{(B_k y^k, y^k)_Q}{(\widetilde{d}^k, y^k)^2_Q}
\end{aligned}
$$

where we consider by binomial formula

$$
\begin{aligned}
= (p, B_k p)_Q &+ \frac{(p, \widetilde{d}^k)^2_Q}{(\widetilde{d}^k, y^k)_Q} - \frac{(B_k y^k, p)^2_Q}{(y^k, B_k y^k)_Q} \\
&+ (B_k y^k, y^k)_Q \left[\frac{(B_k y^k, p)_Q}{(B_k y^k, y^k)_Q} - \frac{(p, \widetilde{d}^k)_Q}{(\widetilde{d}^k, y^k)_Q} \right]^2.
\end{aligned}
$$

Under the assumed sign condition, only the third summand can be negative, using a square root $B_k^{1/2}$ of the positive definite operator B_k, see, e.g., [71], and Cauchy-Schwarz inequality, we obtain

$$
\begin{aligned}
(p, B_{k+1} p)_Q &\geq (p, B_k p)_Q + \frac{(p, \widetilde{d}^k)^2_Q}{(\widetilde{d}^k, y^k)_Q} - \frac{(B_k y^k, p)^2_Q}{(y^k, B_k y^k)_Q} \\
&\geq \|B_k^{1/2} p\|^2_Q + \frac{(p, \widetilde{d}^k)^2_Q}{(\widetilde{d}^k, y^k)_Q} - \frac{\|B_k^{1/2} y^k\|^2_Q \|B_k^{1/2} p\|^2_Q}{\|B_k^{1/2} y^k\|^2_Q} \geq \frac{(p, \widetilde{d}^k)^2_Q}{(\widetilde{d}^k, y^k)_Q} \geq 0.
\end{aligned}
$$

Now, either, $B_k^{1/2} p$ and $B_k^{1/2} y^k$ are linear independent, then the second inequality coming from Cauchy-Schwarz inequality is strict, or there is some $t \neq 0$ such that

$$
B_k^{1/2} p = t B_k^{1/2} y^k
$$

and then

$$
\frac{(p, \widetilde{d}^k)^2_Q}{(\widetilde{d}^k, y^k)_Q} = \frac{(B_k^{-1/2} B_k^{1/2} p, \widetilde{d}^k)^2_Q}{(\widetilde{d}^k, y^k)_Q} = t^2 \frac{(B_k^{-1/2} B_k^{1/2} y^k, \widetilde{d}^k)^2_Q}{(\widetilde{d}^k, y^k)_Q} = t^2 \frac{(y^k, \widetilde{d}^k)^2_Q}{(\widetilde{d}^k, y^k)_Q} > 0
$$

implies positive definiteness of B_{k+1}.

Now, it remains to show that $(y_k, \widetilde{d}^k)_Q > 0$. In the case $\theta = 1$, clearly

$$(y^k, \widetilde{d}^k)_Q \geq 0.2(y^k, B_k y^k)_Q > 0.$$

Otherwise, it is

$$
\begin{aligned}
(y^k, \widetilde{d}^k) &= (y^k, \theta_k \widetilde{d}^k + (1 - \theta_k) B_k y^k)_Q \\
&= 0.8 \frac{(y^k, B_k y^k)_Q}{(y^k, B_k y^k)_Q - (y^k, \widetilde{d}^k)_Q} (y^k, \widetilde{d}^k)_Q \\
&\quad + \left(1 - 0.8 \frac{(y^k, B_k y^k)_Q}{(y^k, B_k y^k)_Q - (y^k, d^k)_Q}\right)(y^k, B_k y^k)_Q \\
&= 0.8 \frac{(y^k, B_k y^k)_Q}{(y^k, B_k y^k)_Q - (y^k, \widetilde{d}^k)_Q} (y^k, \widetilde{d}^k)_Q \\
&\quad + \frac{(y^k, B_k y^k)_Q - (y^k, \widetilde{d}^k)_Q - 0.8(y^k, B_k y^k)_Q}{(y^k, B_k y^k)_Q - (y^k, \widetilde{d}^k)_Q} (y^k, B_k y^k)_Q \\
&= \frac{(y^k, B_k y^k)_Q \cdot \left(0.8(y^k, \widetilde{d}^k)_Q - (y^k, \widetilde{d}^k)_Q + 0.2(y^k, B_k y^k)_Q\right)}{(y^k, B_k y^k)_Q - (y^k, \widetilde{d}^k)_Q} \\
&= \frac{(y^k, B_k y^k)_Q \cdot \left(-0.2(y^k, \widetilde{d}^k)_Q + 0.2(y^k, B_k y^k)_Q\right)}{(y^k, B_k y^k)_Q - (y^k, \widetilde{d}^k)_Q} \\
&= 0.2(y^k, B_k y^k)_Q > 0.
\end{aligned}
$$

Thus the assertion is shown. $\qquad\square$

With that, we conclude that the damping step for the inverse BFGS method ensures the positive definiteness of the operator B_{k+1}. To globalize this method, we check in every iteration, if the computed direction is a descent direction

$$(\nabla_Q j(q^k), d^k)_Q < 0. \tag{4.30}$$

If (4.30) is not fulfilled, then we take a descent direction step instead. The complete damped inverse BFGS method with globalization step (4.30) is shown in Algorithm 4.2.

Remark 4.6. Note, that to assert global convergence, of course a check of the angle between d^k and $\nabla_Q j(q^k)$, see Lemma 2.54, could be added in the algorithm.

Algorithm 4.2 Damped inverse BFGS method

Input: Let $q^0 \in Q$ be an initial guess for the control and the initial inverse
  Hessian approximation be $B_0 \in \mathcal{L}(Q, Q)$ (spd). We choose the parameter
  $k_{\max} \in \mathbb{N}$, and $\gamma \in (0, 0.5)$ for the Armijo Condition (4.21).
  For $k = 1, \ldots, k_{\max}$ **do**
    If $\nabla_Q j(q^k) = 0$ **then**
      STOP
    Compute search direction $d^k = -B_k \nabla_Q j(q^k)$.
    If $\nabla_Q j(q^k)_Q \, d^k < 0$ **then**
      Set $d^k = -\nabla_Q j(q^k)$.
    Compute t_k with Armijo Condition (4.21).
    Set $q_{k+1} = q_k + t_k d^k$.
    If Curvature Condition (4.27) is not fulfilled **then**
      Damping Update by means of Definition 4.4.
    Compute B_{k+1} by means of (4.26).
    $k \leftarrow k + 1$.

However, in our numerical tests convergence to near stationarity was achieved
without such safeguards.

4.2.3. Methods applied to Optimization of Maxwell's Eigenvalue Problem

In this subsection, we explain how we apply the gradient as well as the BFGS
method, which we introduced in the previous two sections, to the considered
Maxwell eigenvalue optimization problem. In order to numerical solve this prob-
lem, we consider the discrete Maxwell eigenvalue problem stated in (4.32) and we
use the following termination criteria implemented in the `DOpElib`-library [49].

Definition 4.7 (Termination Criteria). *The optimization methods applied to the
optimization problem of Maxwell's eigenvalue problem will terminate, if one of
the following cases holds:*

  1. it $\geq$ it$_{\max}$,

  2. $\|\nabla_Q j(q^k)\| < \mathrm{TOL}_{\mathrm{global}}^2$ and $\|\nabla_Q j(q^k)\| < \mathrm{TOL}^2 \cdot \|\nabla_Q j(q^0)\|$,

with it$_{\max}$, $\mathrm{TOL}_{\mathrm{global}}$, $\mathrm{TOL} > 0$, *where* it$_{\max} \in \mathbb{N}$ *is the maximum number of
iterations,* $\mathrm{TOL}_{\mathrm{global}} \in \mathbb{R}$ *is the global tolerance,* $\mathrm{TOL} \in \mathbb{R}$ *is a relative tolerance.*

Algorithm 4.3 Gradient method for optimization of Maxwell's eigenvalue problem

---

Input: Choose initial q_0.

   While Termination criteria 4.7 not fulfilled **do**

     1.   Solve the state eigenvalue problem and normalize u as in (4.12) to obtain the state solution $(\lambda, (u, \psi))$.

     2.   Solve the transposed eigenvalue problem stated in (4.13) and normalize z with (4.14) to obtain the adjoint solution $(\mu, (z, \phi))$.

     3.   Compute $\nabla_Q j(q^k)$ with (4.15) and (4.16) using the state and adjoint solution.

     4.   Compute a search direction $d^k = -\nabla_Q j(q^k)$.

     5.   Compute t_k with line search satisfying Armijo condition (4.28).

     6.   Update $q^{k+1} = q^k + t_k d^k$.

     7.   Set $k \leftarrow k + 1$

The gradient method, see Section 4.2.1, applied to the eigenvalue optimization problem is shown in Algorithm 4.3. The input parameters is a given control vector q_0. Until we fulfill the termination criteria, we solve in a first step the state eigenvalue problem and normalize the state eigenvector as in (4.12), in order to achieve the state solution of the problem. The second step of the method is to solve the adjoint problem, which is in the considered case to solve the transposed eigenvalue problem and to normalize the adjoint eigenvector as in (4.13) and (4.14). With the solutions of the state and adjoint problem, we compute the gradient of the reduced cost functional by computing the derivative of the reduced cost functional Equation (4.15) and the Riesz representation (4.16) in the third step. In the fourth and fifth step, we compute the a search direction as well as the step size, similar to Algorithm 4.1. After updating the iterate q^{k+1} and an increasing the iteration number, we iterate until we fulfill one of the termination criteria.

The damped inverse BFGS method, see Section 4.2.2, applied to the eigenvalue optimization problem is shown in Algorithm 4.4. The input parameters are a given control vector q_0 and an initial approximation matrix B_0.

Algorithm 4.4 Damped inverse BFGS method for optimization of Maxwell's eigenvalue problem

---

Input: Choose initial q_0 and B_0 spd.

   While Termination criteria 4.7 not fulfilled **do**

1. Solve the state eigenvalue problem and normalize u as in (4.12) to obtain the state solution $(\lambda, (u, \psi))$.

2. Solve the transposed eigenvalue problem stated in (4.13) and normalize z with (4.14) to obtain the adjoint solution $(\mu, (z, \phi))$.

3. Compute $\nabla_Q j(q^k)$ with (4.15) and (4.16) using the state and adjoint solution.

4. Compute a search direction $d^k = -B_k \nabla j(q^k)$.

5. **If** $(\nabla_Q j(q^k), d^k)_Q > 0$ **then**
   $d^k = -\nabla_Q j(q^k)$.

6. Compute t_k with line search satisfying Armijo condition (4.28).

7. Update q^{k+1} and $y^k = \nabla_Q j(q^{k+1}) - \nabla_Q j(q^k)$.

8. **If** curvature condition is not fulfilled **then**
   Apply damping step of Definition 4.4

9. Compute B_{k+1} with the update formula, see (4.26).

10. Set $k \leftarrow k + 1$

The operator B_k is never stored but the action $B_k \nabla_Q j(q^k)$ is evaluated using the recursive definition of B_k given by the update formula. To this end, the functions $\widetilde{d}, B_k y^k \in Q$ and the scalars $(\widetilde{d}^k, y^k)_Q$ and $(\widetilde{d}^k - B_k y^k, y^k)$ are stored. To avoid arbitrary increase in memory usage, the implementation allows to specify the number m of previous iterates to be kept. The recursive definition then uses the definition $B_{k-m} = B_0$, where by default we choose $B_0 = 1/\alpha I$ where I denotes the identity on Q. Hence, the BFGS method guarantees fast convergence, see [51, Theorem 5.2], [63, Theorem 2.5].

The first three steps of the method are similar to the steps of the gradient method. With the therein computed gradient, the method is similar to Algorithm 4.2. We compute a search direction in the fourth step and check in the fifth step, if the search direction is a descent direction. Otherwise, we choose the

negative gradient as search direction. Further, we compute the step size with the Armijo condition, update the iterates and apply the damping Definition 4.4 if the curvature condition (4.27) is not satisfied. The final step is to update the matrix B_k to B_{k+1}.

4.3. Discretization of Maxwell's Eigenvalue Problem

In the literature, solving Maxwell's eigenvalue problem in cavities is already investigated. The divergence-free condition of the space X_0, introduced in (3.34), is very difficult to implement because of finding an appropriate finite dimensional subspace of X_0. There are in general three ways to approximate the space of this problem. The first way, and common in engineering, is to neglect the divergence-free constraint, to shift the eigenspace and to filter the physical eigensolutions from the spurious solutions afterwards. Since the number of spurious solutions is not predictable, it is disadvantageous in context of eigenvalue optimization.

Furthermore, there are two other methods for the approximation of Maxwell's eigenvalue problem, which are well explained in [9]. One of these methods is to solve the problem is using a penalty method which neglects the divergence free constraint and uses common linear and quadratic node-based finite elements for the field values. The idea of the penalty method is to consider the problem finding a solution $(\lambda, u) \in \mathbb{R} \times H(\mathrm{curl}; \Omega_q)$, where $u \neq 0$ such that

$$(\nabla \times u, \nabla \times \psi) + s(\nabla \cdot u, \nabla \cdot \psi) = \lambda(u, \psi), \qquad \forall \psi \in H(\mathrm{curl}; \Omega_q), \qquad (4.31)$$

where s is a positive, usually small, parameter, see also [24, 65, 72]. It is clear that a solution of the original variational formulation is a solution of (4.31). However, (4.31) can have solutions other than those of the original problem. For many years, researchers tried this penalty-function approach of constrained minimization to numerically solve Maxwell's eigenvalue problem, since it is easy to implement. For simple computational domains, this approach has a good performance rate, but in general, this approach is a mere fix now being the therein occurring spurious eigenmodes shifted far into the visible spectrum. They are dependent on a user-defined parameter which specifies how strongly the divergenceless condition is imposed. Hence, this approach is not suitable for the eigenvalue optimization, which we consider in this thesis. For more details to this method, we refer to [37–39].

The third method, also explained in [9], is a mixed formulation, such as (4.32), with linear and quadratic finite edge elements, e.g., the elements of Nédélec [83], for the field values and corresponding node-based finite elements for the Lagrange multiplier. For a further mixed formulation, we refer to [26]. This approach avoids the so-called spurious modes which would appear without the divergence-free condition and guarantees the convergence of the finite element solutions to the solutions of the original problem.

In the first two described approaches, the divergence-free condition for the electric field is not treated properly and causes the appearing of spurious modes. For that reason, we solve (4.32) by using a mixed finite element method. The use of mixed elements avoids the problem of spurious solutions. An other advantage of these elements is that, in contrast to the method of modification of the classical elements, also problems modeled with different media could be solved without any modification. We refer to [76] for the analysis of Nédélec's elements which is based on a special theory of mixed methods developed by Boffi et.al., see [21,22,25,27] and also by Kikuchi, see [64–66], or by utilization of discrete analogs of compactness arguments to derive the theory.

In the following, we formulate the discretized variational formulation of Maxwell's eigenvalue problem by Kikuchi (3.4) with the mixed FEM in order to solve it numerically. For a detailed explanation, we refer to [23,76]. The formulation by Kikuchi lives in the Sobolev spaces $H^1(\Omega)$ and $H(\mathrm{curl};\,\Omega)$ and the aim of the method is to replace the infinite-dimensional space X by a finite-dimensional subspace X_h, where X is for example $H^1(\Omega)$ or $H(\mathrm{curl};\,\Omega)$. To construct these spaces, we first discretize the computational domain Ω by a mesh Ω_h, i.e., a finite non-overlapping subdivision into elements T_i of a simple geometry. The discretization is called admissible, if the following properties hold.

1. The elements are non-overlapping, i.e.,

$$\mathrm{interior}(T_i) \cap \mathrm{interior}(T_j) = \emptyset \quad \text{for } i \neq j.$$

2. The discretization Ω_h is a covering of Ω, i.e.,

$$\bigcup_{T_i \in \Omega_h} T_i = \overline{\Omega}.$$

3. The intersection of two different elements is either empty, a vertex, an edge or a face of both elements.

Remark 4.8. For the discretization, the classical elements are typically triangles or quadrilaterals, for two-dimensional domains, and tetrahedral or hexahedral, for three-dimensional domains. In this thesis, we consider exclusively quadrilateral and hexahedral elements because the FE software `deal.II` deals mainly with these elements.

By that, we define the fixed FE space X_h by a sequence of finite-dimensional subspaces X_T, i.e.,

$$X_h := \{v_h \in X : \; v_h|_T \in X_T\}.$$

The interpolation operators π_h, r_h, w_h and $P_{0,h}$ map from suitable subspaces

$$U \subset H^1(\Omega), \qquad V \subset H(\mathrm{curl}; \Omega), \qquad W \subset H(\mathrm{div}; \Omega), \qquad Z \subset L^2(\Omega),$$

into the appropriate finite element spaces. The continuous as well as their discrete subspaces, together with interpolation operators, are linked by the de Rham diagram, see Figure 4.2. The de Rham diagram is of central importance to the analysis, e.g., one can show the existence of an approximate Helmholtz decomposition similar to the continuous one introduced in Lemma 3.10. For the de Rham diagram and more details, we refer to [76].
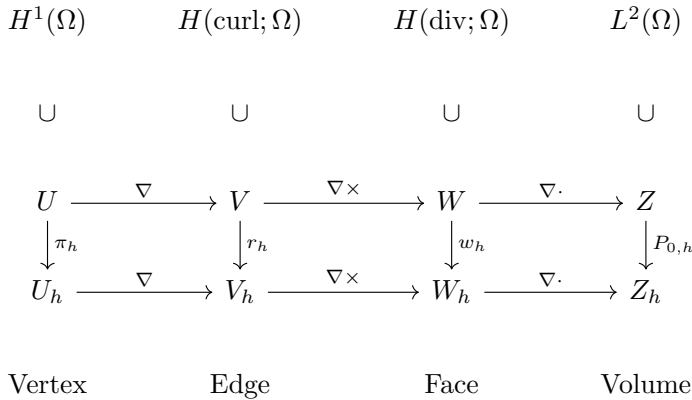
Figure 4.2. Discrete De Rham Diagram

For the discretization of Maxwell's eigenvalue problem, e.g., (3.4), we distinguish between the different spaces. Therefore, we treat finite elements of two different families of elements. A proper discretization of the $H^1(\Omega)$-space,

$$U_h \subset H^1(\Omega),$$

is achieved by using node-based Lagrange elements, see, e.g., [24]. For the discretization of the $H(\mathrm{curl}; \Omega)$-space,

$$V_h \subset H(\mathrm{curl}; \Omega),$$

we introduce a second family of elements, the edge-based Nédélec elements, see [82, 83]. Both families of elements satisfy the discrete de Rham diagram, see Figure 4.2, and will be introduced shortly in the following subsections.

With that, the discretized variational formulation of (3.4) is to find an eigenvalue λ_h and a non-trivial electric field $u_h \in V_h$ with $u_h \neq 0$, and $\psi_h \in U_h$, such that

$$
\begin{aligned}
(\nabla \times u_h, \nabla \times v_h)_{\Omega_h} + (\nabla \psi_h, v_h)_{\Omega_h} &= \lambda_h (u_h, v_h)_{\Omega_h} \quad \forall\, v_h \in V_h, \\
(u_h, \nabla \varphi_h)_{\Omega_h} &= 0 \qquad\qquad\quad \forall\, \varphi_h \in U_h.
\end{aligned}
\tag{4.32}
$$

4.3.1. Finite Element Approximation of $H_0^1(\Omega)$

For the discretization of the scalar potential space $H_0^1(\Omega)$, we consider a conforming approximation by using scalar Lagrange finite elements provided by the `deal.II` library. This element yields the finite element space of continuous, piecewise polynomials of degree p in each coordinate direction. The library uses tensor product polynomials based on one-dimensional Lagrange polynomials with equidistant (degree up to 2), Gauss-Lobatto (starting from degree 3), or given support points. For implementation details, we refer to [10, 11]. This element is $H^1(\Omega)$ conforming and unisolvent. For details, we refer to [76, Lemma 6.9 and Lemma 6.10]. In Figure 4.3, we show two- (a) and three-dimensional (b) first-order Lagrange elements. Further, for a bounded subdomain $\widehat{K} \subset \widehat{\Omega}$ to a bounded subdomain $K \subset \Omega_q$, e.g., a mapping from a discretized finite element reference domain to a discretized finite element domain, it holds the same transformation rules as for the function space of $H^1(\Omega)$ introduced in Section 3.2.1. In this case the shape functions N_i on a general cell K are obtained from the reference shape functions $\widehat{N}_i$ on the reference element $\widehat{K}$ by the pull-back

$$N_i(x) = \left(\widehat{N}_i \circ F^{-1}\right)(x).$$

(a) Two-dimensional   (b) Three-dimensional
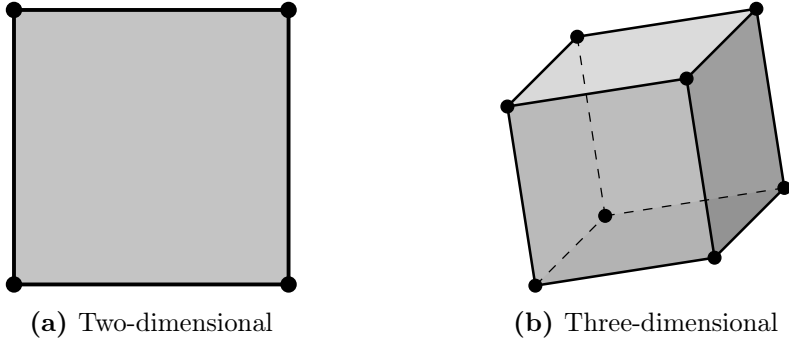
Figure 4.3. First order Lagrange elements

4.3.2. Finite Element Approximation of $H_0(\mathbf{curl};\, \Omega)$

In case of an FE approximation of the space of $H_0(\mathrm{curl};\, \Omega)$, conventional finite element basis functions give rise to spurious solutions because they not guarantee the required tangential continuity. This property is automatically satisfied by edge elements. The approximation of $H_0(\mathrm{curl};\, \Omega)$ requires that degrees of freedom corresponding to the tangential traces match for the $H(\mathrm{curl};\, \Omega)$-conforming discretizations. In this thesis, we use the edge-based Nédélec elements due to [83], introduced, e.g., in [24, 76]. For the implementation in `deal.II`, we refer to the library [10, 11], and a report [98], which introduces the basis for the implementation, i.e., Nédélec's $H(\mathrm{curl};\Omega)$-conforming finite element method of first type. There are several families of Nédélec. We refer to [83] for the first, and to [82] for the second kind. In Figure 4.4, we show two- (a) and three-dimensional (b) lowest-order Nédélec elements. The edge element space has exactly the same continuity requirements as the function space $H_0(\mathrm{curl};\, \Omega)$. The element is curl conforming and unisovlent, see [76, Theorem 6.5]. Furthermore, in case of $H_0(\mathrm{curl})$-conforming subspaces, e.g., a Finite Element space discretized with Nédélec elements, the curl-conforming Piola mapping, introduced in Section 3.2.2, holds. The element shape functions $N_i(x)$ on the element $H_0(\mathrm{curl};\, \Omega_q) \supset K = F_q(\widehat{K})$, with $\widehat{K} \subset H_0(\mathrm{curl};\, \Omega_q)$, are obtained from the reference shape functions by

$$N_i(x) = \left(\mathrm{DF}_q^{-T} \widehat{N}_i \right) \circ F_q^{-1}(x).$$

(a) Two-dimensional   **(b)** Three-dimensional
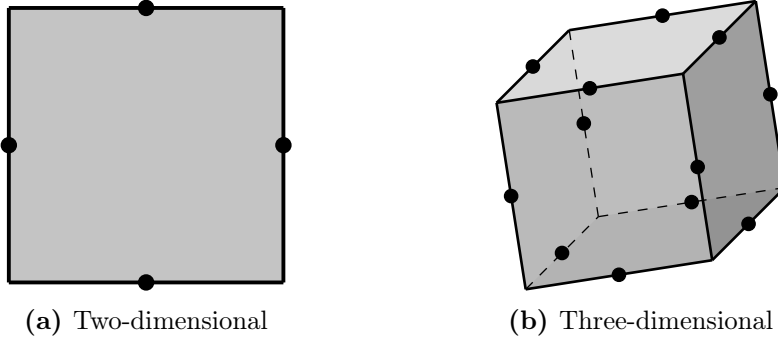
Figure 4.4. Lowest order Nédélec elements

4.3.3. Matrix Formulation

With the given weak formulation we construct a sequence of finite dimensional subsets $U_h \subset H_0(\text{curl};\Omega)$ and $V_h \subset H_0^1(\Omega)$. We construct these discrete spaces with sets of basis functions

$$U_h = \text{span}\{\varphi_i^h\}_{i=1}^{n_U} \qquad \dim U_h = n_U,$$
$$V_h = \text{span}\{v_i^h\}_{i=1}^{n_V} \qquad \dim V_h = n_V.$$

We express and test the solution field with basis functions

$$u^h = \sum_{i=1}^{n_U} u_i^h \varphi_i^h \ \in U_h \qquad \psi^h = \sum_{j=1}^{n_V} \psi_j^h v_j^h \ \in V_h$$

with unknown coefficients u_i^h, $i = 1, \ldots, n_U$ and ψ_j^h, $j = 1, \ldots, n_V$. In terms of basis functions we formulate the discrete weak formulation of Maxwell's eigenvalue problem stated in (4.32) to

$$\sum_{j=1}^{n_U} u_j^h (\nabla \times \varphi_j^h, \nabla \times \varphi_i^h) + \sum_{k=1}^{n_V} \psi_k^h (\nabla v_k^h, \varphi_i^h) = \lambda_h \sum_{j=1}^{n_U} u_j^h (\varphi_j^h, \varphi_i^h) \quad \forall i = 1, \ldots, n_U,$$

$$\sum_{j=1}^{n_U} u_j^h (\varphi_j^h, \nabla v_l^h) = 0 \qquad\qquad \forall l = 1, \ldots, n_V.$$

We obtain the algebraic system of equations in the form

$$\begin{pmatrix} A & B^T \\ B & 0 \end{pmatrix} \begin{pmatrix} u \\ \psi \end{pmatrix} = \lambda \begin{pmatrix} M & 0 \\ 0 & 0 \end{pmatrix} \begin{pmatrix} u \\ \psi \end{pmatrix}, \tag{4.33}$$

where we denote the discrete eigenvalue by $\lambda = \lambda_h$. The finite element matrices $A \in \mathbb{R}^{n_U \times n_U}, B \in \mathbb{R}^{n_U \times n_V}$ and $M \in \mathbb{R}^{n_U \times n_U}$ are

$$(A)_{ji} := a(\varphi_i^h, \varphi_j^h) = \int_\Omega (\nabla \times \varphi_i^h, \nabla \times \varphi_j^h) \mathrm{d}x,$$

$$(B)_{ki} := b(\varphi_i^h, v_k^h) = \int_\Omega (\varphi_i^h, \nabla v_k^h) \mathrm{d}x,$$

$$(M)_{kl} := m(\varphi_l^h, \varphi_k^h) = \int_\Omega (\varphi_l^h, \varphi_k^h) \mathrm{d}x,$$

and the coefficient vectors are

$$(u)_i := u_i^h, \quad u \in \mathbb{R}^{n_V},$$
$$(\psi)_i := \psi_i^h, \quad \psi \in \mathbb{R}^{n_U}.$$

The matrix $K \in \mathbb{R}^{(n_U + n_V) \times (n_U + n_V)}$,

$$K = \begin{pmatrix} A & B^T \\ B & 0 \end{pmatrix},$$

is known as stiffness matrix and the matrix $M \in \mathbb{R}^{(n_U + n_V) \times (n_U + n_V)}$,

$$M = \begin{pmatrix} M & 0 \\ 0 & 0 \end{pmatrix},$$

is called mass matrix. Hence, the generalized eigenvalue problem has the form

$$Kx = \lambda Mx, \tag{4.34}$$

with $x = (u, \psi)^T$

4.3.4. Implementation Details

4.3.4.1. Mixed Finite Elements

In this thesis, we use the open source and `C++`-based FE-library `deal.II` [10, 11] to numerically solve the considered problems. The library constructs discretized domains and trial functions. We implement the weak formulation of the problem including initial and boundary conditions. By that, the library generates a discrete system of equations. Further, the library provides a class of `FESystem` which combines mixed problems containing different classes of FE. The implementation of Nédélec elements in the `deal.II` library is well explained in [98].

Since open source libraries lives from the on-working developers and researchers, the implementation with this kind of software is challenging due to fact that it is not always tested into the finest detail and therefore, it is not free of bugs. As a difficulty of this research, the software development is always a hurdle. The construction of a Mixed Finite Element by `FESystem` enables the usage of a Mixed FEM. While working on this dissertation, we fixed a bug in `deal.II` and correct the method of using a mixed formulation including Nédélec and Lagrange elements. Moreover, the code got tested with several mapping and eigenvalue solver tests, such that we achieve the correct eigensolutions.

4.3.4.2. Saddle Point Problems and Eigenvalue Solver

In Section 4.3.3, we showed the matrix formulation of the discretized Maxwell eigenvalue problem (4.34). This formulation has the form of a saddle point problem, i.e., the following properties hold.

1. A is symmetric: $A = A^T$,
2. The symmetric part of A, $H = \frac{1}{2}(A + A^T)$ is positive semidefinite,
3. $(B^T)^T = B$,
4. the lower right matrix is a zero matrix (and thus symmetric and positive semidefinite).

Furthermore, the considered problem leads to a large sparse system of equations. This kind of problems are also called equilibrium equations, see, e.g., [100] and Karush-Kuhn-Tucker first order optimality conditions, see [84] for precise definitions, and for historical notes, see, e.g., [50].

Since the considered eigenvalue problems are large and sparse, we use an iterative solver for numerical solutions. Therefore, and for more details of solvabil-

Table 4.1. Eigenvalue solver for the optimization

	Solver
A	Subspace iteration
B	Krylov Schur
BS	Krylov Schur with adjusted shift

ity of saddle point problems, we refer to [19] and the therein mentioned literature. Large-scale saddle point problems occur in many areas of computational science and engineering. Some few are constrained optimization [48, 110, 111], electromagnetism [30, 87, 88], mixed finite element approximations of elliptic PDEs [31, 32, 91] and optimal control [16, 17, 20]. The whole field of solving these large-scale saddle point problems is big and a separate topic. For eigenvalue solvers in electromagnetic cavities, we refer to [9], where various algorithms to solve Maxwell's eigenvalue problem stated in (4.32) are compared with each other, i.e., a subspace iteration, a block Lanczos algorithm, implicitly restarted Lanczos algorithm and a Jacobi-Davidson algorithm.

In this thesis, we use the `SLEPc`-library [55,56] for the eigenvalue problem computation which bases on `PETSc`-library [13–15], a Portable, Extensible Toolkit for Scientific Computation. The usage of eigenvalue solver for saddle point problems is challenging. In the end, the for the most examples suitable eigenvalue solvers for the considered Maxwell eigenvalue problems (4.12) as well as (4.13) and (4.14) are the subspace iteration solver as well as the Krylov Schur method. We apply the from the libraries provided shift-invert spectral transformation as well as the Richardson solver and the Cholesky preconditioner.

First, we tested all examples with the subspace iteration solver, which was suitable for the first iterations. However, in not every optimization example, this solver is suitable for the whole optimization process. The eigenvalue solver fails during the optimization using the BFGS method for different reasons, e.g., because of an indefinite matrix or some problems occur intern with the LU factorization. In these examples, we fixed this problem by using the Krylov-Schur method instead. Moreover, a suitable eigenvalue shift at the start of the optimization can turn out badly because the eigenvalue problem changes during the optimization and the initial shift becomes not suitable.

In the examples, we name the finally used solver shown in Table 4.1. For details to the taken parameters in the methods, we refer to Appendix A.1. Further,

for literature for the subspace iteration with shift-and-invert strategy, we refer to [86, 97].

4.4. Numerical Examples of Freeform Optimization for Maxwell's Eigenvalue Problem

In this section, we validate the introduced optimization methods from Section 4.2 by showing examples of freeform optimization problems constrained by Maxwell's eigenvalue problem. In the following, we consider an optimization of the first eigenvalue λ, assumed to be simple, to a target value λ_*. For the optimization, let us consider the functional

$$J(\lambda) := \frac{1}{2}|\lambda - \lambda_*|^2,$$

where $\lambda, \lambda_* \in \mathbb{R}$. Further, we add some regularization terms to the objective functional. We apply a quadratic penalty regularization using the H^1-norm to guarantee the existence of q and ∇q. In addition, the deformation gradient DF_q, defined in (3.8), needs to be invertible and its determinant to be non-negative. To ensure this, we apply a barrier term enforcing $\mathrm{J}_q = \det(\mathrm{DF}_q) \geq \varepsilon$ for some $\varepsilon > 0$. By that, we define the regularization functional as

$$R(q) := \frac{\alpha}{2}\left(\|q\|^2 + \|\nabla q\|^2\right) - \beta \int_{\widehat{\Omega}} \ln(\mathrm{J}_q - \varepsilon)\, d\widehat{x}, \qquad (4.35)$$

where $\|\cdot\|$ is the usual L^2-norm on $\widehat{\Omega}$ with regularization parameters $\alpha, \beta \in \mathbb{R}_+$. We remark here, that in general the choice of α has influence on the convexity of the problem. For that reason, by increasing α, we expect a speed up of the optimization process in the sense of reducing the number of iterations until the method terminates. The barrier term is necessary to guarantee a non-negative J_q but it also changes the optimization problem itself.

The derivative of the regularization functional with respect to q is

$$\mathrm{R}'_q(q)\delta q = \alpha\left((q, \delta q) + (\nabla q, \nabla \delta q)\right) - \beta \int_{\widehat{\Omega}} \frac{1}{\mathrm{J}_q - \varepsilon}\, \mathrm{J}'_q \delta q\, d\widehat{x}.$$

For all numerical examples, it is $\varepsilon = 10^{-4}$ and we consider the Eigenvalue Optimization Problem (4.11) with added regularization functional, i.e.,

find $u \in H_0(\mathrm{curl}; \Omega_q)$ with $u \neq 0$ and $\psi \in H_0^1(\Omega_q)$ by solving

$$
\begin{aligned}
\min \quad & J(q, \lambda) := J(\lambda) + R(q) \\
\text{s.t.} \quad a(q; u, \delta u) + b(q; \delta u, \psi) &= \lambda m(q; u, \delta u) && \forall\, \delta u \in H_0(\mathrm{curl}; \Omega_q), \\
b(q; u, \delta\psi) &= 0 && \forall\, \delta\psi \in H_0^1(\Omega_q), \\
\delta\lambda\,(m(q; u, u) - 1) &= 0 && \forall\, \delta\lambda \in \mathbb{R},
\end{aligned}
\tag{4.36}
$$

with

$$
\begin{aligned}
a(q; u, \delta u) &:= (\nabla \times u, \nabla \times \delta u)_{\Omega_q}, \\
b(q; \delta u, \psi) &:= (\nabla\psi, \delta u)_{\Omega_q}, \\
m(q; u, \delta u) &:= (u, \delta u)_{\Omega_q}.
\end{aligned}
$$

In the following, we show solutions of the optimization problem on two simple geometries, i.e., a rectangle with free boundaries and a quarter circle with fixed edges, in order to validate the code. We compare the optimization processes between the damped inverse BFGS method from Algorithm 4.4 with the gradient method from Algorithm 4.3 with respect to the number of iteration steps and accuracy of the solutions. We determine that the BFGS method provides better convergence results, what we expect and already discussed in Section 4.2. Furthermore, we investigate the influence of the regularization parameters on the concerning optimal shape, accuracy on different refinement levels and element orders. Aside from that, we consider the impact of the choice of the target value on the domain deformation.

To solve the considered optimization problem numerically, we use the PDE optimization library `DOpElib` [49] which bases on the FE library `deal.II` [10,11]. For the mesh refinement and the used finite elements, we use the classes provided by `deal.II`. For all examples, we use a global refinement. For details, we refer to the library.

In the context of this thesis, we extended the `DOpElib` library for eigenvalue optimization problems. We show the documentation of the extension to eigenvalue optimization problems in Appendix A.1. In the previous sections of this chapter, we introduced a gradient method in Algorithm 4.3 and a damped inverse BFGS method in Algorithm 4.4 for the considered Maxwell eigenvalue optimization problem. Within this thesis, we extended the `DOpElib` library by latter. The approximated Hessian matrices can get very costly in memory because of their size and missing sparsity. Instead of fully storing all matrices, we use a

limited-memory BFGS (L-BFGS) method, where we save only a few vectors that represent the approximated Hessian implicitly. In all examples, we use 40 stored vectors. For details for this method, we refer to [84, Chapter 7.2].

Further, we additionally use the `SLEPc`- as well as the `PETSc`-library for solving the containing eigenvalue problems. For the differentiation of the used eigenvalue solver, we name them in the solution tables in the column EVS and refer to Table 4.1. For some comments on the implementation, we refer to Section 4.3.4.2, for more details for the parameters used there, we refer to Appendix A.1 and for an overview of the used library versions to Table A.2.

4.4.1. Rectangle with Free Boundaries

We consider the Freeform Optimization Problem (4.36) with an initial rectangular domain

$$\widehat{\Omega} = \left[0, \frac{\pi}{3}\right] \times \left[0, \frac{\pi}{2}\right],$$

see Figure 4.5, where we allow freeform deformation on the whole domain. With
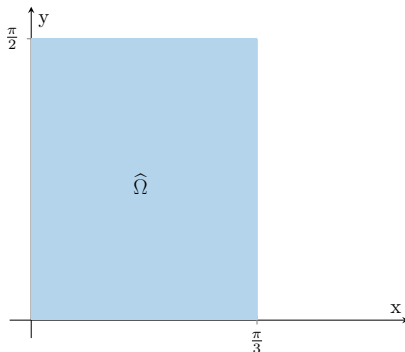
Figure 4.5. Rectangle Geometry

the assumptions to the time-harmonic Maxwell eigenvalue problem in Section 3.1, the initial domain can be interpreted as a rectangular wave guide. For this domain, it is possible to compute the eigenvalues for some particular cases, and also the eigenmode, analytically, see [60]. With that, it is possible to check the convergence of the eigenvalue solver.

For given dimensions $a, b > 0$, there exists two separated sets of solutions, the Transverse Magnetic (TM) and the Transverse Electric (TE) modes, according to the behavior of the electric or magnetic field in the longitudinal direction.

Moreover, the cutoff frequency is defined by

$$\omega_{mn} = \frac{\pi}{\sqrt{\mu_0 \varepsilon_0}} \cdot \sqrt{\frac{m^2}{a^2} + \frac{n^2}{b^2}}, \tag{4.37}$$

with constants μ_0, ε_0 and where m and n cannot both be zero. In this example, it is $a = \frac{\pi}{3}$ and $b = \frac{\pi}{2}$. Further, we are interested in the optimization of the eigenvalue which is determined by the frequency.

In the examples, we solve the considered optimization problems on different refinement levels and two different choices of element orders, either lowest order Nédélec elements and first order Lagrange elements, or first order Nédélec elements and second order Lagrange elements. This has an impact on the number of degrees of freedom (DoFs). We will name the different choices as settings. We observe that, for the first 7 eigenvalues, with increasing the refinement level as well as the element order, the numerical solutions, using the subspace iteration (A), converge to the exact solutions, see Table 4.2.

Table 4.2. Exact and computed first 7 eigenvalues of the initial rectangle domain varying the DoFs by using different refinement levels (ref.) and varying the order of Lagrange (Lagr.) and Nédélec (Néd.) elements using the subspace iteration eigenvalue solver (A).

DoFs	ref.	Lagr.	Néd.	λ_1	λ_2	λ_3	λ_4	λ_5	λ_6	λ_7
387	2	2	1	4.00205	9.00461	13.0067	16.1204	19.4537	19.4537	19.4537
387	3	1	0	4.05166	9.11624	13.1679	16.8382	25.9544	37.8859	40.3212
1411	3	2	1	4.00013	9.00029	13.0004	16.0082	25.0085	36.0184	36.0899
1411	4	1	0	4.01287	9.02895	13.0418	16.2067	25.2356	36.465	37.0525
5389	4	2	1	4.00001	9.00002	13	16.0005	25.0005	36.0012	36.0059
5389	5	1	0	4.00321	9.00723	13.0104	16.0515	25.0587	36.1158	36.261
20995	5	2	1	4	9	13	16	25	36.0001	36.0004
exact solution				4	9	13	16	25	36	36

In the following, we optimize the first eigenvalue $\lambda = \lambda_1$, which is clearly simple, to a target value λ_*. This results in a domain change. First, we compare the gradient method from Algorithm 4.3 with the BFGS method from Algorithm 4.4. In all tables of this section, we show the numerical initial eigenvalue before optimization, named by λ_0. In all settings, we show the number of iterations (it.), the eigenvalue after termination λ_{it}, the value of the cost functional J and the

relative residual of the reduced gradient of the cost functional

$$\mathrm{r}_{\mathrm{rel}} = \frac{\sqrt{\|\nabla_Q j(q^{\mathrm{it}})\|}}{\sqrt{\|\nabla_Q j(q^0)\|}}.$$

Further, we indicate the maximum and minimum values of the determinant of the deformation gradient, which provide information about the domain change. For $\mathrm{J}_q = 1$, the volume of the domain stays the same. Values $\mathrm{J}_q > 1$ indicate a growth, whereas values $\mathrm{J}_q < 1$ indicate a shrinkage of the domain, see Remark 3.7.

First, we consider an initial example and compare the optimization methods. From there, we vary the regularization parameters and study their influence on the deformation of the domain. In general, we see that the BFGS method converges faster than the gradient method. For that reason, we show results for the initial example with different convergence tolerances. Afterwards, we investigate the influence of the choice of different target values λ_* on the deformation of the domain by using the BFGS method.

4.4.1.1. Comparison of the Optimization Methods with Variation of Regularization Parameters

In this subsection, we compare the BFGS method and the gradient method regarding the convergence and we study the influence of the varying the regularization parameters α and β in the same context. Therefore, we choose the target value $\lambda_* = 3.8$ and the parameters for the optimization methods are shown in Table 4.3.

Table 4.3. Parameters for the optimization on the rectangle domain

	BFGS method (Algorithm 4.4)	gradient method (Algorithm 4.3)
$\mathrm{it}_{\max}$	100	1000
$\mathrm{TOL}_{\mathrm{global}}$	10^{-5}	10^{-5}
TOL	10^{-5}	10^{-5}
Armijo Condition		
line $\mathrm{it}_{\max}$	10	10
γ	0.1	0.1
ρ	0.1	0.1

Initial Example: Comparison with $\alpha = 10^{-3}$ and $\beta = 10^{-5}$

Table 4.4 shows results of the freeform optimization with regularization parameters $\alpha = 10^{-3}, \beta = 10^{-5}$. In (a), we observe that the BFGS method from Algorithm 4.4 terminates after 15 iterations in every setting. The method converges in all cases to the chosen target value λ_*. The cost functional value J is in all cases smaller than $3.6 \cdot 10^{-7}$ and r_{rel} converges in every case to values smaller than $3.45 \cdot 10^{-6}$. The minimum values of the determinant of the deformation gradient J_q are between 1.030 and 1.053, and the maximum values are between 1.053 and 1.058.

In (b), we view the results of the gradient method. In every setting, the method terminates after the maximum number of iterations, with only exception of the example with 387 DoFs, refinement level 3 as well as lowest order Nédélec elements and first order Lagrange elements. Here, the method terminates after 30 iterations and converges to $\lambda_{30} = \lambda_*$. In all other settings, the eigenvalue after termination is $\lambda_{1000} = 3.80001$. The cost functional J is in all cases smaller than $4.07 \cdot 10^{-7}$ and decreases with finer meshes and also with a higher order of elements. The relative residual of the gradient r_{rel} is in most settings smaller than $1.35 \cdot 10^{-5}$.

Figure 4.6 shows the deformation of the rectangle corresponding to the example of Table 4.4, where the optimal solution of the BFGS method is illustrated in (a) and the optimal solution of the gradient method is illustrated in (b). The figures show the upper half of the rectangle. The shape of the deformed domain is in both cases similar. In case of optimization with the BFGS method, we obtain a minimally greater deformation on the top than after optimization with the gradient method. Moreover, the shape of the deformed rectangle is after optimization a little bit more curved in the middle part of the domain.

In case of the BFGS method, the results seem to be mesh-independent, the number of iterations is in every setting 15. In case of the gradient method, we can not make a statement yet, because the method stopped after the maximum number of iterations in almost every setting. The runtime of both optimization methods is mainly dependent on the number of eigenvalue solver calls. In each iteration, we solve once the state eigenvalue problem and once the adjoint eigenvalue problem. Therefore, in this example, the BFGS method is definitely faster than the gradient method, as we expected.

Table 4.4. Results of a freeform optimization for the first eigenvalue on a rectangle domain with target value $\lambda_* = 3.8$ and regularization parameters $\alpha = 10^{-3}, \beta = 10^{-5}$ for the tolerance of the termination criteria of $\text{TOL}_{\text{global}} = \text{TOL} = 10^{-5}$. The tables show results varying the DoFs of the mesh, the refinement level (ref.), the order of Lagrange (Lagr.) and Nédélec (Néd.) elements. The initial first (numerical) eigenvalue is given by λ_0. We show the eigenvalue λ_{it} after termination of the method and the resulting value of the cost functional J, the relative residual of the gradient of the cost functional r_{rel} as well as the minimum and maximum value of the determinant of the deformation gradient J_q and the used eigenvalue solver EVS.

(a) BFGS method from Algorithm 4.4

DoFs	ref.	Lagr.	Néd.	λ_0	it.	$\lambda_{\text{it.}}$	J	r_{rel}	$\text{J}_{q,\min}$	$\text{J}_{q,\max}$	EVS
387	2	2	1	4.002	15	3.8	1.128e-07	3.44e-06	1.030	1.057	A
387	3	1	0	4.052	15	3.8	3.522e-07	5.499e-06	1.031	1.054	A
1411	3	2	1	4.000	15	3.8	1.081e-07	3.923e-06	1.042	1.058	A
1411	4	1	0	4.013	15	3.8	1.752e-07	5.818e-06	1.053	1.055	A
5389	4	2	1	4.000	15	3.8	1.265e-07	6.084e-06	1.047	1.055	A
5389	5	1	0	4.003	15	3.8	1.381e-07	6.012e-06	1.053	1.053	A
20995	5	2	1	4.000	15	3.8	1.265e-07	6.085e-06	1.051	1.055	A

(b) Gradient method from Algorithm 4.3

DoFs	ref.	Lagr.	Néd.	λ_0	it.	$\lambda_{\text{it.}}$	J	r_{rel}	$\text{J}_{q,\min}$	$\text{J}_{q,\max}$	EVS
387	2	2	1	4.002	1000	3.80001	1.904e-07	1.309e-05	1.020	1.049	A
387	3	1	0	4.052	30	3.8	4.065e-07	9.659e-05	1.048	1.055	A
1411	3	2	1	4.000	1000	3.80001	1.836e-07	1.340e-05	1.032	1.049	A
1411	4	1	0	4.013	1000	3.80001	2.306e-07	1.196e-05	1.047	1.049	A
5389	4	2	1	4.000	1000	3.80001	1.831e-07	1.340e-05	1.041	1.049	A
5389	5	1	0	4.003	1000	3.80001	1.946e-07	1.304e-05	1.048	1.049	A
20995	5	2	1	4.000	1000	3.80001	1.831e-07	1.341e-05	1.045	1.050	A

Demonstration of the BFGS method

In Table 4.5, we show the functionality of the BFGS Method from Algorithm 4.4, exemplary on the initial example with the setting of 20995 DoFs, a discretization of the domain with Nédélec elements of order 1, Lagrange elements of order 2 and refinement level 5. The method stopped after 15 iteration steps. The table shows the computed eigenvalue after each iteration λ_{it}, the value of the cost functional J, the relative residual of the reduced gradient r_{rel}, the number of line search steps (l.s.), if the damping step has been carried out as well as the minimum and maximum value of the determinant of the deformation gradient J_q. The table displays the convergence of the eigenvalue λ_{it} to the target value $\lambda_* = 3.8$. In this example, the damping step was carried out in the first 6 iterations as well

(a) BFGS method from Algorithm 4.4   (b) Gradient method from Algorithm 4.3
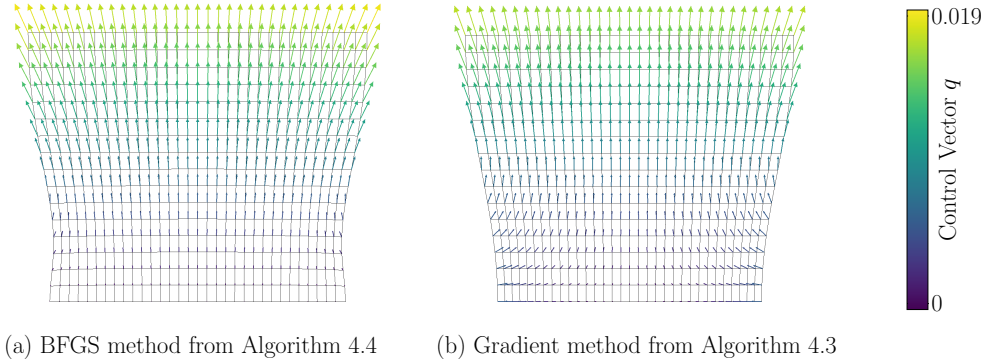
Figure 4.6. Comparison of the optimization methods regarding to the deformed rectangle domain after freeform optimization with target value $\lambda_* = 3.8$ and regularization parameters $\alpha = 10^{-3}$ and $\beta = 10^{-5}$. The figure shows the upper half of the domain, the solution of the lower half is symmetric to the upper part. The deformation is scaled by a factor of 10.

as in iteration 12 to 14. It also shows the change of the deformation as can seen based on the values for J_q up to the final maximum value 1.055.

Influence of increasing the parameter α

In order to investigate the influence of α, we first increase α to 10^{-2}. Table 4.6 indicates the corresponding results. In (a), we see that the BFGS method from Algorithm 4.4 takes 9 to 11 iterations in every setting. With higher number of DoFs, the number of iterations remains 9. The difference between the target value λ_* and the eigenvalue after the last iteration λ_{it} has a difference about $5 \cdot 10^{-5}$. The cost functional J is in all cases smaller than 10^{-6} and the method converges in every setting with r_{rel} smaller than 10^{-7}.

Furthermore, (b) shows the results of the gradient method from Algorithm 4.3. In contrast to the initial example, where $\alpha = 10^{-3}$, the method converges here in every setting to r_{rel} smaller than 10^{-5}. The number of iterations varies, but seems to stay similar with the number of DoFs high enough. The values for λ_{it}, the cost functional and the minimum and maximum value of the determinant of the deformation gradient J_q are comparable to the results of the BFGS method.

Increasing α again, now to $\alpha = 10^{-1}$, has the consequence that the BFGS method converges in every setting after 7 iterations. The gradient method converges to the desired termination tolerance, the number of iterations varies again regarding the choice of lowest order Nédélec elements and first order Lagrange

Table 4.5. Freeform optimization steps of the BFGS method from Algorithm 4.4 on a rectangle domain with target value $\lambda_* = 3.8$ and regularization parameters $\alpha = 10^{-3}$ and $\beta = 10^{-5}$. The chosen refinement level is 5, the number of DoFs is 20995. Lagrange elements of order 2 and Nédélec elements of order 1 are used. The table shows the results of each iteration with the first (numerical) eigenvalue after each iteration λ_{it}, the number of line search steps (l.s.) and if a damping step has been carried out as well as the minimum and maximum value of the determinant of the deformation gradient J_q.

It.	λ_{it}	J	r_{rel}	l.s.	damping	$\mathrm{J}_{q,\min}$	$\mathrm{J}_{q,\max}$
0	4	2.0e-02	1	-	-	1	1
1	3.91852	7.02392e-03	5.77674e-01	5	yes	1.01789	1.01951
2	3.82679	3.58976e-04	1.26861e-01	4	yes	1.03951	1.04332
3	3.78714	8.30135e-05	6.02336e-02	3	yes	1.05016	1.05541
4	3.7909	4.16852e-05	4.26706e-02	3	yes	1.04769	1.05406
5	3.79625	7.27752e-06	1.76422e-02	2	yes	1.04769	1.05266
6	3.80067	4.25193e-07	3.11648e-03	2	yes	1.04947	1.05474
7	3.80047	2.93789e-07	2.19684e-03	1	no	1.05016	1.05537
8	3.80022	1.80904e-07	1.00124e-03	1	no	1.05122	1.05625
9	3.80014	1.56216e-07	6.28121e-04	1	no	1.05157	1.0564
10	3.80013	1.42751e-07	5.70674e-04	1	no	1.05148	1.05606
11	3.80011	1.32559e-07	5.12433e-04	1	no	1.05106	1.05535
12	3.80008	1.29592e-07	3.64495e-04	5	yes	1.05107	1.05536
13	3.79999	1.26622e-07	5.70519e-05	4	yes	1.05109	1.05538
14	3.8	1.26571e-07	3.74452e-05	4	yes	1.05109	1.05538
15	3.8	1.26459e-07	6.08468e-06	3	no	1.05109	1.05538

elements. In constrast, the number of iterations stays stable at 278 by using first order Nédélec elements and second order Lagrange elements. In both methods, the difference between the target value λ_* and the eigenvalue after the last iteration λ_{it} increases again, now to a difference about $5 \cdot 10^{-4}$. Moreover, the minimum and maximum value of the determinant of the deformation gradient J_q are similar to the previous examples, whereas the values of the cost functional increase by a factor of 10. For the results for $\alpha = 10^{-1}$ and $\beta = 10^{-5}$, we refer to Table A.4 in Appendix A.2.1.

Influence of decreasing the parameter α

Now, we investigate the influence of decreasing α to 10^{-4} and keeping $\beta = 10^{-5}$. The results are shown in Table 4.7, where (a) indicates that the number of iterations until convergence in the BFGS method increases up to 39 and stays the same for meshes of at least 1411 DoFs. In (b), the table shows that the gradient method terminates in every setting after 1000 iterations with a

Table 4.6. Results of a freeform optimization for the first eigenvalue on a rectangle domain with target value $\lambda_* = 3.8$ and regularization parameters $\alpha = 10^{-2}, \beta = 10^{-5}$ for the tolerance of the termination criteria of $\text{TOL}_{\text{global}} = \text{TOL} = 10^{-5}$. The tables show results varying the DoFs of the mesh, the refinement level (ref.), the order of Lagrange (Lagr.) and Nédélec (Néd.) elements. The initial first (numerical) eigenvalue is given by λ_0. We show the eigenvalue λ_{it} after termination of the method and the resulting value of the cost functional J, the relative residual of the gradient of the cost functional r_{rel} as well as the minimum and maximum value of the determinant of the deformation gradient J_q and the used eigenvalue solver EVS.

(a) BFGS method from Algorithm 4.4

DoFs	ref.	Lagr.	Néd.	λ_0	it.	λ_{it}	J	r_{rel}	$J_{q,\text{min}}$	$J_{q,\text{max}}$	EVS
387	2	2	1	4.002	9	3.80005	4.933e-06	3.186e-07	1.021	1.050	A
387	3	1	0	4.052	10	3.80007	7.775e-06	1.852e-06	1.049	1.056	A
1411	3	2	1	4.000	9	3.80005	4.836e-06	3.389e-07	1.033	1.050	A
1411	4	1	0	4.013	11	3.80006	5.497e-06	1.155e-07	1.048	1.050	A
5389	4	2	1	4.000	9	3.80005	4.829e-06	4.305e-07	1.042	1.050	A
5389	5	1	0	4.003	9	3.80005	4.992e-06	9.733e-07	1.049	1.049	A
20995	5	2	1	4.000	9	3.80005	4.829e-06	4.325e-07	1.046	1.050	A

(b) Gradient method from Algorithm 4.3

DoFs	ref.	Lagr.	Néd.	λ_0	it.	λ_{it}	J	r_{rel}	$J_{q,\text{min}}$	$J_{q,\text{max}}$	EVS
387	2	2	1	4.002	171	3.80005	4.939e-06	9.972e-06	1.020	1.049	A
387	3	1	0	4.052	24	3.80007	7.781e-06	8.332e-06	1.048	1.055	A
1411	3	2	1	4.000	215	3.80005	4.841e-06	9.960e-06	1.032	1.049	A
1411	4	1	0	4.013	39	3.80006	5.503e-06	9.892e-06	1.047	1.049	A
5389	4	2	1	4.000	215	3.80005	4.835e-06	9.964e-06	1.041	1.049	A
5389	5	1	0	4.003	171	3.80005	4.998e-06	9.922e-06	1.048	1.048	A
20995	5	2	1	4.000	215	3.80005	4.835e-06	9.967e-06	1.045	1.049	A

relative residual around $1.3 \cdot 10^{-5}$, except in case of the example with 387 DoFs, refinement level 3 and lowest order Nédélec elements as well as first order Lagrange elements. Here, the method terminates after 33 iterations. For both methods, the eigenvalue after the last iteration λ_{it} is in every setting equal to the target value λ_*. Moreover, the maximum values of the determinant of the deformation gradient J_q increase for the BFGS method up to 1.118, whereas it stays around 1.055 for the gradient method. The values for the latter are similar to the values we obtained in the previous examples. Decreasing α further to 10^{-5} stabilizes the number of iterations using the BFGS method to 38 iterations in every setting. We notice that the value for J_q increases, e.g., in the last setting from maximum values 1.100 to 1.187. The gradient method

Table 4.7. Results of a freeform optimization for the first eigenvalue on a rectangle domain with target value $\lambda_* = 3.8$ and regularization parameters $\alpha = 10^{-4}, \beta = 10^{-5}$ for the tolerance of the termination criteria of $\text{TOL}_{\text{global}} = \text{TOL} = 10^{-5}$. The tables show results varying the DoFs of the mesh, the refinement level (ref.), the order of Lagrange (Lagr.) and Nédélec (Néd.) elements. The initial first (numerical) eigenvalue is given by λ_0. We show the eigenvalue λ_{it} after termination of the method and the resulting value of the cost functional J, the relative residual of the gradient of the cost functional as well as the minimum and maximum value of the determinant of the deformation gradient J_q and the used eigenvalue solver EVS.

(a) BFGS method from Algorithm 4.4

DoFs	ref.	Lagr.	Néd.	λ_0	it.	$\lambda_{\text{it.}}$	J	r_{rel}	$J_{q,\min}$	$J_{q,\max}$	EVS
387	2	2	1	4.002	28	3.8	-8.012e-07	9.265e-06	1.052	1.096	A
387	3	1	0	4.052	15	3.8	-7.024e-07	9.154e-06	1.076	1.078	A
1411	3	2	1	4.000	38	3.8	-8.522e-07	5.787e-06	1.083	1.102	A
1411	4	1	0	4.013	38	3.8	-9.004e-07	5.049e-06	1.102	1.118	A
5389	4	2	1	4.000	38	3.8	-8.499e-07	8.020e-06	1.093	1.102	A
5389	5	1	0	4.003	39	3.8	-8.385e-07	9.670e-06	1.092	1.097	A
20995	5	2	1	4.000	38	3.8	-8.497e-07	8.051e-06	1.097	1.100	A

(b) Gradient method from Algorithm 4.3

DoFs	ref.	Lagr.	Néd.	λ_0	it.	$\lambda_{\text{it.}}$	J	r_{rel}	$J_{q,\min}$	$J_{q,\max}$	EVS
387	2	2	1	4.002	1000	3.8	-2.845e-07	1.346e-05	1.020	1.049	A
387	3	1	0	4.052	33	3.8	-3.312e-07	9.997e-06	1.048	1.055	A
1411	3	2	1	4.000	1000	3.8	-2.822e-07	1.376e-05	1.032	1.049	A
1411	4	1	0	4.013	1000	3.8	-2.966e-07	1.233e-05	1.047	1.049	A
5389	4	2	1	4.000	1000	3.8	-2.821e-07	1.379e-05	1.041	1.049	A
5389	5	1	0	4.003	1000	3.8	-2.857e-07	1.340e-05	1.048	1.049	A
20995	5	2	1	4.000	1000	3.8	-2.821e-07	1.378e-05	1.045	1.050	A

does not improve with this choice of regularization parameters. For details, we refer to Table A.5.

Influence of decreasing the parameter β

Now, coming back to the initial example, where we chose the regularization parameters $\alpha = 10^{-3}$ and $\beta = 10^{-5}$, we investigate the influence of β on the optimization methods. Table 4.8 shows results after decreasing β to 10^{-8}. In (a), the table indicates that the change of β has nearly no influence on the number of iterations for the BFGS method compared to the initial example. Furthermore, table (b) shows the results for the gradient method. Here, the method converges after 25 to 26 iterations in every setting. In comparison, the initial example

terminated in almost every setting after the maximal number of iterations, which we set to $\text{it}_{\max} = 1000$. In both methods, the difference between the eigenvalue after the last iteration λ_{it} and the target value λ_* is in every setting between 10^{-5} and 0. The values of the determinant of the deformation gradient J_q stay similar to the values of the initial example and the values for the cost functional are less than $5 \cdot 10^{-7}$.

By keeping $\beta = 10^{-8}$ and decreasing α to 10^{-4}, see Table A.6, or 10^{-5}, see Table A.7, the BFGS method converges after 13 to 15 iterations in all settings. It has almost no influence on the value of J_q and the eigenvalue converges in every setting to the target value λ_*. The gradient method converges in both examples again after 25 to 26 iterations in every setting. Moreover, the eigenvalue after the last iteration λ_{it} is equal to the target value λ_*, the values of the reduced cost functional shrink by decreasing β and the values for the determinant of the deformation gradient J_q stay similar to the ones in the initial example.

Table A.8 shows results for $\beta = 10^{-8}$ and increasing α to 10^{-2}, and Table A.9 shows results for increasing α further to 10^{-1}, respectively. In both subtables (a), we observe for the BFGS method that the number of iterations until convergence decreases down to 9 for $\alpha = 10^{-2}$ and 7 for $\alpha = 10^{-1}$, respectively. The gradient method, see each in (b), converges for 10^{-2} after 25 iterations in every setting. By increasing α to 10^{-1} the number of iterations increases to at least 344 for every setting. In both methods, the difference between the eigenvalue after the last iteration λ_{it} and the target value λ_* increases from 10^{-5} to more than $5 \cdot 10^{-4}$ by increasing α. For the values of the determinant of the deformation gradient J_q we do not observe any change.

Influence of increasing the parameter β

In the following, we investigate the influence of increasing β to 10^{-3} on the optimization methods. The results are shown in Table 4.9. In (a), we observe that the BFGS method stops after the maximum number of iterations, which we set to 100 with r_{res} varying between $7 \cdot 10^{-5}$ and 10^{-3}. We identify that the values of $J_{q,\min}$ and $J_{q,\max}$ increase up to 1.812 and 1.91 for the last setting. This implies an increase in volume of the domain. Besides that, the gradient method, see (b), terminates in every setting after the maximum number of iterations with a relative residuum higher than 10^{-3} and a difference between the eigenvalue λ_{it} and the target value λ_* is about 10^{-5}. The values of $J_{q,\min}$ and $J_{q,\max}$ are around 1.065.

Table 4.8. Results of a freeform optimization for the first eigenvalue on a rectangle domain with target value $\lambda_* = 3.8$ and regularization parameters $\alpha = 10^{-3}, \beta = 10^{-8}$ for the tolerance of the termination criteria of $\text{TOL}_{\text{global}} = \text{TOL} = 10^{-5}$. The tables show results varying the DoFs of the mesh, the refinement level (ref.), the order of Lagrange (Lagr.) and Nédélec (Néd.) elements. The initial first (numerical) eigenvalue is given by λ_0. We show the eigenvalue λ_{it} after termination of the method and the resulting value of the cost functional J, the relative residual of the gradient of the cost functional as well as the minimum and maximum value of the determinant of the deformation gradient J_q and the used eigenvalue solver EVS.

(a) BFGS method from Algorithm 4.4

DoFs	ref.	Lagr.	Néd.	λ_0	it.	λ_{it}	J	r_{rel}	$J_{q,\min}$	$J_{q,\max}$	EVS
387	2	2	1	4.002	13	3.80001	5.563e-07	8.762-06	1.017	1.054	A
387	3	1	0	4.052	10	3.80001	7.659e-07	8.597e-06	1.050	1.057	A
1411	3	2	1	4.000	15	3.8	5.350e-07	6.796e-06	1.034	1.055	A
1411	4	1	0	4.013	15	3.8	6.081e-07	5.678e-06	1.049	1.051	A
5389	4	2	1	4.000	15	3.8	5.383e-07	5.704e-06	1.043	1.053	A
5389	5	1	0	4.003	15	3.8	5.558e-07	5.664e-06	1.051	1.051	A
20995	5	2	1	4.000	15	3.8	5.382e-07	5.382e-07	1.048	1.053	A

(b) Gradient method from Algorithm 4.3

DoFs	ref.	Lagr.	Néd.	λ_0	it.	λ_{it}	J	r_{rel}	$J_{q,\min}$	$J_{q,\max}$	EVS
387	2	2	1	4.002	25	3.80001	5.268e-07	9.895e-06	1.020	1.049	A
387	3	1	0	4.052	26	3.80001	8.019e-07	7.749e-06	1.048	1.055	A
1411	3	2	1	4.000	25	3.80001	5.167e-07	9.788e-06	1.032	1.049	A
1411	4	1	0	4.013	26	3.80001	5.849e-07	6.575e-06	1.047	1.049	A
5389	4	2	1	4.000	25	3.80001	5.161e-07	9.781e-06	1.041	1.049	A
5389	5	1	0	4.003	25	3.80001	5.328e-07	9.906e-06	1.048	1.048	A
20995	5	2	1	4.000	25	3.80001	5.161e-07	9.780e-06	1.045	1.049	A

By fixing $\beta = 10^{-3}$ and decreasing α to 10^{-4}, see Table A.10, and 10^{-5}, see Table A.11, the BFGS method stops again after the maximum number of iterations, see (a) each. The value of the determinant of the deformation gradient J_q increases and varies a lot in these settings. For the last setting, we obtain a maximum value of 3.23. Moreover, with these choices of parameters, the gradient method terminates after the maximal number of iterations with a relative residual larger than 10^{-3}, see (b) each. For both choices of α, the maximum value of the determinant of the deformation gradient is 1.066.

Finally, by keeping $\beta = 10^{-3}$ and increasing α to 10^{-2}, see Table A.12, and $\alpha = 10^{-1}$, see Table A.13, the BFGS method terminates for the first choice of parameters with an inconsistent number of iterations between 21 and 79 with

Table 4.9. Results of a freeform optimization for the first eigenvalue on a rectangle domain with target value $\lambda_* = 3.8$ and regularization parameters $\alpha = 10^{-3}, \beta = 10^{-3}$ for the tolerance of the termination criteria of $\text{TOL}_{\text{global}} = \text{TOL} = 10^{-5}$. The tables show results varying the DoFs of the mesh, the refinement level (ref.), the order of Lagrange (Lagr.) and Nédélec (Néd.) elements. The initial first (numerical) eigenvalue is given by λ_0. We show the eigenvalue λ_{it} after termination of the method and the resulting value of the cost functional J, the relative residual of the gradient of the cost functional as well as the minimum and maximum value of the determinant of the deformation gradient J_q and the used eigenvalue solver EVS.

(a) BFGS method from Algorithm 4.4

DoFs	ref.	Lagr.	Néd.	λ_0	it.	$\lambda_{\text{it.}}$	J	r_{rel}	$J_{q,\min}$	$J_{q,\max}$	EVS
387	2	2	1	4.002	100	3.80139	-8.058e-04	4.311e-03	1.91504	2.0232	B
387	3	1	0	4.052	100	3.79999	-8.663e-04	7.572e-05	2.562	2.595	A
1411	3	2	1	4.000	100	3.79961	-8.179e-04	1.170e-03	2.019	2.059	B
1411	4	1	0	4.013	100	3.80003	-7.296e-04	4.923e-04	1.851	2.011	B
5389	4	2	1	4.000	100	3.79987	-7.694e-04	5.344e-04	1.934	1.934	B
5389	5	1	0	4.003	100	3.79974	-5.509e-04	1.026e-03	1.504	1.692	B
20995	5	2	1	4.000	100	3.8009	-5.433e-04	3.002e-03	1.812	1.910	A

(b) Gradient method from Algorithm 4.3

DoFs	ref.	Lagr.	Néd.	λ_0	it.	$\lambda_{\text{it.}}$	J	r_{rel}	$J_{q,\min}$	$J_{q,\max}$	EVS
387	2	2	1	4.002	1000	3.80003	-9.702e-05	1.327e-03	1.061	1.065	A
387	3	1	0	4.052	1000	3.79953	-1.048e-04	1.352e-03	1.074	1.075	A
1411	3	2	1	4.000	1000	3.80004	-9.673e-05	1.366e-03	1.063	1.065	A
1411	4	1	0	4.013	1000	3.80001	-9.872e-05	1.172e-03	1.067	1.068	A
5389	4	2	1	4.000	1000	3.80004	-9.671e-05	1.369e-03	1.064	1.065	A
5389	5	1	0	4.003	1000	3.80003	-9.721e-05	1.315e-03	1.066	1.066	A
20995	5	2	1	4.000	1000	3.80004	-9.6711e-05	1.369e-03	1.064	1.065	A

a difference between the eigenvalue λ_{it} and the target value λ_* of about $2 \cdot 10^{-4}$ and the maximum value of the determinant of the deformation gradient is up to 1.115. In contrast, for $\alpha = 10^{-1}$ the method results in good values with a convergence after 7 to 8 iterations with values of the determinant of the deformation gradient around 1.05. However, the difference between the eigenvalue λ_{it} and the target value λ_* is at least $3.7 \cdot 10^{-4}$. The gradient method, see (b) each, terminates for both choices of α after the maximum number of iterations. With increasing α, also the difference between the eigenvalue λ_{it} and the target value λ_* increases. The residua for $\alpha = 10^{-2}$ are in the range of 10^{-3} and, for $\alpha = 10^{-1}$, they are in the range of $2.5 \cdot 10^{-5}$, respectively. The values of the determinant of the deformation gradient of the first choice of α are around 1.063,

whereas for the second around 1.053. The values for the latter are closer to the ones of the initial example.

Conclusion of the variation of the regularization parameters

In general, the BFGS method provides better results than the gradient method. For the BFGS method, we observe that this example converges to the desired termination tolerance by choosing $\beta \geq 10^{-5}$ or $\beta = 10^{-3}$, $\alpha \geq 10^{-2}$. For other combinations of parameter α and β, the method stops after the maximum number of iterations. Additionally, in these cases, we observe a significant increase of the values of J_q. This indicates an enormous growth of the corresponding domain. Furthermore, we notice that an increase of the parameter α means a reduction of the number of iterations until the method terminates. This holds for a decrease of the parameter β as well. Besides reducing the number of iterations, increasing α also influences the difference between the eigenvalue after the last iteration and the target value, which increases. In the context of eigenvalue optimization in an electromagnetic setting, where we wish to obtain accurate frequencies, we would not decide to chose an α as large as possible. Here, the optimized eigenvalue is not exactly the target value. We have to weigh up between the speed of the method and the accuracy of the eigenvalue. Moreover, the influence of the parameter β is stronger the smaller the choice of α. By taking $\alpha \geq 10^{-3}$, a choice of β between 10^{-5} and 10^{-8} does not have much influence on the optimization results. Finally, we conclude that for the BFGS method the choice of parameters of our initial example, where $\alpha = 10^{-3}$ and 10^{-5}, is already a good choice for the method.

We observed that the gradient method does not converge in the most examples. Nevertheless, we obtain convergence of the method in several settings. We observe the convergence of the gradient method mainly for the choice of $\beta = 10^{-8}$ and the number of iterations stays between 25 and 26 iterations for a choice of $\alpha \leq 10^{-2}$. Furthermore, we notice that increases of β lead to a slight increase in the values of J_q. Finally, even with obtaining convergence for the gradient method, we prefer the BFGS method because it performs better in general.

Visualization of the variation of the regularization parameters

After the discussion of the influence of the regularization parameters for the BFGS method from Algorithm 4.4 and the gradient method from Algorithm 4.3, we visualize the deformed domains after the last iteration for the setting

with 20995 DoFs, refinement level 5 and the choice of first order Nédélec elements and second order Lagrange elements. Figure 4.7 shows the results for the BFGS method and Figure 4.8 for the gradient method, respectively.

The influence of the regularization parameters on the BFGS method can be clearly seen in the solution figure. Taking the initial example with a choice of regularization parameters $\alpha = 10^{-3}$ and $\beta = 10^{-5}$, we observe that the main deformation is the contraction in the vertical center of the domain. This deformation of the domain runs through the examples taking $\beta = 10^{-5}$ or $\beta = 10^{-8}$. In these cases, the parameter α influences for $\beta = 10^{-5}$ the width of the domain and, in both cases, the smoothness of the boundaries. Moreover, taking $\beta = 10^{-3}$ shows that the regularization part of the barrier term has an high impact on the deformation for the case where $\alpha = 10^{-1}$. Here, the domain change behaves similar to the ones by taking a smaller choice for β. In the other cases, we observe that the domain deforms more, the smaller the choice of α. This is consistent with the numerical examples of the discussion above.

In contrast, the influence of the regularization parameters on the gradient descent method has less impact on the deformation. Similar to the BFGS method, the main deformation of the examples with the choice of $\beta = 10^{-5}$ or $\beta = 10^{-8}$ is the contraction in the vertical center of the domain. Taking $\beta = 10^{-3}$ has the consequence that the domain expands on the vertical center except for the choice $\alpha = 10^{-1}$. Here, the domain deformation behaves as in the examples with taking smaller β.
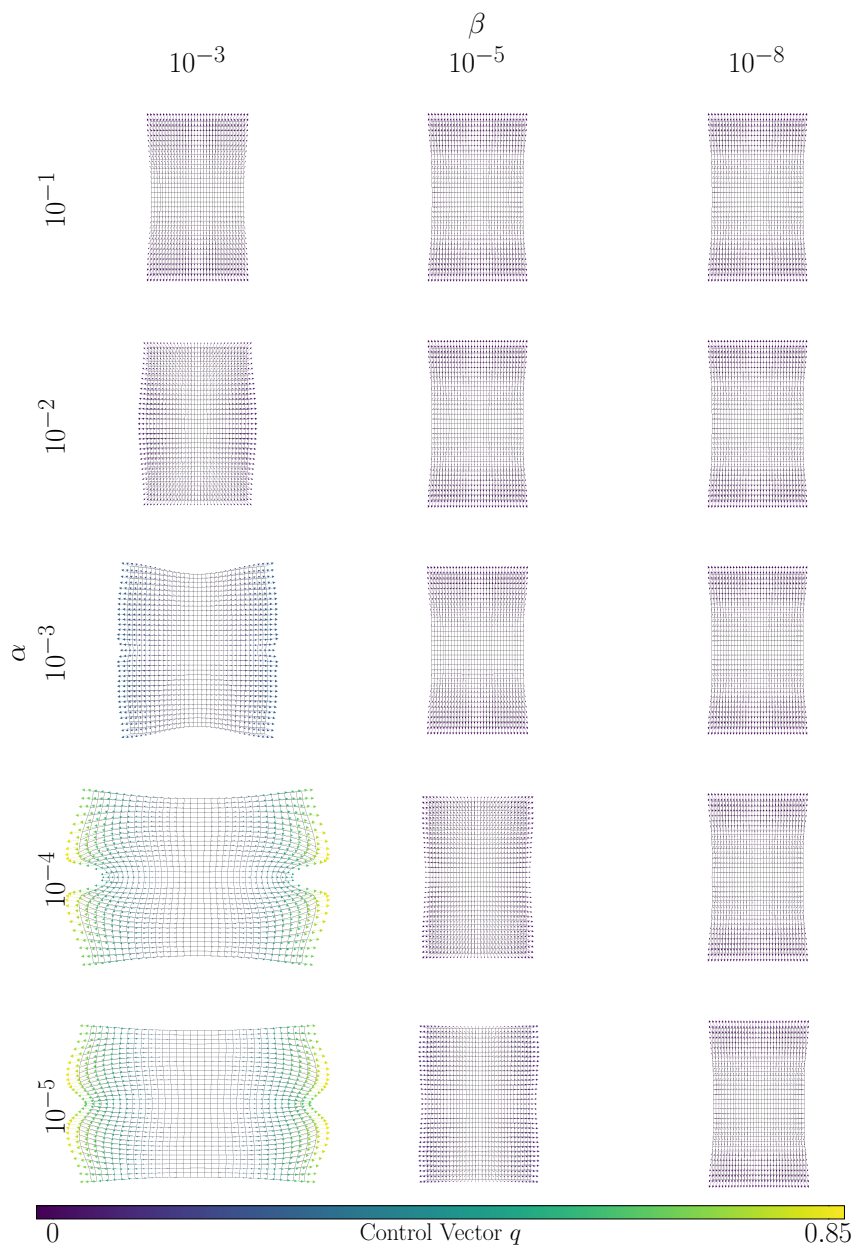
Figure 4.7. Influence of the regularization parameters regarding to the deformed rectangle after freeform optimization using the Damped Inverse BFGS method with target value $\lambda_* = 3.8$. The chosen refinement level is 5, the number of DoFs is 20995 and Lagrange elements of order 2 and first order Nédélec elements are used. The first (numerical) eigenvalue before optimization is $\lambda_0 = 4.0$.

Figure 4.8. Influence on the regularization parameters regarding to the deformed rectangle after freeform optimization using the gradient method with target value $\lambda_* = 3.8$. The chosen refinement level is 5, the number of DoFs is 20995 and Lagrange elements of order 2 and first order Nédélec elements are used. The first (numerical) eigenvalue before optimization is $\lambda_0 = 4.0$.
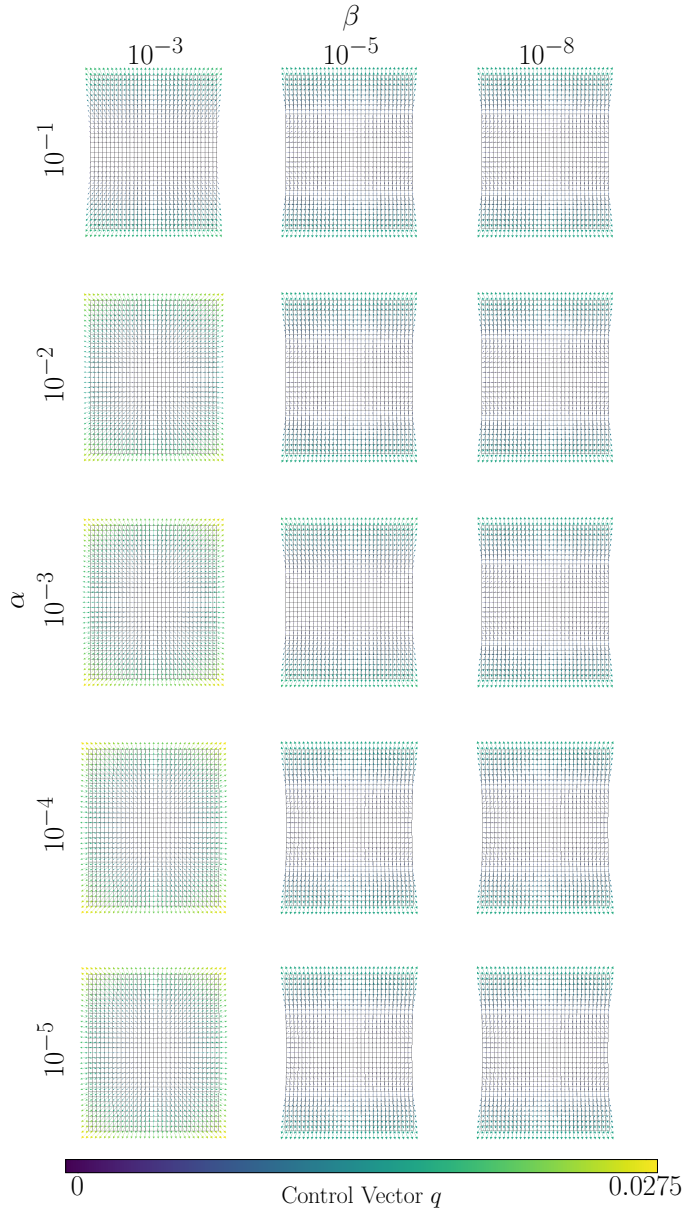
4.4.1.2. BFGS Method with reduction of the termination tolerance

In most of the previous examples, we observe that the gradient method runs out of the chosen maximum number of iterations whereas the BFGS method converges in a few iteration steps. Now, we show the possibility for the BFGS method to reach higher accuracy in sense of a decreasing tolerance for the termination criteria exemplary on the initial example. Therefore, we keep the settings from Table 4.3 with the exception of changing the tolerances $\text{TOL}_{\text{global}}$ and TOL. In these examples, we use the subspace iteration in order to solve the concerning eigenvalue problems. Table 4.10 shows results of the initial example using the BFGS method with varying the choices of termination tolerances, namely

(a) $\text{TOL}_{\text{global}} = \text{TOL} = 10^{-5}$ (initial example),

(b) $\text{TOL}_{\text{global}} = \text{TOL} = 10^{-7}$,

(c) $\text{TOL}_{\text{global}} = \text{TOL} = 10^{-8}$.

We remember the initial example with a tolerance 10^{-5}, see (a), where the method terminates after 15 iterations in every setting with an eigenvalue λ_{it} equal to λ_*. In (b), we observe that the method converges for a tolerance 10^{-7} in every setting but the required number of iterations varies. It seems that with a higher number of DoFs and with the choice of first order Nédélec elements and second order Lagrange elements, the number of iterations stabilizes. In (c) the method converges in mostly every setting to the required tolerance, except for the setting with 5389 DoFs, lowest order Nédélec elements and first order Lagrange elements, as well for the setting with 1411 DoFs, first order Nédélec elements and second order Lagrange elements. Here, it stopped after the maximum number of iterations. Similar to (b), it seems that with a higher number of DoFs and with the choice of first order Nédélec elements and second order Lagrange elements, the number of iterations stabilizes. Furthermore, values of the cost functional J as well as the minimum and maximum values of the determinant of the deformation gradient J_q converge against the same values, see (b) compared with (c). Figure 4.9 shows the deformed upper half of the rectangle domain for the choice of termination tolerances of 10^{-5} in (a) and 10^{-7} in (b). The deformation in both examples behaves similar. In (a) the deformation in the upper corners is slightly stronger than in (b). Moreover, the alignment of the displacement vectors in the lower part of the domain are slightly different.

Table 4.10. Results of a freeform optimization for the first eigenvalue on a rectangle domain with target value $\lambda_* = 3.8$ by using the BFGS method from Algorithm 4.4 with regularization parameters $\alpha = 10^{-3}$ and $\beta = 10^{-5}$ and varying the tolerances of the termination criteria $\mathrm{TOL}_{\mathrm{global}}$ and TOL. The tables show results varying the DoFs of the mesh, the refinement level (ref.), the order of Lagrange (Lagr.) and Nédélec (Néd.) elements. The initial first (numerical) eigenvalue is given by λ_0. We show the eigenvalue λ_{it} after termination of the method and the resulting value of the cost functional J, the relative residual of the gradient of the cost functional as well as the minimum and maximum value of the determinant of the deformation gradient J_q and the used eigenvalue solver EVS.

(a) $\mathrm{TOL}_{\mathrm{global}} = \mathrm{TOL} = 10^{-5}$

DoFs	ref.	Lagr.	Néd.	λ_0	it.	$\lambda_{\mathrm{it.}}$	J	r_{rel}	$\mathrm{J}_{q,\mathrm{min}}$	$\mathrm{J}_{q,\mathrm{max}}$	EVS
387	2	2	1	4.002	15	3.8	1.128e-07	3.44e-06	1.030	1.057	A
387	3	1	0	4.052	15	3.8	3.522e-07	5.499e-06	1.031	1.054	A
1411	3	2	1	4.000	15	3.8	1.081e-07	3.923e-06	1.042	1.058	A
1411	4	1	0	4.013	15	3.8	1.752e-07	5.818e-06	1.053	1.055	A
5389	4	2	1	4.000	15	3.8	1.265e-07	6.084e-06	1.047	1.055	A
5389	5	1	0	4.003	15	3.8	1.381e-07	6.012e-06	1.053	1.053	A
20995	5	2	1	4.000	15	3.8	1.265e-07	6.085e-06	1.051	1.055	A

(b) $\mathrm{TOL}_{\mathrm{global}} = \mathrm{TOL} = 10^{-7}$

DoFs	ref.	Lagr.	Néd.	λ_0	it.	$\lambda_{\mathrm{it.}}$	J	r_{rel}	$\mathrm{J}_{q,\mathrm{min}}$	$\mathrm{J}_{q,\mathrm{max}}$	EVS
387	2	2	1	4.002	69	3.8	1.087e-07	6.554e-08	1.031	1.054	A
387	3	1	0	4.052	47	3.80001	3.201e-07	6.622e-08	1.055	1.060	A
1411	3	2	1	4.000	68	3.8	1.018e-07	9.680e-08	1.040	1.054	A
1411	4	1	0	4.013	49	3.8	1.492e-07	5.870e-08	1.053	1.054	A
5389	4	2	1	4.000	47	3.8	1.013e-07	4.380e-08	1.047	1.054	A
5389	5	1	0	4.003	67	3.8	1.129e-07	7.175e-07	1.053	1.053	A
20995	5	2	1	4.000	47	3.8	1.013e-07	3.914e-08	1.051	1.054	A

(c) $\mathrm{TOL}_{\mathrm{global}} = \mathrm{TOL} = 10^{-8}$

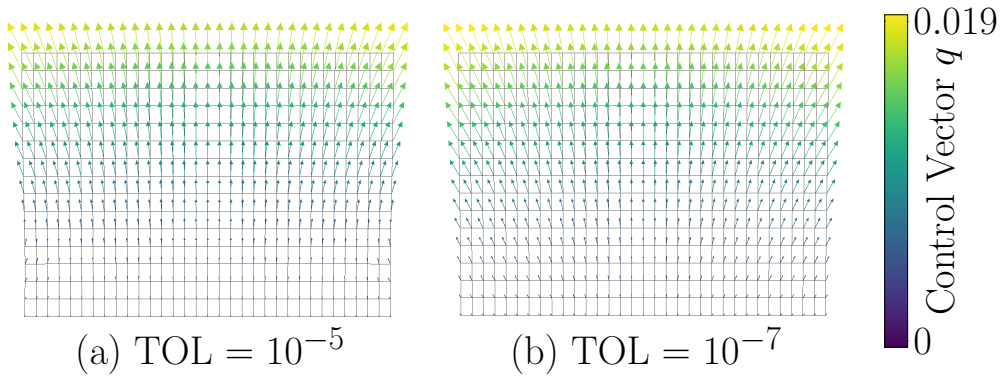| DoFs	ref.	Lagr.	Néd.	λ_0	it.	$\lambda_{\mathrm{it.}}$	J	r_{rel}	$\mathrm{J}_{q,\mathrm{min}}$	$\mathrm{J}_{q,\mathrm{max}}$	EVS
387	2	2	1	4.002	69	3.8	1.087e-07	<1.0e-08	1.031	1.054	A
387	3	1	0	4.052	57	3.80001	3.201e-07	<1.0e-08	1.055	1.060	A
1411	3	2	1	4.000	100	3.8	1.018e-07	3.448e-08	1.040	1.054	A
1411	4	1	0	4.013	58	3.8	1.492e-07	<1.0e-08	1.053	1.054	A
5389	4	2	1	4.000	69	3.8	1.013e-07	<1.0e-08	1.047	1.054	A
5389	5	1	0	4.003	100	3.8	1.129e-07	3.481e-07	1.053	1.053	A
20995	5	2	1	4.000	65	3.8	1.013e-07	<1.0e-08	1.051	1.054	A

Figure 4.9. Comparison the tolerance of the termination criteria of the deformed rectangle domain after freeform optimization with BFGS method with target value $\lambda_* = 3.8$ and regularization parameters $\alpha = 10^{-3}$ and $\beta = 10^{-5}$. The solution is symmetric to the lower half.

4.4.1.3. Influence of the Choice of the Target Value λ_* on the Domain Deformation

In the following examples, we compare the influence of the choice of the target value λ_* on the deformation of the rectangle domain. To this end, we consider the initial example with the choice of regularization parameters $\alpha = 10^{-3}$ and $\beta = 10^{-5}$, the settings from Table 4.3 with termination tolerances $\text{TOL}_{\text{global}} = \text{TOL} = 10^{-7}$. In these examples, we use the subspace iteration in order to solve the concerning eigenvalue problems. In the following, we consider two different refinement levels and a discretization with first order Nédélec elements and second order Lagrange elements. With that, we vary the target value λ_* to 3.95, 4.05 and 4.20 and observe its influence on the domain deformation. The results are shown in Table 4.11 and visualized in Figure 4.10.

For all choices of the target value λ_*, the BFGS method converges with the chosen termination criteria. The target values $\lambda_* = 3.8$ and 3.95 are smaller than the eigenvalue of the initial eigenvalue $\lambda_0 = 4$. Here, we expect the same direction of deformation. Since the analytical first eigenvalue of a rectangle domain depend on the smallest value of width or hight, we expect in our example an shrinkage of the width (x-direction) and a growth of the height (y-direction). In both cases, the number of iterations is for both settings 47 and the eigenvalue after the last iteration λ_{it} is equal to λ_*. Comparing the minimum and maximum value of the

(a) $\lambda_* = 3.8$

(b) $\lambda_* = 3.95$
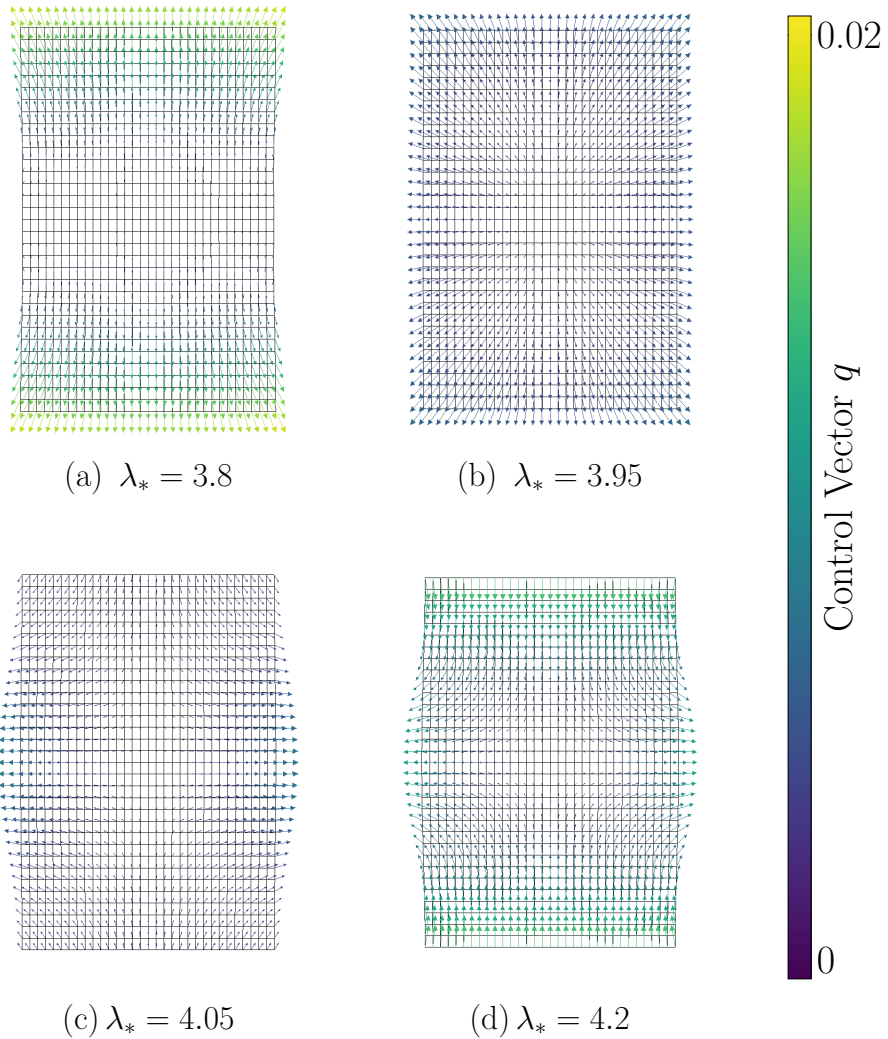
(c) $\lambda_* = 4.05$

(d) $\lambda_* = 4.2$

Figure 4.10. Deformation of a rectangle domain regarding a freeform optimization by using the BFGS method of Algorithm 4.4 with varying the chosen target value λ_* with regularization parameters $\alpha = 10^{-3}$ and $\beta = 10^{-5}$ and the tolerance of termination criteria of $\mathrm{TOL}_{\text{global}} = \mathrm{TOL} = 10^{-7}$. The chosen refinement level is 5, the number of DoFs is 20995. Lagrange elements of order 2 and Nédélec elements of order 1 are used and the initial first (numerical) eigenvalue is $\lambda_0 = 4$.

Table 4.11. Comparison of λ_* on the domain deformation of a freeform optimization on a rectangle domain by using the BFGS method from Algorithm 4.4 for $\alpha = 10^{-3}$ and $\beta = 10^{-5}$ and the tolerance of termination criteria of $\text{TOL}_{\text{global}} = \text{TOL} = 10^{-7}$. The initial first (numerical) eigenvalue is $\lambda_0 = 4$.

DoFs	ref.	Lagr.	Néd.	λ_*	it.	$\lambda_{\text{it.}}$	J	r_{rel}	$J_{q,\text{min}}$	$J_{q,\text{max}}$
5389	4	2	1	3.8	47	3.8	1.013e-07	4.380e-08	1.047	1.054
20995	5	2	1	3.8	47	3.8	1.013e-07	3.914e-08	1.051	1.054
5389	4	2	1	3.95	47	3.95	-1.382e-07	1.535e-07	1.016	1.016
20995	5	2	1	3.95	47	3.95	-1.382e-07	1.541e-07	1.016	1.016
5389	4	2	1	4.05	48	4.05	2.368e-08	1.461e-07	0.993	0.996
20995	5	2	1	4.05	38	4.05	2.370e-08	2.187e-07	0.993	0.994
5389	4	2	1	4.2	30	4.1999	6.919e-07	9.559e-08	0.960	0.969
20995	5	2	1	4.2	30	4.1999	6.912e-07	9.737e-08	0.960	0.964

determinant of the deformation gradient J_q, we observe that the optimization to the target value $\lambda_* = 3.8$ has a greater influence on the domain deformation than optimizing to $\lambda_* = 3.95$. In the first case, it is $J_{q,\text{max}} = 1.054$ and in the second case, it is $J_{q,\text{max}} = 1.016$, which means that in both cases the volume of the domain grows. It is expected that the greater difference between the initial eigenvalue and the target value impacts a greater deformation than the smaller one. The visualization of the two examples are shown in Figure 4.10 (a) and (b). It indicates that in (a) the rectangle expands on the top and bottom of the domain, what results a shrinkage in x-direction and a growth in y-direction. In (b) the deformation is in general much smaller than in (a) and is constantly growing in every direction. This results, that (a) fulfills our expectations to the domain change whereas the deformation in (b) is so small that we cannot make any statement to the deformation of the domain.

The choice of a target values $\lambda_* = 4.05$ or 4.2 is larger than the initial eigenvalue. For $\lambda_* = 4.05$, the method converges after 48 or 38 iterations and the eigenvalue after the last iteration is equal to the target value. For $\lambda_* = 4.2$, it converges after 30 iterations for both settings. Here, the difference between the eigenvalue after the last iteration λ_{it} and the target value is 10^{-4}. Comparing the minimum and maximum value of the determinant of the deformation gradient J_q, the supposition is confirmed. For the first case, it is $J_{q,\text{max}} = 0.996$ or 0.994 and for the second case, it is $J_{q,\text{max}} = 0.969$ or 0.964. The volumes of the domains shrink and also, the closer to the initial value to the target value, the closer is the value of the determinant equal to 1. The visualization of the deformation of

the domain of these examples is shown in Figure 4.10 (c) and (d). In both cases, the domain shrinks in y-direction and grows in x-direction. This is an opposite behavior to (a). Further, we expect this behavior of domain change because by increasing the first eigenvalue, we expect a growth of the smaller side length. Moreover, the deformation in (d) is larger than in (b) as expected, because the difference of the target value to the initial value was bigger in this case.

4.4.2. Quarter Circle with Fixed Edges

In Section 4.4.1, we validated the code for the optimization methods from Algorithms 4.3 and 4.4 to solve the considered Maxwell's eigenvalue optimization problem depending on a domain mapping (4.36) on a simple freeform rectangle domain. In the following, we consider a more complicated setting. Now, the computational domain is a quarter circle with a radius π to verify if the code also works on curved edges. Furthermore, we increase the number of DoFs to obtain more precise results and fix boundaries on the domain by setting $q = 0$, see Figure 4.11. We show the results of various optimization examples to optimize the first eigenvalue $\lambda = \lambda_1$ to a chosen target value λ_*. For the methods, we use the settings shown in Table 4.12.
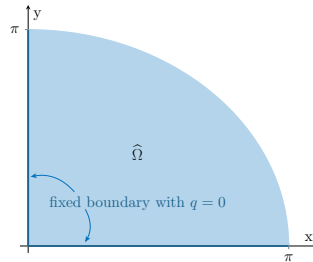

Figure 4.11. Quarter Circle Geometry

Similar to the examples on the rectangle, we show the first numerical eigenvalue before optimization, i.e. λ_0, which gets more precise by increasing the number of DoFs, which we increase by a higher refinement level of the mesh or by increasing the order of elements. In all these settings, we show the number of iterations (it.), the first eigenvalue after termination λ_{it}, the value of the cost functional J and r_{rel}. Further, we indicate the maximum and minimum values of

Table 4.12. Parameters for the optimization on the quarter circle

	BFGS method (Algorithm 4.4)	gradient method (Algorithm 4.3)
$\mathrm{it}_{\mathrm{max}}$	100	1000
$\mathrm{TOL}_{\mathrm{global}}$	10^{-6}	10^{-6}
TOL	10^{-6}	10^{-6}
Armijo condition		
line $\mathrm{it}_{\mathrm{max}}$	10	10
γ	0.1	0.1
ρ	0.1	0.1

the determinant of the deformation gradient, which provides information about the domain change. Again, we consider various settings, which optimize this eigenvalue to a target value λ_*.

In an initial example, we compare the gradient method from Algorithm 4.3 with the BFGS method from Algorithm 4.4. We note that, similar to the examples on the rectangle domain, that the gradient method converges really slow. Hence, we focus then on the BFGS method and show results on the influence of the regularization parameters on the deformation of the domain. Afterwards, we investigate the influence of the choice of different target values λ_*.

4.4.2.1. Comparison of the Optimization Methods

In the following, we compare the BFGS method from Algorithm 4.4 with the gradient method from Algorithm 4.3 on the considered quarter circle domain.

Initial Example: Comparison with $\alpha = 10^{-4}$ and $\beta = 10^{-6}$
We choose for the initial example the regularity parameters $\alpha = 10^{-4}$ and $\beta = 10^{-6}$. Table 4.13 shows results of the optimization, where (a) shows the results after optimization with the BFGS method and (b) the results of the gradient method. The BFGS method converges after 7 iterations for every setting with a relative residual of the reduced gradient smaller than $4.2 \cdot 10^{-6}$ with exception of the first setting, where the relative residual $9.8 \cdot 10^{-6}$. The minimum and maximum values of the determinant of the deformation gradient J_q is between 1.002 and 1.004. In comparison to that terminates the gradient method in every setting after the maximum number of iterations, which is set to 1000, with a relative residual bigger than $1.5 \cdot 10^{-4}$. Here, the minimum and maximum values of the determinant of the deformation gradient J_q is between 0.998

Table 4.13. Results of a freeform optimization on a quarter circle domain with fixed edges and target value $\lambda_* = 0.92$ and regularization parameters $\alpha = 10^{-4}, \beta = 10^{-6}$. The tables show results varying the DoFs of the mesh, the refinement level (ref.), the order of Lagrange (Lagr.) and Nédélec (Néd.) elements. The initial first (numerical) eigenvalue is given by λ_0. We show the eigenvalue λ_{it} after termination of the method and the resulting value of the cost functional J, the relative residual of the gradient of the cost functional as well as the minimum and maximum value of the determinant of the deformation gradient J_q and the used eigenvalue solver EVS.

(a) BFGS method from Algorithm 4.4

DoFs	ref.	Lagr.	Néd.	λ_0	it.	λ_{it}	J	r_{rel}	$J_{q,\min}$	$J_{q,\max}$	EVS
1059	3	1	0	0.9518	7	0.920028	3.827e-07	9.843e-06	1.002	1.004	A
4035	3	2	1	0.9467	7	0.920022	2.409e-07	3.063e-06	1.003	1.004	A
4035	4	1	0	0.9468	7	0.920022	2.483e-07	4.159e-06	1.003	1.004	A
15737	4	2	1	0.9455	7	0.920021	2.172e-07	3.016e-06	1.003	1.003	A
15737	5	1	2	0.9456	7	0.920021	2.190e-07	2.966e-06	1.003	1.003	A
62211	5	2	1	0.9453	7	0.92002	2.114e-07	3.097e-06	1.003	1.003	A

(b) Gradient method from Algorithm 4.3

DoFs	ref.	Lagr.	Néd.	λ_0	it.	λ_{it}	J	r_{rel}	$J_{q,\min}$	$J_{q,\max}$	EVS
1059	3	1	0	0.9518	1000	0.920027	3.954e-07	1.501e-04	0.998	1.000	A
4035	3	2	1	0.9467	1000	0.920022	2.540e-07	1.776e-04	0.999	1.000	A
4035	4	1	0	0.9468	1000	0.920022	2.613e-07	1.777e-04	0.999	1.000	A
15737	4	2	1	0.9455	1000	0.920021	2.303e-07	1.860e-04	0.999	1.000	A
15737	5	1	0	0.9456	1000	0.920021	2.322e-07	1.861e-04	1.000	1.000	A
62211	5	2	1	0.9453	1000	0.92002	2.246e-07	1.883e-04	1.000	1.000	A

and 1.00. In both settings, the difference between the eigenvalue after the last iteration λ_{it} and the target value λ_* is bigger than $2 \cdot 10^{-5}$ and the values of the cost functional are smaller than $4 \cdot 10^{-6}$.

Figure 4.12 visualizes the deformation of the quarter circles after optimization with both methods with the chosen regularization parameters for the refinement level 5, 62212 DoFs and a discretization of the domain with Lagrange elements of order 2 and Nédélec elements of order 1. After both optimization methods, the quarter circle is deformed by pulling apart the corners on the transition from the circular arc to the edges. Further, at the top right, the quarter circle is compressed. The difference between the deformations is, that in (a) the deformation on the transition from the circular arc to the edged is a little stronger than in (b), whereas the compression at the top right is minimal stronger in (b) than in (a).
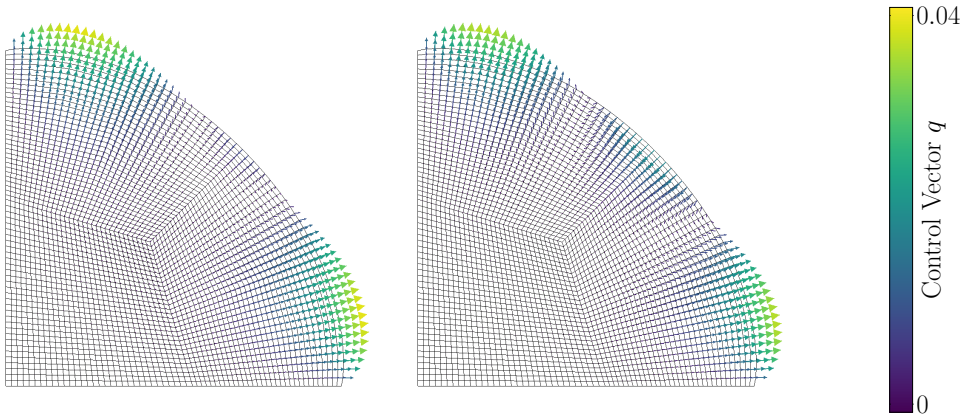
(a) BFGS method from Algorithm 4.4   (b) Gradient method from Algorithm 4.3

Figure 4.12. Comparison of the reduced optimization methods regarding to the deformed quarter circle domain after freeform optimization with target value $\lambda_* = 0.92$ and regularization parameters $\alpha = 10^{-4}, \beta = 10^{-6}$. The chosen refinement level is 5, the number of DoFs is 62211. Lagrange elements of order 2 and Nédélec elements of order 1 are used and the initial first (numerical) eigenvalue is $\lambda_0 = 0.945255$.

4.4.2.2. Comparison of Regularization Parameters on the BFGS Method

Compared to the BFGS method is the gradient method really slow in runtime. Furthermore, we obtain a better convergence results with the BFGS method. For that reason, we focus on the BFGS method in the following and refer to some selected results of the gradient method to Appendix A.2.2.

Influence of increasing the parameter α

In the following, we investigate in the influence of α on the deformation of the domain. Table 4.14 shows results of the optimization problem by increasing α to 10^{-3} and keeping β. The method converges after 5 or 6 iterations to an eigenvalue λ_{it} with a difference to the target value λ_* bigger than $2 \cdot 10^{-4}$ and a relative residual of the reduced gradient varies between 10^{-4} and 10^{-6}. The values for the determinant of the deformation gradient J_q are between 0.998 and 1. The domain deformation is almost negligible.

Influence of decreasing the parameter α

Now, we investigate the influence of decreasing the parameter α to 10^{-5} on the optimization results which we show in Table 4.15. In every setting, the number of

Table 4.14. Results of a freeform optimization on a quarter circle domain with fixed edges by using the BFGS method from Algorithm 4.4 with target value $\lambda_* = 0.92$ and regularization parameters $\alpha = 10^{-3}, \beta = 10^{-6}$. The tables show results varying the DoFs of the mesh, the refinement level (ref.), the order of Lagrange (Lagr.) and Nédélec (Néd.) elements. The initial first (numerical) eigenvalue is given by λ_0. We show the eigenvalue λ_{it} after termination of the method and the resulting value of the cost functional J, the relative residual of the gradient of the cost functional as well as the minimum and maximum value of the determinant of the deformation gradient J_q and the used eigenvalue solver EVS.

DoFs	ref.	Lagr.	Néd.	λ_0	it.	$\lambda_{\mathrm{it.}}$	J	r_{rel}	$J_{q,\mathrm{min}}$	$J_{q,\mathrm{max}}$	EVS
1059	3	1	0	0.9518	5	0.920286	6.859e-05	4.517e-06	0.9982	1.0002	A
4035	3	2	1	0.9467	6	0.920231	3.028e-06	2.263e-06	0.9986	1.000	B
4035	4	1	0	0.9468	5	0.920232	3.105e-06	1.034e-04	0.9992	0.9999	A
15737	4	2	1	0.9455	6	0.920221	2.775e-06	1.953e-06	0.9993	1.0000	B
15737	5	1	0	0.9456	6	0.920222	2.795e-06	1.738e-06	0.9995	1.0000	B
62211	5	2	1	0.9453	6	0.920218	2.714e-06	1.892e-06	0.9995	0.9999	A

Table 4.15. Results of a freeform optimization on a quarter circle domain with fixed edges by using the BFGS method from Algorithm 4.4 with target value $\lambda_* = 0.92$ and regularization parameters $\alpha = 10^{-5}, \beta = 10^{-6}$. The tables show results varying the DoFs of the mesh, the refinement level (ref.), the order of Lagrange (Lagr.) and Nédélec (Néd.) elements. The initial first (numerical) eigenvalue is given by λ_0. We show the eigenvalue λ_{it} after termination of the method and the resulting value of the cost functional J, the relative residual of the gradient of the cost functional as well as the minimum and maximum value of the determinant of the deformation gradient J_q and the used eigenvalue solver EVS.

DoFs	ref.	Lagr.	Néd.	λ_0	it.	$\lambda_{\mathrm{it.}}$	J	r_{rel}	$J_{q,\mathrm{min}}$	$J_{q,\mathrm{max}}$	EVS
1059	3	1	0	0.9518	14	0.920002	-1.679e-07	5.107e-05	1.043	1.046	B
4035	3	2	1	0.9467	14	0.920001	-1.811e-07	2.987e-05	1.032	1.039	A
4035	4	1	0	0.9468	14	0.92	-1.805e-07	3.015e-05	1.034	1.035	A
15737	4	2	1	0.9455	14	0.92	-1.777e-07	4.541e-05	1.030	1.033	A
15737	5	1	2	0.9456	14	0.92	-1.770e-07	4.741e-05	1.031	1.031	A
62211	5	2	1	0.9453	14	0.92	-1.783e-07	4.417e-05	1.031	1.032	A

iterations is 14 and the difference between the eigenvalue of the last iteration λ_{it} and the target value λ_* is between 0 and $2 \cdot 10^{-6}$. The relative residua of the reduced gradient are between $5.1 \cdot 10^{-5}$ and $4.7 \cdot 10^{-5}$. The determinant of the deformation gradient J_q has values around 1.03 which means that the domain grows. For the results of this example solved with the gradient method, we refer to Table A.14. Here, the method stopped after the maximum number of iterations with an eigenvalue equal to the target value. The relative residual of

the reduced gradient is in every setting bigger than $2 \cdot 10^{-4}$ and values of the determinant of the deformation gradient are close to 1 in every setting.

For the BFGS method, decreasing α to 10^{-6} has the consequence that the number of iterations until convergence varies depending on the DoFs on the mesh. For the 159 DoFs it takes 31 iterations, whereas for 4035 DoFs it takes 18, for 15737 Dofs 21 and for 62211 DoFs 27 iterations. Moreover the difference between λ_{it} and λ_* are in the range of 10^{-6}. The relative residua of the reduced gradient of the cost functional vary between 10^{-4} and $7.8 \cdot 10^{-5}$ and the values of J_q vary between 1.028 and 1.381 which is compared to the previous examples a big variation. For the same parameters, the gradient method does not achieve better results compared to the previous example. Again, it stopped for every setting after the maximum number of iterations, where the difference between λ_{it} and λ_* increases to 10^{-6} and the range for the relative residual of the reduced gradient stays the same. For the example with $\alpha = 10^{-3}$ and $\beta = 10^{-6}$, we refer to Table A.15.

Influence of increasing the parameter β

Now, we come back to the initial example and and investigate the influence of increasing the parameter β, i.e., we set $\alpha = 10^{-4}$ and $\beta = 10^{-5}$. Table 4.16 shows that the BFGS method converges for each setting after 9 iterations except for the coarsest mesh. Here, it takes 10 iterations. The difference between the eigenvalue after the last iteration λ_{it} and the target value λ_* is between 10^{-5} for the coarsest mesh and decreases to less than $3 \cdot 10^{-6}$ for the finer ones. The relative residual of the reduced gradient is between $1.2 \cdot 10^{-4}$ and $5 \cdot 10^{-5}$ which is an increase compared to the previous examples. Furthermore, the values for the determinant of the deformation gradient converge for finer meshes to about 1.25. In case of the gradient method, we obtain similar values for λ_{it}. The relative residual is greater than 10^{-3} for every setting after the termination of the method after the maximum number of iterations, see Table A.16.

It turns out that taking $\beta = 10^{-5}$ and decreasing α again to 10^{-5} and 10^{-6} giving no better results, see Table A.17 (a) and (b), respectively. Here, the BFGS method stops in every setting after the maximum number of iterations with a relative residual greater than 10^{-4} which is a debasement to the previous results.

By keeping $\beta = 10^{-5}$ and increasing α to 10^{-3} the method converges after 6 iterations for every setting, the relative residual of the reduced gradient is in every case smaller than $1.8 \cdot 10^{-6}$ and the values for J_q are about 1.003. It is

Table 4.16. Results of a freeform optimization on a quarter circle domain with fixed edges by using the BFGS method from Algorithm 4.4 with target value $\lambda_* = 0.92$ and regularization parameters $\alpha = 10^{-4}, \beta = 10^{-5}$. The tables show results varying the DoFs of the mesh, the refinement level (ref.), the order of Lagrange (Lagr.) and Nédélec (Néd.) elements. The initial first (numerical) eigenvalue is given by λ_0. We show the eigenvalue λ_{it} after termination of the method and the resulting value of the cost functional J, the relative residual of the gradient of the cost functional as well as the minimum and maximum value of the determinant of the deformation gradient J_q and the used eigenvalue solver EVS.

DoFs	ref.	Lagr.	Néd.	λ_0	it.	$\lambda_{\mathrm{it.}}$	J	r_{rel}	$\mathrm{J}_{q,\mathrm{min}}$	$\mathrm{J}_{q,\mathrm{max}}$	EVS
1059	3	1	0	0.9518	10	0.920011	-1.792e-06	5.080e-05	1.038	1.041	A
4035	3	2	1	0.9467	9	0.920003	-1.841e-06	7.350e-05	1.035	1.043	A
4035	4	1	0	0.9468	9	0.920003	-1.838e-06	7.207e-05	1.037	1.039	A
15737	4	2	1	0.9455	9	0.92	-1.846e-06	1.019e-04	1.036	1.040	A
15737	5	1	0	0.9456	9	0.92	-1.845e-06	9.853e-05	1.037	1.038	A
62211	5	2	1	0.9453	9	0.919999	-1.847e-06	1.124e-04	1.034	0.139	A

noticeable that the difference between λ_{it} and λ_* increases in comparison to the other settings, i.e., it increases to $2 \cdot 10^{-4}$. For the results of this choice of parameters, we refer to Table A.17 (c).

Influence of decreasing the parameter β

Finally, we consider the initial example and decrease the parameter β to 10^{-7}. Table 4.17 shows that the method converges in every setting after 6 iterations with a relative residual of the reduced gradient smaller than $3 \cdot 10^{-5}$. Here, the difference between λ_{it} and λ_* is in every setting, except the coarsest one, less than $2.5 \cdot 10^{-5}$. The values of J_q are between 0.999 and 1.

Keeping $\beta = 10^{-7}$ and varying α has the following influences and are shown in Table A.18. By decreasing α to 10^{-5}, see in (a), the number of iterations increases the from the previous example to 7 to 9. Decreasing α again to 10^{-6}, see (b), the number of iterations increases again. Now it is for the most settings 12. Furthermore, decreasing α decreases the difference between λ_{it} and λ_*. For the first case, it is $4 \cdot 10^{-6}$ and for the second, it is less than $2 \cdot 10^{-6}$. Moreover, it is J_q about 1.003 for the first choice of α and between 1.004 to 1.019 for the second. Further, with the choice of $\alpha = 10^{-6}$, the method takes 7 to 12 iterations. The values for the relative residual of the reduced gradient increase compared to taking $\alpha = 10^{-4}$ and by that, we do not obtain better results than before. It as a minimal increasing impact to the values of J_q.

In contrast, increasing α to 10^{-3}, see (c), results that the number of iterations until the method converges differs between 5 and 12. Also the difference between λ_{it} and λ_* differs between $2 \cdot 10^{-4}$ for coarse meshes and 10^{-5} and less for the finer ones. Moreover, the relative residual of the reduced gradient differs between the range of 10^{-4} and 10^{-6}. The values for J_q are between 0.998 and 1.018.

Table 4.17. Results of a freeform optimization on a quarter circle domain with fixed edges by using the BFGS method from Algorithm 4.4 with target value $\lambda_* = 0.92$ and regularization parameters $\alpha = 10^{-4}$ and $\beta = 10^{-7}$. The tables show results varying the DoFs of the mesh, the refinement level (ref.), the order of Lagrange (Lagr.) and Nédélec (Néd.) elements. The initial first (numerical) eigenvalue is given by λ_0. We show the eigenvalue λ_{it} after termination of the method and the resulting value of the cost functional J, the relative residual of the gradient of the cost functional as well as the minimum and maximum value of the determinant of the deformation gradient J_q and the used eigenvalue solver EVS.

DoFs	ref.	Lagr.	Néd.	λ_0	it.	λ_{it}	J	r_{rel}	$\mathrm{J}_{q,\min}$	$\mathrm{J}_{q,\max}$	EVS
1059	3	1	0	0.9518	6	0.998169	4.555e-07	2.904e-05	0.998	1.000	A
4035	3	2	1	0.9467	6	0.920024	3.052e-07	1.743e-05	0.999	1.000	A
4035	4	1	0	0.9468	6	0.920024	3.130e-07	2.398e-05	0.999	0.999	A
15737	4	2	1	0.9455	6	0.920023	2.798e-07	1.671e-05	0.999	0.999	A
15737	5	1	0	0.9456	6	0.920023	2.817e-07	1.851e-05	0.999	1.000	A
62211	5	2	1	0.9453	6	0.920022	2.736e-07	1.661e-05	0.999	1.000	A

Conclusion of the variation of the regularization parameters

The variation of the regularization parameters results similar results to those we observed for the rectangle domain in Section 4.4.1. By increasing α, we reduce the number of iterations until the method converges. Moreover, the difference between the eigenvalue after the last iteration and the target value increases minimally. Again, for a choice of $\alpha \leq 10^{-5}$ and the choice $\beta = 10^{-5}$, the method stops after the maximum number of iterations. Here, the values of J_q increase from a general value near 1 to values up to 1.615. Further, decreasing the parameter β causes a decrease of the number of iterations. In general, the parameter β influences the difference between the obtained eigenvalues and the target value less than the parameter α.

Visualization of the variation of the regularization parameters

After the discussion of the influence of the regularization parameters on the BFGS method from Algorithm 4.4, we visualize the deformed domains in Figure 4.13 after the last iteration for the setting with 62211 DoFs, refinement level 5 and

the choice of first order Nédélec elements and second order Lagrange elements. The influence of the regularization parameters on the BFGS method can be clearly seen in the solution figure. Taking the initial example with a choice of the parameters

- $\alpha = 10^{-4}$ and $\beta = 10^{-6}$,

the quarter circle is deformed by pulling apart the edge of the circular arc. A similar deformation field exists for the choices

- $\alpha = 10^{-3}$ and $\beta = 10^{-5}$
- $\alpha = 10^{-5}$ and $\beta = 10^{-7}$.

This deformation mainly remains for

- $\alpha = 10^{-3}$ and $\beta = 10^{-6}$,
- $\alpha = 10^{-4}$ and $\beta = 10^{-7}$

Here, additionally, there is a small compression at the top right.

A constant deformation over the whole round part of the quarter circle by pulling apart the circular arc at the top right, we obtain for the parameter combinations

- $\alpha = 10^{-3}$ and $\beta = 10^{-7}$,
- $\alpha = 10^{-4}$ and $\beta = 10^{-5}$,
- $\alpha = 10^{-5}$ and $\beta = 10^{-6}$,
- $\alpha = 10^{-6}$ and $\beta = 10^{-7}$,

where for the second and third combination, the deformation in the top right is the biggest. The settings with the biggest deformations are with the parameters

- $\alpha = 10^{-5}$ and $\beta = 10^{-5}$,
- $\alpha = 10^{-6}$ and $\beta = 10^{-5}$,
- $\alpha = 10^{-6}$ and $\beta = 10^{-6}$.

Here, the quarter circle is deformed strongly on the top right, whereas the corners on the transition from the circular arc to the edges remain non-deformed. The biggest deformations obtain the examples with the smallest α and biggest β. The visualization of the domain matches with the expectations of the discussion of the variation of the regularization parameters.
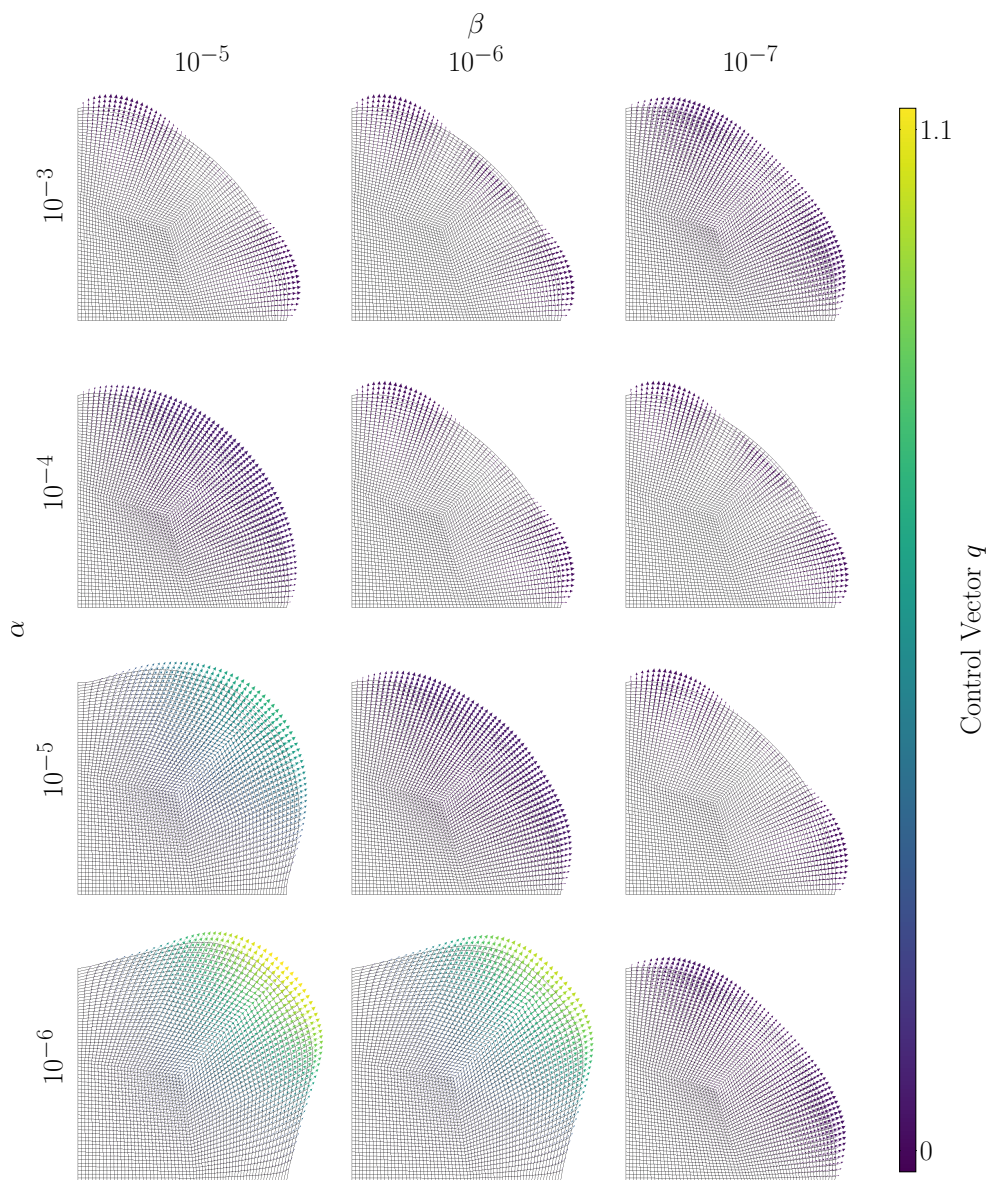
Figure 4.13. Influence of the regularization parameters regarding to the deformed quarter circle after optimization using the BFGS method with target value $\lambda_* = 0.92$. The chosen refinement level is 5, the number of DoFs is 62211 and Lagrange elements of order 2 and first order Nédélec elements are used. The first (numerical) eigenvalue before optimization is $\lambda_0 = 0.9453$.

4.4.2.3. Influence of the Choice of the Target Value λ_* on the Domain Deformation

In this subsection, we compare the influence on the choice of target value λ_* on the deformation on the quarter circle domain. We consider the initial example solved with the BFGS method from Algorithm 4.4 with the choice of regularization parameter $\alpha = 10^{-4}$ and $\beta = 10^{-6}$ and the chosen refinement level 5, 62211 DoFs as well as a discretization with Nédélec elements of order 1 and Lagrange elements of order 2. The first (numerical) eigenvalue is $\lambda_0 = 0.945$. The target value λ_* in the initial example is 0.92 and the results are shown in Table 4.13 and the visualization of the deformed domain is shown in Figure 4.12.

In the following, we consider examples, where we optimize to various target values, namely $1.00, 0.95, 0.94$ and 0.90 and study their influence on the deformation of the domain. The results are shown in Table 4.18 and visualized in Figure 4.14. We observe that the method converges after 7 iterations for every choice of λ_*. The difference of the eigenvalue after the last iteration λ_{it} and the target value is smaller, the closer the target value is chosen from the initial value λ_0, i.e.,

- for $\lambda_* = 1.00$, the difference is $4 \cdot 10^{-5}$,
- for $\lambda_* = 0.95$, the difference is $1 \cdot 10^{-5}$,
- for $\lambda_* = 0.94$, the difference is 0,
- and for $\lambda_* = 0.90$, the difference is $4 \cdot 10^{-5}$.

Furthermore, the relative residua are smaller by a closer chosen target value. Figure 4.14 (a) shows the deformation for $\lambda_* = 1.0$. The quarter circle is deformed by a compression of the corners on the transition from the circular arc to the edges. Further, at the top right, the quarter circle pulls apart. The deformation in (b) for $\lambda_* = 0.95$ is similar. Again, the quarter circle is deformed by a compression of the corners on the transition from the circular arc to the edges and at the top right, the quarter circle pulls apart. Compared to the previous example, the deformation decreases, which we expect because the target value of (b) is closer to the initial eigenvalue. In (c), we see the deformation for $\lambda_* = 0.94$. The quarter circle pulls apart at the complete circular arc. Finally, (d) shows the deformation for $\lambda_* = 0.9$. The quarter circle is deformed by pulling apart at the corners on the transition from the circular arc to the edges. Further, at the top right, the quarter circle deforms by compression. The deformation is the inverse

of the deformation of (a) and (b), where, in contrary to this setting, the target value is higher than the initial eigenvalue.

Table 4.18. Comparison of λ_* on the domain deformation of a freeform optimization on a quarter circle domain with fixed edges by using the BFGS method from Algorithm 4.4 using subspace iteration with $\alpha = 10^{-4}$ and $\beta = 10^{-6}$. The chosen refinement level is 5, the number of DoFs is 62211. Lagrange elements of order 2 and Nédélec elements of order 1 are used and the initial first (numerical) eigenvalue is $\lambda_0 = 0.9453$.

λ_*	it.	$\lambda_{\text{it.}}$	J	r_{rel}	$J_{\min}$	$J_{\max}$
1.00	7	0.99996	1.358e-06	4.295e-05	1.00288	1.00369
0.95	7	0.94999	4.136e-09	1.507e-06	1.00385	1.00417
0.94	7	0.94000	-1.520e-08	3.215e-06	1.00378	1.00398
0.90	7	0.90004	7.995e-07	2.784e-05	1.00263	1.00263

4.4.3. Conclusion of the Numerical Examples

In this section, we showed several examples of freeform optimization problems constrained by Maxwell's eigenvalue problem. We compared the BFGS method from Algorithm 4.4 with the gradient method from Algorithm 4.3 on a rectangle and a quarter circle domain. There, we studied the influence of the regularization parameters as well as the target value λ_* on the domains.

In both domains, we started showing optimization results on an initial example with specified regularization parameters. We observed in both cases a faster convergence of the BFGS method independent on the chosen setting for the mesh. The method converged after 15 iterations for the rectangle domain and after 7 iterations for the quarter circle domain, respectively. In contrast, the gradient method did not converge in both examples. It stopped after the maximum number of iterations, which we set to 1000.

Influence of the regularization parameters
We studied the influence of regularization parameters α and β. Here, we compared their influence on the rectangle domain on both methods, whereas we focused for the quarter circle domain on the BFGS method and restricted to some selected examples for the gradient method to the Appendix. For all choices of regularization parameters, the BFGS method converged faster than the gradient method. Further, the obtained results, where the methods converged, are in almost every setting independent of the refinement level of the mesh. In several

(a) $\lambda_* = 1.00$

(b) $\lambda_* = 0.95$

(c) $\lambda_* = 0.94$

(d) $\lambda_* = 0.90$
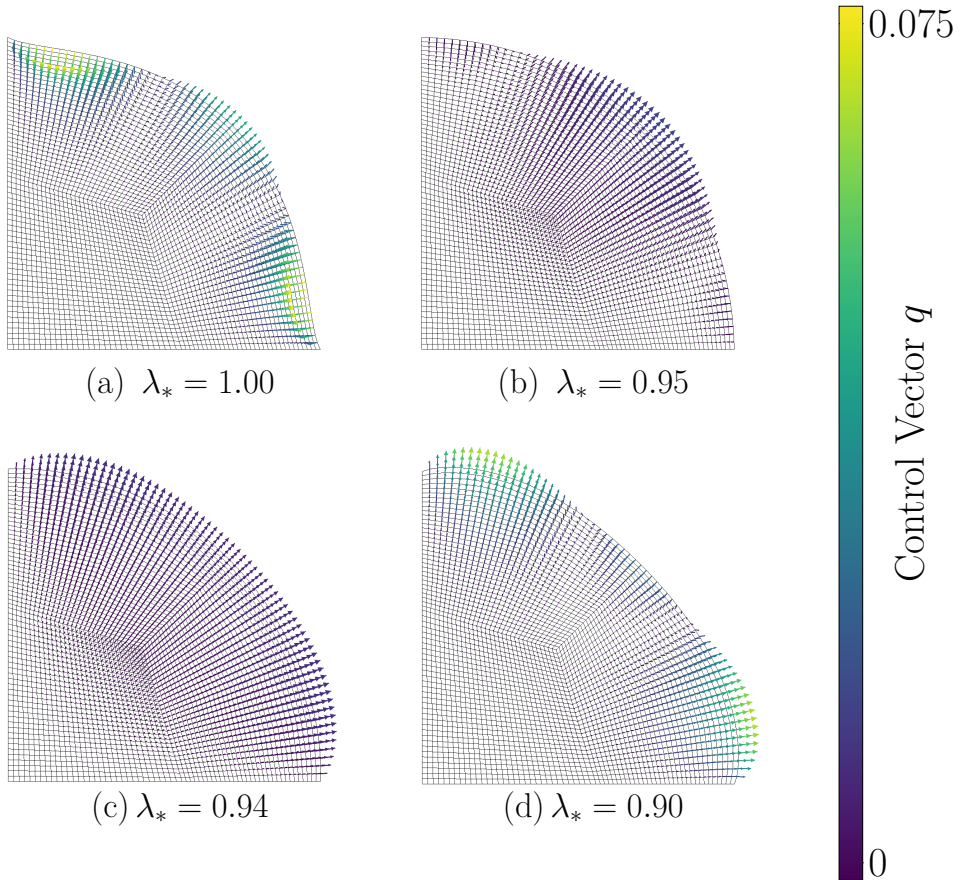
Figure 4.14. Variation of λ_* using the BFGS method from Algorithm 4.4 on quarter circle with fixed edges with $\alpha = 10^{-6}$ and $\beta = 10^{-7}$. The chosen refinement level is 5, the number of DoFs is 62211. Lagrange elements of order 2 and Nédélec elements of order 1 are used and the initial first (numerical) eigenvalue is $\lambda_0 = 0.9453$.

cases, we observe minimal difference between the element orders of the finite elements. The only case where we cannot conclude mesh independence was for the rectangle example with a choice of $\alpha = 10^{-2}$ and $\beta = 10^{-3}$.

As we expected, increasing the parameter α, and by that the influence of the penalty regularization, on the rectangle domain ensured that the number of iterations decreases in both methods. For the gradient method, this holds true with a restriction that the chosen parameter β is small enough. We obtained same results for the quarter circle domain using the BFGS method. In both cases, this increased the difference between the eigenvalue and the target value. We observed that the choice of β also influences, until some limit, the number of iterations. When decreasing β, we observed a decrease in the number of iterations as well. In the rectangle examples, this is also valid when utilizing the gradient method. We conclude that the choice of β influences on the problem itself. A choice of β too large even ensures that the methods do not converge anymore.

For all examples, we visualized the deformation of the optimized domains. We observed that a too-large choice for β combined with a too-small choice for α has an high impact on the domain deformation. Compared with the numerical results, these are the examples, where the methods did not converge after the maximum number of iterations. In these cases, the regularization was not chosen strongly enough.

Influence of the choice of the target value

Another study was the influence of the target value λ_* concerning the influence on the domain change. Here, we obtained the expected results from both examples. The values of J_q showed that the greater the difference between the target value and the initial eigenvalue, the greater the difference of the resulting values to 1. Furthermore, the choice of a smaller or bigger target value than the initial value also influences the value of J_q. The target value decides on which part the domain gets stretched or compressed. Also, depending on the strength of the domain change, the solution changes in accuracy.

Applications

In the previous chapter, we introduced an optimization problem constrained by the Maxwell eigenvalue problem depending on a domain mapping (4.36). In Section 4.1, we computed the gradient of the reduced cost functional with adjoint calculus. Furthermore, we discussed in Section 4.2 two optimization methods applied on the considered eigenvalue optimization problem, i.e., a damped inverse BFGS method in Algorithm 4.4 and a gradient method in Algorithm 4.3. Moreover, we verified both methods on simple geometries in Section 4.4. Here, we concluded that the BFGS method is more suitable in order to solve eigenvalue optimization with respect to shape-variations in electromagnetic systems.

A resulting application is an electromagnetic cavity which is responsible for the acceleration of particles in a particle collider which we already discussed in Chapter 1. Now, the challenge is to transfer our approach to more realistic applications. We have to make several adjustments to this, which we discuss in this chapter.

First, we need to solve the considered optimization problem on more complex geometries. Therefore, we consider in Section 5.1 two-dimensional planar examples of cavity domains. Here, we optimize the first eigenvalue the domain of a 1-cell cavity on several regularization parameters and verify the influence of some target values close the considered eigenvalue on the domain change. Moreover, we verify how an other boundary condition for q influences the solution and the resulting deformation of the domain. Afterwards, we show results on a even more complex domain, a 5-cell cavity domain, inspired by a cavity model seen in [36].

A further extension toward to more realistic examples is, of course, three-dimensional domains. We extend our approach to three-dimensional problems and conclude this chapter by showing optimization results on a cuboid as well as a first example of a cylinder in Section 5.2.

5.1. Numerical Examples of Two-Dimensional Cavities

In this section, we present the results of eigenvalue optimization on two-dimensional planar cavity domains. We consider the optimization on a 1-cell as well as a 5-cell cavity, inspired by the numerical example of [36, Chapter 6.4] on a model for the Superconducting-DArmstadt-LINear-ACcelerator (S-DALINAC), see [2]. The starting design is a so-called low β cavity design, where the cells get longer in order to take into account the increasing speed of the particle bunch. The geometry is described with the parameters shown in Table 5.1, and the initial domain of the 1-cell cavity (a) and the 5-cell cavity (b) is shown in Figure 5.1. For the considered 1-cell cavity, we use the parameters of the first cell.
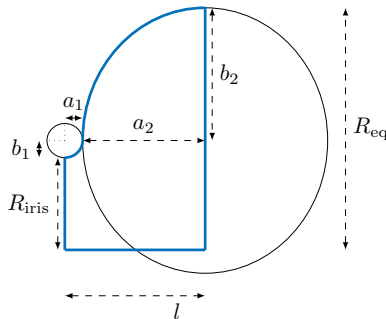
Figure 5.1. Geometry of a Cavity.

Table 5.1. Cavity design parameters for the different cells, see [36]. All dimensions are given in mm.

Cavity Shape Parameter	Cell 1	Cell 2	Cell 3	Cell 4	Cell 5
Equator radius R_{eq}	43.44542	43.44542	43.44542	43.44542	43.44542
Iris radius R_{iris}	16.5627	16.5627	16.5627	16.5627	16.5627
Horizontal half axis at iris a_1	3.2	3.7184	4.32	5.0208	5.8336
Vertical half axis at iris b_1	3.0592	3.0592	3.0592	3.0592	3.0592
Horizontal half axis at equator a_2	21.98	25.54076	29.673	34.48662	40.06954
Vertical half axis at equator b_2	23.82352	23.82352	23.82352	23.82352	23.82352
Length L	25.18	29.25916	33.993	39.50742	45.90314

The meshes of the geometries are created with GMSH [47] and shown in Figure 5.2. For all examples, we use the settings of Table 5.2 and we set $\varepsilon = 10^{-4}$.

(a) 1-cell Cavity

(b) 5-cell Cavity
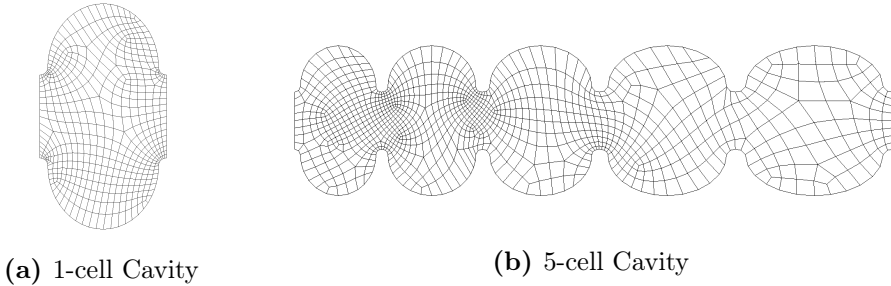
Figure 5.2. Meshes of the Cavites

Table 5.2. Settings for the BFGS method from Algorithm 4.4 for optimization on cavities

BFGS method from Algorithm 4.4	
$\text{it}_{\max}$	100
$\text{TOL}_{\text{global}}$	10^{-7}
TOL	10^{-7}
Armijo Condition	
line $\text{it}_{\max}$	10
γ	0.1
ρ	0.1

To solve the eigenvalue problems during the optimization process, we use the `SLEPc` library. For details on the settings, we refer to Appendix A.1. In Table A.3, we name the concrete shifts of the solver and in Table A.2, the used library versions.

5.1.1. 1-Cell Cavity

In the following, we optimize the first eigenvalue λ of a 1-cell cavity to a target value λ_* using the BFGS method from Algorithm 4.4. In several examples, we observe the influence of the regularization parameters and the choice of the target value on the domain deformation as well as the results of the optimization. Moreover, we consider an example of a variation of the boundary condition.

5.1.1.1. Comparison of Regularization Parameters

For first computational results, we fix the left- and right-hand sides of the domain by setting $q = 0$ on the corresponding boundaries. By remembering the results of Section 4.4, we obtain good results for a choice of $\beta \leq 10^{-5}$ and for $\alpha = 1$. By varying the parameters, we observe that the behavior of the optimization method is similar to the previous examples, see Table 5.3. By increasing α to 1000, we speed up the method. For all examples, we apply the Krylov Schur eigenvalue solver (B). For details, we refer to Table A.1.

5.1.1.2. Influence of the Choice of the Target Value λ_* on the Domain Deformation

By keeping the previous boundary condition and setting the regularization parameters to $\alpha = 1$ and $\beta = 10^{-5}$, we study the influence of the variation of the target value λ_* on the domain deformation. The results are shown in Table 5.4. Here, the BFGS method converges in all cases after 13 to 17 iterations. We observe that choosing a smaller target value compared to the first eigenvalue results in the growth of the domain. We conclude this on the values of the determinant of the deformation gradient J_q. Values bigger than 1 mean a volume growth, whereas values smaller than 1 mean a volume shrink. Furthermore, a bigger difference to the first eigenvalue results in a bigger deformation. Moreover, a bigger target value influences the domain change to shrink. Again, a bigger difference results in a bigger deformation. A visualization of the deformed domains is shown in Figure 5.3, where we observe exactly this phenomenon. The deformation is demonstrated on the upper half of the domain. The lower half is symmetric.

5.1.1.3. Variation of Boundary Condition for the Deformation

In freeform optimization, the whole domain is able to deform in every direction. Sometimes, e.g., in applications for cavities, one is interested in just optimizing parts of the domain. In this last numerical example for 1-cell cavities, we show results for a variation of the boundary condition by the choice of regularization parameters $\alpha = 1$ and $\beta = 10^{-5}$. Here, we fix all parts of the boundary which do not contain the equator of the cavity, by setting $q = 0$ on these places. We observe, that the method converges after 18 iterations for this choice of parameters, whereas in the previous example it terminated after 15 iterations for the same choice of regularization parameters. Furthermore, we obtain that

Table 5.3. Results of a freeform optimization using the BFGS method from Algorithm 4.4 varying α and β on a 1-cell Cavity with fixed R_{iris} on left-hand and right-hand side and target value $\lambda_* = 1650$. The initial first (numerical) eigenvalue is given by λ_0. We show the eigenvalue λ_{it} after termination of the method and the resulting value of the cost functional J, the relative residual of the gradient of the cost functional as well as the minimum and maximum value of the determinant of the deformation gradient J_q.

(a) $\alpha = 10, \beta = 10^{-5}$

DoFs	ref.	Lagr.	Néd.	λ_0	it.	$\lambda_{\text{it.}}$	J	r_{rel}	$J_{q,\min}$	$J_{q,\max}$
2893	0	1	0	1660.77	15	1650	1.880e-07	5.008e-08	1.00504	1.00523
11023	0	2	1	1655.15	15	1650	4.293e-08	3.583e-08	1.00235	1.00240
11023	1	1	0	1653.28	15	1650	1.741e-08	3.154e-08	1.00147	1.00162
43363	2	1	0	1653.75	15	1650	2.273e-08	3.255e-08	1.00169	1.00171

(b) $\alpha = 1, \beta = 10^{-5}$

DoFs	ref.	Lagr.	Néd.	λ_0	it.	$\lambda_{\text{it.}}$	J	r_{rel}	$J_{q,\min}$	$J_{q,\max}$
2893	0	1	0	1660.77	15	1650	1.869e-08	5.008e-08	1.00504	1.00523
11023	0	2	1	1655.15	15	1650	4.245e-09	3.583e-08	1.00235	1.00240
11023	1	1	0	1653.28	15	1650	1.711e-09	3.154e-08	1.00147	1.00162
43363	2	1	0	1653.75	15	1650	2.239e-09	3.255e-08	1.00169	1.00171

(c) $\alpha = 0.1, \beta = 10^{-5}$

DoFs	ref.	Lagr.	Néd.	λ_0	it.	$\lambda_{\text{it.}}$	J	r_{rel}	$J_{q,\min}$	$J_{q,\max}$
2893	0	1	0	1660.77	20	1650	1.764e-09	4.754e-08	1.00500	1.00518
11023	0	2	1	1655.15	19	1650	3.763e-10	6.277e-08	1.00234	1.00239
11023	1	1	0	1653.28	19	1650	1.416e-10	4.015e-08	1.00147	1.00161
43363	2	1	0	1653.75	19	1650	1.897e-10	4.583e-08	1.00169	1.00170

(d) $\alpha = 0.1, \beta = 10^{-7}$

DoFs	ref.	Lagr.	Néd.	λ_0	it.	$\lambda_{\text{it.}}$	J	r_{rel}	$J_{q,\min}$	$J_{q,\max}$
2893	0	1	0	1660.77	15	1650	1.881e-08	5.008e-08	1.00504	1.00523
11023	0	2	1	1655.15	15	1650	4.298e-09	3.583e-08	1.00235	1.00240
11023	1	1	0	1653.28	15	1650	1.744e-09	3.154e-08	1.00147	1.00162
43363	2	1	0	1653.75	15	1650	2.273e-08	3.255e-08	1.00169	1.00171

(e) $\alpha = 1000, \beta = 10^{-7}$

DoFs	ref.	Lagr.	Néd.	λ_0	it.	$\lambda_{\text{it.}}$	J	r_{rel}	$J_{q,\min}$	$J_{q,\max}$
2893	0	1	0	1660.77	11	1650	1.881e-05	3.902e-08	1.005020	1.00520
11023	0	2	1	1655.15	11	1650	4.298e-06	<1.000e-08	1.00235	1.00239
11023	1	1	0	1653.28	11	1650	1.744e-09	<1.000e-08	1.00147	1.00161
43363	2	1	0	1653.75	11	1650	2.277e-08	<1.000e-08	1.00169	1.00171

Table 5.4. Comparison of λ_* on the domain deformation of a freeform optimization on a 1-cell Cavity with fixed R_{iris} on the left and right hand side by using the BFGS method from Algorithm 4.4 with regularization parameters $\alpha = 1, \beta = 10^{-5}$. The chosen refinement level is 2, the number of DoFs is 43363. Lagrange elements of order 1 and lowest order Nédélec elements are used and the initial first (numerical) eigenvalue is $\lambda_0 = 1653.75$.

λ_*	it.	$\lambda_{\text{it.}}$	J	r_{rel}	$J_{q,\text{min}}$	$J_{q,\text{max}}$
1640	17	1640	3.077e-08	5.425e-08	1.00627	1.00633
1650	15	1650	2.239e-09	3.255e-08	1.00169	1.00171
1660	13	1660	6.373e-09	6.155e-08	0.99717	0.99720
1670	15	1670	4.220e-08	2.103e-08	0.99272	0.99279

(a) $\lambda_* = 1640$

(c) $\lambda_* = 1650$

(b) $\lambda_* = 1660$

(d) $\lambda_* = 1670$
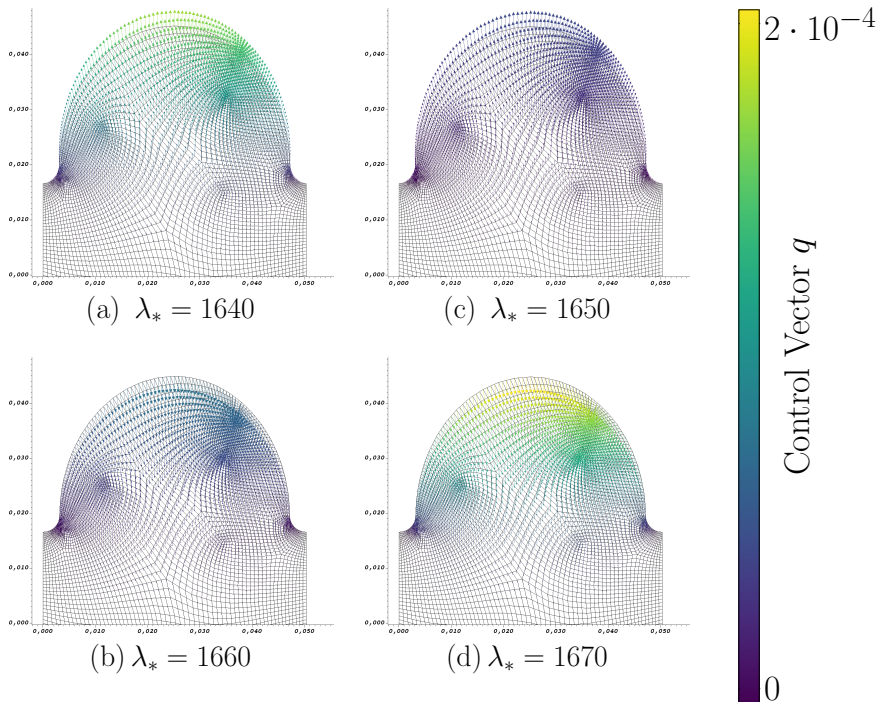
Figure 5.3. Variation of λ_* using BFGS method on a 1-cell Cavity with fixed R_{iris} on left-hand and right-hand side with regularization parameters $\alpha = 1, \beta = 10^{-5}$. The chosen refinement level is 2, the DoFs are 43363. Lagrange elements of order 1 and lowest order Nédélec elements are used and the initial first (numerical) eigenvalue is $\lambda_0 = 1653.75$. The figures show the upper half of the domain.

the values of J_q vary slightly. In the setting with 43363 DoFs, it varies about a difference of 10^{-4}. In Figure 5.4, the deformation of the considered boundary part is visualized in comparison with the example where we choose the iris axis to be the free boundary. Moreover, it is clearly also possible to vary the target value λ_* for this problem setting. Here, we refer to results for the same choice of regularization parameters in Table A.19. These results show no new insights.

(a) Fixed Boundary on the Iris Axis   (b) Free Boundary on the Iris Axis
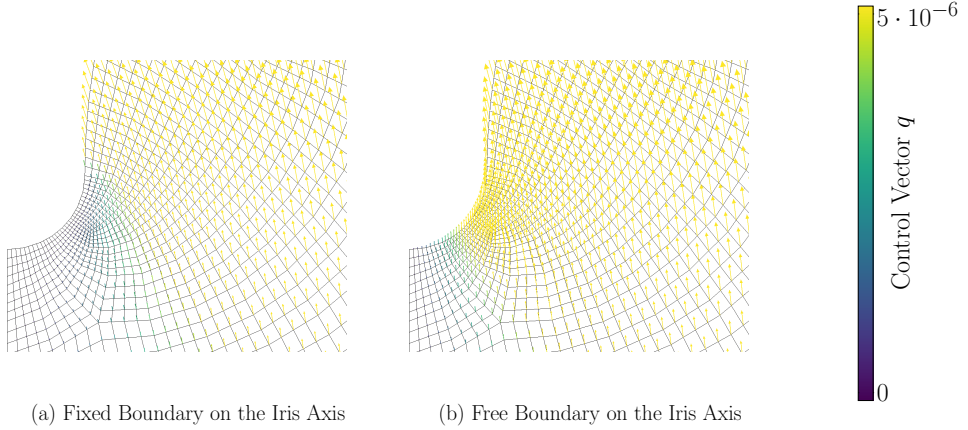
Figure 5.4. Comparison of boundaries of freeform optimization with target value $\lambda_* = 1650$ using the BFGS method from Algorithm 4.4 on a 1-cell cavity with regularization parameters $\alpha = 1$ and $\beta = 10^{-5}$. The chosen refinement level is 2, the number of DoFs is 43363. Lagrange elements of order 1 and lowest order Nédélec elements are used and the initial first (numerical) eigenvalue is $\lambda_0 = 1653.75$.

Table 5.5. Results of a freeform optimization on a 1-cell cavity with fixed R_{iris} on the left and right hand side and with fixed axes at the irises with target value $\lambda_* = 1650$ and regularization parameters $\alpha = 1$ and $\beta = 10^{-5}$. The initial first (numerical) eigenvalue is given by λ_0. We show the eigenvalue λ_{it} after termination of the method and the resulting value of the cost functional J, the relative residual of the gradient of the cost functional as well as the minimum and maximum value of the determinant of the deformation gradient J_q.

DoFs	ref.	Lagr.	Néd.	λ_0	it.	$\lambda_{\mathrm{it.}}$	J	r_{rel}	$J_{q,\mathrm{min}}$	$J_{q,\mathrm{max}}$
2893	0	1	0	1660.77	18	1650	2.038e-08	$< 1.0\text{e-}08$	1.00539	1.00564
11023	0	2	1	1655.15	18	1650	1.856e-09	$< 1.0\text{e-}08$	1.00156	1.00173
11023	1	1	0	1653.28	18	1650	4.609e-09	$< 1.0\text{e-}08$	1.0025	1.00256
43363	2	1	0	1653.75	18	1650	2.427e-09	$< 1.0\text{e-}08$	1.0018	1.00182

5.1.2. 5-Cell Cavity

Now, we extend the optimization domain to a 5-cell cavity, i.e., Figure 5.2 (b), and optimize the first eigenvalue. Table 5.6 shows the results after the optimization to a target value $\lambda_* = 6017$ with regularization parameters $\alpha = 100$ and $\beta = 10^{-6}$. By a discretization with 22103 DoFs or higher, the BFGS method converges after 16 iterations. For a setting with 5438 DoFs, it takes 12. The values of J_q are slightly smaller than 1, which means that we obtain a small shrinkage of the domain.

Table 5.6. Results of a freeform optimization with target value $\lambda_* = 6017$ using the BFGS method from Algorithm 4.4 with $\alpha = 100$ and $\beta = 10^{-6}$ on a 5-cell cavity with fixed R_{iris} on the left and right hand side. The initial first (numerical) eigenvalue is given by λ_0. We show the eigenvalue λ_{it} after termination of the method and the resulting value of the cost functional J, the relative residual of the gradient of the cost functional as well as the minimum and maximum value of the determinant of the deformation gradient J_q.

DoFs	ref.	Lagr.	Néd.	λ_0	it.	$\lambda_{\text{it.}}$	J	r_{rel}	$J_{q,\text{min}}$	$J_{q,\text{max}}$	EVS
5438	0	1	0	6018.47	12	6017	1.728e-10	7.846e-07	0.99998	0.99999	B
22103	0	2	1	6022.89	16	6017	2.691e-09	9.067e-07	0.99987	0.99999	B
22103	1	1	0	6021.91	16	6017	1.878e-09	7.243e-07	0.99993	0.99998	B
86723	2	1	0	6024.65	16	6017	4.532e-09	9.520e-07	0.99991	0.99998	BS

0   Control Vector q $3.38 \cdot 10^{-6}$
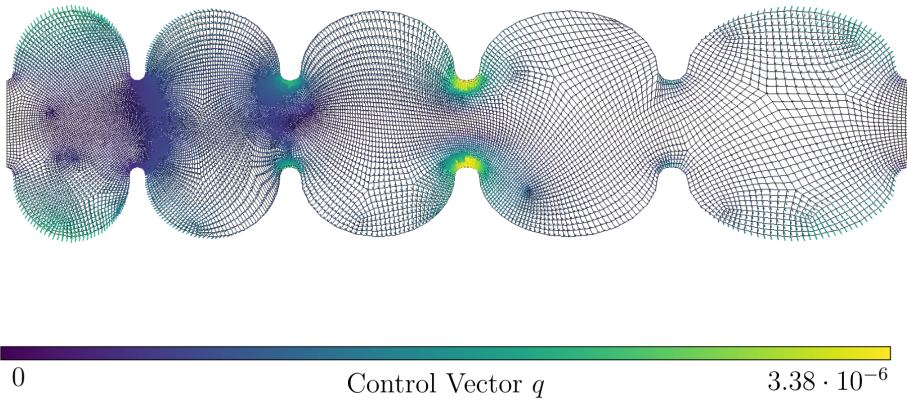
Figure 5.5. Deformation of a 5-cell cavity with fixed R_{iris} on left-hand and right-hand side after optimization of the first eigenvalue to target value $\lambda_* = 6017$ using the BFGS method from Algorithm 4.4 with regularization parameters $\alpha = 100$ and $\beta = 10^{-6}$. The chosen refinement level is 2, the number of DoFs is 86723. Lagrange elements of order 1 and lowest order Nédélec elements are used.

5.2. Eigenvalue Optimization on Three-Dimensional Domains

In this section, we show the results of extending our approach to three-dimensional domains. For the examples, we use the settings of Table 5.7 and we set $\varepsilon = 10^{-4}$.

Table 5.7. Settings for the BFGS method from Algorithm 4.4 for optimization on three-dimensional domains.

BFGS method from Algorithm 4.4	
it_{max}	100
$\text{TOL}_{\text{global}}$	10^{-5}
TOL	10^{-5}
Armijo Condition	
line it_{max}	10
γ	0.1
ρ	0.1

5.2.1. Cuboid

In the following, we optimize the cuboid domain

$$\widehat{\Omega} = \left[0, \frac{\pi}{2}\right] \times \left[0, \frac{\pi}{3}\right] \times \left[0, \frac{\pi}{5}\right], \tag{5.1}$$

where we allow deformation on the whole domain. We optimize the eigenvalue $\lambda \approx 13$ to two different target values, namely $\lambda_* = 12.5$ and 13.5. We validate the results by a short variation of regularization parameters, i.e.,

- $\alpha = 10^{-2}$ and $\beta = 10^{-5}$ in Table 5.8,
- $\alpha = 10^{-1}$ and $\beta = 10^{-5}$ in Table 5.9,
- $\alpha = 10^{-1}$ and $\beta = 10^{-6}$ in Table 5.10,
- $\alpha = 10^{-2}$ and $\beta = 10^{-6}$ in Table 5.11.

We observe that the results behave similarly those on two-dimensional domains, which we discussed in detail in Section 4.4 and Section 5.1. The parameter α influences the speed of the convergence by means of the number of iterations. Moreover, decreasing β stabilizes the number of iterations regarding the chosen settings. The number of iterations varies slightly depending on the different settings concerning the DoFs. We remark here that the three-dimensional numerical

(a) $\lambda_* = 12.5$ (b) $\lambda_* = 13.5$
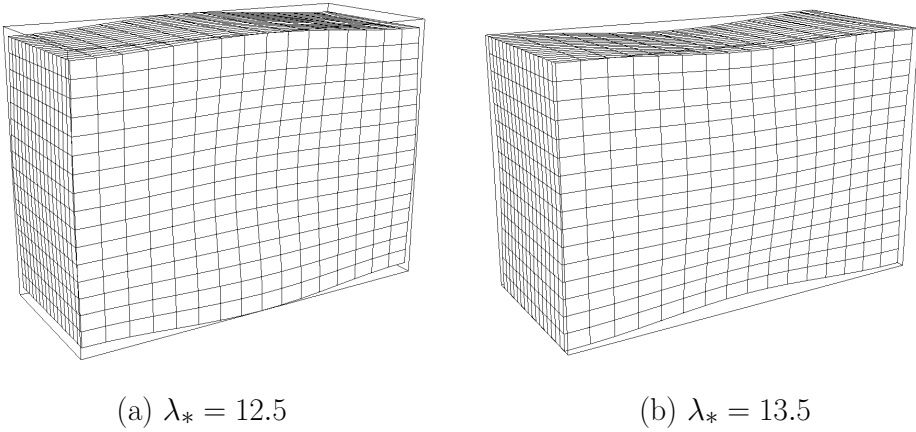
Figure 5.6. Deformation of the cuboid with variation of λ_*.

results are computed on relative coarse meshes. By further refinements, we expect further stabilization regarding the number of iterations. The computation of three-dimensional fine meshes is costly because the number of DoFs increases immensely. For an outlook on finer meshes, we recommend extending the computation to parallel computing. Nevertheless, we observe that all results converge to the chosen termination criteria. The difference between the eigenvalue after the last iteration λ_{it} and the target value λ_* increases slightly by increasing α. Again, this is similar to the obtained two-dimensional results.

In Figure 5.6, we show the deformed cuboid after optimization for 33525 DoFs, by a chosen refinement level 4 as well as first order Lagrange and lowest order Nédélec elements. In (a), we show the cuboid for $\lambda_* = 12.5$ and in (b), for $\lambda_* = 13.5$. To obtain a better view to the behavior of the domain, we further show deformation fields of the y- and z-cross sections after optimization in Figures 5.7 and 5.8. The deformation behaves similar to the results of the two-dimensional rectangle. By optimizing the eigenvalue to a smaller target value $\lambda_* = 12.5$, the domain grows, whereas a larger value, i.e. $\lambda_* = 13.5$, results in the contrary. Here, the domain shrinks. Also, the obtained values for the deformation gradient after optimization J_q are slightly larger than 1 for $\lambda_* = 12.5$ and smaller than 1 for $\lambda_* = 13.5$. This is consistent with our observations.

Table 5.8. Results of a freeform optimization on a on a cuboid varying the target value λ_* and with regularization parameters $\alpha = 10^{-2}$ and $\beta = 10^{-5}$. The tables show results varying the DoFs of the mesh, the refinement level (ref.), the order of Lagrange (Lagr.) and Nédélec (Néd.) elements. The initial first (numerical) eigenvalue is given by λ_0. We show the eigenvalue λ_{it} after termination of the method and the resulting value of the cost functional J, the relative residual of the gradient of the cost functional as well as the minimum and maximum value of the determinant of the deformation gradient J_q and the used eigenvalue solver EVS.

(a) $\lambda_* = 12.5$

DoFs	ref.	Lagr.	Néd.	λ_0	it.	$\lambda_{it.}$	J	r_{rel}	$J_{q,min}$	$J_{q,max}$	EVS
800	2	1	0	13.8610	11	12.5	1.265e-05	3.487e-06	1.0175	1.0177	B
4860	2	2	1	13.0067	14	12.5	2.099e-06	6.669e-06	1.0022	1.0354	B
4860	3	1	0	13.1679	15	12.5	3.781e-06	3.806e-06	1.0069	1.0195	B
33525	3	2	1	13.0004	14	12.5	2.045e-06	9.460e-06	1.0026	1.0174	B
33525	4	1	0	13.0418	14	12.5	2.423e-06	5.453e-06	1.0036	1.0071	B

(b) $\lambda_* = 13.5$

DoFs	ref.	Lagr.	Néd.	λ_0	it.	$\lambda_{it.}$	J	r_{rel}	$J_{q,min}$	$J_{q,max}$	EVS
800	2	1	0	13.8610	14	13.5	2.075e-07	4.839e-06	1.0025	1.0106	B
4860	2	2	1	13.0067	11	13.5	2.179e-06	6.987e-06	0.9687	0.9971	B
4860	3	1	0	13.1679	15	13.5	1.043e-06	6.228e-06	0.9911	0.9966	B
33525	3	2	1	13.0004	15	13.5	2.230e-06	3.497e-05	0.9840	0.9979	B
33525	4	1	0	13.0418	16	13.5	1.895e-06	1.074e-06	0.9944	0.9978	B

Table 5.9. Results of a freeform optimization on a cuboid varying the target value λ_* and with regularization parameters $\alpha = 10^{-1}$ and $\beta = 10^{-5}$. The tables show results varying the DoFs of the mesh, the refinement level (ref.), the order of Lagrange (Lagr.) and Nédélec (Néd.) elements. The initial first (numerical) eigenvalue is given by λ_0. We show the eigenvalue λ_{it} after termination of the method and the resulting value of the cost functional J, the relative residual of the gradient of the cost functional as well as the minimum and maximum value of the determinant of the deformation gradient J_q and the used eigenvalue solver EVS.

(a) $\lambda_* = 12.5$

DoFs	ref.	Lagr.	Néd.	λ_0	it.	$\lambda_{\mathrm{it.}}$	J	r_{rel}	$\mathrm{J}_{q,\mathrm{min}}$	$\mathrm{J}_{q,\mathrm{max}}$	EVS
800	2	1	0	13.8610	10	12.5002	1.308e-04	9.220e-06	1.0174	1.0732	B
4860	2	2	1	13.0067	10	12.5001	2.278e-05	5.773e-06	1.0027	1.0359	B
4860	3	1	0	13.1679	8	12.5001	4.009e-05	7.134e-06	1.0073	1.0189	B
33525	3	2	1	13.0004	9	12.5001	2.220e-05	7.648e-06	1.0012	1.0175	B
33525	4	1	0	13.0418	8	12.5001	2.611e-05	8.897e-07	1.0038	1.0067	B

(b) $\lambda_* = 13.5$

DoFs	ref.	Lagr.	Néd.	λ_0	it.	$\lambda_{\mathrm{it.}}$	J	r_{rel}	$\mathrm{J}_{q,\mathrm{min}}$	$\mathrm{J}_{q,\mathrm{max}}$	EVS
800	2	1	0	13.8610	7	13.5000	2.739e-06	2.468e-06	1.0025	1.0106	B
4860	2	2	1	13.0067	9	13.4999	2.004e-05	1.259e-05	0.9673	0.9975	B
4860	3	1	0	13.1679	21	13.4999	9.222e-06	8.433e-06	0.9914	0.9965	B
33525	3	2	1	13.0004	8	13.4999	2.052e-05	8.126e-06	0.9838	0.9988	B
33525	4	1	0	13.0418	8	13.4999	1.733e-05	8.727e-06	0.9947	0.9969	B

Table 5.10. Results of a freeform optimization on a cuboid varying the target value λ_* and with regularization parameters $\alpha = 10^{-1}$ and $\beta = 10^{-6}$. The tables show results varying the DoFs of the mesh, the refinement level (ref.), the order of Lagrange (Lagr.) and Nédélec (Néd.) elements. The initial first (numerical) eigenvalue is given by λ_0. We show the eigenvalue λ_{it} after termination of the method and the resulting value of the cost functional J, the relative residual of the gradient of the cost functional as well as the minimum and maximum value of the determinant of the deformation gradient J_q and the used eigenvalue solver EVS.

(a) $\lambda_* = 12.5$

DoFs	ref.	Lagr.	Néd.	λ_0	it.	$\lambda_{\text{it.}}$	J	r_{rel}	$J_{q,\min}$	$J_{q,\max}$	EVS
800	2	1	0	13.8610	9	12.5002	1.312e-04	3.290e-06	1.0174	1.0732	B
4860	2	2	1	13.0067	9	12.5001	2.296e-05	1.483e-07	1.0026	1.036	B
4860	3	1	0	13.1679	8	12.5001	4.033e-05	7.134e-06	1.0073	1.0189	B
33525	3	2	1	13.0004	12	12.5001	2.237e-05	8.344e-06	1.0011	1.0174	B
33525	4	1	0	13.0418	10	12.5001	2.630e-05	6.973e-06	1.0039	1.0067	B

(b) $\lambda_* = 13.5$

DoFs	ref.	Lagr.	Néd.	λ_0	it.	$\lambda_{\text{it.}}$	J	r_{rel}	$J_{q,\min}$	$J_{q,\max}$	EVS
800	2	1	0	13.8610	7	13.4999	2.805e-06	2.468e-06	1.0025	1.0106	B
4860	2	2	1	13.0067	10	13.4999	1.986e-05	4.456e-06	0.9677	0.9970	B
4860	3	1	0	13.1679	8	13.4999	9.102e-06	8.218e-06	0.9913	0.9965	B
33525	3	2	1	13.0004	8	13.4999	2.034e-05	8.126e-06	0.9836	0.9990	B
33525	4	1	0	13.0418	8	13.4999	1.716e-05	8.728e-06	0.9947	0.9969	B

Table 5.11. Results of a freeform optimization on a cuboid varying the target value λ_* and with regularization parameters $\alpha = 10^{-2}$ and $\beta = 10^{-6}$. The tables show results varying the DoFs of the mesh, the refinement level (ref.), the order of Lagrange (Lagr.) and Nédélec (Néd.) elements. The initial first (numerical) eigenvalue is given by λ_0. We show the eigenvalue λ_{it} after termination of the method and the resulting value of the cost functional J, the relative residual of the gradient of the cost functional as well as the minimum and maximum value of the determinant of the deformation gradient J_q and the used eigenvalue solver EVS.

(a) $\lambda_* = 12.5$

DoFs	ref.	Lagr.	Néd.	λ_0	it.	$\lambda_{\mathrm{it.}}$	J	r_{rel}	$\mathrm{J}_{q,\min}$	$\mathrm{J}_{q,\max}$	EVS
800	2	1	0	13.8610	11	12.5	1.309e-05	3.079e-06	1.0177	1.0745	B
4860	2	2	1	13.0067	14	12.5	2.279e-06	8.976e-06	1.0015	1.0356	B
4860	3	1	0	13.1679	15	12.5	4.024e-06	3.8066e-06	1.0069	1.0195	B
33525	3	2	1	13.0004	15	12.5	2.220e-06	6.260e-06	0.9985	1.0173	B
33525	4	1	0	13.0418	14	12.5	2.615e-06	5.477e-06	1.0036	1.0071	B

(b) $\lambda_* = 13.5$

DoFs	ref.	Lagr.	Néd.	λ_0	it.	$\lambda_{\mathrm{it.}}$	J	r_{rel}	$\mathrm{J}_{q,\min}$	$\mathrm{J}_{q,\max}$	EVS
800	2	1	0	13.8610	12	13.5	2.741e-07	7.023e-06	1.0025	1.0106	B
4860	2	2	1	13.0067	11	13.5	2.004e-06	7.003e-06	0.9687	0.9971	B
4860	3	1	0	13.1679	15	13.5	9.229e-07	6.096e-06	0.9914	0.9964	B
33525	3	2	1	13.0004	10	13.5	2.053e-06	3.624e-05	0.9840	0.9980	B
33525	4	1	0	13.0418	16	13.5	1.734e-06	9.177e-06	0.9947	0.9968	B

(a) $\lambda_* = 12.5$

(b) $\lambda_* = 13.5$
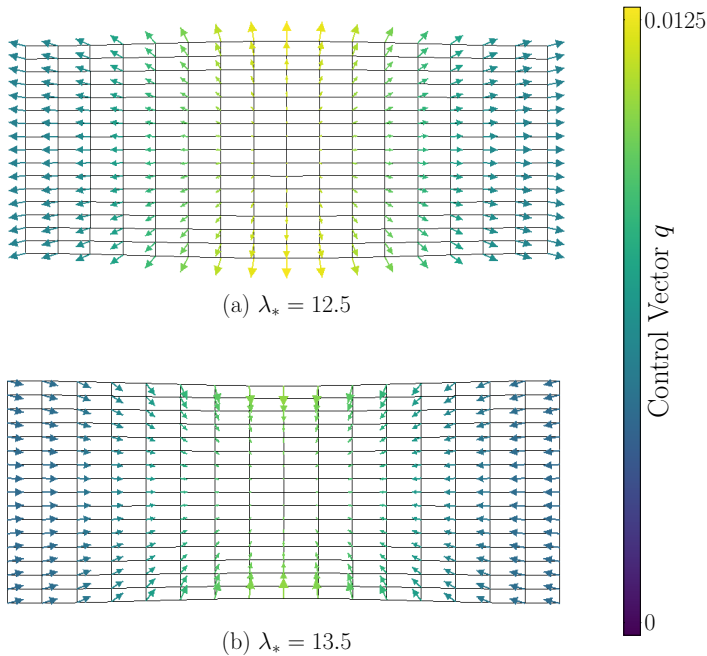
Figure 5.7. Cross-section y-axis of the deformation of a cuboid after optimization using the BFGS method from Algorithm 4.4 with regularization parameters $\alpha = 10^{-2}$ and $\beta = 10^{-5}$. The chosen refinement level is 4, the number of DoFs is 33525. Lagrange elements of order 1 and lowest order Nédélec elements are used.

(a) $\lambda_* = 12.5$

(b) $\lambda_* = 13.5$
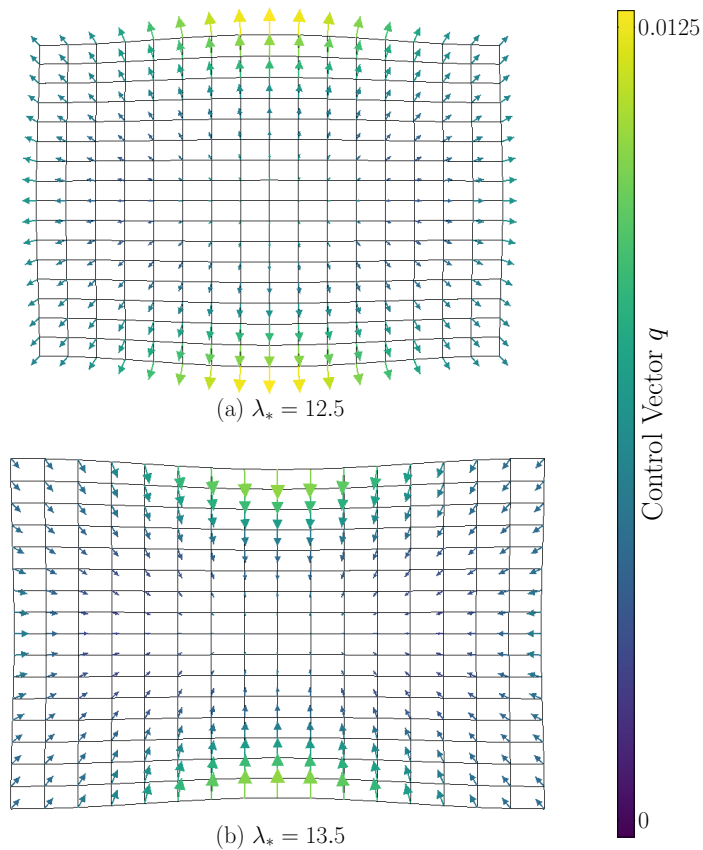
Figure 5.8. Cross-section z-axis of the deformation of a cuboid domain after optimization using the BFGS method from Algorithm 4.4 with regularization parameters $\alpha = 10^{-2}$ and $\beta = 10^{-5}$. The chosen refinement level is 4, the number of DoFs is 33525. Lagrange elements of order 1 and lowest order Nédélec elements are used.

5.2.2. Cylinder

In the context of particle collider, a pill-box is a particular case of interest, i.e., a cylindrical cavity. The extension to three-dimensional domains with curved boundaries is challenging because a good approximation of the domain requires a high resolution on the domain. Here, by the approximation of the domain with FE, the problem becomes very large. In the following, we show a first optimization example of a cylinder with radius $r = 1$ and length $l = 10$. We fix the left and right hand side of the cylinder by fixing $q = 0$. Table 5.12 shows the results of the optimization of the first eigenvalue to the target value $\lambda_* = 4$. Here, the chosen regularization parameters are $\alpha = 10^{-6}$ and $\beta = 10^{-4}$.

Table 5.12. Results of a freeform optimization to a target value $\lambda_* = 4$ with regularization parameters $\alpha = 10^{-6}$ and $\beta = 10^{-4}$ using the BFGS method from Algorithm 4.4 on on a cylinder with radius $r = 1$ and length $l = 10$. The initial first (numerical) eigenvalue is given by λ_0. We show the eigenvalue λ_{it} after termination of the method and the resulting value of the cost functional J, the relative residual of the gradient of the cost functional as well as the minimum and maximum value of the determinant of the deformation gradient J_q.

DoFs	ref.	Lagr.	Néd.	λ_0	it.	$\lambda_{\text{it.}}$	J	r_{rel}	$J_{q,\text{min}}$	$J_{q,\text{max}}$
25044	2	1	0	3.66322	14	4	2.970e-04	2.874e-06	0.99644	0.99989
189284	3	1	0	3.53257	14	4	4.189e-04	4.290e-06	0.99631	0.99888

The method converges after 14 iterations in every setting. The value of J_q is between 0.996 and 0.999 which means a shrinkage of the domain. This will be confirmed by considering the deformation of the domain, shown as a cross-section in Figure 5.10. The domain shrinks in the middle part of the cylindrical domain. In Figure 5.9, we show the three-dimensional domain of the cylinder before and after optimization.
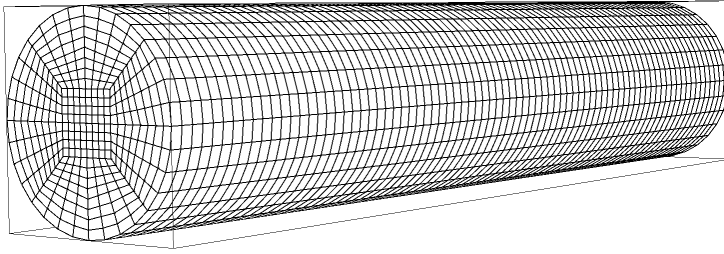
(a) Initial Cylinder
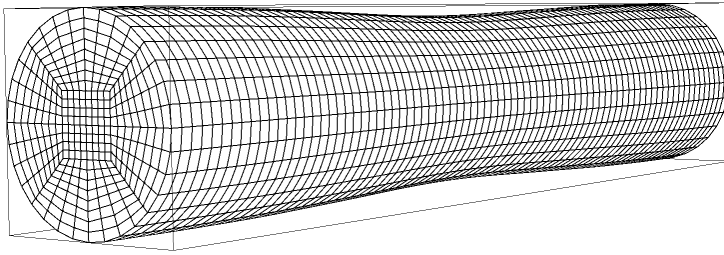
(b) Optimized Cylinder

Figure 5.9. Domain of the cylinder before and after optimization.
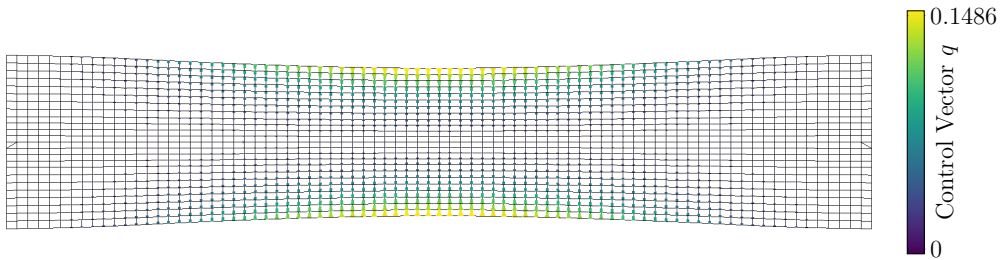
Figure 5.10. Cross-section of the deformation of a cylinder after optimization of the first eigenvalue to target value $\lambda_* = 4$ using the BFGS method from Algorithm 4.4 with regularization parameters $\alpha = 10^{-6}$ and $\beta = 10^{-4}$. The chosen refinement level is 3, the number of DoFs is 189284. Lagrange elements of order 1 and lowest order Nédélec elements are used.

Conclusion and Outlook

6.1. Conclusion

In this thesis, we considered an eigenvalue optimization problem with respect to shape-variations in electromagnetic systems motivated by particle accelerator cavities, such as superconducting TESLA cavities, see [12, 36, 46]. For a suitable problem formulation, we discussed the theory of Maxwell's eigenvalue problem in Chapter 3. Because of the context of particle accelerator cavities, we considered a time-harmonic formulation. In order to solve the considered problem, we discussed variants of possible variational formulations of this problems regarding the occurrence of so-called spurious modes. We decided to take the mixed formulation by Kikuchi even if this enlarges the problem by taking the divergence-free condition into account. Using this approach, we obtained a mixed saddle point problem formulation preventing that the obtained solutions are physical solutions. Afterwards, we formulated the Maxwell eigenvalue problem depending on a domain mapping, where we distinguished between the function spaces of $H_0(\mathrm{curl})$ and H_0^1. We concluded Chapter 3 by a discussion of the existence and properties of eigenvalues and associated eigenfunctions of the domain-dependent Maxwell eigenvalue problem.

In Chapter 4, we analyzed an eigenvalue optimization constrained by the previously considered Maxwell eigenvalue problem. First, we discussed the approach of adjoint calculus for general eigenvalue optimization problems. Afterwards, we applied adjoint calculus to the concrete problem. In order to solve this optimization problem, we discussed two optimization methods, a gradient method and a damped inverse BFGS method. For the latter, we proved the preservation of the

positive definiteness property of the updating operator which ensures that the curvature condition is fulfilled. Furthermore, we discussed a proper discretization of the Maxwell eigenvalue problem by using a mixed FEM, where we discretized the $H_0^1(\Omega)$-space with Lagrange elements and the $H_0(\mathrm{curl}; \Omega)$ with Nédélec elements. Moreover, we pointed out to some details on the implementation, which solved the eigenvalue problem. We made some comments to the hurdles by using mixed FEM and on the eigenvalue solver applied to the considered saddle point problem.

The main contribution of this thesis is the implementation and simulation of the considered freeform optimization problem constrained by Maxwell's eigenvalue problem with respect to shape-variations. All computations base on the finite element library `deal.II` [10,11] and are implemented within the optimization library `DOpElib` [49]. In the context of this thesis, we extended the framework for PDE optimization problems of the `DOpElib` library for eigenvalue optimization problems. In order to validate the implementation and the mentioned approach, we presented numerical results of eigenvalue optimization problems on simple geometries with different refinement levels and finite element orders, where we also considered curved domains, in Section 4.4. Finally, we concluded Chapter 4 by a discussion of the obtained numerical results. First, we compared the two considered optimization methods regarding convergence and the influence of the regularization parameters on the methods and, also, on the deformation of the domain after optimization. Second, we validated the influence of a change of the target value in the cost functional to which we optimize the considered eigenvalue. As expected, the BFGS method converges faster than gradient method with a suitable choice of regularization parameters.

In Chapter 5, we concluded this thesis with a discussion of necessary extensions to more realistic applications. Numerical examples were presented using the damped inverse BFGS method on two-dimensional planar cavity geometries for a validation of the approach on more complex and detailed geometries. We showed solutions on 1-cell and 5-cell cavity geometries, based on a model seen in [36]. Finally, we showed numerical examples in three-dimensional geometries, such as a cuboid and a cylinder.

6.2. Outlook

Let us consider some open questions for future research and investigations. In Chapter 3, we computed the Fréchet derivatives by assuming differentiability for the time-harmonic Maxwell eigenvalue problem depending on a domain mapping. One possible investigation is the analysis of the considered problem. To this, one needs to extend the proofs for the continuity as well as for differentiability of eigenvalues and associated eigenfunctions in the context of linear elasticity problems in [44] to the context of Maxwell's eigenvalue problem. Doing that, we could use the properties discussed in Chapter 3 to show continuity. In detail, we could prove the sequential continuity and local Lipschitz continuity of the eigenvalues with respect to control variations in the domain mapping. Further, with help of a sign convention for the eigenfunctions, we should be able to prove continuity of the eigenfunctions and the differentiability of the eigenvalues and associated eigenfunctions. In detail, one has to show semi-differentiability of the first eigenvalue and with that, we could prove Fréchet-differentiability of the considered problem. For the proofs of the analysis for problems depending on a domain mapping, we refer to [42], where Fréchet differentiability is proved in context of Navier-Stokes and the Boussinesq equations. The analysis is based on the assumption of simple eigenvalues. In the application of particle accelerator cavities, this is sufficient because the acceleration frequencies are in general simple. From a mathematical perspective, an extension to semi-simple eigenvalue it would be conceivable but unnecessary for the application.

Further, there are many tasks for the extension of this approach to more realistic problems. In Chapter 5, we showed numerical examples on two-dimensional planar cavities as well as on a three-dimensional cuboid and cylinder. By computing on three-dimensional domains, the system of equations enlarges fast by the increasing number of DoFs. We expect that an extension of parallel computing is necessary in order to save runtime. Another geometry of interest is a three-dimensional cavity domain.

In our numerical examples, we just considered the optimization of a certain eigenvalue to a target value. In the optimization process, we did not check if the obtained eigenvalue stays at the same position in the optimization process. Here, an eigenvalue tracking could be useful because if we optimize the acceleration frequency we want guarantee that it is still the acceleration frequency after optimization. The tracking of eigenvalues is already done in the context of accelerator cavities, e.g., see [36, 46, 61] and could be applied to our freeform

optimization problem. By the consideration of more quantities of interest on the application, several extensions are conceivable, e.g., field flatness and cavity tuning. For these quantities, we refer, e.g., to [36, 85, 112].

It is also conceivable to optimize a spectrum of eigenvalues. By a computation of more than one eigenvalue, it is possible that we have reconsider the choice of eigenvalue solver. Until now, in all numerical examples, the choice of eigenvalue solver is chosen by the assumption of solving just one eigenvalue at a time.

Appendix

A.1. Optimization of Eigenvalue Problems in `DOpElib`

In this thesis, the examples of the optimization of eigenvalue problems are implemented with the `DOpElib`-library [49], based on the FE library `deal.II` [10, 11]. The implementations are tested for `deal.II version 9.4.0`. The utilization of the `DOpElib`-library allows an easy implementation and numerical solving of PDE problems

$$a(u, \psi) = 0 \quad \forall \, \psi \in V,$$

with some appropriate space V, and PDE optimization problems of the form

$$
\begin{aligned}
\min \quad & J(q, u) \\
\text{s.t.} \quad & a(q; u, \psi) = 0 \qquad \forall \, \psi \in V, \\
& a \leq q \leq b, \\
& g(q, u) \leq 0,
\end{aligned}
$$

where u is a FE-function and q is either a FE-function or some fixed number of parameters, $J(\cdot, \cdot)$ is the cost functional, a and b are constraint bounds for the control q, and $g(\cdot)$ is some control or state constraint.

During this thesis, we extended the library to solve eigenvalue optimization problems of the form

$$
\begin{aligned}
\min \quad & J(q, \lambda) \\
\text{s.t.} \quad & k(q; u, \psi) &&= \lambda\, m(q; u, \psi) && \forall\, \psi \in V, \\
& m(q; u, u) &&= 1;
\end{aligned}
\tag{A.1}
$$

where (λ, u) denotes the eigensolution with the eigenvalue λ and the eigenvector u. Further, $k(\cdot; \cdot, \cdot)$ and $m(\cdot; \cdot, \cdot)$ denote the stiffness and mass matrix.

In the following, we describe the extension of the library. With the Lagrangian

$$
\begin{aligned}
\mathcal{L}(q, (\lambda, u), z) &= J(q, (\lambda, u)) - k(q, u)(z) + \lambda m(q, u)(z) \\
&= J(q, (\lambda, u)) - \tilde{a}(q, (\lambda, u))(z),
\end{aligned}
$$

where $\tilde{a}(q, (\lambda, u))(z) = k(q, u)(z) - \lambda m(q, u)(z)$, we formulate the optimality (KKT) system

$$
\begin{aligned}
\tilde{a}'_{\underline{u}}(q, \underline{u}, \underline{z})(\underline{\phi}) &= J'_{\underline{u}}(q, \underline{u})(\underline{\phi}) \\
\tilde{a}'_q(q, \underline{u})(\chi, \underline{z}) &= J'_q(q, \underline{u})(\chi) \\
\tilde{a}(q, \underline{u})(\underline{\psi}) &= 0
\end{aligned}
$$

with $\underline{u} = (\lambda, u)^T$ and $\underline{z} = (\mu, z)^T$.

In PDE optimization, the state is a vector. In contrary, the state of an eigenvalue optimization problem consists of one or more eigenvalues and their associated eigenfunctions. Therefore, define a vector for the eigenvalues and a vector containing the eigenfunctions, i.e.,

```
std::vector<double> uvals_,
std::vector<StateVector<VECTOR>> uvecs_.
```

We define the adjoint solutions similarly, i.e.,

```
std::vector<double> zvals_,
std::vector<StateVector<VECTOR>> zvecs_.
```

A.1.1. Extension and Implementation Details

Problem Container
To save the complete problem description in a common data format and to

pass data between the objects, the library contains container, named by their problem type. For the structure of eigenvalue optimization problems, we add a container called `eigenvalueproblemcontainer.h` to the library. This container contains the data, i.e., the semilinear forms $k(\cdot)(\cdot)$ (`ElementMatrix`), $m(\cdot)(\cdot)$ `ElementMassMatrix`. and a target functional $J(\cdot)$, which describe the problem and builds the element right-hand side (`ElementRhs`).

Space-time Handler

To numerically solve the problem on require a space-time handler which handle all dofs in space and time. In the eigenvalue optimization with Maxwell's equation, we utilize a mixed finite element discretiziation with Lagrange and Nédélec elements. Therefore, we need to differentiate between two different kinds of boundary conditions. We apply these conditions in the space-time handler. More concrete, we added the case for mixed finite elements by using the function

```
VectorTools::interpolate_boundary_values(...)
```

for the Lagrange elements and the curl-conforming (perfect electrical conductor) boundary conditions

```
VectorTools::project_boundary_values_curl_conforming_l2(...)
```

for the Nédélec elements.

Integrator

The library contains several integrator routines which computes integrals over a given triangulation. The original class `integrator.h` computes the matrix corresponding to the linearized equation. To integrate over a triangulation of a generalized eigenvalue problem, we need a calculation of two matrices, namely the stiffness and the mass matrix. Therefore, we extend the class `integrator.h`. There, the function

```
void ComputeMassMatrix(PROBLEM &pde, MATRIX &matrix)
```

integrates over the mass matrix, where the stiffness matrix is computed in the function

```
void ComputeMatrix(PROBLEM &pde, MATRIX &matrix),
```

similary to the function in the original class.

Reduced Problem

We extend the library with the class `eigenvaluereducedproblem.h` which implicitly solve the reduced optimization problem whenever it is required. For algorithmic aspects, we refer to [18]. This class is an abstraction which contains methods to solve the reduced problem by solving intern the eigenvalue problem.

It returns the function values and derivatives of the reduced functional by using adjoint calculus. The reduced problem class consists the method to compute the reduced gradient (`ReducedGradient`) by applying a Newton solver. The settings of this solver for the optimization in this thesis are shown in Table A.1.

Table A.1. Settings of the Newton solver for the optimization on rectangle (R), quarter circle (C), 1-cell cavity (1C), 5-cell cavity (5C), cuboid (CU) and cylinder (CY) domains

	R, C, 1C	5C,CU,CY
maximal number of linesearch steps	8	8
reduction rate for the linesearch damping parameter	0.9	0.9
global tolerance for the newton iteration	10^{-12}	10^{-8}
maximal number of newton iterations	100	100
minimal newton reduction	0.1	0.1
relative tolerance for the newton iteration	10^{-10}	10^{-6}

Reduced Optimization Methods

The library contains also several optimization algorithms to solve reduced optimization problems where the PDE, or eigenvalue problem, constraint has been eliminated as explained above. For the numerical examples, we implemented the BFGS method from Algorithm 4.4 in the class

> `reduceddampedbfgsalgorithm.h.`

Further, we compared this method with the gradient method from Algorithm 4.3, which is implemented in the class

> `reducedgradientalgorithm.h.`

Problemdata

We extended the library by the problemdata `eigenvaluestateproblem` and `eigenvalueadjointproblem` which is similar to the 'standard' `stateproblem`/ `adjointproblem` with appropriate extension for the `ElementMassMatrix` or `ElementMassMatrix_U`.

Eigenvalue Solver

In order to solve generalized eigenvalue problems, we use `SLEPc`-library based on the `PETSc`-library, more details in Table A.2. Within the `deal.II`-library, a wrapper to the `SLEPc`-library exists and contains some basis eigenvalue solver with basic settings. An example is class `eigenvalue_solver_lapack.h`, where we used the wrapper to use the in `SLEPc` implemented `LAPACK` solver. For some

Table A.2. Libraries for the eigenvalue optimization with `DOpElib` used for the results of this thesis

library	version	
`deal.ii`	9.4.0	FE-library [10, 11]
`PETSc`	3.18.5	Portable Extendable Toolkit for Scientific Computations [55, 56, 95]
`SLEPc`	3.18.2	Scalable Library for Eigenvalue Problem Computations [13–15]

basic tests, this works well. Nevertheless, for more flexibility, we interfaced some eigenvalue solver independently from the wrapper class.

For the numerical examples of this thesis, we use either the subspace iteration (A) or the Krylov Schur (B) eigenvalue solver, provided by `SLEPc`. We apply a shift-invert spectral transformation with the target shifts shown in Table A.3. A target magnitude is chosen equally. The tolerance for the eigenvalue solver is set to 10^{-5}. The eigenvalue solver applies a Richardson solver and the Cholesky preconditioner. For the numerical examples in Section 4.4, we use the default properties of the `SLEPc`- and `PETSc`-libraries, whereas in the Chapter 5, we set the relative convergence tolerance of the Richardson Krylov solver to 10^{-5} and allow this method to automatically determine optimal scaling at each iteration to minimize the 2-norm of the preconditioned residual. Furthermore, the eigenvalue solver classes contain a normalization method for the eigenfunctions.

Table A.3. Shift parameter for the eigenvalue solver

Example	Solver	Shift
Rectangle	Subspace Iteration (A)	4
Rectangle	Krylov Schur (B)	4
Rectangle	Krylov Schur (BS)	3.8
Quarter Circle	Subspace Iteration (A)	0.9
Quarter Circle	Krylov Schur (B)	0.9
Quarter Circle	Krylov Schur (BS)	0.94
1-Cell Cavity	Krylov Schur (B)	1650
5-Cell Cavity	Krylov Schur (B)	6000
5-Cell Cavity	Krylov Schur (BS)	6024
Cuboid	Krylov Schur (B)	13
Cylinder	Subspace Iteration (A)	2

A.1.2. Implementation Details to Maxwell's Eigenvalue Optimization Problem

In the numeric examples in Section 4.4 and Chapter 5, we consider an eigenvalue optimization problem of the form: Find λ_i, u_i, such that

$$\min \ J(\lambda_i, q)$$
$$\text{s.t.} \quad Ku_i = \lambda_i M u_i \quad \text{in } \Omega_q,$$
$$\|u_i\|_{\Omega_q} = 1$$

of a domain Ω_q and where K, M are the stiffness and mass matrix, respectively.

The mixed finite elements for the state are defined in a `FESystem` with Nédélec-elements to discretize the $H_0(\text{curl})$-space and Lagrange elements to discretize the H_0^1-space:

```
FESystem<DIM> state_fe(FE_Q<DIM>(order_lagr), 1,
   FE_Nedelec<DIM>(order_ned),1).
```

For the control we use Lagrange-elements:

```
FE<DIM> control_fe(FE_Q<DIM>(order_lagrange), 2).
```

In the examples, the choice of element order is either

$\quad$ `order_lagr` $= 1$ and `order_ned` $= 0$, or

$\quad$ `order_lagr` $= 2$ and `order_ned` $= 1$.

In the `localpde.h`, we implement all functions needed for the compuation of the reduced state, adjoint and gradient. For the state and adjoint solution, we need an eigenvalue computation. Therefore, we implement the `ElementMatrix` and `ElementMassMatrix` of our problem. The `ElementMatrix_Q` and `ElementMassMatrix_Q` consist of the derivatives of the associated matrix with respect to the control variable q. Further, the `ControlElementEquation` and `ControlElementMatrix` implement the inner product associated to the control space to invert the respective Riesz mapping.

For the domain mapping, introduced in Section 3.2, we implement in `functions.h` subroutines for the deformation gradient with respect to the control variable q

```
Tensor<2,DIM> deformation_tensor_(Tensor<2,DIM>)
double determinante_(Tensor<2,DIM>)
Tensor<2,DIM> adjunkte_(Tensor<2,DIM>)
Tensor<2,DIM> transpose_(Tensor<2,DIM>)
Tensor<2,DIM> adjunkte_transposed_(Tensor<2,DIM>)
Tensor<2,DIM> inverse_(Tensor<2,DIM>)
Tensor<2,DIM> inverse_transpose_(Tensor<2,DIM>)
```

and the required derivatives

```
double determinante_DF_dq_(Tensor<2,DIM> ,Tensor<2,DIM>)
double determinante_DF_inv_dq_(Tensor<2,DIM>,Tensor<2,DIM>)
Tensor<2,DIM> DF_inv_T_dq_(Tensor<2,DIM>,Tensor<2,DIM>)
Tensor<2,DIM> DF_inv_dq_(Tensor<2,DIM>,Tensor<2,DIM>).
```

In the class `localfunctional.h` , we implement all information regarding the `ReducedCostfunctional`. We split the cost functional in two parts. The first part is the evaluation of the algebraic value of the cost functional. This is done in the function `AlgebraicValue`. And second, for the regularization terms, we need the evaluation of a domain integral. This is computed in `ElementValue`. To handle this, we determine the type of the cost functional by `"domain algebraic"`. Further, for the optimization process, the method `ElementValue_Q` is implemented for the computation of the reduced gradient.

A.2. Further Numerical Solution Tables

A.2.1. Rectangle with Free Boundaries

Table A.4. Results of a freeform optimization for the first eigenvalue on a rectangle domain with target value $\lambda_* = 3.8$ and regularization parameters $\alpha = 10^{-1}, \beta = 10^{-5}$ for the tolerance of the termination criteria of $\text{TOL}_{\text{global}} = \text{TOL} = 10^{-5}$. The tables show results varying the DoFs of the mesh, the refinement level (ref.), the order of Lagrange (Lagr.) and Nédélec (Néd.) elements. The initial first (numerical) eigenvalue is given by λ_0. We show the eigenvalue λ_{it} after termination of the method and the resulting value of the cost functional J, the relative residual of the gradient of the cost functional as well as the minimum and maximum value of the determinant of the deformation gradient J_q and the used eigenvalue solver EVS.

(a) BFGS method from Algorithm 4.4

DoFs	ref.	Lagr.	Néd.	λ_0	it.	$\lambda_{\text{it.}}$	J	r_{rel}	$\text{J}_{q,\text{min}}$	$\text{J}_{q,\text{max}}$	EVS
387	2	2	1	4.002	7	3.80054	5.224e-05	2.417e-06	1.019	1.049	A
387	3	1	0	4.052	7	3.80067	8.131e-05	7.379e-06	1.048	1.055	A
1411	3	2	1	4.000	7	3.80053	5.124e-05	2.683e-06	1.032	1.049	A
1411	4	1	0	4.013	7	3.80056	5.802e-05	3.583e-06	1.047	1.049	A
5389	4	2	1	4.000	7	3.80053	5.117e-05	2.704e-06	1.041	1.049	A
5389	5	1	0	4.003	7	3.80054	5.284e-05	2.907e-06	1.048	1.049	A
20995	5	2	1	4.000	7	3.80053	5.117e-05	2.704e-06	1.045	1.050	A

(b) Gradient method from Algorithm 4.3

DoFs	ref.	Lagr.	Néd.	λ_0	it.	$\lambda_{\text{it.}}$	J	r_{rel}	$\text{J}_{q,\text{min}}$	$\text{J}_{q,\text{max}}$	EVS
387	2	2	1	4.002	278	3.80054	5.224e-05	9.538e-06	1.020	1.049	A
387	3	1	0	4.052	350	3.80067	8.131e-05	9.672e-06	1.048	1.055	A
1411	3	2	1	4.000	278	3.80053	5.124e-05	9.529e-06	1.032	1.049	A
1411	4	1	0	4.013	300	3.80056	5.802e-05	9.479e-06	1.047	1.049	A
5389	4	2	1	4.000	278	3.80053	5.117e-05	9.528e-06	1.041	1.049	A
5389	5	1	0	4.003	281	3.80054	5.284e-05	9.762e-06	1.048	1.048	A
20995	5	2	1	4.000	278	3.80053	5.117e-05	9.522e-06	1.045	1.049	A

Table A.5. Results of a freeform optimization for the first eigenvalue on a rectangle domain with target value $\lambda_* = 3.8$ and regularization parameters $\alpha = 10^{-5}, \beta = 10^{-5}$ for the tolerance of the termination criteria of $\text{TOL}_{\text{global}} = \text{TOL} = 10^{-5}$. The tables show results varying the DoFs of the mesh, the refinement level (ref.), the order of Lagrange (Lagr.) and Nédélec (Néd.) elements. The initial first (numerical) eigenvalue is given by λ_0. We show the eigenvalue λ_{it} after termination of the method and the resulting value of the cost functional J, the relative residual of the gradient of the cost functional as well as the minimum and maximum value of the determinant of the deformation gradient J_q and the used eigenvalue solver EVS.

(a) BFGS method from Algorithm 4.4

DoFs	ref.	Lagr.	Néd.	λ_0	it.	$\lambda_{\text{it.}}$	J	r_{rel}	$J_{q,\min}$	$J_{q,\max}$	EVS
387	2	2	1	4.002	38	3.8	-2.037e-06	8.388e-06	1.109	1.189	B
387	3	1	0	4.052	38	3.8	-1.403e-06	7.410e-06	1.109	1.132	B
1411	3	2	1	4.000	38	3.8	-2.128e-06	8.418e-06	1.169	1.202	B
1411	4	1	0	4.013	38	3.8	-1.369e-06	8.713e-06	1.107	1.123	B
5389	4	2	1	4.000	38	3.8	-2.048e-06	8.456e-06	1.178	1.192	B
5389	5	1	0	4.003	38	3.8	-2.834e-06	9.904e-06	1.249	1.281	B
20995	5	2	1	4.000	38	3.8	-2.048e-06	8.456e-06	1.182	1.187	B

(b) Gradient method from Algorithm 4.3

DoFs	ref.	Lagr.	Néd.	λ_0	it.	$\lambda_{\text{it.}}$	J	r_{rel}	$J_{q,\min}$	$J_{q,\max}$	EVS
387	2	2	1	4.002	1000	3.8	-3.320e-07	1.348e-05	1.020	1.0492	A
387	3	1	0	4.052	55	3.8	-4.051e-07	9.955e-06	1.048	1.055	A
1411	3	2	1	4.000	1000	3.8	-3.288e-07	1.381e-05	1.032	1.049	A
1411	4	1	0	4.013	1000	3.8	-3.493e-07	1.237e-05	1.047	1.049	A
5389	4	2	1	4.000	1000	3.8	-3.286e-07	1.382e-05	1.041	1.049	A
5389	5	1	0	4.003	1000	3.8	-3.338e-07	1.344e-05	1.048	1.049	A
20995	5	2	1	4.000	1000	3.8	-3.286e-07	1.382e-05	1.054	1.050	A

Table A.6. Results of a freeform optimization for the first eigenvalue on a rectangle domain with target value $\lambda_* = 3.8$ and regularization parameters $\alpha = 10^{-4}, \beta = 10^{-8}$ for the tolerance of the termination criteria of $\text{TOL}_{\text{global}} = \text{TOL} = 10^{-5}$. The tables show results varying the DoFs of the mesh, the refinement level (ref.), the order of Lagrange (Lagr.) and Nédélec (Néd.) elements. The initial first (numerical) eigenvalue is given by λ_0. We show the eigenvalue λ_{it} after termination of the method and the resulting value of the cost functional J, the relative residual of the gradient of the cost functional as well as the minimum and maximum value of the determinant of the deformation gradient J_q and the used eigenvalue solver EVS.

(a) BFGS method from Algorithm 4.4

DoFs	ref.	Lagr.	Néd.	λ_0	it.	$\lambda_{\text{it.}}$	J	r_{rel}	$J_{q,\text{min}}$	$J_{q,\text{max}}$	EVS
387	2	2	1	4.002	13	3.8	5.568e-08	3.188e-06	1.014	1.059	A
387	3	1	0	4.052	15	3.8	8.681e-08	1.368e-06	1.052	1.061	B
1411	3	2	1	4.000	14	3.8	5.456e-08	6.696e-06	1.034	1.058	A
1411	4	1	0	4.013	15	3.8	6.126e-08	2.108e-06	1.051	1.053	B
5389	4	2	1	4.000	15	3.8	5.455e-08	9.292e-07	1.046	1.058	A
5389	5	1	0	4.003	15	3.8	5.642e-08	1.220e-06	1.056	1.057	A
20995	5	2	1	4.000	15	3.8	5.455e-08	9.401e-07	1.052	1.058	B

(b) Gradient method from Algorithm 4.3

DoFs	ref.	Lagr.	Néd.	λ_0	it.	$\lambda_{\text{it.}}$	J	r_{rel}	$J_{q,\text{min}}$	$J_{q,\text{max}}$	EVS
387	2	2	1	4.002	25	3.8	5.239e-08	9.896e-06	1.020	1.049	A
387	3	1	0	4.052	26	3.8	8.155e-08	7.746e-06	1.048	1.055	A
1411	3	2	1	4.000	25	3.8	5.138e-08	9.789e-06	1.032	1.049	A
1411	4	1	0	4.013	26	3.8	5.818e-08	6.572e-06	1.047	1.049	A
5389	4	2	1	4.000	25	3.8	5.132e-08	9.782e-06	1.041	1.049	A
5389	5	1	0	4.003	25	3.8	5.299e-08	9.907e-06	1.048	1.048	A
20995	5	2	1	4.000	25	3.8	5.131e-08	9.780e-06	1.045	1.049	A

Table A.7. Results of a freeform optimization for the first eigenvalue on a rectangle domain with target value $\lambda_* = 3.8$ and regularization parameters $\alpha = 10^{-5}, \beta = 10^{-8}$ for the tolerance of the termination criteria of $\text{TOL}_{\text{global}} = \text{TOL} = 10^{-5}$. The tables show results varying the DoFs of the mesh, the refinement level (ref.), the order of Lagrange (Lagr.) and Nédélec (Néd.) elements. The initial first (numerical) eigenvalue is given by λ_0. We show the eigenvalue λ_{it} after termination of the method and the resulting value of the cost functional J, the relative residual of the gradient of the cost functional as well as the minimum and maximum value of the determinant of the deformation gradient J_q and the used eigenvalue solver EVS.

(a) BFGS method from Algorithm 4.4

DoFs	ref.	Lagr.	Néd.	λ_0	it.	$\lambda_{\text{it.}}$	J	r_{rel}	$J_{q,\text{min}}$	$J_{q,\text{max}}$	EVS
387	2	2	1	4.002	13	3.8	5.329e-09	7.454e-06	1.013	1.060	A
387	3	1	0	4.052	15	3.8	8.405e-09	9.111e-07	1.053	1.062	B
1411	3	2	1	4.000	14	3.8	5.213e-09	7.044e-06	1.034	1.059	B
1411	4	1	0	4.013	15	3.8	5.957e-09	1.531e-06	1.055	1.058	B
5389	4	2	1	4.000	14	3.8	5.211e-09	9.974e-06	1.046	1.060	A
5389	5	1	0	4.003	15	3.8	5.390e-09	9.976e-07	1.056	1.057	B
20995	5	2	1	4.000	15	3.8	5.208e-09	7.111e-07	1.053	1.060	A

(b) Gradient method from Algorithm 4.3

DoFs	ref.	Lagr.	Néd.	λ_0	it.	$\lambda_{\text{it.}}$	J	r_{rel}	$J_{q,\text{min}}$	$J_{q,\text{max}}$	EVS
387	2	2	1	4.002	25	3.8	4.944e-09	9.897e-06	1.020	1.049	A
387	3	1	0	4.052	26	3.8	7.786e-09	7.746e-06	1.048	1.055	A
1411	3	2	1	4.000	25	3.8	4.846e-09	9.789e-06	1.032	1.049	A
1411	4	1	0	4.013	26	3.8	5.506e-09	6.572e-06	1.047	1.049	A
5389	4	2	1	4.000	25	3.8	4.840e-09	9.782e-06	1.041	1.049	A
5389	5	1	0	4.003	25	3.8	5.002e-09	9.907e-06	1.048	1.048	A
20995	5	2	1	4.000	25	3.8	4.839e-09	9.781e-06	1.045	1.049	A

Table A.8. Results of a freeform optimization for the first eigenvalue on a rectangle domain with target value $\lambda_* = 3.8$ and regularization parameters $\alpha = 10^{-2}, \beta = 10^{-8}$ for the tolerance of the termination criteria of $\mathrm{TOL}_{\mathrm{global}} = \mathrm{TOL} = 10^{-5}$. The tables show results varying the DoFs of the mesh, the refinement level (ref.), the order of Lagrange (Lagr.) and Nédélec (Néd.) elements. The initial first (numerical) eigenvalue is given by λ_0. We show the eigenvalue λ_{it} after termination of the method and the resulting value of the cost functional J, the relative residual of the gradient of the cost functional as well as the minimum and maximum value of the determinant of the deformation gradient J_q and the used eigenvalue solver EVS.

(a) BFGS method from Algorithm 4.4

DoFs	ref.	Lagr.	Néd.	λ_0	it.	λ_{it}	J	r_{rel}	$\mathrm{J}_{q,\mathrm{min}}$	$\mathrm{J}_{q,\mathrm{max}}$	EVS
387	2	2	1	4.002	9	3.80005	5.269e-06	5.214e-07	1.019	1.049	A
387	3	1	0	4.052	10	3.80007	8.192e-06	3.375e-06	1.048	1.055	A
1411	3	2	1	4.000	9	3.80005	5.168e-06	9.175e-07	1.032	1.049	A
1411	4	1	0	4.013	9	3.80006	5.850e-06	6.211e-07	1.047	1.049	A
5389	4	2	1	4.000	9	3.80005	5.162e-06	9.620e-07	1.041	1.050	A
5389	5	1	0	4.003	9	3.80005	5.330e-06	7.144e-07	1.005	1.049	A
20995	5	2	1	4.000	9	3.80005	5.162e-06	9.683e-07	1.045	1.050	A

(b) Gradient method from Algorithm 4.3

DoFs	ref.	Lagr.	Néd.	λ_0	it.	λ_{it}	J	r_{rel}	$\mathrm{J}_{q,\mathrm{min}}$	$\mathrm{J}_{q,\mathrm{max}}$	EVS
387	2	2	1	4.002	26	3.80006	5.270e-06	6.815e-6	1.020	1.049	A
387	3	1	0	4.052	26	3.80007	8.194e-06	8.365e-05	1.048	1.055	A
1411	3	2	1	4.000	26	3.80005	5.169e-06	6.746e-06	1.032	1.049	A
1411	4	1	0	4.013	26	3.80006	5.851e-05	7.118e-06	1.047	1.049	A
5389	4	2	1	4.000	26	3.80005	5.163e-06	6.742e-06	1.041	1.049	A
5389	5	1	0	4.003	26	3.80006	5.330e-06	6.834e-06	1.048	1.048	A
20995	5	2	1	4.000	26	3.80005	5.162e-06	6.741e-06	1.045	1.049	A

Table A.9. Results of a freeform optimization for the first eigenvalue on a rectangle domain with target value $\lambda_* = 3.8$ and regularization parameters $\alpha = 10^{-1}, \beta = 10^{-8}$ for the tolerance of the termination criteria of $\text{TOL}_{\text{global}} = \text{TOL} = 10^{-5}$. The tables show results varying the DoFs of the mesh, the refinement level (ref.), the order of Lagrange (Lagr.) and Nédélec (Néd.) elements. The initial first (numerical) eigenvalue is given by λ_0. We show the eigenvalue λ_{it} after termination of the method and the resulting value of the cost functional J, the relative residual of the gradient of the cost functional as well as the minimum and maximum value of the determinant of the deformation gradient J_q and the used eigenvalue solver EVS.

(a) BFGS method from Algorithm 4.4

DoFs	ref.	Lagr.	Néd.	λ_0	it.	$\lambda_{\text{it.}}$	J	r_{rel}	$J_{q,\text{min}}$	$J_{q,\text{max}}$	EVS
387	2	2	1	4.002	7	3.80054	5.257e-05	2.413e-06	1.019	1.049	A
387	3	1	0	4.052	7	3.80067	8.172e-05	7.367e-06	1.048	1.055	A
1411	3	2	1	4.000	7	3.80053	5.156e-05	2.680e-06	1.032	1.049	A
1411	4	1	0	4.013	7	3.80057	5.836e-05	3.577e-06	1.047	1.049	A
5389	4	2	1	4.000	7	3.80053	5.150e-05	2.699e-06	1.041	1.049	A
5389	5	1	0	4.003	7	3.80054	2.9030e-06	5.317e-05	1.048	1.048	A
20995	5	2	1	4.000	7	3.80053	5.149e-05	2.700e-06	1.045	1.050	A

(b) Gradient method from Algorithm 4.3

DoFs	ref.	Lagr.	Néd.	λ_0	it.	$\lambda_{\text{it.}}$	J	r_{rel}	$J_{q,\text{min}}$	$J_{q,\text{max}}$	EVS
387	2	2	1	4.002	344	3.80054	5.257e-05	9.385e-06	1.019	1.049	A
387	3	1	0	4.052	394	3.80067	8.172e-05	9.495e-06	1.048	1.055	A
1411	3	2	1	4.000	344	3.80053	5.156e-05	9.386e-06	1.032	1.049	A
1411	4	1	0	4.013	347	3.80057	5.836e-05	9.829e-06	1.047	1.049	A
5389	4	2	1	4.000	344	3.80053	5.150e-05	9.388e-06	1.041	1.049	A
5389	5	1	0	4.003	344	3.80054	5.317e-05	9.470e-06	1.048	1.048	A
20995	5	2	1	4.000	344	3.80053	5.149e-05	9.385e-06	1.045	1.049	A

Table A.10. Results of a freeform optimization for the first eigenvalue on a rectangle domain with target value $\lambda_* = 3.8$ and regularization parameters $\alpha = 10^{-4}, \beta = 10^{-3}$ for the tolerance of the termination criteria of $\text{TOL}_{\text{global}} = \text{TOL} = 10^{-5}$. The tables show results varying the DoFs of the mesh, the refinement level (ref.), the order of Lagrange (Lagr.) and Nédélec (Néd.) elements. The initial first (numerical) eigenvalue is given by λ_0. We show the eigenvalue λ_{it} after termination of the method and the resulting value of the cost functional J, the relative residual of the gradient of the cost functional as well as the minimum and maximum value of the determinant of the deformation gradient J_q and the used eigenvalue solver EVS.

(a) BFGS method from Algorithm 4.4

DoFs	ref.	Lagr.	Néd.	λ_0	it.	$\lambda_{\text{it.}}$	J	r_{rel}	$J_{q,\min}$	$J_{q,\max}$	EVS
387	2	2	1	4.002	100	3.79974	-2.393e-03	4.400e-04	4.012	13.748	BS
387	3	1	0	4.052	100	3.79984	-2.063e-03	2.450e-04	2.063	3.732	B
1411	3	2	1	4.000	100	3.79975	-2.006e-03	3.559e-04	2.485	3.661	B
1411	4	1	0	4.013	100	3.80102	-1.235e-03	5.001e-03	2.582	3.009	B
5389	4	2	1	4.000	100	3.79957	-1.241e-03	1.113e-03	2.622	2.780	B
5389	5	1	0	4.003	100	3.799	-2.277e-03	2.178e-03	11.576	12.424	B
20995	5	2	1	4.000	100	3.79923	-1.361e-03	2.865e-03	2.963	3.232	B

(b) Gradient method from Algorithm 4.3

DoFs	ref.	Lagr.	Néd.	λ_0	it.	$\lambda_{\text{it.}}$	J	r_{rel}	$J_{q,\min}$	$J_{q,\max}$	EVS
387	2	2	1	4.002	1000	3.80003	-9.971e-05	1.343e-03	1.061	1.066	A
387	3	1	0	4.052	1000	3.79952	-1.078e-04	1.350e-03	1.075	1.075	A
1411	3	2	1	4.000	1000	3.80004	-9.941e-05	1.381e-03	1.063	1.066	A
1411	4	1	0	4.013	1000	3.8	-1.015e-04	1.190e-03	1.068	1.068	A
5389	4	2	1	4.000	1000	3.80004	-9.939e-05	1.384e-03	1.064	1.066	A
5389	5	1	0	4.003	1000	3.80003	-9.990e-05	1.331e-03	1.066	1.066	A
20995	5	2	1	4.000	1000	3.80004	-9.939e-05	1.384e-03	1.065	1.066	A

Table A.11. Results of a freeform optimization for the first eigenvalue on a rectangle domain with target value $\lambda_* = 3.8$ and regularization parameters $\alpha = 10^{-5}, \beta = 10^{-3}$ for the tolerance of the termination criteria of $\text{TOL}_{\text{global}} = \text{TOL} = 10^{-5}$. The tables show results varying the DoFs of the mesh, the refinement level (ref.), the order of Lagrange (Lagr.) and Nédélec (Néd.) elements. The initial first (numerical) eigenvalue is given by λ_0. We show the eigenvalue λ_{it} after termination of the method and the resulting value of the cost functional J, the relative residual of the gradient of the cost functional as well as the minimum and maximum value of the determinant of the deformation gradient J_q and the used eigenvalue solver EVS.

(a) BFGS method from Algorithm 4.4

DoFs	ref.	Lagr.	Néd.	λ_0	it.	λ_{it}	J	r_{rel}	$J_{q,\min}$	$J_{q,\max}$	EVS
387	2	2	1	4.002	100	3.79961	-1.944e-03	7.788e-04	3.800	3.936	B
387	3	1	0	4.052	100	3.79965	-2.884e-03	3.755e-04	1.079	6.984	B
1411	3	2	1	4.000	100	3.80053	-1.401e-03	3.317e-03	2.876	3.605	B
1411	4	1	0	4.013	100	3.80072	-5.028e-03	1.210e-03	4.960	6.768	B
5389	4	2	1	4.000	100	3.79911	-1.328e-03	3.159e-03	2.854	3.009	B
5389	5	1	0	4.003	100	3.80028	-2.024e-03	2.011e-03	3.408	3.986	B
20995	5	2	1	4.000	100	3.80018	-1.463e-03	1.724e-03	2.872	3.010	B

(b) Gradient method from Algorithm 4.3

DoFs	ref.	Lagr.	Néd.	λ_0	it.	λ_{it}	J	r_{rel}	$J_{q,\min}$	$J_{q,\max}$	EVS
387	2	2	1	4.002	1000	3.80003	-9.999e-05	1.345e-03	1.061	1.066	A
387	3	1	0	4.052	1000	3.79952	-1.081e-04	1.350e-03	1.075	1.075	A
1411	3	2	1	4.000	1000	3.80003	-9.968e-05	1.383e-03	1.063	1.066	A
1411	4	1	0	4.013	1000	3.8	-1.017e-04	1.192e-03	1.068	1.068	A
5389	4	2	1	4.000	1000	3.80003	-9.966e-05	1.386e-03	1.064	1.066	A
5389	5	1	0	4.003	1000	3.80002	-1.002e-04	1.332e-03	1.066	1.066	A
20995	5	2	1	4.000	1000	3.80003	-9.966e-05	1.385e-03	1.065	1.066	A

Table A.12. Results of a freeform optimization for the first eigenvalue on a rectangle domain with target value $\lambda_* = 3.8$ and regularization parameters $\alpha = 10^{-2}, \beta = 10^{-3}$ for the tolerance of the termination criteria of $\text{TOL}_{\text{global}} = \text{TOL} = 10^{-5}$. The tables show results varying the DoFs of the mesh, the refinement level (ref.), the order of Lagrange (Lagr.) and Nédélec (Néd.) elements. The initial first (numerical) eigenvalue is given by λ_0. We show the eigenvalue λ_{it} after termination of the method and the resulting value of the cost functional J, the relative residual of the gradient of the cost functional as well as the minimum and maximum value of the determinant of the deformation gradient J_q and the used eigenvalue solver EVS.

(a) BFGS method from Algorithm 4.4

DoFs	ref.	Lagr.	Néd.	λ_0	it.	$\lambda_{\text{it.}}$	J	r_{rel}	$J_{q,\min}$	$J_{q,\max}$	EVS
387	2	2	1	4.002	35	3.79988	-1.105e-04	6.667e-06	1.089	1.127	A
387	3	1	0	4.052	21	3.79989	-1.156e-04	4.620e-06	1.104	1.115	A
1411	3	2	1	4.000	69	3.79988	-1.103e-04	5.567e-06	1.090	1.108	A
1411	4	1	0	4.013	22	3.79988	-1.117e-04	3.070e-06	1.095	1.098	A
5389	4	2	1	4.000	79	3.79988	-1.103e-04	3.602e-06	1.089	1.098	A
5389	5	1	0	4.003	36	3.79988	-1.107e-04	6.220e-06	1.091	1.093	A
20995	5	2	1	4.000	68	3.79988	-1.103e-04	7.510e-06	1.088	1.094	A

(b) Gradient method from Algorithm 4.3

DoFs	ref.	Lagr.	Néd.	λ_0	it.	$\lambda_{\text{it.}}$	J	r_{rel}	$J_{q,\min}$	$J_{q,\max}$	EVS
387	2	2	1	4.002	1000	3.80011	-7.480e-05	1.246e-03	1.054	1.063	A
387	3	1	0	4.052	1000	3.79954	-7.993e-05	1.415e-03	1.070	1.072	A
1411	3	2	1	4.000	1000	3.80012	-7.459e-05	1.293e-03	1.058	1.063	A
1411	4	1	0	4.013	1000	3.80008	-7.597e-05	1.064e-03	1.064	1.065	A
5389	4	2	1	4.000	1000	3.80012	-7.458e-05	1.296e-03	1.060	1.063	A
5389	5	1	0	4.003	1000	3.80011	-7.493e-05	1.233e-03	1.063	1.063	A
20995	5	2	1	4.000	1000	3.80012	-7.458e-05	1.296e-03	1.062	1.063	A

Table A.13. Results of a freeform optimization for the first eigenvalue on a rectangle domain with target value $\lambda_* = 3.8$ and regularization parameters $\alpha = 10^{-1}, \beta = 10^{-3}$ for the tolerance of the termination criteria of $\text{TOL}_{\text{global}} = \text{TOL} = 10^{-5}$. The tables show results varying the DoFs of the mesh, the refinement level (ref.), the order of Lagrange (Lagr.) and Nédélec (Néd.) elements. The initial first (numerical) eigenvalue is given by λ_0. We show the eigenvalue λ_{it} after termination of the method and the resulting value of the cost functional J, the relative residual of the gradient of the cost functional as well as the minimum and maximum value of the determinant of the deformation gradient J_q and the used eigenvalue solver EVS.

(a) BFGS method from Algorithm 4.4

DoFs	ref.	Lagr.	Néd.	λ_0	it.	$\lambda_{\text{it.}}$	J	r_{rel} .	$J_{q,\text{min}}$	$J_{q,\text{max}}$	EVS
387	2	2	1	4.002	8	3.80037	1.080e-05	2.806e-08	1.031	1.054	A
387	3	1	0	4.052	7	3.80051	3.188e-05	9.300e-06	1.055	1.060	A
1411	3	2	1	4.000	8	3.80037	1.011e-05	2.907e-08	1.040	1.053	A
1411	4	1	0	4.013	8	3.8004	1.484e-05	4.272e-08	1.053	1.054	A
5389	4	2	1	4.000	8	3.80037	1.007e-05	2.978e-08	1.047	1.054	A
5389	5	1	0	4.003	8	3.80038	1.122e-05	3.243e-08	1.053	1.053	A
20995	5	2	1	4.000	8	3.80037	1.006e-05	2.962e-08	1.050	1.054	A

(b) Gradient method from Algorithm 4.3

DoFs	ref.	Lagr.	Néd.	λ_0	it.	$\lambda_{\text{it.}}$	J	r_{rel}	$J_{q,\text{min}}$	$J_{q,\text{max}}$	EVS
387	2	2	1	4.002	1000	3.80037	1.080e-05	3.715e-05	1.030	1.053	A
387	3	1	0	4.052	1000	3.80051	3.189e-05	2.176e-05	1.055	1.060	A
1411	3	2	1	4.000	1000	3.80036	1.011e-05	3.820e-05	1.040	1.053	A
1411	4	1	0	4.013	1000	3.8004	1.485e-05	3.307e-05	1.053	1.054	A
5389	4	2	1	4.000	1000	3.80036	1.007e-05	3.830e-05	1.047	1.054	A
5389	5	1	0	4.003	1000	3.80037	1.122e-05	3.692e-05	1.053	1.053	A
20995	5	2	1	4.000	1000	3.80036	1.007e-05	3.829e-05	1.050	1.054	A

A.2.2. Quarter Circle with Fixed Edges

Table A.14. Results of a freeform optimization on a quarter circle domain with fixed edges by using the gradient method from Algorithm 4.3 with target value $\lambda_* = 0.92$ and regularization parameters $\alpha = 10^{-5}, \beta = 10^{-6}$. The tables show results varying the DoFs of the mesh, the refinement level (ref.), the order of Lagrange (Lagr.) and Nédélec (Néd.) elements. The initial first (numerical) eigenvalue is given by λ_0. We show the eigenvalue λ_{it} after termination of the method and the resulting value of the cost functional J, the relative residual of the gradient of the cost functional as well as the minimum and maximum value of the determinant of the deformation gradient J_q and the used eigenvalue solver EVS.

DoFs	ref.	Lagr.	Néd.	λ_0	it.	$\lambda_{\mathrm{it.}}$	J	r_{rel}	$J_{q,\min}$	$J_{q,\max}$	EVS
1059	3	1	0	0.9518	1000	0.92	-2.118e-08	1.716e-04	0.998	1.000	A
4035	3	2	1	0.9467	1000	0.92	-2.626e-08	2.003e-04	0.999	1.000	A
4035	4	1	0	0.9468	1000	0.92	-2.594e-08	2.006e-04	0.999	1.001	A
15737	4	2	1	0.9455	1000	0.92	-2.675e-08	2.093e-04	0.999	1.000	A
15737	5	1	0	0.9456	1000	0.92	-2.667e-08	2.094e-04	1.000	1.000	A
62211	5	2	1	0.9453	1000	0.92	-2.685e-08	2.117e-04	1.000	1.000	A

Table A.15. Results of a freeform optimization on a quarter circle domain with fixed edges and target value $\lambda_* = 0.92$ and regularization parameters $\alpha = 10^{-6}, \beta = 10^{-6}$. The tables show results varying the DoFs of the mesh, the refinement level (ref.), the order of Lagrange (Lagr.) and Nédélec (Néd.) elements. The initial first (numerical) eigenvalue is given by λ_0. We show the eigenvalue λ_{it} after termination of the method and the resulting value of the cost functional J, the relative residual of the gradient of the cost functional as well as the minimum and maximum value of the determinant of the deformation gradient J_q and the used eigenvalue solver EVS.

(a) BFGS method from Algorithm 4.4

DoFs	ref.	Lagr.	Néd.	λ_0	it.	λ_{it}	J	r_{rel}	$J_{q,\min}$	$J_{q,\max}$	EVS
1059	3	1	0	0.9518	31	0.919999	-1.005e-06	7.816e-05	1.164	1.176	A
4035	3	2	1	0.9467	18	0.919997	-8.793e-07	1.088e-04	1.123	1.152	A
4035	4	1	0	0.9468	18	0.919997	-9.020e-07	1.028e-04	1.028	1.142	A
15737	4	2	1	0.9455	21	0.919997	-1.005e-06	8.504e-05	1.337	1.381	A
15737	5	1	2	0.9456	21	0.919998	-1.006e-06	8.695e-05	1.351	1.358	A
62211	5	2	1	0.9453	27	0.919997	-1.012e-06	8.469e-05	1.342	1.364	A

(b) Gradient method from Algorithm 4.3

DoFs	ref.	Lagr.	Néd.	λ_0	it.	λ_{it}	J	r_{rel}	$J_{q,\min}$	$J_{q,\max}$	EVS
1059	3	1	0	0.9518	1000	0.919998	-6.290e-08	1.741e-04	0.998	1.000	A
4035	3	2	1	0.9467	1000	0.919998	-5.432e-08	2.028e-04	0.999	1.000	A
4035	4	1	0	0.9468	1000	0.919998	-5.470e-08	2.031e-04	0.999	1.000	A
15737	4	2	1	0.9455	1000	0.919990	-5.249e-08	2.118e-04	0.999	1.000	A
15737	5	1	0	0.9456	1000	0.919998	-5.258e-08	2.120e-04	1.000	1.000	A
62211	5	2	1	0.9453	1000	0.919998	-5.203e-08	2.142e-04	1.000	1.000	A

Table A.16. Results of a freeform optimization on a quarter circle domain with fixed edges by using the gradient method from Algorithm 4.3 with target value $\lambda_* = 0.92$ and regularization parameters $\alpha = 10^{-4}$ and $\beta = 10^{-5}$. The tables show results varying the DoFs of the mesh, the refinement level (ref.), the order of Lagrange (Lagr.) and Nédélec (Néd.) elements. The initial first (numerical) eigenvalue is given by λ_0. We show the eigenvalue λ_{it} after termination of the method and the resulting value of the cost functional J, the relative residual of the gradient of the cost functional as well as the minimum and maximum value of the determinant of the deformation gradient J_q and the used eigenvalue solver EVS.

DoFs	ref.	Lagr.	Néd.	λ_0	it.	λ_{it}	J	r_{rel}	$J_{q,\min}$	$J_{q,\max}$	EVS
1059	3	1	0	0.9518	1000	0.92001	-4.825e-07	1.561e-03	1.002	1.004	A
4035	3	2	1	0.9467	1000	0.920004	-5.340e-07	1.821e-03	1.003	1.003	A
4035	4	1	0	0.9468	1000	0.920004	-5.308e-07	1.823e-03	1.003	1.004	A
15737	4	2	1	0.9455	1000	0.920003	-5.391e-07	1.903e-03	1.003	1.003	A
15737	5	1	0	0.9456	1000	0.920003	-5.383e-07	1.904e-03	1.003	1.003	A
62211	5	2	1	0.9453	1000	0.920002	-5.399e-07	1.924e-03	1.003	1.003	A

Table A.17. Results of a freeform optimization varying the regularization parameters α and β by using the BFGS method from Algorithm 4.4 on a quarter circle domain with fixed edges and target value $\lambda_* = 0.92$. The tables show results varying the DoFs of the mesh, the refinement level (ref.), the order of Lagrange (Lagr.) and Nédélec (Néd.) elements. The initial first (numerical) eigenvalue is given by λ_0. We show the eigenvalue λ_{it} after termination of the method and the resulting value of the cost functional J, the relative residual of the gradient of the cost functional as well as the minimum and maximum value of the determinant of the deformation gradient J_q and the used eigenvalue solver EVS.

(a) $\alpha = 10^{-5}$ and $\beta = 10^{-5}$

DoFs	ref.	Lagr.	Néd.	λ_0	it.	$\lambda_{\text{it.}}$	J	r_{rel}	$\mathrm{J}_{q,\min}$	$\mathrm{J}_{q,\max}$	EVS
1059	3	1	0	0.9518	63	0.92002	-1.327e-05	8.882e-05	1.459	1.495	A
4035	3	2	1	0.9467	100	0.919973	-1.218e-05	1.486e-04	1.268	1.336	B
4035	4	1	0	0.9468	100	0.919981	-1.227e-05	2.668e-04	1.302	1.314	BS
15737	4	2	1	0.9455	100	0.919973	-1.209e-05	2.095e-04	1.276	1.308	A
15737	5	1	0	0.9456	100	0.919953	-1.180e-05	1.442e-03	1.253	1.267	A
62211	5	2	1	0.9453	100	0.919953	-1.180e-05	1.44203	1.253	1.267	A

(b) $\alpha = 10^{-6}$ and $\beta = 10^{-5}$

DoFs	ref.	Lagr.	Néd.	λ_0	it.	$\lambda_{\text{it.}}$	J	r_{rel}	$\mathrm{J}_{q,\min}$	$\mathrm{J}_{q,\max}$	EVS
1059	3	1	0	0.9518	100	0.919938	-3.308e-05	1.109e-03	1.554	1.615	B
4035	3	2	1	0.9467	100	0.920088	-3.306e-05	3.436e-03	1.482	1.547	B
4035	4	1	0	0.9468	100	0.919555	-3.115e-05	9.538e-03	1.465	1.476	B
15737	4	2	1	0.9455	100	0.919868	-2.696e-05	3.184e-03	1.400	1.419	A
15737	5	1	0	0.9456	100	0.920065	-3.278e-05	2.919e-03	1.479	1.485	B
62211	5	2	1	0.9453	100	0.919868	-2.696e-05	3.184e-03	1.400	1.419	A

(c) $\alpha = 10^{-3}$ and $\beta = 10^{-5}$

DoFs	ref.	Lagr.	Néd.	λ_0	it.	$\lambda_{\text{it.}}$	J	r_{rel}	$\mathrm{J}_{q,\min}$	$\mathrm{J}_{q,\max}$	EVS
1059	3	1	0	0.9518	6	0.920272	3.793e-06	1.125e-06	1.0020	1.0040	A
4035	3	2	1	0.9467	6	0.920214	2.388e-06	1.381e-06	1.0030	1.0036	A
4035	4	1	0	0.9468	6	0.920218	2.461e-06	1.626e-06	1.0029	1.0036	A
15737	4	2	1	0.9455	6	0.920204	2.153e-06	1.633e-06	1.0032	1.0034	A
15737	5	1	0	0.9456	6	0.920205	2.171e-06	1.701e-06	1.0032	1.0035	A
62211	5	2	1	0.9453	6	0.920201	2.096e-06	1.652e-06	1.0033	1.0034	A

Table A.18. Results of a freeform optimization varying the regularization parameters α and β by using the BFGS method from Algorithm 4.4 on a quarter circle domain with fixed edges and target value $\lambda_* = 0.92$. The tables show results varying the DoFs of the mesh, the refinement level (ref.), the order of Lagrange (Lagr.) and Nédélec (Néd.) elements. The initial first (numerical) eigenvalue is given by λ_0. We show the eigenvalue λ_{it} after termination of the method and the resulting value of the cost functional J, the relative residual of the gradient of the cost functional as well as the minimum and maximum value of the determinant of the deformation gradient J_q and the used eigenvalue solver EVS.

(a) $\alpha = 10^{-5}$ and $\beta = 10^{-7}$

DoFs	ref.	Lagr.	Néd.	λ_0	it.	$\lambda_{\text{it.}}$	J	r_{rel}	$J_{q,\min}$	$J_{q,\max}$	EVS
1059	3	1	0	0.9518	9	0.920004	3.831e-08	4.089e-05	1.002	1.004	A
4035	3	2	1	0.9467	7	0.920005	2.427e-08	1.012e-04	1.002	1.003	A
4035	4	1	0	0.9468	9	0.920003	2.485e-08	3.740e-05	1.003	1.003	A
15737	4	2	1	0.9455	7	0.920004	2.188e-08	7.823e-05	1.003	1.003	A
15737	5	1	0	0.9456	7	0.920004	2.208e-08	9.096e-05	1.003	1.003	A
62211	5	2	1	0.9453	7	0.920004	2.130e-08	6.969e-05	1.003	1.003	A

(b) $\alpha = 10^{-6}$ and $\beta = 10^{-7}$

DoFs	ref.	Lagr.	Néd.	λ_0	it.	$\lambda_{\text{it.}}$	J	r_{rel}	$J_{q,\min}$	$J_{q,\max}$	EVS
1059	3	1	0	0.9518	7	0.92	-6.003e-09	1.825e-05	1.004	1.006	B
4035	3	2	1	0.9467	12	0.920002	-1.365e-08	7.669e-05	1.016	1.019	A
4035	4	1	0	0.9468	7	0.919998	-6.361e-09	8.983e-05	1.004	1.005	A
15737	4	2	1	0.9455	12	0.920002	-1.383e-08	8.217e-05	1.017	1.018	A
15737	5	1	0	0.9456	12	0.920001	-1.296e-08	2.562e-05	1.015	1.015	A
62211	5	2	1	0.9453	12	0.920001	-1.393e-08	8.456e-05	1.017	1.018	B

(c) $\alpha = 10^{-3}$ and $\beta = 10^{-7}$

DoFs	ref.	Lagr.	Néd.	λ_0	it.	$\lambda_{\text{it.}}$	J	r_{rel}	$J_{q,\min}$	$J_{q,\max}$	EVS
1059	3	1	0	0.9518	5	0.920288	4.574e-06	6.746e-05	0.998	1.000	A
4035	3	2	1	0.9467	6	0.920232	3.077e-06	2.487e-06	0.9984	1.000	A
4035	4	1	0	0.9468	5	0.920234	3.154e-06	1.018e-04	0.999	1.000	A
15737	4	2	1	0.9455	6	0.920223	2.822e-06	2.158e-06	0.999	1.000	A
15737	5	1	0	0.9456	5	0.920221	2.842e-06	1.144e-04	0.999	0.999	B
62211	5	2	1	0.9453	6	0.920220	2.760e-06	2.093e-06	1.000	1.000	B

A.2.3. 1-Cell Cavity

Table A.19. Comparison of λ_* on the domain deformation of a freeform optimization on a 1-cell Cavity with fixed R_{iris} on left-hand and right-hand side and with fixed axes at the irises by using the BFGS method from Algorithm 4.4 with regularization parameters $\alpha = 1, \beta = 10^{-5}$. The chosen refinement level is 2, the number of DoFs is 43363. Lagrange elements of order 1 and lowest order Nédélec elements are used and the initial first (numerical) eigenvalue is $\lambda_0 = 1653.75$.

λ_*	it.	$\lambda_{\mathrm{it.}}$	J	r_{rel}	$J_{\min}$	$J_{\max}$
1650	18	1650	2.427e-09	< 1.0e-08	1.00180	1.00182
1640	18	1640	3.330e-08	4.410e-08	1.00662	1.00670
1660	18	1660	6.889e-09	1.163e-08	0.99698	0.99702
1670	18	1670	4.587e-08	4.002e-08	0.99220	0.99230

Bibliography

[1] Cern accelerators. `https://home.cern/science/accelerators`. Accessed: 2023-12-13. [→1]

[2] Superconducting darmstadt electron linear accelerator s-dalinac. `http://www.ikp.tu-darmstadt.de/sdalinac_ikp/`. Accessed: 2023-12-12. [→122]

[3] V. Akçelik, G. Biros, O. Ghattas, D. Keyes, K. Ko, L.-Q. Lee, and E. G. Ng. Adjoint methods for electromagnetic shape optimization of the low-loss cavity for the international linear collider. *Journal of Physics: Conference Series*, 16:435–445, 2005. [→3]

[4] G. Allaire, C. Dapogny, and P. Frey. Shape optimization with a level set based mesh evolution method. *Computer Methods in Applied Mechanics and Engineering*, 282:22–53, 2014. [→3]

[5] G. Allaire, C. Dapogny, and F. Jouve. *Chapter 1 - Shape and topology optimization*, volume 22 of *Handbook of Numerical Analysis*, pages 1–132. Elsevier, 2021. [→1]

[6] G. Allaire and F. Jouve. Minimum stress optimal design with the level set method. *Engineering Analysis with Boundary Elements*, 32(11):909–918, 2008. Shape and Topological Sensitivity Analysis: Theory and Applications. [→3]

[7] G. Allaire, F. Jouve, and A.-M. Toader. Structural optimization using sensitivity analysis and a level-set method. *Journal of Computational Physics*, 194(1):363–393, 2004. [→3]

[8] G. Allaire, F. Jouve, and N. Van Goethem. Damage and fracture evolution in brittle materials by shape optimization methods. *Journal of Computational Physics*, 230(12):5010–5044, 2011. [→3]

[9] P. Arbenz and R. Geus. Eigenvalue solvers for electromagnetic fields in cavities. In *High Performance Scientific and Engineering Computing*, pages

363–373. Springer Berlin Heidelberg, 1999. [→1, 5, 56, 75, 76, 83]

[10] D. Arndt, W. Bangerth, B. Blais, T. C. Clevenger, M. Fehling, A. V. Grayver, T. Heister, L. Heltai, M. Kronbichler, M. Maier, P. Munch, J.-P. Pelteret, R. Rastak, I. Thomas, B. Turcksin, Z. Wang, and D. Wells. The `deal.II` library, version 9.2. *Journal of Numerical Mathematics*, 28(3):131–146, 2020. [→6, 78, 79, 82, 85, 140, 143, 147]

[11] D. Arndt, W. Bangerth, T. C. Clevenger, D. Davydov, M. Fehling, D. Garcia-Sanchez, G. Harper, T. Heister, L. Heltai, M. Kronbichler, R. M. Kynch, M. Maier, J.-P. Pelteret, B. Turcksin, and D. Wells. The `deal.II` library, version 9.1. *Journal of Numerical Mathematics*, 27(4):203–213, 2019. [→6, 78, 79, 82, 85, 140, 143, 147]

[12] B. Aune, R. Bandelmann, D. Bloess, B. Bonin, A. Bosotti, M. Champion, C. Crawford, G. Deppe, B. Dwersteg, D. A. Edwards, H. T. Edwards, M. Ferrario, M. Fouaidy, P.-D. Gall, A. Gamp, A. Gössel, J. Graber, D. Hubert, M. Hüning, M. Juillard, T. Junquera, H. Kaiser, G. Kreps, M. Kuchnir, R. Lange, M. Leenen, M. Liepe, L. Lilje, A. Matheisen, W.-D. Möller, A. Mosnier, H. Padamsee, C. Pagani, M. Pekeler, H.-B. Peters, O. Peters, D. Proch, K. Rehlich, D. Reschke, H. Safa, T. Schilcher, P. Schmüser, J. Sekutowicz, S. Simrock, W. Singer, M. Tigner, D. Trines, K. Twarowski, G. Weichert, J. Weisend, J. Wojtkiewicz, S. Wolff, and K. Zapfe. Superconducting tesla cavities. *Physical Review Special Topics - Accelerators and Beams*, 3:092001, 2000. [→2, 139]

[13] S. Balay, S. Abhyankar, M. F. Adams, J. Brown, P. Brune, K. Buschelman, L. Dalcin, A. Dener, V. Eijkhout, W. D. Gropp, D. Kaushik, M. G. Knepley, D. A. May, L. C. McInnes, R. T. Mills, T. Munson, K. Rupp, P. Sanan, B. F. Smith, S. Zampini, H. Zhang, and H. Zhang. PETSc users manual. Technical Report ANL-95/11 - Revision 3.15, Argonne National Laboratory, 2021. [→83, 147]

[14] S. Balay, S. Abhyankar, M. F. Adams, J. Brown, P. Brune, K. Buschelman, L. Dalcin, A. Dener, V. Eijkhout, W. D. Gropp, D. Kaushik, M. G. Knepley, D. A. May, L. C. McInnes, R. T. Mills, T. Munson, K. Rupp, P. Sanan, B. F. Smith, S. Zampini, H. Zhang, and H. Zhang. PETSc Web page. `https://petsc.org/`, 2021. [→83, 147]

[15] S. Balay, W. D. Gropp, L. C. McInnes, and B. F. Smith. Efficient management of parallelism in object oriented numerical software libraries. In

Modern Software Tools in Scientific Computing, pages 163–202. Birkhauser Press, 1997. [→83, 147]

[16] A. Battermann and M. Heinkenschloss. Preconditioners for karush-kuhn-tucker matrices arising in the optimal control of distributed systems. In *Control and Estimation of Distributed Parameter Systems*, pages 15–32. Birkhäuser Basel, 1998. [→83]

[17] A. Battermann and E. W. Sachs. Block preconditioners for kkt systems in pde - governed optimal control problems. In *Fast Solution of Discretized Optimization Problems*, pages 1–18. Birkhäuser Basel, 2001. [→83]

[18] R. Becker, D. Meidner, and B. Vexler. Efficient numerical solution of parabolic optimization problems by finite element methods. *Optimization Methods and Software*, 22, 2007. [→31, 57, 145]

[19] M. Benzi, G. H. Golub, and J. Liesen. Numerical solution of saddle point problems. *Acta Numerica*, 14:1–137, 2005. [→83]

[20] J. T. Betts. *Practical Methods for Optimal Control and Estimation Using Nonlinear Programming, Second Edition.* Society for Industrial and Applied Mathematics, second edition, 2010. [→83]

[21] D. Boffi. Discrete compactness and fortin operator for edge elements. *Numerische Mathematik*, 87:229–246, 2000. [→76]

[22] D. Boffi. A note on the derham complex and a discrete compactness property. *Applied Mathematics Letters*, 14(1):33–38, 2001. [→76]

[23] D. Boffi. Finite element approximation of eigenvalue problems. *Acta Numer.*, 19:1–120, 2010. [→37, 38, 40, 76]

[24] D. Boffi, F. Brezzi, and M. Fortin. *Mixed Finite Element Methods and Applications*, volume 44 of *Springer Series in Computational Mathematics*. Springer Berlin Heidelberg, 2013. [→10, 22, 56, 75, 78, 79]

[25] D. Boffi, F. Brezzi, and L. Gastaldi. On the problem of spurious eigenvalues in the approximation of linear elliptic problems in mixed form. *Math. Comput.*, 69:121–140, 2000. [→76]

[26] D. Boffi, P. Fernandes, L. Gastaldi, and I. Perugia. Computational models of electromagnetic resonators: Analysis of edge element approximation. *SIAM Journal on Numerical Analysis*, 36(4):1264–1290, 1999. [→76]

[27] D. Boffi and L. Gastaldi. Edge finite elements for the approximation of Maxwell resolvent operator. *ESAIM: Mathematical Modelling and Numerical Analysis*, 36(2):293–305, 2002. [→76]

[28] J. Bonet and R. D. Wood. *Nonlinear Continuum Mechanics for Finite Element Analysis*. Cambridge University Press, 2 edition, 2008. [→41]

[29] A. Bossavit. Solving maxwell equations in a closed cavity, and the question of spurious modes. *Magnetics, IEEE Transactions on*, 26:702 – 705, 1990. [→5]

[30] A. Bossavit and I. Mayergoyz. *Computational Electromagnetism: Variational Formulations, Complementarity, Edge Elements*. Electromagnetism. Elsevier Science, 1998. [→83]

[31] F. Brezzi and M. Fortin. Mixed and hybrid finite element method. *Springer Series In Computational Mathematics; Vol. 15*, page 350, 1991. [→45, 83]

[32] Brezzi, F. On the existence, uniqueness and approximation of saddle-point problems arising from lagrangian multipliers. *R.A.I.R.O. Analyse Numérique*, 8:129–151, 1974. [→83]

[33] J. Cea. Conception optimale ou identification de formes, calcul rapide de la dérivée directionnelle de la fonction coût. *M2AN - Modélisation mathématique et analyse numérique*, 20(3):371–402, 1986. [→3]

[34] A. Chatterjee, J. Jin, and J. Volakis. Computation of cavity resonances using edge-based finite elements. *IEEE Transactions on Microwave Theory and Techniques*, 40(11):2106–2108, 1992. [→5]

[35] G. Cohen. *Higher-Order Numerical Methods for Transient Wave Equations*. Scientific computation. Springer, 2002. [→38]

[36] J. Corno. *Numerical Methods for the Estimation of the Impact of Geometric Uncertainties on the Performance of Electromagnetic Devices*. PhD thesis, Technische Universität, Darmstadt, 2017. [→2, 37, 121, 122, 139, 140, 141, 142, xviii]

[37] M. Costabel and M. Dauge. Maxwell and lamé eigenvalues on polyhedra. *Mathematical Methods in the Applied Sciences*, 22(3):243–258, 1999. [→75]

[38] M. Costabel and M. Dauge. Weighted regularization of maxwell equations in polyhedral domains. *Numerische Mathematik*, 93(2):239–277, 2002. [→75]

[39] M. Costabel, M. Dauge, and D. Martin. Numerical investigation of a boundary penalization method for maxwell equations. *Proceedings of the 3rd European Conference on Numerical Mathematics and Advanced Applications*, 2000. [→75]

[40] J. De los Reyes. *Numerical PDE-Constrained Optimization*. Springer, 2015. [→3, 55, 63]

[41] M. C. Delfour and J. P. Zolésio. *Shapes and Geometries*. Society for Industrial and Applied Mathematics, second edition, 2011. [→4]

[42] M. Fischer, F. Lindemann, M. Ulbrich, and S. Ulbrich. Fréchet differentiability of unsteady incompressible navier–stokes flow with respect to domain variations of low regularity by using a general analytical framework. *SIAM Journal on Control and Optimization*, 55(5):3226–3257, 2017. [→4, 37, 141]

[43] T. Galek, K. Brackebusch, T. Flisgen, U. van Rienen, J. Knobloch, A. Neumann, B. Riemann, and T. Weis. BERLinPro Seven-cell SRF Cavity Optimization and HOMs External Quality Factors Estimation. In *4th International Particle Accelerator Conference*, page WEPWO010, 2013. [→2]

[44] H. Garcke, P. Hüttl, and P. Knopf. Shape and topology optimization involving the eigenvalues of an elastic structure: A multi-phase-field approach. *Advances in Nonlinear Analysis*, 11:159–197, 2021. [→4, 141]

[45] J. E. Gentle. Matrix algebra: Theory, computations, and applications in statistics. *International Statistical Review*, 75(3):435–435, 2007. [→23]

[46] N. Georg, W. Ackermann, J. Corno, and S. Schöps. Uncertainty quantification for maxwell's eigenproblem based on isogeometric analysis and mode tracking. *Computer Methods in Applied Mechanics and Engineering*, 350, 2019. [→2, 37, 139, 141]

[47] C. Geuzaine and J.-F. Remacle. Gmsh: A 3-d finite element mesh generator with built-in pre- and post-processing facilities. *International Journal for Numerical Methods in Engineering*, 79(11):1309–1331, 2009. [→123]

[48] P. E. Gill, W. Murray, and M. H. Wright. *Practical optimization*. Academic Press Inc. [Harcourt Brace Jovanovich Publishers], London, 1981. [→83]

[49] C. Goll, T. Wick, and W. Wollner. DOpElib: Differential equations and optimization environment; A goal oriented software library for solving pdes and optimization problems with pdes. *Archive of Numerical Software*, 5(2):1–14, 2017. [→6, 72, 85, 140, 143]

[50] G. H. Golub and C. Greif. On solving block-structured indefinite linear systems. *SIAM Journal on Scientific Computing*, 24(6):2076–2092, 2003. [→82]

[51] A. Griewank. The local convergence of Broyden-like methods on Lipschitzian problems in Hilbert spaces. *SIAM J. Numer. Anal.*, 24(3):684–705, 1987. [→74]

[52] J. Haslinger and R. A. E. Mäkinen. *Introduction to Shape Optimization*. Society for Industrial and Applied Mathematics, 2003. [→4]

[53] P. Haupt. *Continuum Mechanics and Theory of Materials*. Springer, 2002. [→37, 41]

[54] J. Heners, L. Radtke, M. Hinze, and A. Düster. Adjoint shape optimization for fluid–structure interaction of ducted flows. *Computational Mechanics*, 61(3):259 – 276, 2018. [→3]

[55] V. Hernandez, J. E. Roman, and V. Vidal. SLEPc: Scalable Library for Eigenvalue Problem Computations. *Lect. Notes Comput. Sci.*, 2565:377–391, 2003. [→83, 147]

[56] V. Hernandez, J. E. Roman, and V. Vidal. SLEPc: A scalable and flexible toolkit for the solution of eigenvalue problems. *ACM Trans. Math. Software*, 31(3):351–362, 2005. [→83, 147]

[57] C. Herter, S. Schöps, and W. Wollner. Eigenvalue optimization with respect to shape-variations in electromagnetic cavities. *PAMM*, 22(1):e202200122, 2023. [→3, 6, 55]

[58] V. Heuveline and R. Rannacher. A posteriori error control for finite approximations of elliptic eigenvalue problems. *Adv. Comput. Math.*, 15:107–138, 2001. [→3, 55]

[59] M. Hinze, R. Pinnau, M. Ulbrich, and S. Ulbrich. *Optimization with PDE Constraints*, volume 23, pages xii+270. Springer, 2009. [→3, 9, 15, 20, 26, 28, 29, 31, 32, 34, 63, 64]

[60] J. D. Jackson. *Klassische Elektrodynamik*. De Gruyter, 2011. [→4, 37, 38, 40, 86]

[61] P. Jorkowski and R. Schuhmann. Mode tracking for parametrized eigenvalue problems in computational electromagnetics. In *2018 International Applied Computational Electromagnetics Society Symposium (ACES)*, pages 1–2, 2018. [→141]

[62] H. Kasumba, K. Kunisch, and K.-F.-U. Graz. On shape sensitivity analysis of the cost functional without shape sensitivity of the state variable. *Control and Cybernetics*, 40:989–1017, 2011. [→3]

[63] C. T. Kelley and E. W. Sachs. A new proof of superlinear convergence for Broyden's method in Hilbert space. *SIAM J. Optim.*, 1(1):146–150, 1991. [→74]

[64] F. Kikuchi. An isomorphic property of two hilbert spaces appearing in electromagnetism: Analysis by the mixed formulation. *Japan Journal of Applied Mathematics*, 3:53–58, 1986. [→76]

[65] F. Kikuchi. Mixed and penalty formulations for finite element analysis of an eigenvalue problem in electromagnetism. *Applied Mechanics and Engineering*, 64:509–521, 1987. [→5, 37, 40, 52, 75, 76]

[66] F. Kikuchi. On a discrete compactness property for the nedelec finite elements. *J. Fac. Sci. Univ. Tokyo, Sect. IA. Math.*, 36, 1989. [→76]

[67] N. Kikuchi, H.-C. Cheng, and Z.-D. Ma. *Optimal Shape and Topology Design of Vibrating Structures*. Springer Netherlands, Dordrecht, 1995. [→3]

[68] H.-J. Kowalsky. *Vektoranalysis Teil 2*. De Gruyter, Berlin, Boston, 1976. [→37]

[69] M. Kranjčević, S. Gorgi Zadeh, A. Adelmann, P. Arbenz, and U. van Rienen. Constrained multiobjective shape optimization of superconducting rf cavities considering robustness against geometric perturbations. *Phys. Rev. Accel. Beams*, 22:122001, 2019. [→2]

[70] M. Kranjčević, A. Adelmann, P. Arbenz, A. Citterio, and L. Stingelin. Multi-objective shape optimization of radio frequency cavities using an evolutionary algorithm. *Nuclear Instruments and Methods in Physics Research Section A: Accelerators, Spectrometers, Detectors and Associated Equipment*, 920:106–114, 2019. [→2]

[71] C. S. Kubrusly. *Spectral Theorem*, pages 55–89. Birkhäuser Boston, Boston, 2012. [→70]

[72] R. Leis. Zur theorie elektromagnetischer schwingungen in anisotropen inhomogenen medien. *Mathematische Zeitschrift*, 106(3):213–224, 1968. [→5, 75]

[73] J. C. Maxwell. On physical lines of force. *Philosophical Magazine and Journal of Science*, 1861. [→37, 38]

[74] J. C. Maxwell. A dynamical theory of the electromagnetic field. *Royal Society Transactions*, 155:459–512, 1864. [→37, 38]

[75] J. C. Maxwell. *A treatise on electricity and magnetism*. Clarendon Press, 1873. [→37, 38]

[76] P. Monk, P. Department of Mathematics Sciences Peter Monk, and O. U. Press. *Finite Element Methods for Maxwell's Equations*. Numerical Mathematics and Scientific Computation. Clarendon Press, 2003. [→10, 22, 25, 37, 38, 39, 41, 45, 51, 53, 54, 56, 76, 77, 78, 79]

[77] G. Mur. Edge elements, their advantages and their disadvantages. *IEEE Transactions on Magnetics*, 30(5):3552–3557, 1994. [→5]

[78] F. Murat. *Calculus of Variations and Homogenization*, pages 139–173. Birkhäuser Boston, Boston, MA, 1997. [→3]

[79] F. Murat and J. Simon. Etude de problemes d'optimal design. In *Optimization Techniques Modeling and Optimization in the Service of Man Part 2*, pages 54–62, Berlin, Heidelberg, 1976. Springer Berlin Heidelberg. [→4, 37]

[80] F. Murat and J. Simon. Sur le contrôle par un domaine géométrique. *Laboratoire d'Analyse Numérique de l'Université de Paris VI*, 1976. [→4, 37]

[81] J. Muscat. *Functional Analysis: An Introduction to Metric Spaces, Hilbert Spaces, and Banach Algebras.* Springer International Publishing, 2014. [→9]

[82] J. Nédélec. A new family of mixed finite elements in r3. *Numerische Mathematik*, 50:57–82, 1986/87. [→78, 79]

[83] J. C. Nédélec. Mixed finite elements in r3. *Numerische Mathematik*, 35:315–341, 1980. [→5, 76, 78, 79]

[84] J. Nocedal and S. J. Wright. *Numerical Optimization.* Springer, New York, NY, USA, 2e edition, 2006. [→3, 55, 63, 65, 66, 67, 68, 82, 86]

[85] H. Padamsee, T. Hays, and J. Knobloch. *RF superconductivity for accelerators.* Wiley series in beam physics and accelerator technology. Wiley, New York, NY, 1998. [→142]

[86] B. Parlett. *The Symmetric Eigenvalue Problem.* Prentice-Hall International Series in Computer Science. Prentice-Hall, 1980. [→84]

[87] I. Perugia. A field-based mixed formulation for the two-dimensional magnetostatic problem. *SIAM Journal on Numerical Analysis*, 34(6):2382–2391, 1997. [→83]

[88] I. Perugia, V. Simoncini, and M. Arioli. Linear algebra methods in a mixed approximation of magnetostatic problems. *SIAM Journal on Scientific Computing*, 21(3):1085–1101, 1999. [→83]

[89] M. J. D. Powell. A fast algorithm for nonlinearly constrained optimization calculations. In *Numerical Analysis*, pages 144–157. Springer Berlin Heidelberg, 1978. [→3, 55, 63, 65, 68]

[90] P. Putek, S. G. Zadeh, M. Wenskat, and U. van Rienen. Multi-objective design optimization of a quadrupole resonator under uncertainties, 2020. [→2]

[91] A. M. Quarteroni and A. Valli. *Numerical Approximation of Partial Differential Equations.* Springer Publishing Company, Incorporated, 2008. [→83]

[92] R. Rannacher, A. Westenberger, and W. Wollner. Adaptive finite element solution of eigenvalue problems: Balancing of discretization and iteration error. *Journal of Numerical Mathematics*, 18(4):303–327, 2010. [→3, 55]

[93] M. Renardy and R. Rogers. *An Introduction to Partial Differential Equations.* Texts in applied mathematics. Springer, 1993. [→9, 11]

[94] M. E. Rognes, R. C. Kirby, and A. Logg. Efficient assembly of h(div) and h(curl) conforming finite elements. *SIAM Journal on Scientific Computing*, 31(6):4130–4151, 2010. [→45]

[95] J. E. Roman, C. Campos, L. Dalcin, E. Romero, and A. Tomas. SLEPc users manual. Technical Report DSIC-II/24/02 - Revision 3.16, D. Sistemes Informàtics i Computació, Universitat Politècnica de València, 2021. [→147]

[96] B. Rousselet and D. Chenais. Continuité et différentiabilité d'éléments propres: application à l'optimisation de structures. *Applied Mathematics and Optimization*, 22, 1990. [→26]

[97] H. Rutishauser. *Simultaneous Iteration Method for Symmetric Matrices*, pages 284–302. Springer Berlin Heidelberg, 1971. [→84]

[98] A. Schneebeli. An h(curl,ω)-conforming fem: Nédélec's elements of first type. `https://www.dealii.org/reports/nedelec/nedelec.pdf`, 2003. [→79, 82]

[99] J. Sokolowski and J.-P. Zolesio. *Introduction to shape optimization.* Springer Berlin Heidelberg, 1992. [→4]

[100] G. Strang. Introduction to applied mathematics. *ZAMM - Journal of Applied Mathematics and Mechanics*, pages 311–312, 1989. [→82]

[101] A.-M. Toader and C. Barbarosie. *6. Optimization of eigenvalues and eigenmodes by using the adjoint method*, pages 142–158. De Gruyter, Berlin, Boston, 2017. [→3, 55]

[102] F. Tröltzsch. *Optimal control of partial differential equations.* Graduate Studies in Mathematics. American Mathematical Society, Providence, RI, 2010. [→31, 57]

[103] M. Ulbrich and S. Ulbrich. *Nichtlineare Optimierung.* Mathematik Kompakt. Springer Basel, 2012. [→3, 55, 63, 69]

[104] T. P. Wangler. *RF Linear Accelerators*. Physics Textbook. Wiley. [→40]

[105] J. Webb. Edge elements and what they can do for you. *IEEE Transactions on Magnetics*, 29(2):1460–1465, 1993. [→5]

[106] C. Weber and P. Werner. A local compactness theorem for maxwell's equations. *Mathematical Methods in the Applied Sciences*, 2(1):12–25, 1980. [→53]

[107] T. Weiland. On the Numerical Solution of Maxwell's Equations and Applications in the Field of Accelerator Physics. *Particle Accelerators*, 15:245–292, 1984. [→4]

[108] T. Weiland. On the unique numerical solution of maxwellian eigenvalue problems in three-dimensions. *Particle Accelerators*, 17:227–242, 1985. [→4]

[109] T. Wick and W. Wollner. Optimization with nonstationary, nonlinear monolithic fluid-structure interaction. *International Journal for Numerical Methods in Engineering*, 122(19):5430–5449, 2021. [→65]

[110] M. H. Wright. Interior methods for constrained optimization. *Acta Numerica*, 1:341–407, 1992. [→83]

[111] S. J. Wright. Primal-dual interior-point methods. In *Other Titles in Applied Mathematics*, 1997. [→83]

[112] A. Ziegler, R. Hahn, V. Isensee, A. D. Nguyen, and S. Schöps. Gradient-based eigenvalue optimization for electromagnetic cavities with built-in mode matching. *IET Science, Measurement & Technology*, 2023. [→142]

[113] A. Ziegler, M. Merkel, P. Gangl, and S. Schöps. On the computation of analytic sensitivities of eigenpairs in isogeometric analysis. *Computer Methods in Applied Mechanics and Engineering*, 409:115961, 2023. [→2]

List of Algorithms

List of Figures

List of Tables

Wissenschaftlicher Werdegang

04/2022-09/2024	Wissenschaftliche Mitarbeiterin am Fachbereich Mathematik der Universität Hamburg in der Arbeitsgruppe Optimierung
04/2019 - 03/2022	Wissenschaftliche Mitarbeiterin am Fachbereich Mathematik der Technischen Universität Darmstadt in der Arbeitsgruppe Optimierung
12/2018	Abschluss Master of Science in Computational Engineering
10/2011 - 12/2018	Studium Computational Engineering mit Schwerpunkt angewandte Mathematik und Mechanik an der Technischen Universität Darmstadt
05/2011	Abitur am Gymnasium Gernsheim